PhD Thesis

Complexation on the Surface of Zinc Chalcogenide Quantum Dots: Binding, Kinetics and Application

by

Shilaj Roy

Department of Chemistry

Indian Institute of Technology Guwahati

Assam, India - 781039

August 2018

Complexation on the Surface of Zinc Chalcogenide Quantum Dots: Binding, Kinetics and Application

A thesis submitted by

Shilaj Roy

Roll No. 126122025

to

Indian Institute of Technology Guwahati

for the award of the degree of

Doctor of Philosophy

Department of Chemistry

Indian Institute of Technology Guwahati
Guwahati – 781039
India
August 2018

Abstract

As the surface of quantum dot (Qdot) emerges pivotal in every aspect of its real-life applications, intensive investigation of surface phenomenon becomes inevitable. Apart from surface ions, surface ligands have also played the determining role in the physico-chemical properties of a Qdot. In addition to the ligand manipulation strategy, formation of inorganic complexes on the surface of Qdots has also become a convenient way for engineering the surface for controllably tuning the properties of Qdots. Hence, probing the surface complexation reaction is important for understanding surface structure, stability and reactivity for properly defining the system called 'quantum dot complex (QDC)', i.e., composite consisting of complex attached to the surface of Qdot. In this regard, kinetic study coupled with modelling of the reaction of surface complexes seems to be an interesting way to probe the surface chemistry of complexation and mechanism of its formation. Besides, probing the surface complexation at few particle level is more interesting in taking advantage of coexistence of complex and Qdot in a single entity called QDC.

Focusing on basic understanding of surface complexation reaction and subsequent application, the thesis presents results of investigations on some issues such as –

i. Binding chemistry of ligands like 8-hydroxyquinoline on the surface of ZnS Qdot.
ii. Extraordinary reactivity of surface of Qdot in accomplishing anomalous reactions
iii. Role of surface anions in providing stability to surface complex.
iv. Time dependent photoluminescence based kinetic study for understanding the mechanism of surface complexation reaction.
v. Identifying two different species within a QDC at few particle level.
vi. Application of complexation strategy in generating white light emission and formulating broad-spectrum sun protection formula.

The present thesis contains seven chapters. Here are the glimpses of contents of each chapters.

Chapter 1 of the thesis is a brief introduction to the basics of Qdots and literature survey on various types of surface reactions of Qdots. The chapter is focused on the idea of interaction between ligands and dangling ions on the surface of Qdots.

Chapter 2 contains a discussion about the binding of 8-hydroxyquinoline (HQ) on the surface of the ZnS Qdot and probable coordination chemistry of the surface ZnQ_2 complex.

Chapter 3 describes the experimental results of an unprecedented reaction between surface Zn^{2+} and copper quinolato complex.

Chapter 4 is a description of mechanistic approach to study a complex transfer reaction from ZnO to ZnS Qdot driven by surface dangling anions.

Chapter 5 contains description of dual photoluminescence intermittency observed in a Quantum dot complex.

Chapter 6 describes application of surface complexation of Qdots. This chapter is divided into two parts. Part-A is a description of formation of white light emitting material by complexation on the surface of ZnO Qdot. Part-B contains preparation method of a broad spectrum sun protection formula (SPF) using herbal nanocomposite of ZnO Qdot.

Chapter 7, the last chapter of the thesis, is the summary of the work. It provides the overview of the thesis and future prospect of the works presented in the current thesis.

Statement

This thesis entitled **"Complexation on the Surface of Zinc Chalcogenide Quantum Dots: Binding, Kinetics and Application"** is a work of research and investigation carried out by me under the supervision of Dr. Arun Chattopadhyay, Professor, Department of Chemistry, Indian Institute of Technology Guwahati. This thesis has been submitted by me to the Department of Chemistry, Indian Institute of Technology Guwahati for the award of the degree of Doctor of Philosophy. I further declare that this work has not been submitted anywhere else for any degree, diploma, associateship or membership etc. of any Institute or University to the best of my knowledge.

_____

Shilaj Roy
Roll No. 126122025
Department of Chemistry
IIT Guwahati,
Guwahati-781039, Assam, India

Date:

Place: Guwahati, Assam

Certificate

It is certified that the thesis entitled **"Complexation on the Surface of Zinc Chalcogenide Quantum Dots: Binding, Kinetics and Application"** being submitted to the Indian Institute of Technology Guwahati by Shilaj Roy (Roll. No. 126122025) for the award of the degree of Doctor of Philosophy in Chemistry, is a bonafide record of research work carried out by him. The information and data reported by him are solely the results of his original findings. He has meticulously carried out the investigations and followed the guidelines of the laboratory. This work has not been submitted elsewhere for any degree or diploma.

_____

Prof. Arun Chattopadhyay
Thesis Supervisor
Professor,
Department of Chemistry,
IIT Guwahati,
Guwahati-781039, Assam, India.

Date:

Place: Guwahati, Assam

Dedicated to my

Grandparents, Parents, Wife

and

other Family Members

An offering to the Lord 'Bhairab'

Acknowledgements

It is my privilege to be a disciple of Prof. Arun Chattopadhyay, who has always inspired me to be an honest scientist with self-dignity and dynamism. The freedom of work, which he has provided me during my PhD days, has enormously helped me to build up self-confidence and to cultivate my scientific ideas. Definitely, I can never repay the debt to my master (guru); however, I pledge to keep his inspiration and scientific views alive in my mind in the course of my life.

I am grateful to my doctoral committee members for providing me with valuable suggestions and evaluating my thesis progress periodically.

I was very lucky to spend the period of two months under guidance of Prof Puspendu Kumar Das at IISc, Bangalore in 2013. His motivation to continue my career with science, has helped me lot to stimulate myself.

I am also thankful to Prof. Anumita Paul for her kind cooperation.

I cannot help but express my gratitude to my teachers at Paikar High School and Ramakrishna Mission Vidyamandira, who has really helped cherish my dreams.

I am thankful to my friends and labmates for their support and company. The sweet memories at IITG, especially in cricket field, has certainly refreshed my mind with fresh enthusiasm.

I am proud to be a part of IIT Guwahati community. The facility and assistance from Dept. of Chemistry, Centre for Nanotechnology, Central Instrument Facility, IIT Guwahati is really appreciable for carrying out my research work.

I do believe that no word in the lexicon is sufficient to define the sacrifice and support of my parents, my wife and my other family members. The spirit of their well wish always insists my endeavour to achieve the best. Without them, I might suffer from existential crisis.

I owe to my motherland, India, which has nurtured me with tolerance, has enlightened me with the spirituality and has endowed me with the truthfulness. I wish, I may devote myself to the science for the sake of my country.

Finally, I bow down to the almighty by uttering few lines of R N Tagore:

"That I want thee, only thee – let my heart repeat without end.
All desires that distract me, day and night, are false and empty to the core."

..... *Shilaj Roy*

Table of Contents

Chapter 1

Introduction

As the world realizes the potential of nanoscale particles, intense research is currently being carried out for their applications. Among the nanoparticles, quantum dot (Qdot) or semiconductor nanoparticle was introduced in the 1980s and then emerged as versatile material very soon. Qdots exhibited promising potential in wide range of application ranging from solar cell to water splitting, from light emitting device to bio-imaging, from biomedicine to catalysis and many more. Importantly, their unique optoelectronic properties have elevated Qdots as important materials among nanoparticles. Apart from this, the surface of Qdot has also contributed a lot in widening area of its application. Not only this, surface of Qdot has a great prospect ahead for exploring chemistry.

1.1 Quantum Dots.

1.1.1 History.

In the year 1981, Alexey Ekimov, discovered quantum dots (Qdots) in glass matrix.[1] Following this, Louis E. Brus has discovered colloidal semi-conductor nanocrystals in the year 1985.[2] But, the term 'Quantum Dot' was first coined by Mark Reed following his observation regarding discrete electronic states of Qdot.[3]

1.1.2 Definition.

Quantum Dot – otherwise known as semiconductor nanocrystal (NC) – is semiconductor nanoparticle (typical size: 1 – 10 nm) that exhibits quantum confinement effect in all three spatial dimensions.

1.1.3 Quantum Confinement.

Owing to very small size, the excited electron hole pair i.e., exciton of Qdot becomes confined in all three spatial dimensions, which can be described as excitonic confinement or quantum confinement.[3-6] As a result, energy states of Qdot becomes discretized when radius of a Qdot is less than or comparable to excitonic bohr radius (Figure 1.1).[3-4] Moreover, the extent of confinement depends on the size of Qdot, e.g. strong confinement occurs when radius of Qdot is less than excitonic bohr radius, while

weak confinement occurs when radius of Qdot is little higher that excitonic bohr radius.[4-9] Furthermore, band gap between conduction band and valence band is a function of size of Qdot, i.e., as size decreases band gap increases and vice versa.[3-7] Hence, quantum confinement stands responsible for unique optoelectronic behavior of Qdot that further depends on the energy of electronic states.[3-9]

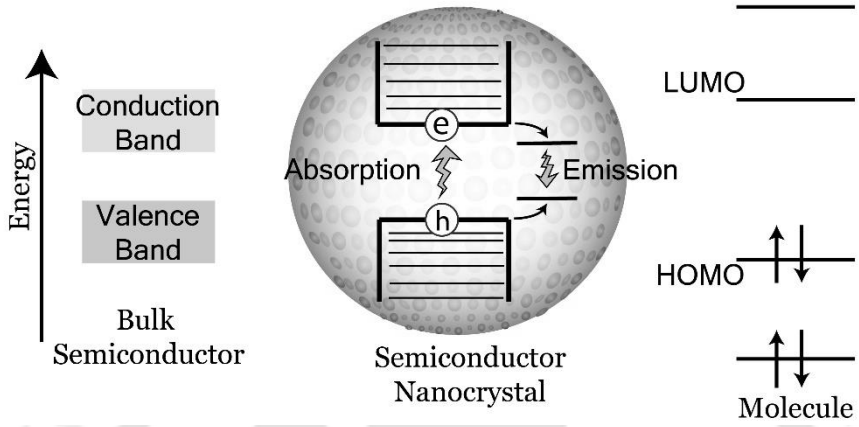

Figure 1.1. Schematic representation depicting the comparison of electronic structure and band gap energy among bulk semiconductor, semiconductor nanocrystals (i.e., quantum dots) and single molecule.[4]

1.1.4 Unique Optoelectronic properties.

Energy level of electronic states of semiconductor nanocrystal or Qdot lies in between bands and bonds – making it a unique material.[3-7] As mentioned earlier, band gap energy is dependent on size of Qdot, thus, absorption energy for generation of exciton (i.e., excited electron hole pair) would be much higher in case of Qdot compared to its bulk counterpart. [4-9] Hence, simple variation in size of Qdot results in change in absorption band edge. In addition, Qdots usually have photoluminescence property notwithstanding, non-fluorescent nature of bulk semiconductor. Moreover, in contrary to organic molecules, Qdot usually exhibits large Stokes shift – which may be attributed to the emission from surface defect states. [10-14] Briefly, surface states are generated by means of a few factors like lattice defects, impurity and this states are usually placed in between band edge and help relaxation of excited electron and hole.[10-14] Thus, significant Stokes shift occurs when radiative recombination takes place by transition from these surface states (Figure 1.1).[10-14]

1.1.5 Structure of Quantum Dot.

Quantum dot usually comprises of – (i) core consisting of crystalline inorganic lattice and (ii) surface ligand shell. For typical aqueous based synthesis, crystallinity of inorganic core apparently deviates from core to surface – as for example, the trend can be perceived as inorganic crystalline core shielded by a layer of co-ordination saturated distorted atoms followed by co-ordination unsaturated atoms at the surface.[15] On the other hand, the surface ligands are supposed to play important roles in saturating the surface atoms.[15-19] Thus, surface of a Qdot mainly contains peripheral inorganic ions – considered as a part of the lattice – and associated capping ligands.

1.2 Surface of Quantum Dots.

From the viewpoint of a chemist, the surface of a Qdot is of immense importance as it is the only interface to deal with various aspects of chemistry while keeping the core intact. In this regard, the surface plays a unique role in accomplishing various chemical reactions for making Qdot more amenable towards real-life applications.[14,17,20-21]

1.2.1 Surface Ions and their Importance.

Surface ions may be considered as the penultimate layer of a Qdot, being protected by surface ligands. Although being a part of lattice, the co-ordinations of the surface ions are not saturated and are called as dangling ions. In some cases, surface ions may not have balanced charge – which are then neutralized by surface ligands or ion pairs.[16,22-29] Hence, the nature of surface ions determines the nature of ligands to be attached on the surface for stabilization of the Qdot.[16,22-29] Importantly, surface defects are often considered as the origin of surface states – which are considered responsible for emission of Qdot.[10-14] In addition, surface ions are also a determinant of chemical nature of the Qdot.[14,16,19,21-23,30-32] For example, catalytic role, redox behavior and energy harvesting involving Qdots are critically dependent on surface ions and passivation of the surface.

1.2.2 Surface Ligand: Basic Idea.

Capping agents or surface ligands are the outer most part of a Qdot that help protect the inner lattice and determine the chemical reactivity of the Qdot to a significant extent. Surface ligands are often considered as functionalization unit – which help widening the application potential of a nanocrystal.[16,33-38]

According to covalent bond classification (CBC), surface ligands can be classified into three categories – namely, L, X and Z –type – based on number of electron

donating capability in neutral form (Figue 1.2).[22-26,39-40] L-type ligands are two electron donors and preferably bind with surface cations by forming dative bonds. While, X-type ligands are one electron donor and likely to form covalent bond primarily with surface cations. Whereas, Z-type ligands are zero electron donor or more precisely electron acceptor and possibly attach with surface anions through formation of dative bond. Thus, in neutral form L, X and Z-type ligands are, respectively, Lewis base (e.g. $MeNH_2$, PMe_3, TOPO, pyridine etc.), radical (e.g. Cl, Br, MeS, MeO, MeCOO, H, CH_3 etc.) and Lewis acid (e.g. BF_3, Me_3Al etc.) in nature.[22-26,39] Due to unambiguity and consistency, CBC method (considering two centred two electron covalent bond) is a well accepted method to describe bonding between capping ligand and surface ions of Qdot.[16,22,39-40]

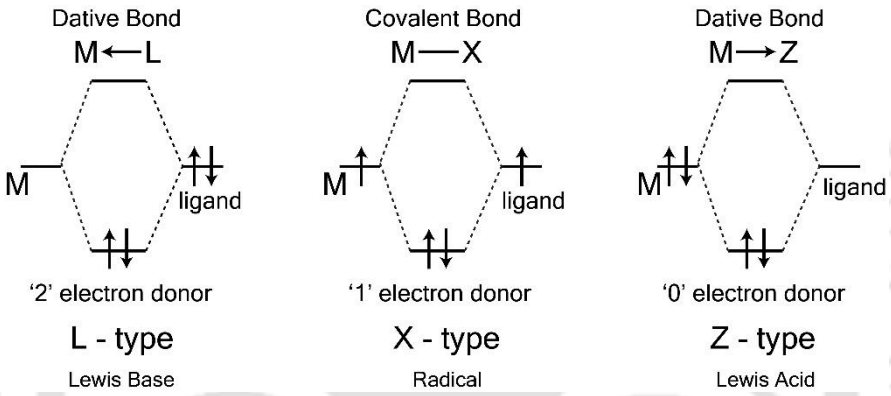

Figure 1.2. Classification of L, X and Z ligands based on covalent bond theory. [Adapted from *ref 40*, Copyright *2014, The American Chemical Society and Division of Chemical Education, Inc.*]

1.2.3 Ligand Surface Ion Interaction.

While surface ions primarily determine the chemical behavior of a Qdot – it is the surface ligand that dictates the ultimate applicability in terms of stability, conductivity, solubility and so on.[16,33-38] Thus, mode of attachment of the ligand on Qdot surface is the key to manipulate the properties of a Qdot for further applications. As surface consists of both the positively charged cations and negatively charged anions – surface ligands can bind through either cation or anion.[16,22-29] For simplicity, the surface of a nanocrystal (Qdot) as a whole can be readily compared to cluster of inorganic complexes within a single unit. Hence, surface ion - ligand interaction can be anticipated as complex formation phenomenon – that certainly follows the code of co-ordination chemistry. Co-ordination – or stoichiometry – on the surface is primarily controlled by lattice termination fashion and nature of capping ligand – maintaining charge

neutrality.[16,22-29] Being labile in nature, L-type ligands bind with surface cations and unable to form stable species. Usually, X-type ligand binds with surface cations and terminate the lattice in case of metal ion rich Qdot, although, binding with surface anion is also known, such as – adsorption of proton (H^+) through surface anion.[22-23,26-27] Whereas, Z-type ligand exclusively binds with surface anions (Figue 1.3). Interestingly, excess metal ions can reversibly bind (adsorb) with surface anions in the form of metal complexes as a Z-type ligand. Importantly, surface ligands are accountable for saturating surface co-ordination, forming stable bond and more importantly, passivating the mid gap surface states for better photoluminescence quantum yield (PLQY).

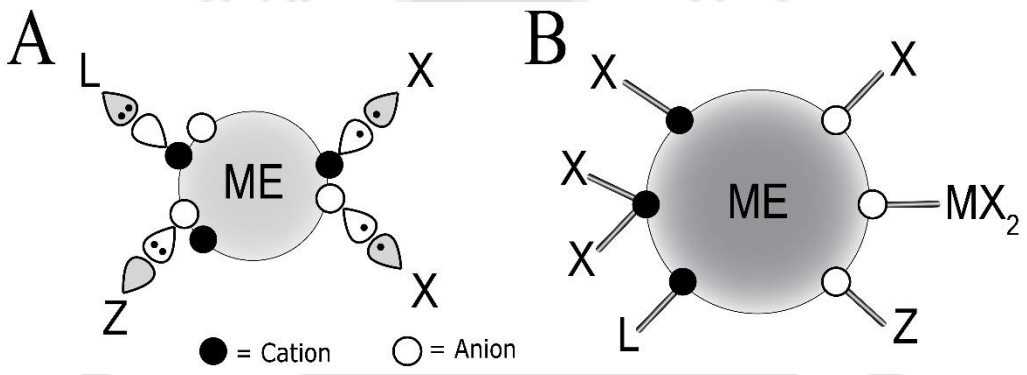

Figure 1.3. **(A)** Bonding with surface ions according to covalent bond classification and **(B)** different binding motifs of L, X and Z-type ligands on the surface of Qdot. [Adapted from *ref 22,* with permission from The Royal Society of Chemistry]

1.2.4 Importance of Surface Ligands.

Surface ligands coupled with surface ions are solely responsible for defining the quality of Qdot meant for end applications. Importantly, surface ligands critically affect some important aspects like – optical properties, catalytic properties, colloidal stability, surface passivation, energy of surface states, surface charge separation and so on.

1.2.4.1 Colloidal Stability and Dispersibility.

Application of colloidal Qdots depends on their dispersibility in polar or non-polar solvent. Layer of surface ligands – which is apparently exposed to the solvent medium as the outer-most part of a Qdot – readily interacts with solvent molecules; thus, determines the degree of colloidal stability and aggregation of Qdots in a particular solvent.[16,41] Hence, ligand with hydrophobic ending prefers non-polar solvents, whereas, hydrophilic ending prefers polar solvents. Moreover, little change in polarity of solvent may lead to flocculation of nanocrystals i.e., deterioration of colloidal stability. The

colloidal stability of nanocrystals can be explained using two different fundamental mechanisms – which are steric stabilization and electrostatic stabilization. Briefly, steric stabilization depends on the free energy of ligand-solvent mixing and ligand-ligand interaction. Whereas, electrostatic stabilization depends on adsorption of charged species for neutralization of excess surface charge and consequently stability of this oppositely charged counter-ions further depends on the dielectric constant of the solvent.[16,22-26]

1.2.4.2 Surface Ligand and Electronic Structure.

Surface states – originating from coordination unsaturated surface ions or any other surface defects – may be significantly affected by surface ligands. Frontier orbitals (i.e., HOMO and LUMO) of surface ligands can readily mix with mid gap surface states to produce new bonding and anti-bonding orbital and thus, can passivate the surface states (Figure 1.4A).[16,24] In addition, the dipole moment of the bond between ligand head and surface ion can affect the absolute electronic structure of a Qdot. For example, direction of dipole moment towards NC reduces the energy of all states, whereas dipole moment towards ligand head increases the energy of all states. (Figure 1.4B).[16,42-43]

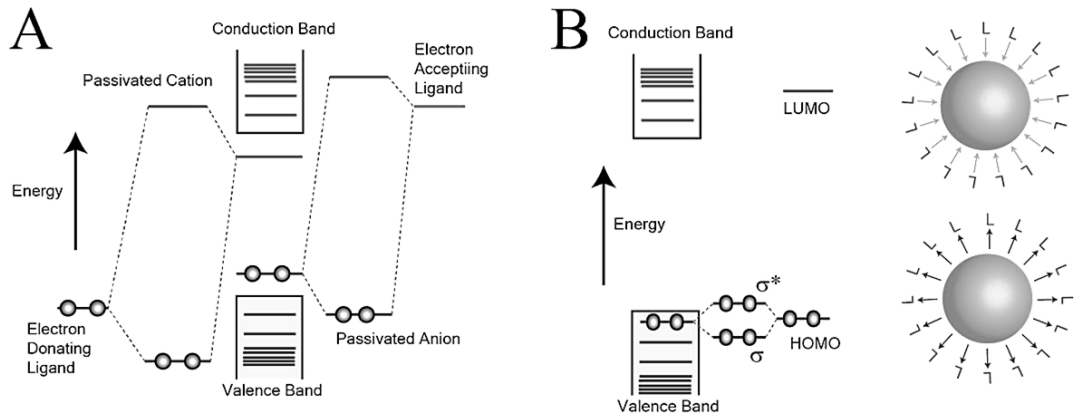

Figure 1.4. Dependence of **(A)** surface states and **(B)** absolute electronic structure of Qdot on surface ligands. [Reproduced from *ref 16*, Copyright 2016 *Springer Nature*]

1.2.4.3 Functionalization.

As mentioned earlier, surface ligands are the functionalization units and hold the key of all applications. The field of application drives the choice and design of surface ligands. For example, biological application demands water dispersible non-toxic Qdots, photovoltaic applications demand ligands those can conduct charge, LED application demands ligands capable of efficiently passivating the surface and so on. It is the surface

functionalization that makes almost all Qdot applicable for different purpose by manipulating the surface after synthesis.

1.3 Reactions on the Surface of Quantum Dots.

A few factors – such as quantum yield, surface reactivity, band gap energy, dispersibility – are the key determinants of quality and applicability of the Qdots.[16-17,20-21,30-32] In this aspect, surface passivation has turned out to be noteworthy in enhancing the quality of Qdots.[16-17,44] As the surface of Qdot extensively controls its physicochemical properties, surface modification appears to be very useful technique for manipulating the properties of Qdots for desired applications.[14,16,19-37,42-44] To achieve this, both the surface constituents – i.e., surface ions and surface ligands – can be manipulated by means of chemical reactions on the surface of Qdots. As for example, ions exchange, redox reactions, ligand exchange, functionalization of surface ligands, complex formation reaction are a few instances of chemical reactions involved for surface modification.[16,22-29,31-32,45-54]

1.3.1 Ion Exchange.

Manipulation of dangling surface ions of Qdot has turned out to be a convenient way for tuning the optoelectronic properties, especially, photoluminescence properties of Qdot.[31] Importantly, surface ions may be considered as important source of PL emission of Qdot by virtue of surface states – basically, originating form surface defects.[31]In this regard, engineering of surface ions provides the opportunity to have control over photoluminescence properties of Qdot. As for example, surface ion removal by cation exchange resin bead from the surface of Mn(II) doped ZnS Qdot results in initial increment in PL quantum yield followed by significant decrease in PLQY (Figure 1.5A).[31] Illustratively, the clusters of surface cations – probably responsible for quenching of surface state emission – are perhaps subjected to rupture followed by removal, which accounts for initial PLQY increment. In addition, further removal of surface ions leads to reducing the number of emitting surface states and consequently PLQY decreases.

1.3.2 Redox Reaction.

Transition metal ions – like Mn or Cu – having variable oxidation states may be doped in the lattice of host like ZnS or CdS Qdot and can affect the intrinsic physical and chemical properties of host lattice.[32,45] Interestingly, it is possible to tune PL emission of a Qdot by simply changing the oxidation states of the doped transition metal ions present

on the surface.[32,45] It is important to mention here that particular oxidation state of the transition metal ion (e.g. '+2' for Mn or '+1' for Cu) is responsible for emission that originates from atomic transition.[32,45] As for example, emission intensity of Mn(II) doped ZnS Qdot decreases while treating with oxidizing agent due to oxidation of surface Mn(II) ions to higher non-emissive oxidation state (Figure 1.5B).[32,45] Importantly, this redox active Qdot, more precisely the surface, helps detect oxidizing or reducing environment even in the biological system.[32]

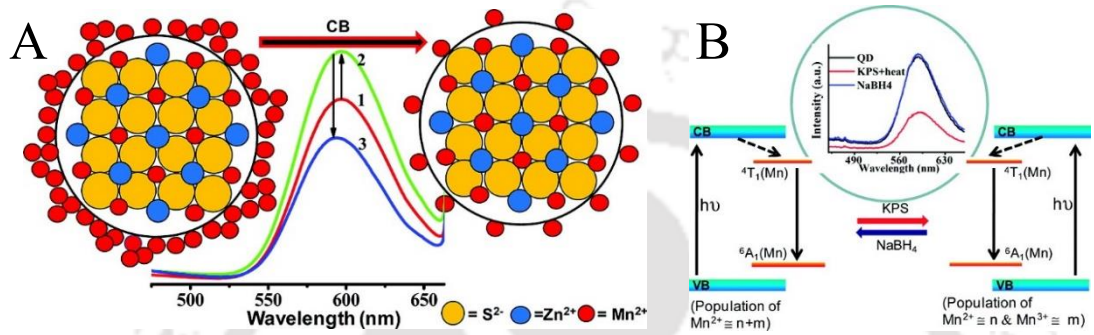

Figure 1.5. Schematic representation of **(A)** effect of cation exchange resin bead on the photoluminescence of Mn doped ZnS Qdots and **(B)** reversible tuning of photoluminescence of Mn doped ZnS Qdot usinf redox chemistry. [Reprinted from *ref 31 and 45*, Copyright *2012 The Americal Chemical Society*, Copyright *2011 The Americal Chemical Society*]

1.3.3 Ligand Exchange.

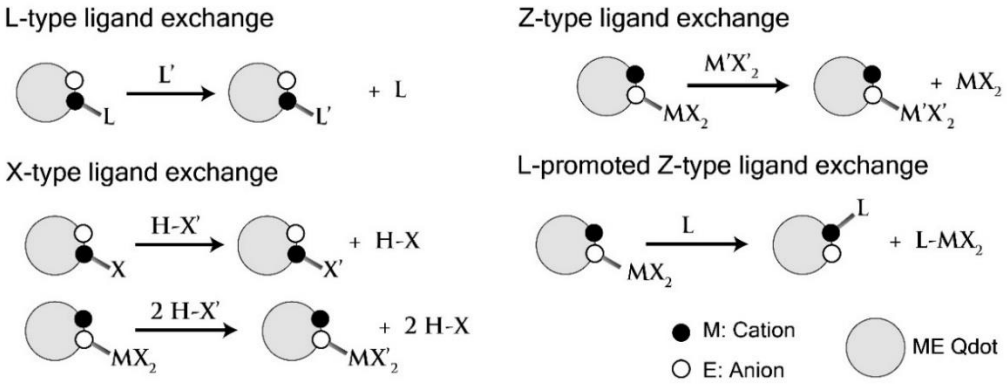

Figure 1.6. Schematic representation of possible different kind of ligand displacement reaction on the surface of Qdot. [Reproduced from ref 24, Copyright 2013, *The American Chemical Society*]

Importance of capping ligand in determining the physicochemical behavior as well as quality of Qdots is worth mentioning.[22-29] Hence, ligand exchange on the surface is deemed crucial for functionalization of Qdots meant for various applications.[17,22-29,42-

[44] Moreover, ligand exchange seems very useful in phase transfer, surface passivation, improvising PL emission, enhancing conductivity, functionalization of Qdots and so on.[16,17,42-45,55-58] A surface ligand can be replaced by another one depending on the relative stability of the surface ion-ligand complex. As per L, X, Z-type classification of ligands, ligand exchange can also be of different types, such as, X-type ligand transfer, L-type ligand transfer, Z-type ligand transfer, and L promoted Z-type ligand transfer (Figure 1.6).[22-26]

1.3.4 Complex Formation.

Apart from conventional interaction between ligand and surface ion, typical inorganic complex of chelating ligand can also be formed on the surface of a Qdot – forming quantum dot complex or QDC i.e., complex attached on the surface of Qdot.

1.4 Complexation Reaction on the Surface of Quantum Dots.

Until now, focus on the surface of a Qdot was primarily focused on improving the surface or functionalization for achieving the best performance from the Qdot itself. Beyond this, inorganic complexes, having application prospective, may gain better properties while attached on the surface of a Qdot for more precise applications. Therefore, it would be more useful to get dual character within a single QD where each component contributes to improve the properties of another.

1.4.1 Tuning Photoluminescence.

Formation of surface complex has find its utility in tuning photoluminescence of Qdot by virtue of formation of luminescence complex on the surface of Qdot – called as quantum dot complex (QDC). Upon complexation, intrinsic emission of Qdot usually suffers quenching as surface ions become involved in complexation – which are responsible for surface state emission as well. [46-54] In addition to emission from Qdot, new emission arises from luminescent complex(es) formed on the surface of Qdot. [46-51] Hence, it is possible to generate various colors from QDC by simply varying the amount of reactant ligand as relative emission intensity of Qdot and surface complex is solely dependent on the extent of surface complexation. For example, complexation using 8-hydroxyquinoline on the surface of Mn doped ZnS Qdot leads to formation of dual channel emission with excitation tunable chromaticity (Figure 1.7A).[46]

1.4.2 Dictating Colloidal Dispersibility.

As exposed part of capping ligand dictates the polar or non-polar nature of a Qdot, likewise, attached complex on the surface also determines behavior of quantum dot

complex, thus, it helps in the dispersibility of QDC in different solvent systems. As for example, oleate capped Zn doped CdS Qdot – upon complexation with 8-hydroxyquinoline – can be readily transferred from non-polar to polar medium by simply replacing the native oleate ligand by surface quinolato complex (Figure 1.7B).[47]

1.4.3 Improved Light Emitting Material.

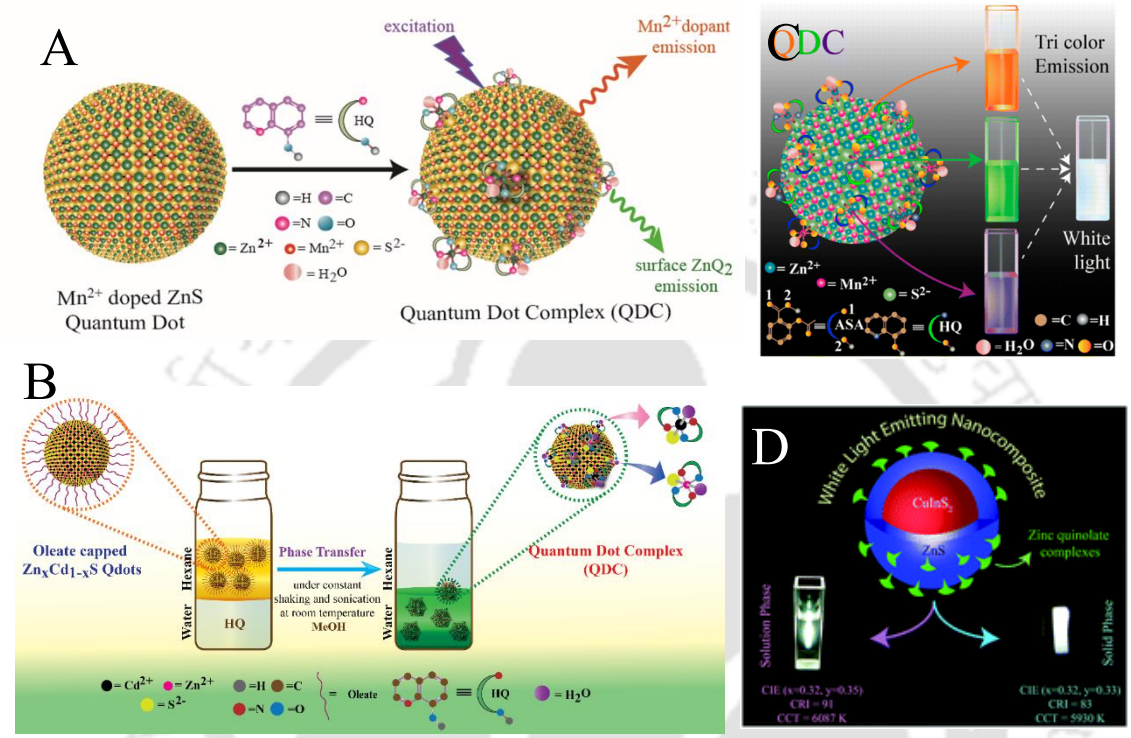

Figure 1.7. Schematic representation of **(A)** generation of dual channel emitting QDC upon reaction between 8-hydroxyquinoline and Mn doped ZnS Qdot, **(B)** complexation assited phase transfer of oleate capped Zn doped CdS Qdot from non-polar to polar solvent, **(C)** white light generation by dual complexation on the surface of Mn doped ZnS Qdot and **(D)** white light generation by means of reaction between $CuInS_2$@ZnS Qdot and 8-hydroxyquinoline. [Fig 1.7A reprinted from *ref 48*, Copyright 2014 *The American Chemical Society;* Fig 1.7B reprinted from *ref 47*, Copyright 2014 *The American Chemical Society;* Fig 1.7C reprinted from *ref 49*, Copyright 2015 *The American Chemical Society;* Figure 1.7D reprinted from *ref 51*, with permission from *The Royal Society of Chemistry*]

Complexes attached to the surface of Qdots usually gain higher stability, better QY than their counterparts i.e., simple inorganic complexes. This enhanced photo and thermal stability coupled with higher QY of surface complexes may be attributed to the higher structural rigidity while attached on the surface of Qdot probably through surface anions. [46,48-52] As for example, reaction between ZnS Qdot and 8-hydroxyquinoline results in the formation of quantum dot complex, i.e., zinc quinolato complex attached

on the surface of ZnS Qdot, which possesses better stability and higher QY and thus making it better LED material compared to simple zinc quinolato complex. [46]

In addition, using this strategy of surface complexation it is possible to achieve white light emission from Qdots. Briefly, emission from surface complexes coupled with emission from Qdot may produce white light – when the different emissive sources emit colors complementary to each other (Figure 1.7C-D). Notably, this strategy of white light emission from complexed Qdot or QDC seems superior compared to conventional white light generation by mixing different colors. In case of WLE QDC, white light usually obtained by means of synchronous multi-color emission from a single QDC having different emission sources (Figure 1.7C-D). [49-52]

It is very clear from the previous discussions that phenomenon of complexation on the surface of Qdot is a convenient tool for surface modification and possibly has a great prospect ahead in various applications. However, application of this concept in a well-defined manner is of utmost importance to achieve the best out of it. Hence, detailed study of surface complexation is required to understand the chemistry occurring on the surface of a Qdot. In this regard, time dependent photoluminescence study turns out to be a useful way to follow the kinetics of the surface reactions – which further helps decipher the mechanism of the surface reaction. Additionally, these studies might be useful to understand the structure, stability and reactivity of the surface of Qdots. Briefly, this thesis is focused on the physical insights of surface complexation reaction and relevant application of complexation strategy in white light emission and formulating superior sun protection formula.

1.5 Bibliography.

1. Ekimov, A. I.; Onushchenko A. A. Quantum size effect in three-dimensional microscopic semiconductor crystals. *JETP Lett* **1981** *34*, 345–349.
2. Brus, L. Electron-electron and electron-hole interactions in small semiconductor crystallites: the size dependence of the lowest excited electronic state. *J Chem Phys* **1984,** *80*, 4403–4409.
3. Reed, M.A.; Randall, J.N.; Aggarwal, R. J.; Matyi, R. J.; Moore, T, M.; Wetsel, A. E. Observation of discrete electronic states in a zero-dimensional semiconductor nanostructure. *Phys. Rev. Lett.* **1988**, *60*, 535–537.
4. Murphy, C. J.; Coffer, J. L. Quantum Dots: A Primer. *Applied Spectroscopy* **2002**, *56*, 16A-27A.
5. Kambhampati, P. Fundamentals of the Quantum Confinement Effect, Book chapter in *Handbook of Photoluminescent Semiconductor Materials – Taylor & Francis*, **2011**.
6. Alivisatos, A. P. Semiconductor Clusters, Nanocrystals, and Quantum Dots. *Science*, **1996**, *271*, 933–937.
7. Kippeny, T.; Swafford, L. A.; Rosenthal, S. J. Semiconductor nanocrystals: A Powerful Visual Aid for Introducing the Particle in a Box. *J. Chem. Ed.* **2002,** *79*, 1094-1100.
8. Rossetti, R.; Nakahara, S.; Brus, L. E. Quantum Size Effects in the Redox Potentials, Resonance Raman Spectra, and Electronic Spectra of CdS Crystallites in Aqueous Solutions. *J. Chem. Phys*. **1983**, *79*, 1086-1088.
9. Kambhampati, P. Unraveling the Structure and Dynamics of Excitons in Semiconductor Quantum Dots. *Acc. Chem. Res.* **2011**, *44*, 1– 13.
10. Efros, A. L.; Rosen, M.; Kuno, M.; Nirmal, M.; Norris, D. J.; Bawendi, M. Band-Edge Exciton in Quantum Dots of Semiconductors with a Degenerate Valence Band: Dark and Bright Exciton States. *Phys. Rev. B: Condens. Matter Mater. Phys*. **1996**, *54*, 4843−4856.
11. Beaulac, R.; Archer, P. I.; Liu, X. Y.; Lee, S.; Salley, G. M.; Dobrowolska, M.; Furdyna, J. K.; Gamelin, D. R. Spin-Polarizable Excitonic Luminescence in Colloidal Mn^{2+}-Doped CdSe Quantum Dots. *Nano Lett.* **2008**, *8*, 1197−1201.
12. Bloom, B.; Zhao, L.-B.; Wang, Y.; Waldeck, D.; Liu, R.; Zhang, P.; Beratan, D. Ligand-Induced Changes in the Characteristic Size- Dependent Electronic Energies of CdSe Nanocrystals. *J. Phys. Chem. C* **2013**, *117*, 22401−22411.
13. Kilina, S. V.; Tamukong, P. K.; Kilin, D. S. Surface Chemistry of Semiconducting Quantum Dots: Theoretical Perspectives. *Acc. Chem. Res.* **2016**, *49*, 2127−2135.
14. Jing, L.; Kershaw, S. V.; Li, Y.; Huang, X.; Li, Y.; Rogach, A. L.; Gao, M. Aqueous Based Semiconductor Nanocrystals. *Chem. Rev.* **2016**, *116*, 10623−10730.
15. Khalkhali, M.; Liu, Q.; Zeng, H.; Zhang, H. A size-dependent structural evolution of ZnS nanoparticles, *Scientific reports*, **2015**, *5*, 14267
16. Boles, M. A.; Ling, D.; Hyeon, T.; Talapin, D. V. The surface science of nanocrystals. *Nature Materials* **2016**, *15*, 141–153.
17. Teunis, M. B.; Liyanage, T.; Dolai, S.; Muhoberac, B. B.; Sardar, R.; Agarwal, M. Unraveling the Mechanism Underlying Surface Ligand Passivation of Colloidal Semiconductor Nanocrystals: A Route for Preparing Advanced Hybrid Nanomaterials. *Chem. Mater.* **2017**, *29*, 8838–8849.

18. Thanh, N.; Maclean, N.; Mahiddine, S. Mechanisms of Nucleation and Growth of Nanoparticles in Solution. *Chem. Rev.* **2014**, *114*, 7610−7630.
19. Weiss, E. A. Organic Molecules as Tools To Control the Growth, Surface Structure, and Redox Activity of Colloidal Quantum Dots. *Acc. Chem. Res*. **2013**, *46*, 2607−2615.
20. Talapin, D. V.; Lee, J. S.; Kovalenko, M. V.; Shevchenko, E. V. Prospects of Colloidal Nanocrystals for Electronic and Optoelectronic Applications. *Chem. Rev*. **2010**, *110*, 389–458.
21. Seker, F.; Meeker, K.; Kuech, T. F.; Ellis, A. B. Surface Chemistry of Prototypical Bulk II-VI and III-V Semiconductors and Implications for Chemical Sensing. *Chem. Rev.* **2000,** *100,* 2505-2536**.**
22. De Roo, J.; De Keukeleere, K.; Hens, Z.; Van Driessche, I. From ligands to binding motifs and beyond; the enhanced versatility of nanocrystal surfaces. *Dalton Trans.* **2016**, *45*, 13277-13283.
23. Owen, J. The coordination chemistry of nanocrystal surfaces. *Science* **2015**, *347*, 615-616.
24. Anderson, N. C.; Hendricks, M. P.; Choi, J. J.; Owen, J. S. Ligand Exchange and the Stoichiometry of Metal Chalcogenide Nanocrystals: Spectroscopic Observation of Facile Metal-Carboxylate Displacement and Binding. *J. Am. Chem. Soc.* **2013**, *135*, 18536–18548.
25. Hassinen, A.; Moreels, I.; Nolf, K. De; Smet, P. F.; Martins, J. C.; Hens, Z. Short-Chain Alcohols Strip X-Type Ligands and Quench the Luminescence of PbSe and CdSe Quantum Dots, Acetonitrile Does Not. *J. Am. Chem. Soc*. **2012**, *134*, 20705−20712.
26. Roo, J. D.; Justo, Y.; Keukeleere, K. D.; Broeck, F. V. D.; Martins, J. C.; Driessche, I. V.; Hens, Z. Carboxylic-Acid-Passivated Metal Oxide Nanocrystals: Ligand Exchange Characteristics of a New Binding Motif. *Angew. Chem. Int. Ed*. **2015**, *54*, 6488–6491.
27. Fritzinger, B.; Capek, R. K.; Lambert, K.; Martins, J. C.; Hens, Z. Utilizing Self-Exchange To Address the Binding of Carboxylic Acid Ligands to CdSe Quantum Dots. *J. Am. Chem. Soc*. **2010**, *132*, 10195−10201.
28. Owen, J. S.; Park, J.; Trudeau, P.-E.; Alivisatos, A. P. Reaction Chemistry and Ligand Exchange at Cadmium−Selenide Nanocrystal Surfaces. *J. Am. Chem. Soc*. **2008**, *130*, 12279−12281.
29. Moreels, I.; Fritzinger, B.; Martins, J. C.; Hens, Z. Surface Chemistry of Colloidal PbSe Nanocrystals. *J. Am. Chem. Soc*. **2008**, *130*, 15081−15086.
30. Hines, D. A.; Kamat, P. V. Recent Advances in Quantum Dot Surface Chemistry. *ACS Appl. Mater. Interfaces* **2014**, *6*, 3041−3057.
31. Begum, R.; Bhandari, S.; Chattopadhyay, A. Surface Ion Engineering of Mn^{2+}-Doped ZnS Quantum Dots Using Ion-Exchange Resins. *Langmuir* **2012**, *28*, 9722- 9728.
32. Begum, R.; Chattopadhyay, A. Redox-Tuned Three-Color Emission in Double (Mn and Cu) Doped Zinc Sulfide Quantum Dots. *J. Phys. Chem. Lett*. **2014**, *5*, 126-130.
33. Dubertret, B. *et al. In vivo* Imaging of Quantum Dots Encapsulated in Phospholipid Micelles. *Science* **2002**, *298*, 1759–1762.
34. Osaki, F.; Kanamori, T.; Sando, S.; Sera, T.; Aoyama, Y. A quantum dot conjugated sugar ball and its cellular uptake. On the size effects of endocytosis in the subviral region. *J. Am. Chem. Soc.* **2004**, *126*, 6520–6521.

35. Gao, X.; Cui, Y.; Levenson, R. M.; Chung, L. W. K.; Nie, S. *In vivo* cancer targeting and imaging with semiconductor quantum dots. *Nature Biotechnol.* **2004**, *22***,** 969–976.
36. Kovalenko, M. V.; Bodnarchuk, M. I.; Zaumseil, J.; Lee, J.-S.; Talapin, D. V. Expanding the chemical versatility of colloidal nanocrystals capped with molecular metal chalcogenide ligands. *J. Am. Chem. Soc.* **2010**, *132*, 10085–10092.
37. Dirin, D. N. et al. Lead halide perovskites and other metal halide complexes as inorganic capping ligands for colloidal nanocrystals. *J. Am. Chem. Soc*. **2014**, *136*, 6550–6553.
38. Zhang, H.; Jang, J.; Liu, W.; Talapin, D. V. Colloidal nanocrystals with inorganic halide, pseudohalide, and halometallate ligands. *ACS Nano* **2014**, *8*, 7359–7369.
39. Green, M. L. H. A new approach to the formal classification of covalent compounds of the elements. *Journal of Organometallic Chemistry* **1995**, *500*, 127-148.
40. Green, M. L. H.; Parkin, G. Application of the covalent bond classification method for the teaching of inorganic chemistry. *J. Chem. Educ.* **2014**, *91*, 807–816.
41. Israelachvili, J. N. Intermolecular and Surface Forces (Elsevier, 2011).
42. Brown, P. R. et al. Energy level modification in lead sulfide quantum dot thin films through ligand exchange. *ACS Nano* **2014**, *8*, 5863–5872.
43. Frederick, M. T.; Weiss, E. A. Relaxation of exciton confinement in CdSe quantum dots by modification with a conjugated dithiocarbamate ligand. *ACS Nano* **2010**, *4*, 3195–3200.
44. Cao1, Y.; Stavrinadis1, A.; Lasanta1, T.; So1, D.; Konstantatos, G. The Role of Surface Passivation for Efficient and Photostable PbS Quantum Dot Solar Cells. *Nat Energy* **2016**, *1*, 16035.
45. Begum, R.; Chattopadhyay, A. In Situ Reversible Tuning of Photoluminescence of Mn^{2+} Doped ZnS Quantum Dots by Redox Chemistry. *Langmuir* **2011**, *27*, 6433– 6439.
46. Bhandari, S.; Roy, S.; Chattopadhyay, A. Enhanced photoluminescence and thermal stability of zinc quinolate following complexation on the surface of quantum dots. *RSC Adv*. **2014**, *4*, 24217-24221.
47. Bhandari, S.; Roy, S.; Pramanik, S.; Chattopadhyay, A. Surface Complexation Reaction for Phase Transfer of Hydrophobic Quantum Dot from Nonpolar to Polar Medium. *Langmuir* **2014**, *30*, 10760–10765.
48. Bhandari, S.; Roy, S.; Pramanik, S.; Chattopadhyay, A. Double Channel Emission from a Redox Active Single Component Quantum Dot Complex. *Langmuir* **2015**, *31*, 551- 561.
49. Pramanik, S.; Bhandari, S.; Roy, S.; Chattopadhyay, A. Synchronous Tricolor Emission-Based White Light from Quantum Dot Complex. *J. Phys. Chem. Lett*. **2015**, *6*, 1270- 1274.
50. Bhandari, S.; Pramanik, S.; Khandelia, R.; Chattopadhyay, A. Gold Nanocluster and Quantum Dot Complex in Protein for Biofriendly White-Light-Emitting Material. *ACS Appl. Mater. Interfaces* **2016**, *8*, 1600−1605.
51. Pramanik, S.; Bhandari, S.; Chattopadhyay, A. Zinc quinolate complex decorated CuInS2/ZnS core/shell quantum dots for white light emission. *J. Mater. Chem. C*, **2017**, *5*, 7291-7296.

52. Pramanik, S.; Bhandari, S.; Pan, U. N.; Roy, S.; Chattopadhyay, A. A White Light-Emitting Quantum Dot Complex for Single Particle Level Interaction with Dopamine Leading to Changes in Color and Blinking Profile. *Small* **2018**, *14*, 1800323.
53. Bhandari, S.; Khandelia, R.; Pan, U. N.; Chattopadhyay, A. Surface Complexation-Based Biocompatible Magnetofluorescent Nanoprobe for Targeted Cellular Imaging. *ACS Appl. Mater. Interfaces* **2015**, *7*, 17552–17557.
54. Pan, U. N.; Sanpui, P.; Paul, A.; Chattopadhyay, A. Surface-Complexed Zinc Ferrite Magnetofluorescent Nanoparticles for Killing Cancer Cells and Single-Particle-Level Cellular Imaging. *ACS Appl. Nano Mater.* **2018**, *1*, 2496–2502.
55. Tang, J.; Kemp, K. W.; Hoogland, S.; Jeong, K. S.; Liu, H.; Levina, L.; Furukawa, M.; Wang, X.; Debnath, R.; Cha, D.; Chou, K.W.; Fischer, A.; Amassian, A.; Asbury, J. B.; Sargent, E. H. Colloidal-quantum-dot photovoltaics using atomic-ligand passivation. *Nature Materials* **2011**, *10*, 765-771.
56. Krause, M. M.; Jethi, L.; Mack, T. G.; Kambhampati, P. Ligand Surface Chemistry Dictates Light Emission from Nanocrystals. *J. Phys. Chem. Lett.* **2015**, *6*, 4292–4296.
57. Quilettes, D. W.; Koch, S.; Burke, S.; Paranji, R. K.; Shropshire, A. J.; Ziffer, M. E.; Ginger, D. S. Photoluminescence Lifetimes Exceeding 8 μs and Quantum Yields Exceeding 30% in Hybrid Perovskite Thin Films by Ligand Passivation. *ACS Energy Lett*. **2016**, *1*, 438–444.
58. Dai, M. Q.; Yung, L. Y. L. Ethylenediamine-Assisted Ligand Exchange and Phase Transfer of Oleophilic Quantum Dots: Stripping of Original Ligands and Preservation of Photoluminescence. *Chem. Mater.* **2013**, *25*, 2193–2201.

Chapter 2

The Nature of Binding of Quinolate Complex on the Surface of ZnS Quantum Dot

It is reported that the Z-type, compared to X-type, binding was favored when 8-hydroxyquinoline (HQ) reacted with a presynthesized ZnS quantum dot (Qdot) to form surface zinc quinolinate complex, with preferable stoichiometry of 1:2 (surface Zn^{2+}:HQ). Importantly, the higher solubility in polar solvents and high desorption coefficient (following Langmuir binding isotherm) of HQ treated ZnS Qdot in DMSO solvent, compared to methanol, clearly indicated the favorable Z-type binding of HQ and thus to the formation of surface octahedral ZnQ_2 complex. Furthermore, the characteristics peaks in the ^1H- nuclear magnetic resonance (NMR) spectrum of the desorbed species and the ligand density calculation of the surface complex (formed out of the reaction between HQ and ZnS Qdot) supported octahedral ZnQ_2 complex formation. Interestingly, the presence of dangling sulphide and the loss of planarity of ZnQ_2 complex on the surface of ZnS Qdots (in turn gaining structural rigidity) may be the reasons for the Z-type binding of HQ. The specific binding might have favored superior optical properties and thermal stability of the surface ZnQ_2 complex compared to the complex as such. The results can be considered important towards understanding the coordination chemistry of inorganic complex on the surface of Qdot and thus for their application potentials.

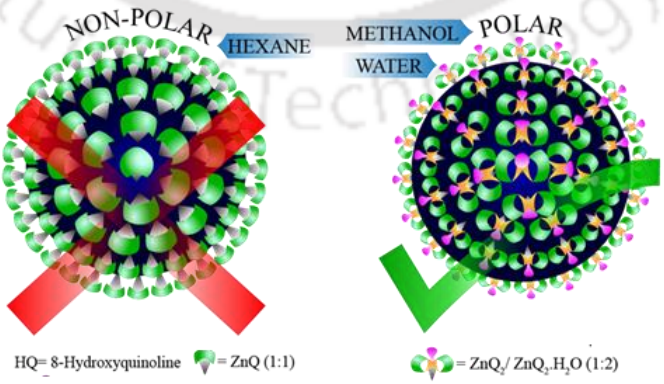

*Manuscript to be submitted

2.1 Experimental Section

2.1.1 Materials.

Zinc acetate dihydrate (Merck), sodium sulfide (Na_2S, Merck), ethylene diamine (Merck), methanol (MeOH, Merck), 8-amino quinoline (Alfa Aesar), 2-chloroacetyl chloride (Spectrochem), potassium carbonate (K_2CO_3, Merck), potassium iodide (KI, Sigma Aldrch), trimethylamine (Et_3N, Sigma Aldrich), N-dimethyl formamide (DMF, Sigma Aldrich), chloroform ($CHCl_3$, Merck), hexane (Merck), ethyl acetate (Merck) were purchased and used directly without any purification. Milli-Q grade water used for ZnS synthesis.

2.1.2 Synthesis of ZnS Qdots.

Synthesis of ethylene diamine capped ZnS quantum dots (Qdots) has been performed by following a reported protocol.[1-2] Firstly, 0.25 millimoles of zinc acetate dehydrate ($Zn(OAc)_2.2H_2O$) was added to a 100 mL round bottom flask containing 50 mL water – placed on a hotplate under stirring condition. Next, 500 mL of ethylene diamine and 0.25 millimoles of sodium sulphide were sequentially added to that solution. Then, the solution was refluxed for 2 h and the temperature was fixed at 393 K. After that, the opaque milky white dispersion was observed and it was centrifuged at 25,000 rpm for 15 min. To remove all the unreacted salts, the obtained pellet was redispersed in water and centrifuged. The washing process was repeated twice and then it was washed by methanol. Finally, the so-obtained pellet was redispersed in 200 mL of methanol and used for carrying out the experiments. As-synthesized ZnS Qdot was characterized with TEM analysis, UV-vis and PL emission spectra (Figure A.2.1, Appendix).

2.1.3 Synthesis of L1.

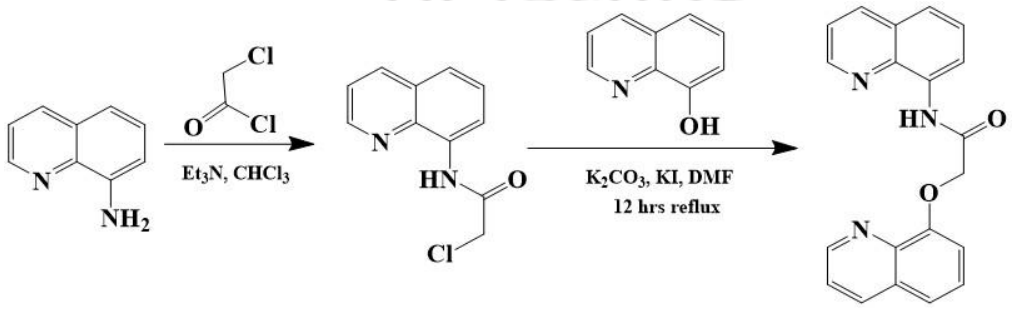

Scheme 2.1. Schematic representation of synthetic route of Ligand-1.

Ligand L1 was synthesized by the two step reaction as per reported protocol.[3] Firstly, 2-chloro-N-(quinol-8-yl)-acetamide was synthesized out of reaction between 2-chloroacetyl chloride and 8-aminoquinoline. Shortly afterwards, 20 mmol of 8-aminoquinoline and ~ 3.0 mL of Et_3N were dissolved in 15 mL of chloroform in a round bottom flask – being kept at low temperature (i.e., < 277 K) under vigorous stirring. After that, ~ 5.5 mL of 2-chloroacetyl chloride (dissolved in 10 mL of chloroform) solution was poured dropwise to that solution for ~ 30 min. Then, the reaction mixture was kept at the same condition for 3 h. Then, the solvent mixture was evaporated by reducing the pressure using vacuum pump to obtain white solid, which was purified by column chromatography (silica gel) using solvent dichloromethane as eluent to obtain pure chloro-N-(quinol-8-yl)-acetamide.

Now, chloro-N-(quinol-8-yl)-acetamide was used to prepare N-(Quinolin-8-yl)-2-(quinolin-8-yloxy)acetamide (L1). For this purpose, 5.0 mmol of chloro-N-(quinol-8-yl)-acetamide, 5.0 mmol of 8-hydroxyquinoline (8-HQ), ~ 900 mg of K_2CO_3 and ~ 10 mg of KI were mixed to ~ 30.0 mL of DMF in a round bottom flask. Following this, the reaction mixture was stirred vigorously under refluxing condition for ~ 12 h. After completion of the reaction, the reaction mixture was cooled down to room temperature. The solvent was removed by evaporation under reduced pressure. Pure N-(quinolin-8-yl)-2-(quinolin-8-yloxy)acetamide (L1) was collected after performing silica gel column chromatographic separation. The as synthesized L1 was characterized by using NMR and mass spectrometry (Figure A.2.2 – A2.3, Appendix).

2.1.4 Calculation of Concentration of ZnS Qdot.

From particle size distribution of TEM analyses, the average diameter of a ZnS Qdot was calculated to be, d = 3.37 nm (Figure A.2.1B); So, the average radius, r = 1.685 nm.

Therefore, considering each single Qdot to be a sphere, the volume of a ZnS Qdot sphere was calculated to be, $V = 20.04 \times 10^3$ Å^3 and surface area of a ZnS Qdot was found to be, $A = 3.57 \times 10^3$ Å^2.

Now, from diffraction pattern it was found that lattice structure of ZnS Qdots was wurtzite.[1] As single ZnS wurtzite cell has volume of, a = 79.11 Å^3, a single ZnS Qdot consist of 253 (i.e., V/a) unit of wurtzite cell. It is important to mention here that a unit ZnS wurtzite cell consists of '2' Zn^{2+} ion. So, number of Zn^{2+} ion per single ZnS Qdot = 506.

The total concentration of Zn^{2+} in as prepared Qdot dispersion was = 0.9 mM.

Hence, concentration of ZnS Qdot is as prepared Qdot dispersion = 1.77 μM.

2.1.5 Calculation of Ligand Density.

For calculating the ligand density of 8-HQ on the surface of ZnS Qdot, excess amount of 8-HQ (which was determined from titration of 8-HQ and ZnS Qdot) was reacted with ZnS in methanolic medium (i.e., methanol-d_4) and amount of unreacted 8-HQ was determined by using NMR spectroscopy (Figure A.2.4 – A2.5, Appendix). Consequently, attached amount of HQ was calculated. For this experiment, we have taken 1/8 part of ZnS Qdot (i.e., 25 mL as synthesized ZnS Qdot) from one-time synthesis (5 mM 50 mL scale synthesis – as described before) and centrifuged to get the pellet. The solvent was evaporated and it was redispersed in 500 μL of methanol-d_4. Then, 30 μL of 50 mM of HQ (in methanol-d_4) was added to that Qdot dispersion. Additionally, 10 μL DMSO solution (5 μL in 500 μL methanol d_4) was added to that dispersion as internal standard. NMR spectra of the mixture was recorded and absolute integration values for each peak corresponding to 8-HQ and DMSO were calculated (Figure A.2.4, Appendix). NMR spectrum of 500 μL of 1 mM HQ in methanol-d_4 (added with same amount of internal standard) was used as reference standard (Figure A.2.5, Appendix).

So, amount of free ligand (HQ) in the sample = 3.52 μL of 50 mM HQ.

Now, the attached ligand is = 26.48 μL of 50 mM HQ.

So, ligand per Qdot = 29.4≈30.

So, 1:2 complex (ZnQ2) per Qdot = 15.

So, footprint area per complex = 2.38 nm^2 and footprint per ligand = 1.19 nm^2.

2.1.6 Instruments.

(i) 600 MHz nuclear magnetic resonance (NMR) spectrometer (Bruker) (ii) Agilent Accurate Mass (LC/MS Q-TOF 6520) spectrometer (iii) Perkin Elmer LAMBDA 750 UV/Vis/NIR spectrophotometer and (iv) HORIBA Jobin Yvon FluoroMax-4 spectrofluorimeter, (v) JEOL JEM-2100 transmission electron microscope (maximum accelerating voltage 200 kV), (vi) Perkin-Elmer (Model: Spectrum Two) FTIR spectrophotometer, were used.

2.2 Results and Discussion

2.2.1 Formation and Characterization of QDC out of Reaction between HQ and ZnS Qdot.

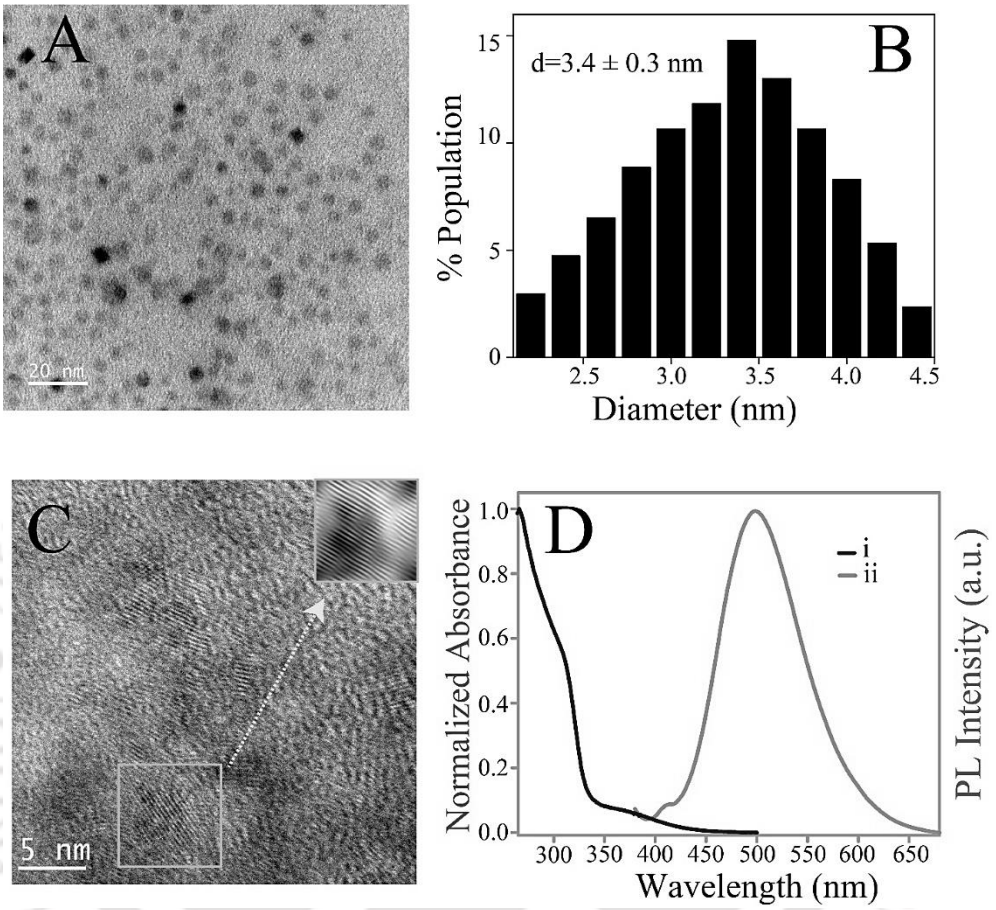

Figure 2.1. (A) Transmission electron microscopic (TEM) image (scale bar- 10 nm) and **(B)** corresponding particle size distribution, **(C)** high resolution TEM image (scale bar - 5 nm) and corresponding inverse fast Fourier transform (IFFT) image (inset) and **(D)** UV-vis and emission spectra (λ_{ex}-365 nm) of QDC (in DMSO).

The ethanolic dispersion of as synthesized ZnS Qdots showed an absorption edge at 320 nm and a broad emission centered at 440 nm, which is typical of emission from surface trap states [2] (Figure A.2.1D – A2.1E, Appendix). The treatment of HQ to the ZnS Qdots resulted in the formation of new luminescent nanocomposite, the absorption spectrum of which consisted of two peaks at 320 nm (due to ZnS Qdots) and 365 nm (appeared due to the formation of surface Zn-quinolate complex).[1-2] In the emission spectrum the peak due to the Qdot disappeared and a new peak at 500 nm appeared (Figure 2.1D). Additionally, QDC exhibited an excitation peak at 365 nm when probed with emission maximum at 500 nm while only ZnS Qdots showed excitation peak at 320

nm upon probing through emission maximum at 440 nm (Figure A.2.6, Appendix). There was no significant change in terms of the size and structure (i.e., lattice fringe) of ZnS Qdots [1] in the QDC as observed in the TEM (and corresponding particle size distribution), high resolution TEM (and IFFT) (Figure 2.1C). Importantly, the presence of the characteristics peaks in the FTIR spectrum of the functional group of the zinc quinolate complex [4] in the QDC also supported its formation (Figure A.2.7 and Table A.2.1, Appendix).

Our earlier observations suggested that when HQ reacted with ZnS Qdots formation of product with properties akin to ZnQ_2 complex on the surface of the Qdots was favored. This was further supported by reaction of ZnQ_2 with ZnS Qdots, leading to product with similar properties. In addition, it was observed that thermal stability and photo–stability of ZnQ_2 complex was enhanced when attached to the surface of the Qdots. The results also indicated important roles of surface sulphide ions and Zn^{2+} ions in the stability of the complex and reactivity of the Qdots.These bring us to the question on the nature of the surface species and their properties in a dispersion medium.

2.2.2 Interpretation of Nature of Binding of Surface Zinc Quinolato Complex

2.2.2.1 Dispersibility and Stability of QDC.

An important first test of the nature of the species present on the surface of the Qdots could be the ability to disperse in a liquid medium. This will not only depend on the nature of ligand attached to the surface but the fashion of the attachment. According to Green's classification, bidentate chelating ligand HQ has two parts – one is pyridyl (i.e., L-type) and other one is phenolic (i.e., X-type).[5-6] Consequently, two possible fashions can be anticipated for binding of HQ to the surface of ZnS Qdot. These are: (i) 1:1 binding - where one HQ moiety binds with a surface Zn^{2+} ion like X-type binding, which can be visualized as cation capping and (ii) 1:2 binding – where two HQ moieties bind with Zn^{2+} to form ZnQ_2 complex, which would be attached to ZnS surface through dangling sulfide – and that can be visualized as anion capping. In this regard, ability to disperse and corresponding stability (as measured through the luminescence at 500 nm; Figure 2.2A) of the dispersion of QDC (HQ treated ZnS Qdot) in different solvents (namely (i) MeOH, (ii) MeOH-H_2O, (iii) DMSO, (iv) H_2O and (v) hexane) were tested.

Among the five solvent systems used, DMSO and MeOH-water polar solvent systems provided better dispersibility and stability of QDC in the dispersion phase. This was

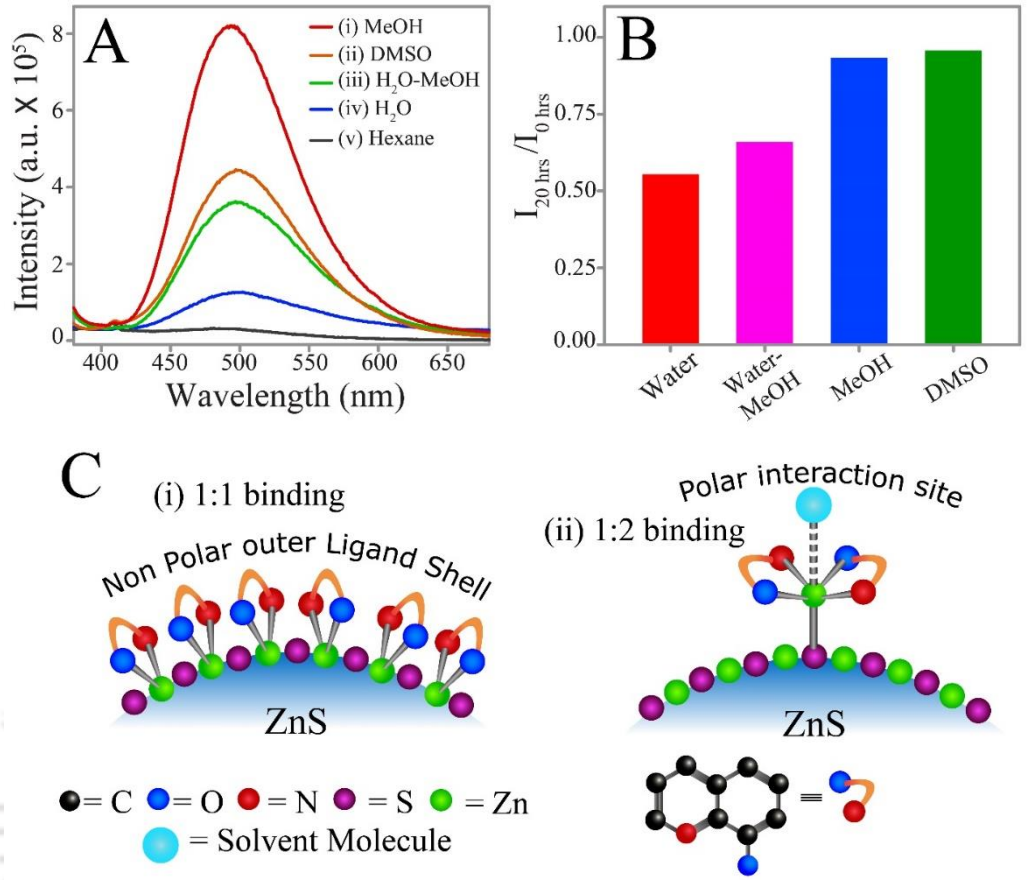

Figure 2.2. (A) Emission spectra (λ_{ex}-365 nm) and **(B)** bar diagram of the ratio of luminescence (in terms of intensity at 500 nm) recorded at time interval of 20 and 0 h of the QDC (i.e., HQ added ZnS Qdots) in solvents: (i) DMSO (ii) MeOH (iii) MeOH-H_2O (iv) H_2O and (v) Hexane. **(C)** Schematic illustration of (i) 1:1 and (ii) 1:2 binding modes of HQ to the surface Zn^{2+} of ZnS Qdot.

measured through the luminescence intensity of the QDC. The bar diagram of the ratio of luminescence intensity at 500 nm at time intervals of 20 h to 0 h of the QDC in different solvents are shown in Figure 2.2B**.** The results indicated that among the solvent medium of (i) DMSO, (ii) MeOH, (iii) MeOH-H_2O or (iv) H_2O, stability of QDC was better in aprotic polar solvents (like DMSO and MeOH; Figure 2.2B). It is to be mentioned here that QDC was not dispersible in nonpolar solvent like hexane. Thus, if 1:1 binding mode (X type) of HQ favored over 1:2 (Z type), then the outer surface of the QDC might have consisted of exposed aromatic rings of HQ (as visualized in Figure 2.2C). This would have rendered the QDC dispersible in nonpolar solvent (like hexane: since as such HQ is highly soluble in hexane medium). The observed dispersibility in polar solvents (like

DMSO and MeOH-H_2O: since octahedral or distorted octahedral ZnQ_2 is highly soluble in the mentioned polar solvents) of QDC pointed towards the Z type (1:2) binding of HQ to the surface of ZnS Qdot. This may also indicate the binding of ZnQ_2 complex to the Qdot via dangling sulphide bond as a fifth coordination (as visualized in Figure 2.2C(ii)). The sixth coordination of the complex might have been occupied by the solvent molecule [7] and thus accounted for the dispersibility as well as stability of QDC in a particular solvent. The results supported the affinity of the surface bound complex for polar solvents, as like the case of ordinary ZnQ_2. This is further supported from our earlier results of complexation assisted phase transfer of hydrophobic Qdots from nonpolar to polar medium. [8]

2.2.2.2 Solvent Dependent Adsorption of HQ on the Surface of ZnS Qdot.

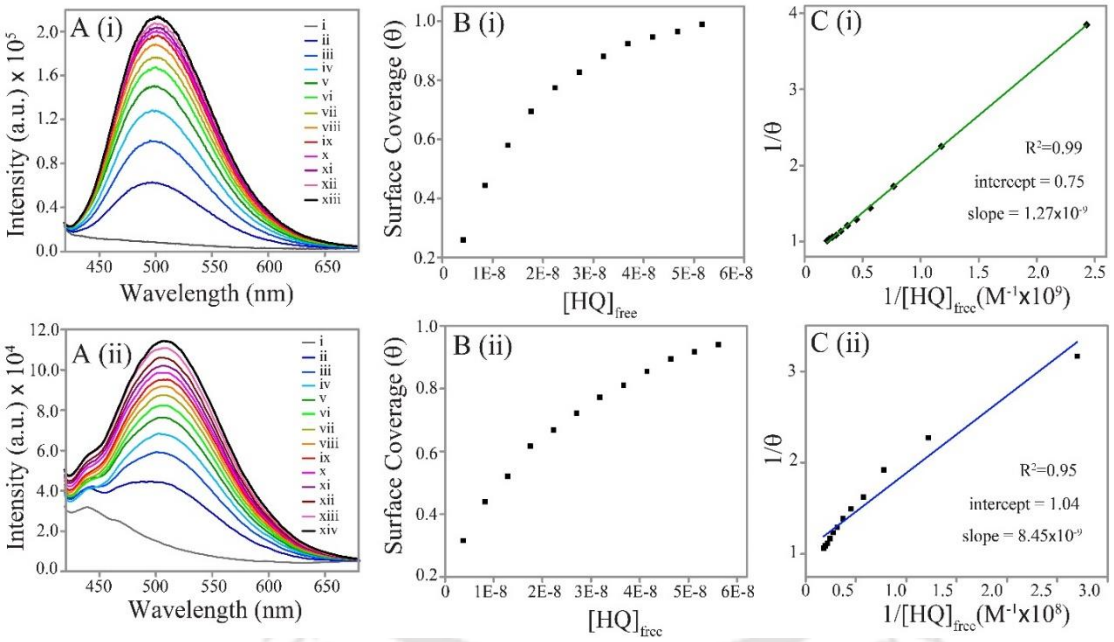

Figure 2.3. (A) Emission spectra (λ_{ex}-365 nm) of the different amount of HQ added ZnS Qdots (with absorbance $\leq$ 0.1 at 320 nm) recorded using (i) MeOH and (ii) DMSO as solvents respectively. **(B)** Plot of emission intensity (at 500 nm) vs concentration of HQ and corresponding **(C)** Langmuir binding isotherm with a linear fitting in (i) MeOH and (ii) DMSO solvents, respectively.

Next, we investigated the binding of ligand (HQ) on the surface of Qdot based on monitoring of the evolution of PL emission intensity (at 500 nm) upon addition of HQ to the dispersion of ZnS Qdot in two different solvent systems (DMSO and MeOH). Further, based on earlier observations,[1-2, 9-10] we made the following assumptions in this

regard - (i) PL emission intensity originating from the ZnS Qdot and HQ reaction mixture is directly proportional to the concentration of surface Zn-quinolate complex; (ii) at its low concentration, ligand(HQ) completely binds to the surface of ZnS Qdot; (iii) surface coverage could be considered to be '1' when ZnS Qdot was treated with high amount of HQ. Using PL spectroscopy, we monitored the reaction between HQ and ZnS Qdots in both the MeOH and DMSO media (Figure 2.3A). It was observed that the HQ attachment on the surface of ZnS Qdot followed Langmuir type binding in both the solvent systems (Figure 2.3B-C). It can be speculated that HQ adsorption on the surface of ZnS Qdot follows reaction with surface Zn^{2+} ions in order to form Zn-quinolate complex (either 1:1 or 1:2). Interestingly, value of adsorption constant (K) obtained from methanolic dispersion was found to be higher than that of the adsorption constant obtained from DMSO solvent (i.e., $K_{DMSO} < K_{MeOH}$). This can be explained on the basis of the adsorption equilibrium that persists between adsorbed species on the surface of ZnS Qdot species and free desorbed present in the medium. The equilibrium is highly affected by solubility of the desorbed species, as the extent of desorption increases as solubility of the desorbed species increases. It is to be mentioned here that ZnQ_2 is highly soluble in DMSO as compared to MeOH while HQ is soluble in both the solvents. So, it is desorption of ZnQ_2 – more precisely solubility of the same in a particular solvent – that determines the value of adsorption constant (K). The above can be better explained by a relevant reaction model as discussed in the subsequent section.

2.2.2.3 Modelling the Adsorption Phenomenon.

The reaction can be visualized as two-step process –

(i) Adsorption of HQ followed by complexation on the surface of ZnS Qdot (X-type ligand bonding with surface cation):

$$Surface - Zn^{2+} + 2HQ \underset{k_d}{\overset{k_a}{\rightleftharpoons}} surface - ZnQ_2$$

(ii) Adsorption equilibrium between adsorbed complex and desorbed complex (Z-type ligand binding):

$$Surface - ZnQ_2 \underset{k_d'}{\overset{k_a'}{\rightleftharpoons}} Desorbed - ZnQ_2$$

Now, HQ is attached on the surface the Qdot via the formation luminescent ZnQ_2 complex. Thus, surface coverage of Qdot can be expressed as a function of PL intensity – which is as follows; $\theta = \frac{I}{I_{max}}$

Where θ= average surface coverage; I_{max} = maximum fluorescent intensity which was determined using highly concentrated HQ.

Now, considering the two step reaction the surface equilibrium can be expressed as –

$$k_a(1-\theta)[HQ] + k_a'(1-\theta)[ZnQ_2] = k_d\theta + k_d'\theta$$

As, free ZnQ_2 is the intermediate species and HQ is added to the mixture externally, so, we have [HQ]>>[ZnQ_2]. Thus the equation can be written as –

$$k_a(1-\theta)[HQ] = (k_d + k_d')\theta$$

$$\theta = \frac{K_{ca}[HQ]}{K_{ca}[HQ]+1}, where, K_{ca} = \frac{k_a}{k_d + k_d'}$$

We term the new constant 'K_{ca}' as complexation adsorption constant. 'k_a/k_d' is similar to surface complexation constant. Thus 'K_{ca}' herein represents adsorption constant (K). Importantly, 'K_{ca}' takes care of complexation assisted adsorption of HQ as well as solubility driven desorption of ZnQ_2 – occurring in parallel on the surface. Due to higher solubility of ZnQ_2 of in DMSO than in MeOH, the extent of desorption would be higher in case of DMSO. As a result, desorption coefficient of ZnQ_2 in DMSO would be much higher than that of MeOH, [$(k_d')_{DMSO}$ >> $(k_d')_{MeOH}$] – which would result in the lower value of 'K_{ca}' in DMSO than in MeOH. The above model projects the ZnQ_2 in the binding and thus supports Z type (1:2) binding of HQ to the surface of the ZnS Qdot. However, this requires further experimental substantiation.

2.2.2.4 Identification of Desorbed Species from the Surface of QDC.

That the desorption of zinc-quinolato complex from the surface of QDC in DMSO took place was substantiated by using NMR spectroscopic analysis. The supernatant obtained – following centrifugation of QDC dispersion in DMSO-d_6 – was used for ^{1}H NMR analyses. Notably, when complexation reaction of HQ with Zn^{2+} ions in a liquid medium (DMSO) was carried out, the shift in the characteristic peaks of HQ was observed (Figure 2.4). For example, the characteristic peak of HQ at 7.1 ppm (which was assigned to proton number 6) was shifted to 6.88 ppm following complexation with Zn^{2+} ions (i.e., the formation of normal ZnQ_2 complex; Figure 2.4). Interestingly, the supernatant of the

HQ treated ZnS Qdot (QDC) exhibited characteristics peaks at 6.88 (for the proton number 6 of HQ) – which is akin to that of ZnQ_2 complex (Figure 2.4). This clearly indicated the presence of ZnQ_2 complex in the supernatant of the HQ treated ZnS Qdot (QDC). Besides, the additional peaks present in the NMR spectrum of supernatant of HQ treated ZnS Qdot may be attributed to the presence of HQ and impurity in the supernatant solution. The detailed spectral analyses have been produced in the appendix (Figure A.2.8-A.2.10, Appendix). Thus, the results indicated zinc-quinolato complex as the desorbed species, which might have been attached to the surface reversibly as a consequence of adsorption equilibrium. Thus, the structure of the surface zinc quinolate complex (i.e. the desorbed species of the HQ treated ZnS Qdots) can be anticipated as octahedral or distorted octahedral ZnQ_2 with one axial position occupied by the dangling sulphide bond (which helps in the stabilization and attachment of the complex on the surface of ZnS Qdot) and the other axial position occupied by one solvent molecule (here DMSO; which defines the higher solubility of the Qdot in the polar solvents).

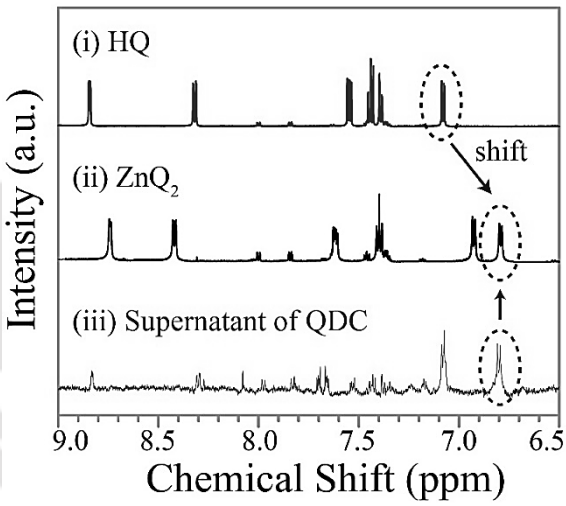

Figure 2.4. ^{1}H nuclear magnetic resonance (NMR) spectra of (i) only HQ (in d6-DMSO), (ii) only ZnQ_2 (in d_6-DMSO) and (iii) supernatant of HQ treated ZnS Qdots (obtained following centrifugation of the as-synthesized product and redispersion in DMSO-d6). The peaks representing aromatic ^{1}H of the spectra (δ = 6.5 – 9 ppm) are highlighted by dotted ellipses.

2.2.2.5 Solid State Emission of QDC & Evidence of Attachment of L1 on the Surface of ZnS Qdot.

It is to be mentioned here that the emission maximum (at 500 nm –with an excitation wavelength of 365 nm) of the QDC was similar to that of ZnQ_2 complex in solid form (Figure 2.5A). The electronic transition from the electron rich phenoxide ring (HOMO; highest occupied molecular orbital) to the electron deficient pyridyl ring

(LUMO; lowest occupied molecular orbital) may account for the origin of the luminescence of the QDC. [11] Additionally, when a modified ligand of HQ (L1) – with the ability to form distorted pentagonal luminescent crystal with normal Zn^{2+} ions - was used for complexation on the surface of ZnS Qdots, the newly form QDC showed a similar emission in the solid form (i.e., at 500 nm – with an excitation wavelength of 365 nm) (Figure 2.5B). The results also indicated that when HQ reacted with ZnS Qdot, the formation of 1:2 binding mode (Z type: ZnQ_2 complex with octahedral/distorted octahedral structure) was preferred over 1:1 binding mode. Thus the dangling sulphide accounted for the stabilization of the ZnQ_2 complex on the surface of ZnS Qdots (following replacement of the existing (as-synthesized) stabilizer, if any) and thus to the structural rigidity and loss of planarity of the ZnQ_2 complex – which may be the reason behind the superior optical properties and extraordinary stability of QDC in comparison to the ordinary octahedral trans planar $ZnQ_2.(solvent)_2$ complex.

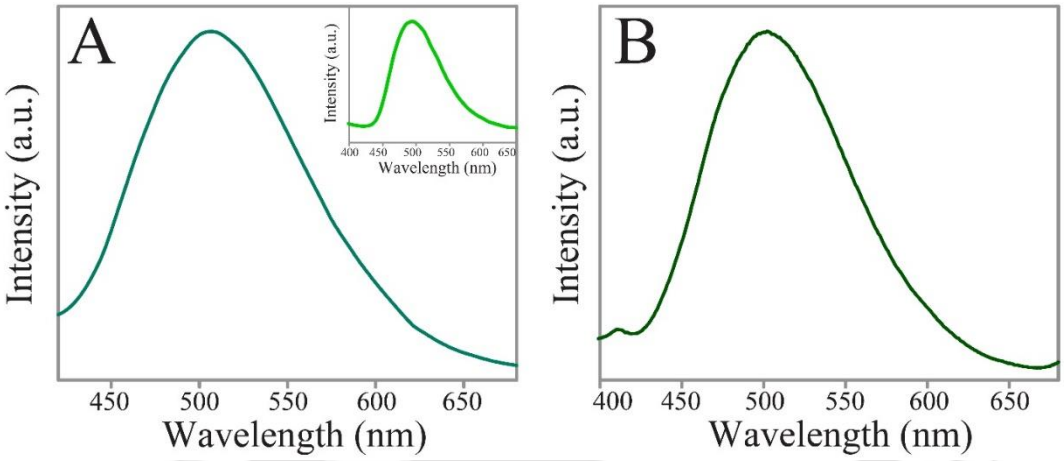

Figure 2.5. (A) Emission spectra (λ_{ex}-365 nm) of QDC and (inset) only ZnQ_2 in their solid phases. **(B)** Emission spectra (λ_{ex}-365 nm) of L1 treated ZnS Qdots (solid) obtained following centrifugation.

2.2.2.6 Calculation of Ligand Density of the Surface of QDC.

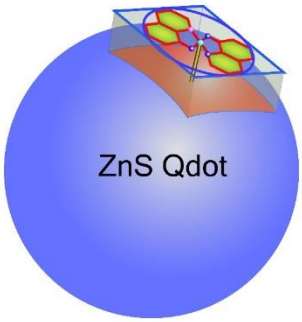

Scheme 2.2. Schematic representation of the projection of zinc quinolato complex on the surface of ZnS Qdot

Furthermore, the ligand density of HQ on the surface of Qdot was determined to support the presence of the octahedral ZnQ_2 complex on the surface of ZnS Qdot or the Z type binding of HQ to the surface of ZnS Qdot. This was achieved from the results obtained from (i) NMR spectroscopy – which was used to quantify the ligand (HQ), (ii) transmission electron microscopy (TEM) – which was used for determination of the size of the Qdot and (iii) atomic absorption spectroscopy (AAS) – which was used to obtain total concentration of Zn^{2+} ions present in the dispersion of QDC. [12-13] The details of calculation have been described in the experimental section. Notably, the ligand density on the surface of ZnS was calculated to be ~0.84 nm^{-2} (0.42 nm^{-2} for 1:2 complex). From reported crystal structure of $ZnQ_2.2H_2O$, the ligand density of HQ on the ZnS surface was found to be 1.18 nm^{-2} (0.56 nm^{-2} for ZnQ_2 complex) (considering close packing of ZnQ_2 on the surface of Qdot). The closeness of the ligand density value as obtained from the experimental results and calculation (which is pictorially shown in the scheme 2.2) clearly supported the presence of octahedral ZnQ_2 complex (1:2; Z type binding) – attached via dangling sulphide coordination - on the surface of ZnS Qdot.

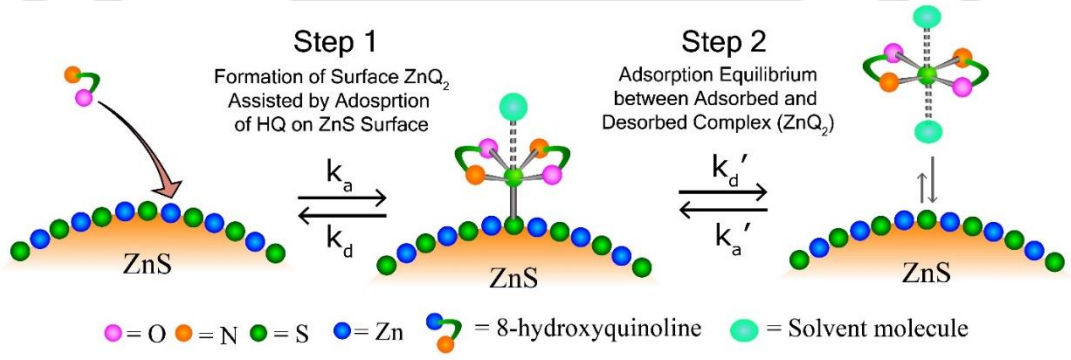

Scheme 2.3. Schematic representation of the binding mode of HQ to ZnS Qdot leading to the formation of of QDC.

Therefore, Z type binding mode of HQ preferred over X type binding mode when HQ reacted with ZnS to form QDC and accordingly QDC has octahedral ZnQ_2 complex – with dangling sulphide in the fifth coordination and the solvent molecule (which was used during synthesis of QDC) in the sixth coordination (as is visualize in the Scheme 2.3). Hence, two parallel chemical events are taking place while HQ is attached on the surface of ZnS Qdots. Initially, HQ forms complex with Zn^{2+} ions originating from Qdot surface, then, the complex gets attached on the surface through dangling sulphide ion. So, the phenomenon of complexation on the surface is controlled by two parameters –

i.e. complexation constant of the ligand with the metal ion and adsorption constant of the complex on the surface of Qdot.

2.3 Conclusions

In summary, the presented results indicated that complexation reaction between ZnS Qdot and HQ lead to the formation of ZnQ_2 on the surface of the Qdot. The dispersibility of the product QDC in polar solvent, solvent-dependent Langmuir model based binding and density of ligand (otherwise termed as surface coverage) clearly supported the preferable formation of zinc quinolate complex, with stoichiometry of surface Zn^{2+}: HQ – 1:2 (thus to the Z-type binding of HQ) on the surface of ZnS Qdot. Additionally, ^{1}H-NMR signals of the desorbed species, which was similar to that of bare octahedral ZnQ_2 complex, clearly supported the aforesaid conclusion. Remarkably, the dangling sulphide accounted for the formation of surface octahedral ZnQ_2 complex and its stability and loss of planarity (in turn gaining structural rigidity) and thus to the superior optical features, in comparison to ordinary ZnQ_2.This may provide a new idea in unfolding the ligand binding chemistry on the surface of Qdot. The products so obtained may find use in light emitting devices, healthcare, energy and in addressing environmental issues. Future work will focus on unravelling the nature of binding of different types of chelating ligands on the surface of various quantum dots and effort will be on generalization of the concept. It would be of immense urge to understand the chemistry behind the preferable Z-type binding. Future work will focus on unravelling the nature of binding of different types of chelating ligands on the surface of various quantum dots and effort will be on generalization of the concept. It would be of immense urge to understand the chemistry behind the preferable Z-type binding.

2.4 Bibliography.

1. Roy, S.; Bhandari, S.; Chattopadhyay, A. Quantum Dot Surface Mediated Unprecedented Reaction of Zn^{2+} and Copper Quinolate Complex. *J. Phys. Chem. C* **2015**, *119*, 21191–21197.
2. Roy, S.; Manna, M.; Chattopadhyay, A. Complex Transfer Reaction from ZnO to ZnS Quantum Dots Driven by Surface Anions. *J. Phys. Chem. C* **2018**, *122*, 9939-9946.
3. Zhou, X.; Li, P.; Shi, Z.; Tang, X.; Chen, C.; Liu, W. A Highly Selective Fluorescent Sensor for Distinguishing Cadmium from Zinc Ions Based on a Quinoline Platform**.** *Inorg. Chem.* **2012**, *51*, 9226-9231.
4. Bhandari, S.; Roy, S.; Chattopadhyay, A. Enhanced Photoluminescence and Thermal Stability of Zinc Quinolate Following Complexation on the Surface of Quantum Dots. *RSC Adv.* **2014**, *4*, 24217-24221.
5. Green, M. L. H. A new approach to the formal classification of covalent compounds of the elements. *Journal of Organometallic Chemistry* **1995**, *500*, 127-148.
6. Owen, J. The coordination chemistry of nanocrystal surfaces. *Science* **2015**, *347*, 615-616.
7. Grice, K. A.; Griffin, G. B.; Cao, P. S.; Saucedo, C.; Niyazi, A. H.; Aldakheel, F. A.; Sterbinsky, G. E.; LeSuer, R. J. Elucidating the Solution-Phase Structure and Behavior of 8-Hydroxyquinoline Zinc in DMSO. *J. Phys. Chem. A* **2018**, *122*, 2906-2914.
8. Bhandari, S.; Roy, S.; Pramanik, S.; Chattopadhyay, A. Surface Complexation Reaction for Phase Transfer of Hydrophobic Quantum Dot from Nonpolar to Polar Medium. *Langmuir* **2014**, *30*, 10760–10765.
9. Koole, R.; Schapotschnikow, P.; Donegá, C. M.; Vlug, T. J. H.; Meijerink, A. Time-Dependent Photoluminescence Spectroscopy as a Tool to Measure the Ligand Exchange Kinetics on a Quantum Dot Surface. *ACS Nano* **2008**, *2*, 1703−1714.
10. Bullen, C.; Mulvaney, P. The Effects of Chemisorption on the Luminescence of CdSe Quantum Dots. *Langmuir* **2006,** *22*, 3007–3013.
11. Hopkins, T. A.; Meerholz, K.; Shaheen, S.; Anderson, M. L.; Schmidt, A.; Kippelen, B.; Padias, A. B.; Hall, H. K.; Peyghambarian, N.; Armstrong, N. R. Substituted Aluminum and Zinc Quinolates with Blue-Shifted Absorbance/Luminescence Bands: Synthesis and Spectroscopic, Photoluminescence, and Electroluminescence Characterization. *Chem. Mater.* **1996**, *8*, 344– 351.
12. Hinterwirth, H.; Kappel, S.; Waitz, T.; Prohaska, T.; Lindner, W.; Lämmerhofer, M. Quantifying Thiol Ligand Density of Self-Assembled Monolayers on Gold Nanoparticles by Inductively Coupled Plasma–Mass Spectrometry. *ACS Nano* **2013**, *7*, 1129– 1136.
13. Leatherdale, C. A.; Woo, W. K.; Mikulec, F. V.; Bawendi, M. G. On the Absorption Cross Section of CdSe Nanocrystal Quantum Dots. *J. Phys. Chem. B* **2002,** *106*, 7619-7622.

Chapter 3

Quantum Dot Surface Mediated Unprecedented Reaction of Zn^{2+} and Copper Quinolate Complex

This chapter is a report of the reaction between Zn^{2+} ions, being present on the surface of ZnS quantum dot (Qdot), and copper(II)-bis(8-hydroxyquinoline) (copper quinolate; CuQ_2) complex, leading to the formation of luminescent ZnQ_2 on the surface. This is contrary to the reactivity of copper complex based on Irving-William series in the liquid medium and thus indicating catalytic role of the Qdot surface. The rate of the reaction was observed to be first order with respect to the concentrations of both the reactants, with activation energy measured to be 74.3 kJ mol^{-1}. Further, the reaction of the Zn^{2+} ions on the Qdot was observed to be fastest with HQ, slower with MnQ_2 and slowest with CuQ_2, all leading to the formation of ZnQ_2 on the surface of the Qdot. The enhanced stability of the product complex on the surface, in the presence of dangling sulphide ions, indicated a new type of chemical reaction deserving special attention.

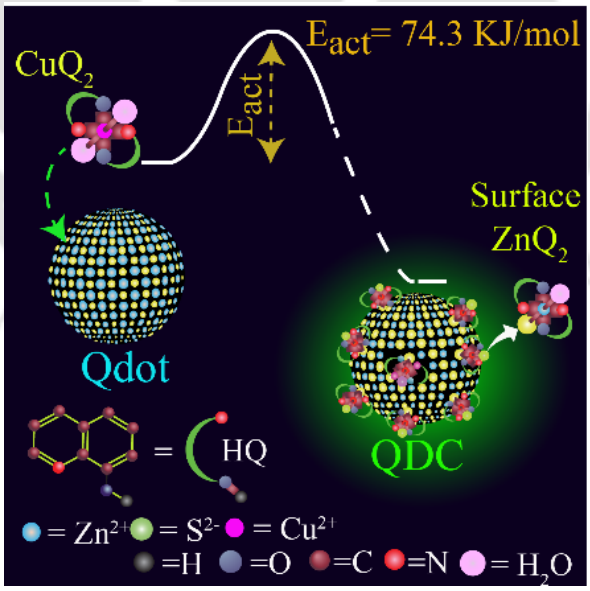

*[Roy et al. *J. Phys. Chem. C*, **2015**, *119*, 21191–21197.] - Reproduced with permission from The American Chemical Society.

3.1 Experimental.

3.1.1 Materials.

Zinc acetate dihydrate (Merck), ethylene diamine (en, Merck), 8-hydroxyquinoline (HQ, Merck), sodium sulphide (58%, Merck), copper (II) acetate monohydrate (Merck), manganese acetate tetra hydrate (99%, Merck), quinine sulphate (Sigma Aldrich) and ethanol (Merck) were purchased and used without further purification. Mili-Q grade water was used for the synthesis and in other experiments.

3.1.2 Synthesis of ethylene diamine capped ZnS Qdots.

The ZnS Qdots were synthesized following precipitation method using ethylene diamine (en) as the capping ligand. Briefly, 500.0 μL of ethylene diamine (en) was poured into a round bottom flask containing 50.0 mL of Mili-Q water. To that solution, 0.25 millimoles of zinc acetate dihydrate ($Zn(OAc)_2.2H_2O$) and 0.25 millimoles of sodium sulphide (Na_2S) were sequentially added and the resulting mixture was allowed to stir for 1 h at 100-120 $^{\circ}C$ temperature under reflux condition. The resulting colloidal dispersion was centrifuged at 25,000 rpm speed for 10 min. The obtained pellet was washed repeatedly with water and then was redispersed into same amount of solvent and the cycle was repeated for another two times. Finally, the pellet was dispersed into 100.0 mL ethanol and was used for further experiments.

3.1.3 Preparation of CuQ_2 complex.

The complex of $CuQ_2.2H_2O$ was synthesized following very simple method. Briefly, 10.0 mL ethanolic solution of 20.0 mM of HQ was added drop-wise to 10.0 mL aqueous solution of 10.0 mM copper acetate and was kept under sonication for 30 min. After sonication, the reaction mixture was filtered using Whatman filter paper. The filtrate was then thoroughly washed with water and hexane, respectively, in order to remove the unreacted salts. The obtained precipitate was then dried at room temperature. Further, the precipitate was crystallized by dissolving into a minimum amount of ethanol. Finally, the crystals were collected and purified followed by washing with water and hexane. The purified crystals were further used for experiments. The x-ray diffraction pattern, thermo-gravimetric analysis (TGA), Fourier transform infrared (FTIR) and UV-Vis spectroscopy were used to characterize the $CuQ_2.2H_2O$ complex (Figure A.3.1, Appendix). Similarly, $MnQ_2.2H_2O$ complex was synthesized using manganese acetate tetrahydrate (99%,

Merck) instead of copper acetate and following the same procedure of the synthesis of $CuQ_2.2H_2O$ complex.

3.1.4 Synthesis of Qdot complex (QDC).

To a 2.0 mL ethanolic dispersion of as prepared Qdots, 40.0 μL of 0.1 mM CuQ2 (in ethanol) was added and kept at room temperature for 20 min. Then the resulting mixture was centrifuged at a speed of 25000 rpm for 10 min. The so-obtained pellet was redispersed into the same amount of Mili-Q water. The resulting dispersion was characterized by using UV-Vis analysis, photoluminescence (PL), zeta potential measurement, atomic absorption spectroscopy (AAS), transmission electron microscopy (TEM), while the solid form of the dispersion (following centrifugation) was used for Fourier transform infrared (FTIR) spectroscopy and X-ray diffraction (XRD) analysis.

3.1.5 Effect of different concentration of Zn2+ ions (added as salt) on the luminescence of CuQ_2 in absence and presence of S^{2-} ions.

(i) To a solution containing 10.0 μL of 0.1 mM CuQ_2 and 3.0 mL ethanol, 2.4 μL of 2.5 mM zinc acetate (in ethanol) was added and the PL was measured. Next, the PL of the same resulting mixture was recorded after 12 h. To that resulting mixture, 2.4 μL of 2.5 mM sodium sulphide (in ethanol) was added and the PL was recorded just after the addition and after 12 h of sodium sulphide addition.

(ii) To a solution of 10.0 μL 0.1 mM CuQ_2 and 2.59 mL ethanol, 200.0 μL 2.5 mM of zinc acetate (in ethanol) was added and the PL was measured. To that resulting mixture, 200.0 μL of 2.5 mM sodium sulphide (in ethanol) was added and the PL was recorded.

(iii) On the other hand, to a solution of 10.0 μL 0.1 mM CuQ_2 (in ethanol) and 2.59 mL ethanol, 200.0 μL of 2.5 mM sodium sulphide (in ethanol) were added and the PL was monitored. To that, 200.0 μL 2.5 mM of zinc acetate (in ethanol) and the PL was measured. The excitation wavelength used to monitor the PL was 361 nm.

3.1.6 Effect of Zn^{2+} (added as salt) on the luminescence of ZnQ_2 in absence and presence of S^{2-} ions.

To a solution containing 10.0 μL of 0.1 mM ZnQ_2 and 2.59 mL ethanol, 200.0 μL of 2.5 mM sodium sulphide (in ethanol) was added and the PL was measured. To that resulting mixture, 200.0 μL of 2.5 mM zinc acetate (in ethanol) was added and the PL was recorded.

3.1.7 Study of kinetics of the formation of QDC following complexation between en-capped ZnS quantum dots and $CuQ_2.2H_2O$.

In order to calculate the order of the reaction and the rate of the formation of QDC, with respect to both the reactants (CuQ_2 and Qdot), the time-dependent change in area under the emission curve was measured, by varying the concentration of one reactant (at five different concentrations), while the concentration of other was kept fixed (refer to appendix). This was done at five different temperatures.

3.1.7.1 Calculation of order of reaction for the formation of QDC with respect to CuQ_2 and Qdot.

2.0 μL, 4.0 μL, 6.0 μL, 8.0 μL and 10.0 μL of 0.1 mM CuQ_2 (in ethanol) were separately added to solutions containing each of 2.8 mL ethanol and 200.0 μL of as-prepared Qdots (with absorbance of 0.106 at 317 nm) in a cuvette set at a particular temperature (T = 20 °C). Further details of the solutions are tabulated in the appendix, Table A.3.5. Then the time-dependent changes in emission intensity (at 361 nm excitation) were monitored for each set of the resulting solution until the maximum emission intensity was reached. On the other hand, for five different amounts of as-prepared Qdot dispersion (50.0 μL, 100.0 μL, 150.0 μL, 200.0 μL and 250.0 μL of Qdot dispersion), 10.0 μL of 0.1 mM CuQ_2 (in ethanol) was added to each of them and finally the total volume of the resulting mixture was adjusted to 3.0 mL by adding ethanol. The resulting mixtures were used to monitor the time-dependent changes in emission intensity at 20 °C.

3.1.7.2 Calculation of activation energy of the formation of QDC (with respect to CuQ_2).

Experiments similar to (i) above (for finding the order with respect to [CuQ_2]) were carried out at different temperatures, namely, T = 15 ºC, 20 ºC, 25 ºC and 30 ºC, in order to calculate activation energy of the formation of QDC. The rate constant was calculated from the intercept value obtained from the plot of ln(Rate) vs ln([CuQ_2]) of the reaction at different temperatures. The results were further used to make Arrhenius plot (lnk vs 1/T), in order to calculate the activation energy of the reaction with regard to CuQ_2.

3.1.8 Kinetic study of the formation of QDC following complexation of en-capped ZnS Qdots with HQ and $MnQ_2.2H_2O$.

To a solution containing 2.8 mL ethanol and 200.0 μL of as prepared Qdots (with absorbance 0.106 at 317 nm), 10.0 μL 0.2 mM HQ and 10.0 μL 0.1 mM MnQ_2 (in ethanol) were separately added in the cuvette and the time-dependent photoluminescence spectra were recorded until the emission intensity of the resulting mixture stopped increasing.

3.1.9 Calculation of equilibrium constant of the formation of QDC.

To a solution containing 2.8 mL ethanol and 200.0 μL ethanolic dispersion of as-prepared Qdots (with absorbance of 0.106 at 317 nm) in a cuvette at a particular temperature (T = 20 ºC), 2.0 μL of 0.1 mM CuQ2 (in ethanol) was added sequentially in order to obtained saturation in emission intensity (at 497 nm) of the resulting mixture. Additionally, the resulting mixture after each sequential addition was kept for 20 min, under same experimental condition, before the measurement was made.

3.1.10 Instruments.

The visual images of the samples were recorded under UV light (365 nm) using a UV-lamp. Perkin Elmer Lambda-750 and HORIBA-Fluoromax4 spectrofluorimeter were used to record the UV-Vis and PL spectra, respectively. The pH of the samples were measured using a JENWAY 3510- pH meter. HORIBA-JOBIN Yvon Flurolog spectrofluorimeter (using 340 nm LED excitation source with pulse width <1ns) was used to record the time-resolved photoluminescence (TRPL) spectra of the samples. The elemental analysis of the aqueous dispersion of the samples, following their acid digestion, was done using atomic absorption spectrometer (Varian AA240FS model). The FTIR spectra and XRD patterns of the solid samples were recorded using Perkin-Elmer (Model: Spectrum One) spectrophotometer and Brucker D2 Phaser X-ray diffractometer (having CuKα radiation at 1.5418Å), respectively. The transmission electron microscopic (TEM), high resolution TEM (HRTEM) and selected area electron diffraction (SAED) pattern of the samples - following deposition of their aqueous dispersion on formvar-carbon-coated copper grids - were obtained using a JEOL JEM-2100 transmission electron microscope (operated at a maximum accelerating voltage of 200 kV). The inverse fast Fourier transform (IFFT) images and particle size distribution of the samples were obtained using the Gatan Digital Micrograph software.

3.2 Results and Discussion.

3.2.1 Reaction between CuQ_2 and Ethylene-diamine Capped ZnS Qdot and Characterization of the Product.

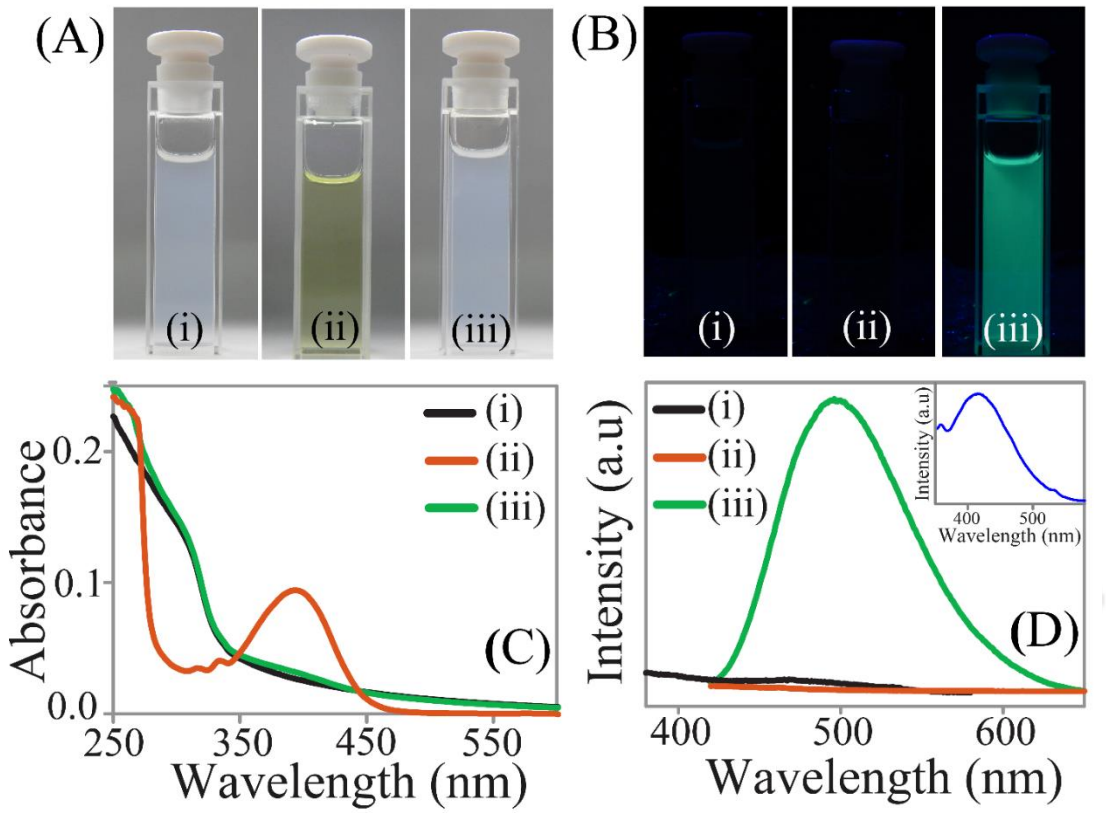

Figure 3.1. Digital photographs under (**A**) white light and (**B**) UV light (365 nm); (**C**) UV-Vis and (**D**) emission spectra (λ_{ex} – 361 nm) of (i) *en*-capped ZnS Qdots, (ii) CuQ_2 and (iii) CuQ_2 added *en*-capped ZnS Qdots, recorded following centrifugation and redispersion into the same amount of ethanol. (**D**) Inset: emission spectrum of *en*-capped ZnS Qdots (in ethanol) at an excitation wavelength of 324 nm.

Under white light, the en-capped Qdot dispersion in ethanol appeared milky white; the color of CuQ_2 solution was pale green; while the mixture of the two indicated milky white color (Figure 3.1A). On the other hand, under UV-light (365 nm), both the precursor solutions appeared dark, while the mixture appeared bright green (Figure 3.1B), indicating the occurrence of reaction between the precursors. Earlier results from the laboratory associated QDC (having ZnQ_2 on the surface of the Qdot) with green color emission from the reaction of ZnS Qdot with HQ.[1-4] Thus similar product formation might have occurred herein. The UV-vis absorption spectrum of the Qdot consisted of an edge at 317 nm and that of CuQ_2 a peak at 394 nm, while the reaction mixture

consisted of the edge at 317 nm and in addition, a broad shoulder centered around 370 nm (Figure 3.1C). It may be mentioned here that the UV-vis spectrum of the product was measured after centrifugation of the reaction mixture (followed by redispersion in ethanol).

On the other hand, at an excitation wavelength of 361 nm, ZnS Qdots (in ethanol) did not exhibit significant PL at 440 nm, while treatment with CuQ_2 led to generation of green emission at 497 nm (recorded following centrifugation and redispersion; Figure 3.1D). An ethanolic solution of CuQ_2 exhibited negligible PL (at λ_{ex} -361 nm) in the region (Figure 3.1D). Additionally, the surface defect trap emission of ZnS Qdots at 440 nm - which was absent at an excitation wavelength of 361 nm - was observed when excited at 324 nm light (Inset; Figure 3.1D).[5] Similarly, the peak of the excitation spectrum of Qdots shifted from 320 to 370 nm following reaction with CuQ_2 (Appendix, Figure A.3.2). Further, when the ethanolic dispersion of CuQ_2 treated Qdots were centrifuged and the so-obtained pellets were redispersed (into the same amount of ethanol), similar green emission at 497 nm was obtained (Appendix, Figure A.3.3), which clearly indicated the formation and attachment of green luminescent ZnQ_2 complexes on the surface of ZnS Qdot.[1-4] The quantum yield (QY) of PL (when excited at 361 nm) of the QDC, obtained from CuQ_2 and Qdot reaction, was found to be 2.1%, which was close to the QY (2.8%) of the QDC obtained from treating Qdots with only HQ (Table A.3.1, Appendix). The average life time of the CuQ_2 treated Qdots was 10.52 ns (Figure A.3.4 and Table A.3.2, Appendix). Additionally, the changes in zeta potential from 18.9 $\pm$ 0.36 to 25.3 $\pm$ 0.98 mV of Qdots, following complexation reaction with CuQ_2, indicated the modification of the surface of the Qdot. In the present case, the observed zeta potential value, of 25.3 $\pm$ 0.98 mV of CuQ_2 treated ZnS Qdot, is close to the zeta potential value of HQ treated ZnS Qdot from our earlier results. [2-4] This clearly supported the formation of similar type of complexes on the surface in the current context (Table A.3.3, Appendix).[2-4]

The results from X-ray diffraction (XRD) and transmission electron microscopy (TEM) experiments showed that the morphology and dimension of the ZnS Qdots remained unaltered following complexation reaction with CuQ_2 (Figure A.3.5-A.3.7, Appendix).[6] Further, Fourier transform infrared spectroscopic (FTIR) measurements of the QDC indicated the presence of octahedral MQ_2 (M=Zn or Cu) complexes on the surface of Qdots (Figure A.3.8, Appendix).[1-4] Atomic absorption spectroscopic (AAS)

measurements indicated the incorporation of small amount of Cu^{2+} ions (2.2 mol %) in Qdot (which may be in the form of CuS or CuQ_2), following complexation reaction with CuQ_2, while there was no significant change in the Zn^{2+} concentration (Table A.3.4, Appendix). Hence, the apperance of green PL at 497 nm in the QDC - following reaction between Qdots and CuQ_2 - was mainly due to the formation and attachment of luminescent ZnQ_2 complexes on the surface of Qdot, akin to reaction between ZnS Qdot and HQ as observed earlier.[1-4] Further, the incorporation of Cu^{2+} could be due to formation of CuS (which has a higher solubility product than ZnS) or adsorption of CuQ_2 on the surface.

3.2.2 Role of Dangling Sulfide in Accomplishing the Unprecedented Reaction.

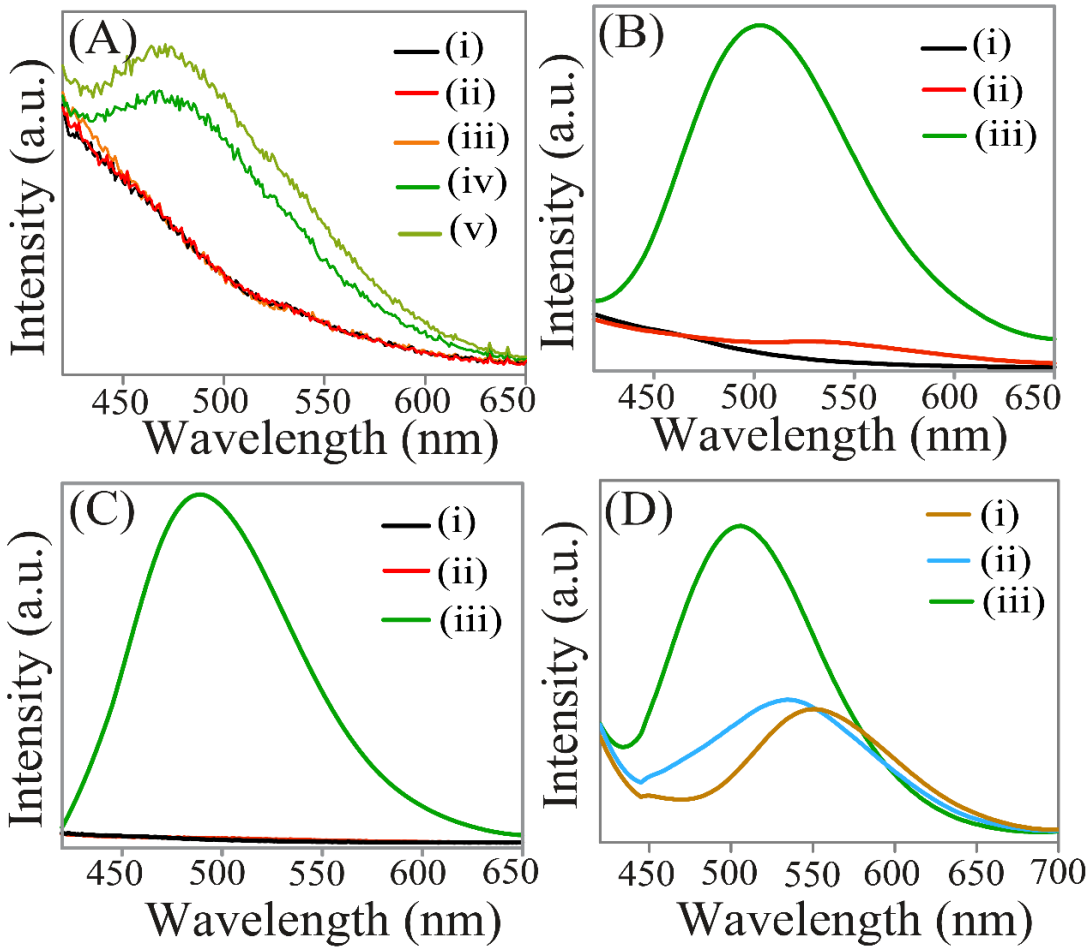

Figure 3.2. (**A**) Emission spectra (λ_{ex}= 361 nm) of (i) 3.0 mL ethanolic dispersion containing 10.0 µL of 0.1 mM CuQ_2, (ii) that with 2.4 µL of 2.5 mM of Zn^{2+} added (in ethanol; i.e. CuQ_2 + Zn^{2+}), (iii) the resulting solution after keeping for 12 h, (iv) following addition of 2.4 µL of 2.5 mM of sodium sulphide to the medium (in ethanol; CuQ_2 + Zn^{2+} (after 12 h) + S^{2-}) and (v) the

final resulting mixture after keeping for another 12 h. (**B**) Emission spectra (λ_{ex}= 361 nm) of (i) 2.59 mL ethanolic dispersion containing 10.0 μL of 0.1 mM CuQ_2, (ii) that with 200.0 μL of 2.5 mM of Zn^{2+} added (in ethanol; CuQ_2+Zn^{2+}) and (iii) that following addition of 200.0 μL of 2.5 mM sodium sulphide (in ethanol; $CuQ_2 + Zn^{2+} + S^{2-}$). (**C**) Emission spectra (λ_{ex}= 361 nm) of (i) 2.59 mL ethanolic dispersion containing 10.0 μL of 0.1 mM CuQ_2, (ii) that with 200.0 μL of 2.5 mM of sodium sulphide added (in ethanol; $CuQ_2 + S^{2-}$) and (iii) that following addition of 200.0 μL of 2.5 mM of Zn^{2+} (in ethanol; $CuQ_2 + S^{2-} + Zn^{2+}$). (**D**) Emission spectra (λ_{ex}= 361 nm) of (i) 2.59 mL ethanolic dispersion containing 10.0 μL of 0.1 mM ZnQ_2, (ii) that following addition of 200.0 μL of 2.5 mM of sodium sulphide (in ethanol; i.e. $ZnQ_2 + S^{2-}$) and (iii) that following addition of 200.0 μL of 2.5 mM Zn^{2+} (in ethanol; i.e. $ZnQ_2 + S^{2-} + Zn^{2+}$).

Importantly, the reaction of CuQ_2 with Zn^{2+} (and hence the formation of ZnQ_2) is unfavourable, according to Irving William series.[7] Thus when $Zn(acetate)_2$ (2.0 μM) was added to CuQ_2 (0.33 μM) solution, no changes in PL was observed even after 12 h of addition (Figure 3.2A). However, a strong luminescence at 497 nm, corresponding to ZnQ_2 (as in the presence of ZnS)[1] was observed, when Na_2S was added to that solution (Figure 3.2A). Similar observations (with higher luminescence) were made when higher concentration of $Zn(acetate)_2$ (167.0 μM) was added to CuQ_2 (0.33 μM) solution, which was followed by addition of higher concentration of sodium sulphide (167.0 μM) (Figure 2B). Furthermore, no change in PL of CuQ_2 (0.33 μM) was observed following the addition of only sodium sulphide (167.0 μM), while the same resulted in a strong PL at 497 nm when $Zn(acetate)_2$ (167.0 μM) was added into that medium (Figure 3.2C). Also, luminescence was observed only when $Zn(acetate)_2$ was added to a mixture of $Cu(acetate)_2$, Na_2S and HQ (results not shown). It is to be mentioned here that the addition of only Na_2S to CuQ_2 or ZnQ_2 was not sufficient to exert similar effect in terms of changes in emission maximum and intensity as compared to when CuQ_2 or ZnQ_2 reacted with ZnS Qdots (Figure 3.2C-D). The presence of $Zn(acetate)_2$ and Na_2S led to the similar kind of emission behavior as was obtained when CuQ_2 or ZnQ_2 reacted with ZnS Qdots.[1] This clearly indicated that the presence of the dangling S- bonds (in the ZnS crystal) is important to facilitate the complexation reaction with CuQ_2. However, it was found difficult to monitor the kinetics of the reaction of CuQ_2 with the mixture of free Zn^{2+} and S^{2-} ions (added independently), which led to the sudden change in the PL at 497 nm (Figures 3.2B and 3.2C). On the other hand, following the synthesis of the ZnS Qdots, that problem could be alleviated and it was easier to follow the kinetics and obtain thermodynamics parameters for the formation of ZnQ_2 from CuQ_2. In the current context, the presence of both Zn^{2+} ans S^{2-} ions on the surface of the *en* capped ZnS Qdot may be

facilitating its reaction with CuQ_2**.** Overall, the stability constant value of copper quinolate complex (CuQ_2) is 29.0, wheras zinc quinolate complex (ZnQ_2) has the stability constant value of 20.81.[8] Thus the formation of zinc quinolate from copper quinolate complex via mere ligand exchange in bare ionic form is thermodynamically not feasible. In the current case, the surface of the Qdot mediated the reaction as well as provided staibilty to the formed complex on it. This may possibly be through the attchment of ZnQ_2 on the surface via dangling sulphide bond.[1]

3.2.3 Kinetic Study of the Reaction.

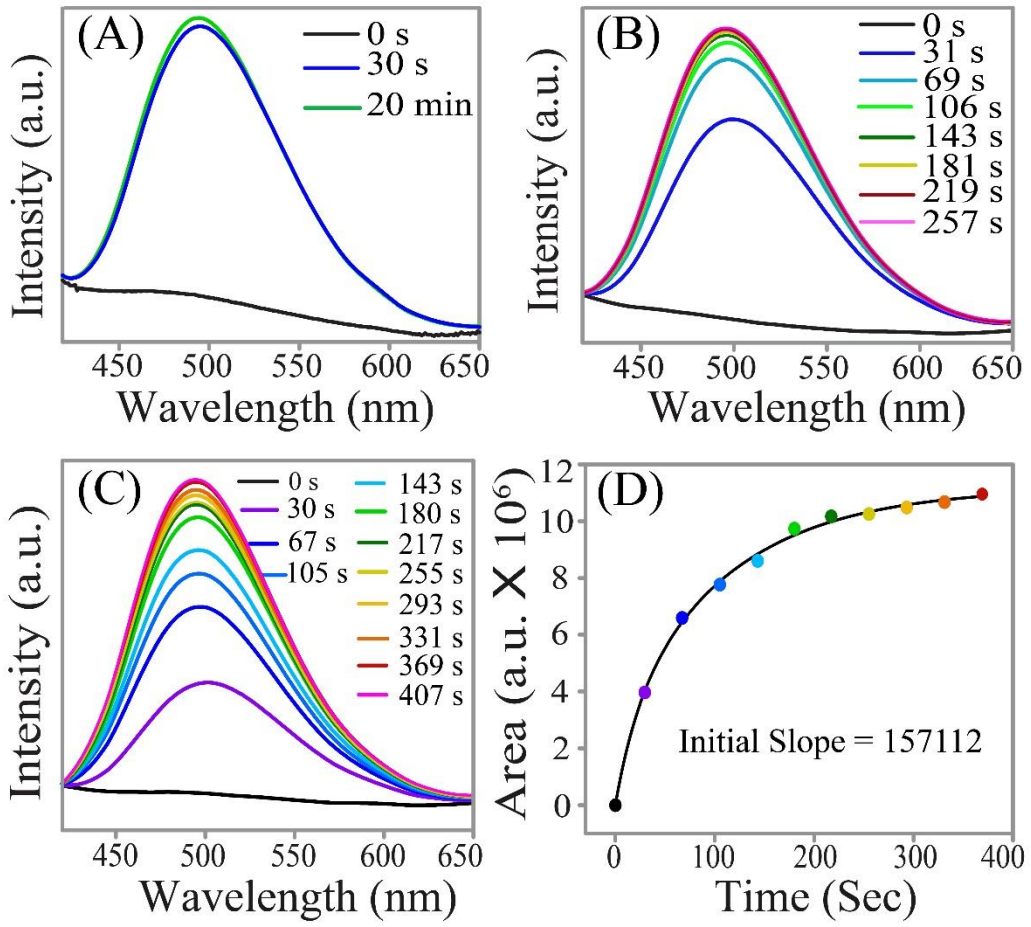

Figure 3.3. Time dependent changes (at T= 20 °C) in emission (λ_{ex} – 361 nm) intensity following addition of (**A**) 10.0 µL 0.2 mM HQ, (**B**) 10.0 µL 0.1 mM MnQ_2 and (**C**) 10.0 µL 0.1 mM CuQ_2 (in ethanol) to a solution containing 200.0 µL of as prepared Qdots (of fixed conc.) and 2.8 mL ethanol. (**D**) Variation in the area under the emission curve (following subtraction of area under the emission curve of Qdot) with time (in s) of CuQ_2 added Qdots (obtained from Figure 3.3C). Data points were fitted to an exponential function and the slope was equated to initial rate of the reaction (i.e. 157112.0 a.u./sec).

It was further observed that when ZnS Qdots with absorbance of 0.107 at 317 nm was treated with 0.66 μM (or even lower i.e. 0.066 μM) HQ, the reaction was over instantly (as probed by the luminescence of the product QDC, Figure 3.3A and Figure A.3.9A, Appendix). On the other hand, reaction of the Qdots (having absorbance of 0.107 at 317 nm) with 0.33 μM MnQ_2 (or even lower i.e. 0.033 μM) was nearly complete in 139 s (Figure 3.3B and Appendix, Figure A.3.9B). For either of the reactions, the time taken for completion - at both the reactant concentrations - was the same as mentioned above. Since the reaction of the Qdots with CuQ_2 was comparatively slower (it took about 5 min to be completed while using 0.33 mM CuQ_2), it was deemed feasible to study the reaction kinetics using an ordinary spectrofluorimeter (Figure 3.3C and 3.3D).

3.2.3.1 Determination of Order of the Reaction.

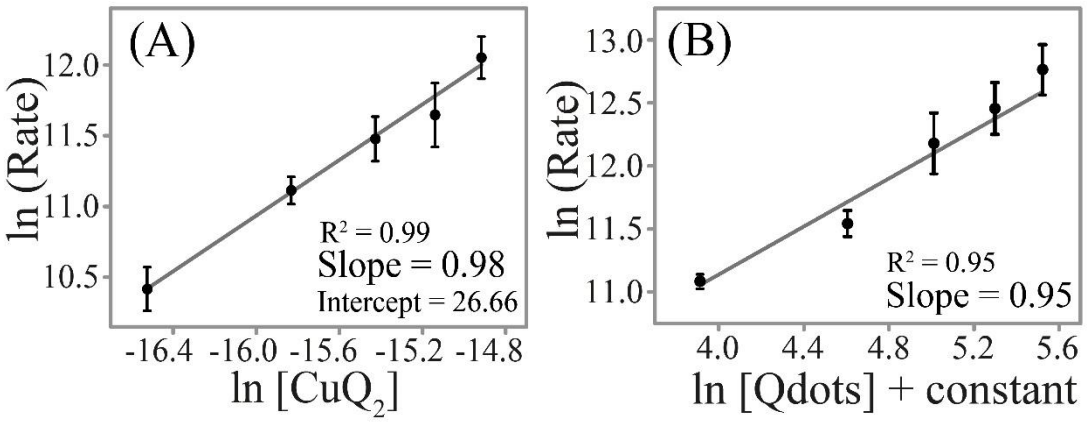

Figure 3.4. Plot of (**A**) ln(Rate) Vs ln[CuQ_2] and (**B**) ln(Rate) Vs ln[Qdots]. Data points were fitted to a linear function and the slope was equated to order of the reaction (i.e. 1) while the intercept denoted the logarithmic value of rate constant at T = 20 °C.

As shown in Figure 3.3C, the time-dependent progress of the reaction of Qdots with CuQ_2 (0.33 μM) at 20 °C led to the appearance of a peak at 497 nm, the intensity of which increased monotonically. Further, the plot of area (under the emission curve) vs time (Figure 3.3D) showed that the formation of the QDC followed exponential growth with time. Additionally, the rate of the reaction of the Qdots with CuQ_2 was measured, at 20 °C, to be first order with respect to the concentrations of both the reactants (Figure 3.4A, 3.4B and Figure A.3.10-A.3.15, Appendix).

Thus the overall reaction can be written as,

Zn^{2+} *(on the surface of ZnS Qdot)* + $CuQ_2 \rightleftharpoons ZnQ_2$ *(QDC)* + Cu^{2+} ….. (3.1)

$$\frac{d[QDC]}{dt} = k[Zn^{2+}][CuQ_2] \qquad \text{…….. (3.2)}$$

The rate of the formation of the QDC - with the overall reaction following second order kinetics – can be expressed as in equation 3.2.

3.2.3.2 Calculation of Equilibrium Constant of the Reaction.

Although the nature of reaction involving the dispersion of the Qdots and dissolved metal complex could be considered microheterogeneous, for simplicity, the concept of chemical equilibrium can be applied for reaction (3.1), considering it as a solution phase reaction. Hence, equilibrium constant can be calculated from the photoluminescence spectra of different amount of CuQ_2 added ZnS Qdot dispersion (Figure 3.5A)

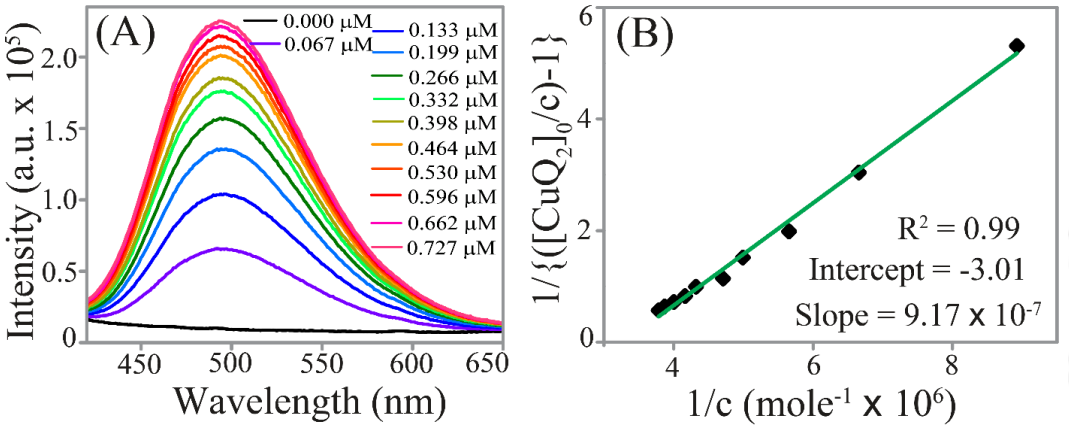

Figure 3.5. (A) Photoluminescence emission spectra (λ_{ex} – 361 nm) and **(B)** corresponding plot of $\frac{1}{\left(\frac{[CuQ_2]_0}{c}-1\right)}$ vs. $\frac{1}{c}$ of Qdot treated with various amounts of CuQ_2.

The equilibrium constant can then be expressed as,

$$K_{eq} = \frac{[Cu^{2+}][ZnQ_2]}{[CuQ_2][Zn^{2+}]} \quad \text{..... (3.3)}$$

Now, at equilibrium, $[ZnQ_2] = [Cu^{2+}]$ = a × area under emission curve = c (where 'a' is the proportionality constant).

The proportionality constant 'a' was calculated from emission spectrum of 0.01 mM 2.0 µL HQ added 3.0 mL of Qdots (i.e. 2.8 mL ethanol + 0.2 mL as prepared Qdots dispersion) solution, assuming full conversion of HQ to ZnQ_2 on the surface of the Qdots.

$$[Zn^{2+}] = [Zn^{2+}]_0 - [ZnQ_2] \quad \text{..... (3.4)}$$

$$[CuQ_2] = [CuQ_2]_0 - [ZnQ_2] \quad \text{..... (3.5)}$$

$$K_{eq} = \frac{[Cu^{2+}][ZnQ_2]}{([Zn^{2+}]_0-[ZnQ_2])([CuQ_2]_0-[ZnQ_0])} \quad \text{..... (3.6)}$$

Finally, $\frac{[Zn^{2+}]_0}{c} K_{eq} - K_{eq} = \frac{1}{\left(\frac{[CuQ_2]_0}{c} - 1\right)}$ …….. (3.7)

From the plot (Figure 3.5B) of $\frac{1}{\left(\frac{[CuQ_2]_0}{c} - 1\right)}$ vs. $\frac{1}{c}$ one could derive K_{eq} from the slope of the linear graph. $[Zn^{2+}]_0$, which indicates the initial value of surface $[Zn^{2+}]$, also can be obtained from the same plot. This (i.e. $[Zn^{2+}]_0$) can also be used to calculate rate constant of the reaction.

Equilibrium constant value was found to be 3.01 at T = 20 °C and coresponding ΔG° value was calculated to be -2.7 kJ mol^{-1}.

3.2.3.3 Calculation of Rate Constant of the Reaction.

Differential rate law for the reaction 3.1 can be presented as,

Rate of formation of surface ZnQ_2 complex,

$$r = \frac{d[ZnQ_2]}{dt} = k[Zn^{2+}][CuQ_2] \quad \text{....(3.8)}$$

Here the concentration of surface Zn^{2+} i.e. $[Zn^{2+}]$ was kept fixed by using a constant amount of Qdot (having an absorbance value of 0.106 at 317 nm) for ease of calculation of order of the reaction with respect to $[CuQ_2]$.

$$\ln (\text{Rate}) = \ln (k \times [\text{surface } Zn^{2+}]) + \ln [CuQ_2] \quad (3.9)$$

$$\ln (\text{Rate} / a) = \ln (k \times [\text{surface } Zn^{2+}] / a) + \ln [CuQ_2] \quad (3.10)$$

From this relationship the rate constant at T = 20 °C was found to be,

k = (2.93 ± 0.45) x10^4 $mol^{-1}s^{-1}$ L.

3.2.3.4 Calculation of Activation Energy (E_a) of the Reaction.

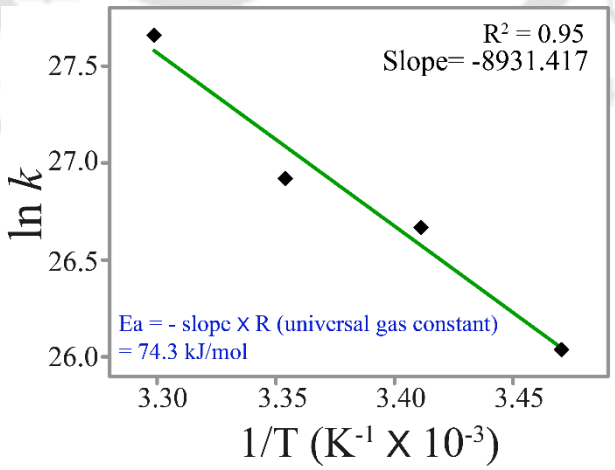

Figure 3.6. Plot of ln (k) vs 1/T of the formation of QDC (with respect to CuQ_2). Data points were fitted to a linear function and the negative of slope multiplied by R (universal gas constant) was considered equal to the activation energy of the reaction.

Further, in order to determine the activation energy of the reaction, temperature-dependent reaction kinetics was followed. (Figure 3.4A and Figure A.3.14, Appendix) The results are shown in Figure 3.6. The activation energy was calculated to be 74.3 kJ mol^{-1}. It is to be mentioned here that, the activation energy was calculated from the results of reaction being carried out in the temperature range of 15-30 °C. Also, the effect of Cu^{2+} ions adsorbed on the Qdot surface, if any, on the emission of the QDC, was ignored in the calculation. An earlier report suggests that elimination of quinolate moiety from copper complexes requires activation energy in the range of 25.0 – 131.0 kJ mol^{-1}. Hence, the activation energy of reaction 3.1 may be primarily attributed to the dissociation of Q^- from CuQ_2.[8]

3.2.4 Plausible Mechanism.

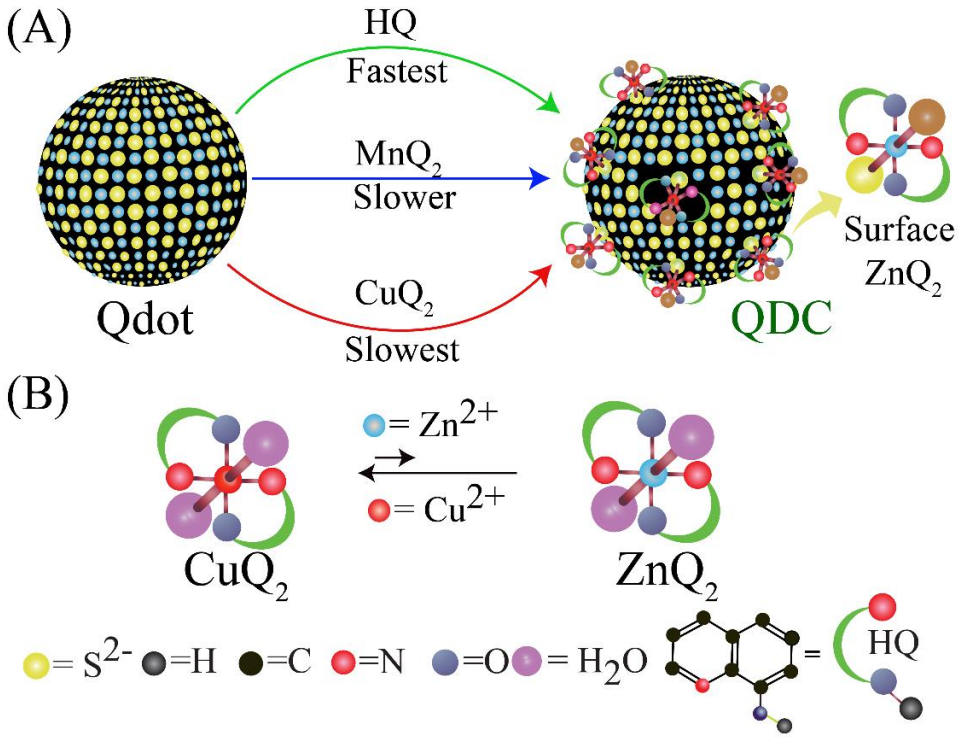

Scheme 3.1. Schematic representation of the (A) favourable formation of ZnQ_2 on the surface of ZnS Qdot (as QDC) followed by reacting Qdot with HQ, MnQ_2 and CuQ_2 and (B) unfavourable formation of ZnQ_2 following reaction between CuQ_2 and free Zn^{2+} ions (as salt form) in a liquid medium.

The overall observations from the current experiments are represented schematically in Scheme 3.1A. Thus the reaction of Zn^{2+} ions present on the surface of the ZnS Qdot was fastest with HQ, slower with MnQ_2 and the slowest with CuQ_2, leading to the

formation of the same product (ZnQ_2) on the surface. As is known from the Irving-William series,[8] the reaction of Zn^{2+} with HQ and MnQ_2 leading to the formation of ZnQ_2 in a liquid medium ought to be facile. The same was observed in the reaction involving surface Zn^{2+} ions. The slowness of the reaction with MnQ_2 could be due to the reaction being a two-step process, where the salt is in equilibrium with Q^-, which reacts with Qdot. On the other hand, CuQ_2 has the highest stability constant in the medium and thus the reaction with Zn^{2+} is not facile under ordinary condition (Scheme 3.1B). However, the reaction became facile when carried out with the Zn^{2+} present on the surface of Qdot. This clearly indicates the catalytic role of the surface of Qdot. The dangling S^{2-} bonds, which may not only provide additional stability to the product on the surface,[1] but also may lower the energy barrier of the complexation reaction, leading to the formation of QDC.

3.3 Conclusion.

In conclusion, we have reported a new type of reaction involving Zn^{2+} ions present on the surface of ZnS Qdot with CuQ_2, leading to the formation of ZnQ_2 on the surface. This is against the trend of Irving-William series, which stipulates that the reaction is not facile when Zn^{2+} ions are present as solute in a liquid medium. The reaction followed first order kinetics with respect to the concentrations of both the reactants i.e. CuQ_2 and Qdots, while the activation energy was found to be 74.3 kJ mol^{-1}. Further, the role of the surface of Qdots especially the dangling bonds was attributed to the formation of surface ZnQ_2 from CuQ_2. Finally, the current study, involving reaction kinetics of the formation of inorganic complexes on the surface of Qdots, can be expected to bring newer avenues towards the surface coordination chemistry of the Qdots and thus may have important consequences with regard to chemistry of Qdot and inorganic complex. As the phenomenon is unconventional, establishing the reaction pathway remains a point of interest.

3.4 Bibliography.

1. Bhandari, S.; Roy, S.; Chattopadhyay, A. Enhanced Photoluminescence and Thermal Stability of Zinc Quinolate Following Complexation on the Surface of Quantum Dots. *RSC Adv*. **2014**, *4*, 24217- 24221.
2. Bhandari, S.; Roy, S.; Pramanik, S.; Chattopadhyay, A. Double Channel Emission from a Redox Active Single Component Quantum Dot Complex. *Langmuir* **2015**, *31*, 551- 561.
3. Pramanik, S.; Bhandari, S.; Roy, S.; Chattopadhyay, A. Synchronous Tricolor Emission-Based White Light from Quantum Dot Complex. *J. Phys. Chem. Lett*. **2015**, *6*, 1270- 1274.
4. Bhandari, S.; Roy, S.; Pramanik, S.; Chattopadhyay, A. Surface Complexation Reaction for Phase Transfer of Hydrophobic Quantum Dot from Nonpolar to Polar Medium. *Langmuir* **2014**, *30*, 10760- 10765.
5. Kambhampati, P. On the Kinetics and Thermodynamics of Excitons at the Surface of Semiconductor Nanocrystals: Are There Surface Excitons? *Chem. Phys.* **2015**, *446*, 92- 107.
6. Acharya, S. A.; Maheshwari, N.; Tatikondewar, L.; Kshirsagar, A.; Kulkarni, S. K. Ethylenediamine-Mediated Wurtzite Phase Formation in ZnS. *Cryst. Growth Des*. **2013**, *13*, 1369- 1376.
7. Irving, H.; Williams, R. J. P. The Stability of Transition-Metal Complexes. *J. Chem. Soc.* **1953**, 3192- 3210.
8. EL-Gahami, M. A.; Khafagy, Z. A.; Ali, A. M. M.; Ismail, N. M. Thermal, Spectroscopic, Cyclic Voltammetric, and Biological Activity Studies of Cobalt(II), Nickel(II), and Copper(II) Complexes of Dicarboxylic Amino Acids and 8-Hydroxyquinoline. *J. Inorg. Organomet. Polym.* **2004**, *4*, 117- 129.

Chapter 4

Complex Transfer Reaction from ZnO to ZnS Quantum Dots Driven by Surface Anions

The work demonstrates preferential transfer of 8-hydroxyquinoline-5-sulphonic acid (HQS) from surface of ZnO quantum dots to ZnS quantum dots in the form of $Zn(QS)_2$ complex. This is an instance of inter quantum dot complex or Z-type ligand transfer that depends on solvent system – more precisely solubility of the migrating complex. The migration can be explained using Langmuir model by considering two parallel adsorption equilibria on ZnO and ZnS surfaces. It was also proposed that higher stability of the zinc quinolato complex on ZnS surface in comparison to that of ZnO is the driving force of the reaction.

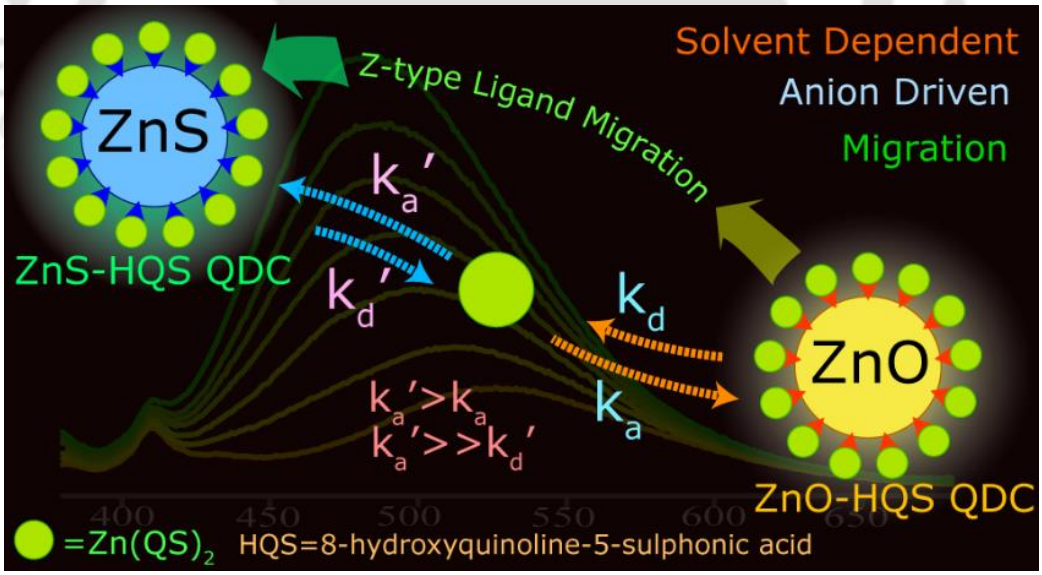

*[Roy et al. *J. Phys. Chem. C*, 2018, *122*, 9939–9946.] - Reproduced with permission from The American Chemical Society.

4.1 Experimental.

4.1.1 Materials.

Zinc acetate dihydrate (Merck), potassium hydroxide (Merck), ethylene diamine (en, Merck), 8-hydroxyquinoline-5-sulphonic acid (HQS, Merck), 8-hydroxyquinoline (HQ, Merck), sodium sulphide (58%, Merck), iron(III) chloride (Sigma Aldrich), sodium oleate (Sigma Aldrich), oleylamine (Sigma Aldrich), 2-propanol (Merck), methanol (MeOH, Merck), ethanol (TEDIA), DMSO (Merck), DMSO-d6 (Sigma Aldrich), chloroform (Merck), HPLC grade acetonitrile (Merck), sodium dihydrogen phosphate dehydrate (Merck), di-sodium hydrogen phosphate (Merck) were purchased and used without further purification. Mili-Q grade water was used for synthesis and in other experiments.

4.1.2 Synthesis of ZnO Qdots.

As per reported protocol, synthesis of ZnO quantum dots was carried out in ethanolic medium under basic condition.[1] Precisely, 5.0 mM of 50.0 mL ethanolic zinc acetate solution was taken in a round bottom flask. Then, 0.5 M of 2.0 mL ethanolic KOH solution was added to that solution under vigorous stirring and allowed to stir for ~ 40 min at room temperature. The opaque solution – so obtained was centrifuged at speed of 25,000 rpm for 15 min. The resulting pellet was washed twice with water by redispersing the obtained pellet followed by centrifugation. Same washing method was followed with methanol. Finally, the pellet was redispersed in 200 mL MeOH and was used as stock for further experiments. Formation of ZnO Qdot was confirmed through transmission electron microscopic image (Figure A.4.1A – A4.1B, Appendix). Zeta potential of as prepared ZnO Qdot dispersion in water was measured to be 18.6 mV.

4.1.3 Preparation of ZnS Qdot.

Following previously reported precipitation method, synthesis of ethylene diamine capped ZnS Qdots was carried out.[2] Precisely, 0.25 mmol zinc acetate dihydrate ($Zn(OAc)_2,2H_2O$) was solubilized in 40 ml of Milli-Q water taken in a round bottom flask and 500 μL of ethylene diamine was poured gently followed by addition of 25 mM 10 ml aqueous solution of Na_2S under stirring condition and allowed to maintain same reaction condition for 1 h at 383 K under reflux condition. Resulting milky white reaction

mixture was centrifuged at 25,000 rpm for 15 min and so obtained pellet was washed several times (centrifugation followed by redispersion) with water in order to remove the unreacted compounds. Lastly, the pellet was redispersed in MeOH and centrifuged and so obtained pellet was finally dispersed in 200 mL MeOH, which was used as stock solution for further use and characterization. The formation of ZnS Qdots was confirmed by TEM images (Figure A.4.2A – A4.2C, Appendix) and was further supported by characteristic absorption band edge at 310 nm and emission maximum at 425 nm (Figure A.4.2D, Appendix). Zeta potential of aqueous dispersion of as prepared ZnS Qdots was measured to be 15.1 mV.

4.1.4 Synthesis of quantum dot complex (QDC) of ZnO and 8-hydroxyquinoline-5-sulphonic acid (HQS) (i.e. ZnO-HQS QDC):

3.50 mL of 5.0 mM HQS (in 3:7 water:methanol solvent system) was added dropwise to 200 mL of as synthesized ZnO Qdots in stirring condition and was kept for 15 min. The reaction mixture was centrifuged for 15 min at 25000 rpm speed. The pellet so obtained was redispersed in methanol and centrifuged again maintaining same instrumental parameters. The final pellet was redispersed into 50 mL MeOH and used for further experiments.

The same protocol was followed to prepare ZnO-HQ QDC taking 8-hydroxyquinoline, (HQ) in lieu of HQS.

4.1.5 Synthesis of Fe_3O_4 Nanoparticles.

Synthesis of water dispersible Fe_3O_4 nanoparticles were performed following previously reported protocol.[3] At first, we synthesized Fe-oleate complex, which was used as starting material for synthesis of Fe_3O_4 nanoparticles soluble in organic solvent. Lastly, phase transfer agent was used for transferring water insoluble Fe_3O_4 nanoparticles to water. In a solvent mixture of hexane (18.0 mL), water (15.0 mL) and ethanol (8.0 mL), 18.25 g of sodium oleate were mixed with 3.24 g of iron chloride hexahydrate to synthesize Fe-oleate complexes and the reaction mixture was kept under constant stirring and temperature at 70 ºC. After refluxing for 4 h, dark brown precipitate was collected from hexane layer and washed with water-ethanol solvent mixture.

In a solvent mixture of olylamine and oleic acid (3:1) 300.0 mg of synthesized Fe-oleate complex was added and was refluxed for 1 h at 120 ºC until the solution turned black. Then the temperature was increased to 200 °C under nitrogen gas passing through the

mixture. Temperature was again increased to 300 °C and the reaction mixture was kept at the same condition for 2 hr. As the reaction was over, ethanol was added as precipitating agent of the product. Following this, removal of excess oleic acid and oleyl amine was performed by washing with hexane and ethanol. Then, aqueous 1 M tetramethylammonium hydroxide (TMAOH) was used for transferring product to water medium. Lastly, magnet was used to collect the final product and washed with water several times. Product was finally dispersed in 500 mL Milli-Q water for further use.

4.1.6 Synthesis of Fe_3O_4-ZnS nanocomposites (NCs).

Cysteine capped Fe_3O_4-ZnS composite was synthesized by previously reported method.[4] In short, 10 mL of as-prepared Fe_3O_4 was added to 20 mL Mili-Q water followed by 0.25 mmol zinc acetate dihydrate. Then the mixture was heated up to 100 °C with stirring. 10 mL of basic 25.0 mM cysteine hydrochloride aqueous solution (pH = 11.0) and 10 mL of 25.0 mM aqueous solution of sodium sulfide were then added to that hot mixture and kept the reaction mixture under reflux for 3 h at the same temperature. After 3 h the reaction mixture became light brown, thus indicating completion of the reaction. Then the resulting mixture was centrifuged at 20000 rpm for 15 min. The pellet was collected and washed twice by redispersing in water and centrifuged to remove all reactants. Then the pellet was dispersed in water and external magnet was applied to separate Fe_3O_4-ZnS Qdots from the unbound ZnS Qdots. After keeping the magnetic field for 12 h, the particles those were accumulated near the magnet were collected by removing the rest of the solution. The particles were dispersed in water and centrifuged. This process was repeated once by dispersing the pellet in MeOH. Finally, the pellet was dispersed in 10 mL MeOH for further experiment.

4.1.7 Monitoring reaction between ZnO-HQS (or ZnO-HQ) QDC with Fe_3O_4-ZnS nanocomposites (NCs).

For this experiment, the as-prepared solid pellets of ZnO-HQS and ZnO-HQ QDC were dispersed in 5.0 mL MeOH (instead of 50 mL MeOH). Then, we have monitored the reaction of Fe_3O_4-ZnS NCs with ZnO-HQS QDC and ZnO-HQ QDC separately. Reaction between Fe_3O_4-ZnS NCs and ZnO-HQS QDC was monitored in three solvent systems and three different sets were prepared as follows: (i) 5 mL DMSO + 0.25 mL ZnO-HQS QDC + 0.50 mL Fe_3O_4-ZnS NCs, (ii) 5 mL MeOH + 0.25 mL

ZnO-HQS QDC + 0.50 mL Fe_3O_4-ZnS NCs and (iii) 5 mL H_2O + 0.25 mL ZnO-HQS QDC + 0.50 mL Fe_3O_4-ZnS NCs. After mixing, reaction mixtures were allowed to stir for ~ 5 min followed by placing the culture tubes (containing reaction mixtures) beside magnet for 6 h. Then, the solvents were decanted from the culture tubes and the remaining magnetically separated pellets were dispersed in 3 mL of MeOH each for further experiments. Same sort of experiments were repeated for monitoring reaction between Fe_3O_4-ZnS NCs and ZnO-HQ QDC using another set of solvent systems. Three different sets used were as follows - (i) 5 mL DMSO + 0.25 mL ZnO-HQ QDC + 0.50 mL Fe_3O_4-ZnS NCs, (ii) 5 mL MeOH + 0.25 mL ZnO-HQ QDC + 0.50 mL Fe_3O_4-ZnS NCs and (iii) 5 mL $CHCl_3$ + 0.25 mL ZnO-HQ QDC + 0.50 mL Fe_3O_4-ZnS NCs.

4.1.8 Kinetic study of reaction between ZnO-HQS QDC and ethylene diamine capped ZnS Qdot.

Reaction between ZnO-HQS QDC and ZnS Qdot resulted in transfer of the complex, $Zn(QS)_2$ from the surface of ZnO Qdot to surface of ZnS Qdot. It was considered considered that increment in photoluminescence (PL) emission intensity is directly proportional to the attachment of $Zn(QS)_2$ on the surface of ZnS Qdots (i.e. concentration of Zn-HQS complex attached on the surface of ZnS Qdots). Time dependent PL emission spectra were recorded to find out the kinetic dependence of the reaction on both the reactants. Dependence on ZnS Qdot was followed by recording time dependent PL emission spectra by varying the amount of as-prepared ZnS Qdot in the dispersion while keeping amount of ZnO-HQS QDC fixed. In brief, 50 μL of as prepared methanolic ZnO-HQS in 2.5 mL 2-propanol taken in a cuvette was used as aliquot and either of 30, 40, 50, 60, 70, 80, 90, 100, 125, 150, 175, 200, 225, 250 and 275 μL of as prepared methanolic ZnS Qdot were added separately to the aliquot solution in stirring condition in a temperature controller system (T= 288 K). Before addition of ZnS Qdot certain amount of MeOH was added to each set so that final volume became 3.2 mL. Before addition of methanolic ZnS Qdot the PL emission was considered as emission profile at the starting of the reaction i.e., at time = 0 sec. Stopwatch was started just after the addition of ZnS Qdot and first spectrum was recorded at ~ 7 s interval after addition of ZnS Qdot and several spectra were recorded sequentially up to ~ 5 min to reach the saturation and time-gaps were noted. Likewise, same sort of experiments were repeated by varying the amount of ZnO-HQS QDC, while keeping concentration of ZnS Qdot constant to find out dependence of the reaction kinetics on ZnO-HQS QDC. For this

experiment, 10, 20, 30, 40, 50, 60, 80, 100, 125, 150, 175, 200, 250 and 300 μL of as prepared methanolic ZnO-HQS QDC were added separately to 2.5 mL 2-propanol taken in a cuvette, which were used as aliquots. For each set, 50 μL of as prepared methanolic ZnS Qdots was added to aliquot solution in stirring condition in a temperature controller system (T= 288 K) and time dependent PL emission were recorded.

4.1.9 Calculation of concentration of ZnO and ZnS Qdot.

Initial rate was calculated from the initial enhancement of PL emission intensity at 485 nm. Initial rate of the reaction was obtained by simply dividing the intensity enhancement value by the time.

(i) Concentration of ZnO Quantum Dot Complex (ZnO-HQS QDC).

From TEM analysis diameter of the ZnO-HQS QDC was found to be, d = 3.02 ± 0.30 nm.

So, radius = 1.51 nm or 15.1 ≈ 15 Å.

Hence, for a single ZnO QD volume, V = 14.14×10^3 Å^3 and area, A = 2.83×10^3Å^2.

From powder XRD and SAED pattern of ZnO Qdot, wurtzite lattice structure was found.[2]

Now, volume of single wurtzite cell, a = 47.66 Å^3. So, number of unit wurtzite cell per ZnO QDC = (V/a) = 297. So, number of Zn per QDC = 2 × 297 = 594 [as a unit wurtzite cell consist two metal ions]. From AAS analysis, it was found that concentration of total Zn^{2+} ion present in stock solution of as prepared ZnO-HQS QDC = 3.793 mM.

So, concentration of ZnO-HQS QDC, [QDC_{ZnO}] = 6.40 μM.

(ii) Concentration of ZnS Quantum dot.

From TEM analysis diameter of the ZnS QD was found to be, d = 3.20 nm.

So, radius = 1.6 nm or 16 Å.

Hence, for a single ZnS QD volume, V = 17.16×10^3 Å^3 and area, A = 3.22×10^3 Å^2.

From powder XRD and SAED pattern of ZnS Qdot, wurtzite lattice structure was found.[3]

Now, volume of single wurtzite cell, a = 79.11 Å^3. So, number of unit wurtzite cell per ZnS QD = (V /a) = 217. So, number of Zn per QD = 2 × 217 = 434 [as a unit wurtzite cell consist two metal ions]. From AAS analysis, it was found that concentration of total Zn^{2+} ion present in stock solution of as prepared ZnS QD= 0.99 mM.

So, concentration of ZnS QD, [QD_{ZnO}] = 2.30 μM.

4.1.10 Instruments.

The photographs of the samples were taken under UV light (365 nm) using a UV-lamp and digital camera. Perkin Elmer Lambda-750 and HORIBA-Fluoromax4 spectrofluorometer were used to record the UV-vis and PL spectra respectively. Life-Spec-II spectrofluorometer (Edinburgh Instrument, using Pico Quant 375 nm LASER source) for time-resolved photoluminescence measurement for time-resolved photoluminescence study. The elemental analyses of the aqueous dispersion of the samples, following their acid digestion, were done using atomic absorption spectrometer (Varian AA240FS model). The Fourier transform-Infrared (FTIR) spectra of the solid samples were recorded using the Perkin-Elmer (Model: Spectrum One) spectrophotometer. The transmission electron microscopic (TEM), high resolution TEM (HRTEM) and selected area electron diffraction (SAED) pattern of the samples - following deposition of their aqueous dispersion on formvar-carbon-coated copper grids - were obtained using a JEOL JEM-2100 and JEOL JEM-2100F transmission electron microscope (operated at a maximum accelerating voltage of 200 kV). The Gatan Digital Micrograph software was used to obtain particle size distribution of the samples. Bruker 600 MHz NMR spectrometer was used for NMR analysis. Zetasizer Nano-ZS90 (Malvern) was used for zeta potential measurement.

4.2 Results and Discussion.

4.2.1 Formation and Characterization of ZnO-HQS QDC.

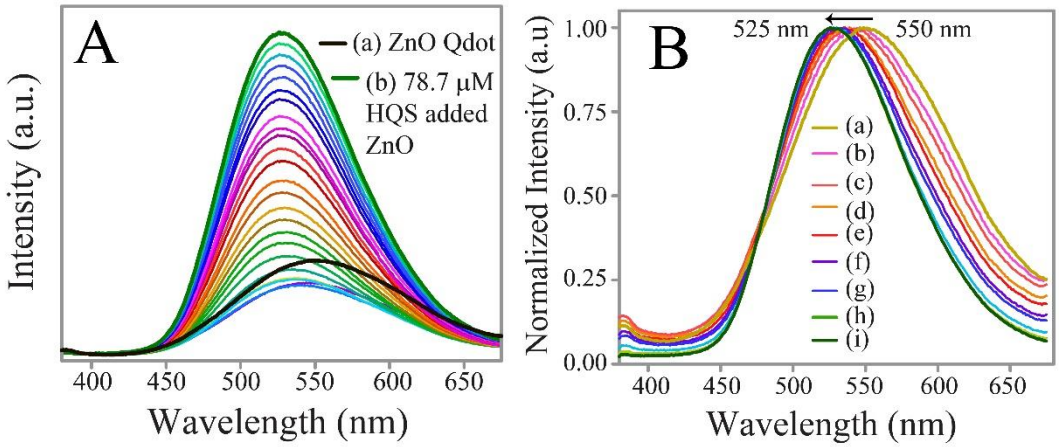

Figure 4.1. (A) Photoluminescence (PL) emission spectra of (a) as synthesized ZnO Qdots (3 mL) and of that sample after sequentially addition of 2 μL 5 mM aqueous-methanolic 8-hydroxyquinoline-5-sulphonic acid (HQS) each up to (b) 48 μL 5 mM HQS corresponding to final concentration of HQS 78.7 μM. (B) Corresponding normalized PL emission spectra of (a) as synthesized ZnO Qdots dispersion and that dispersion after addition of (b) 3.3 μM, (c) 6.7 μM, (d) 10.0 μM, (e) 13.3 μM, (f) 19.9 μM, (g) 39.7 μM, (h) 59.3 μM and (i) 78.7 μM methanolic HQS.

As synthesized dispersion of ZnO Qdots had absorbance maximum at 345 nm and showed yellow emission (λ_{em} ~ 550 nm) (Figure A.4.1C, Appendix). Upon reaction with HQS, ZnO Qdot exhibited initial decrease in emission intensity, which was followed by its gradual enhancement accompanied by blue shift towards 525 nm (Figure 4.1 and Figure A.4.3, Appendix). The initial decrease might have resulted from the decrease in the number of emitting surface defect states due to complex formation with surface Zn^{2+} ion(s). But, as the concentration of $Zn(QS)_2$ complex on the surface of ZnO increased, PL – originating from it – dominated the emission of the ZnO-HQS QDC. Importantly, when the reaction was carried out in phosphate buffer medium (buffer pH ~ 6.77) the results obtained were similar to those performed in methanol. Thus, pH might not have significant effect on the luminescence of ZnO Qdot. On the other hand, the increase in emission intensity with shift of the maximum to 525 nm was observed when HQS was added to ZnO Qdot in phosphate buffer medium (Figure A.4.4, Appendix). The results indicated the formation of $Zn(QS)_2$ complex on the surface of the Qdot as the primary reason for enhancement in PL and blue shift of the peak. Additionally, the appearance of

absorption peak at 375 nm (Figure A.4.5, Appendix) – that resembles absorbance peak of Zn^{2+} added HQS solution (Figure A.4.6A, Appendix) – indicated the formation of zinc - HQS complex on ZnO Qdot surface i.e., ZnO-HQS QDC, which was further supported by FTIR results (Figure A.4.7, Appendix). Zeta potential of aqueous colloidal dispersion of ZnO-HQS QDC was measured to be 12.1 mV. It may be mentioned here that although the zeta potential values indicated that the dispersions did not have high colloidal stability; however, they were sufficiently stable for carrying out experiments reported herein. From TEM analysis, it was evident that complexation did not significantly affect the size and shape of ZnO Qdots (Figure A.4.8, Appendix).

4.2.2 Reaction between ZnS Qdot and ZnO-HQS QDC.

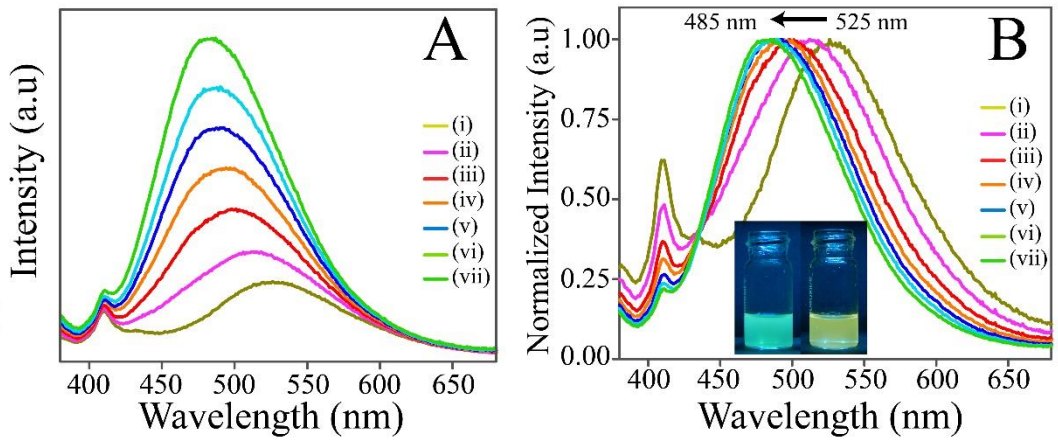

Figure 4.2. (A) PL emission spectra (λ_{ex} – 365 nm) and **(B)** corresponding normalized spectra of (i) as synthesized 100 µL ZnO-HQS QDC in 3.0 mL methanol and that after addition of (ii) 20 µL, (iii) 40 µL, (iv) 60 µL, (v) 80 µL, (vi) 100 µL and (vii) 120 µL as synthesized en-capped ZnS Qdots.

When as-synthesized ZnS Qdot was added to methanolic ZnO-HQS QDC dispersion, there was significant increase in PL intensity with gradual shift towards 485 nm from 525 nm (λ_{ex} – 365 nm) (Figure 4.2A – 4.2B). This was also visualized under UV light (λ_{ex} – 365 nm). Briefly, near yellow emitting dispersion containing ZnO-HQS QDC turned luminescent cyan after addition of ZnS Qdots (Figure 4.2B, inset). Importantly, ZnS-HQS QDC – formed out of reaction between ZnS Qdot and HQS – emitted at 485 nm (Figure A.4.9 – A4.10, Appendix).[5] Hence, this considerable blue shift of ~ 40 nm possibly was an outcome of the formation of ZnS-HQS QDC as a result of ligand transfer from the surface of ZnO to ZnS Qdot. Ligand transfer was further supported by centrifugation and time resolved photoluminescence experiments (Figure A.4.11-A.4.12,

Appendix).[2,6] The pellet obtained after centrifugation of reaction mixture was dispersed in the same volume of the solvent, which exhibited almost same PL emission intensity (λ_{max} – 485 nm) as the reaction mixture, thus indicating that stable product was formed out of the ligand transfer reaction from ZnO to ZnS surface in order to attain superior stability. Earlier observations indicated stability of the surface zinc complex of the ligand on ZnS Qdot by means of attachment through dangling sulphide.[2,6] The enhanced stability of the complex with attachment to sulphide ion instead of oxide might have driven the ligand transfer reaction. From time - resolved photoluminescence (TRPL) measurements, it was observed that ZnS-HQS QDC had higher luminescence lifetime compared to ZnO-HQS QDC (Table A.4.1, Appendix). Hence, the higher lifetime of the reaction mixture – comprising of ZnS Qdots and ZnO-HQS – may be attributed to the formation of ZnS-HQS QDC. Thus, it can be concluded that following reaction between ZnS-HQS QDC and ZnS Qdots, the steady-state luminescence intensity as well as lifetime of the emission increased.

4.2.3 Proof of Ligand Transfer.

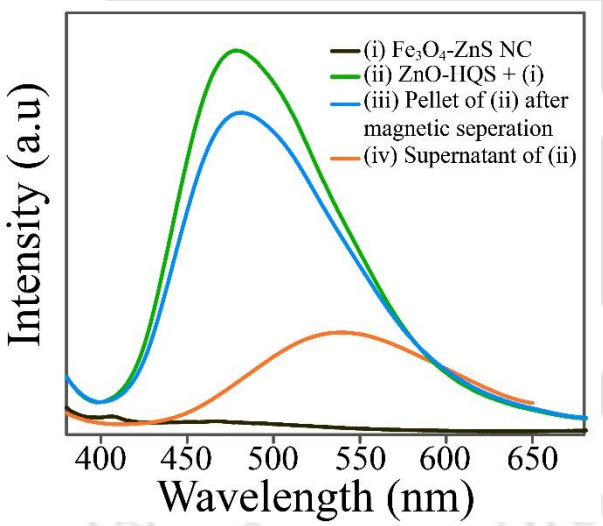

Figure 4.3. (A) PL emission spectra (λ_{ex} – 365 nm) of (i) as synthesized Fe_3O_4-ZnS nanocomposite in methanol, (ii) that after addition of as synthesized ZnO-HQS QDC, (iii) dispersion of pellet to same volume of methanol and (iv) supernatant obtained after overnight magnetic separation of reaction mixture (ii).

Experimental substantiation of the ligand transfer reaction between ZnO and ZnS Qdots was achieved by magnetic separation using Fe_3O_4-ZnS nanocomposites (NCs).[4] A new emission peak at λ_{em} – 485 nm was observed when as-synthesized non-fluorescent Fe_3O_4-ZnS NCs were added to the dispersion of ZnO-HQS QDC (Figure 4.3).

Importantly, when the product was separated by using a magnet and then was dispersed in methanol, strong luminescence at the above wavelength was observed. The results indicated that luminescent Zn-HQS complex was attached to the surface of Fe_3O_4-ZnS with the ligand originating from the ZnO surface. FTIR spectrum of the pellet obtained after magnetic separation further supported the ligand transfer phenomenon as peaks appeared in the FTIR spectrum indicated attachment of HQS on Fe_3O_4-ZnS NCs (Figure A.4.13, Appendix).

4.2.4 Identification of Migrating Species.

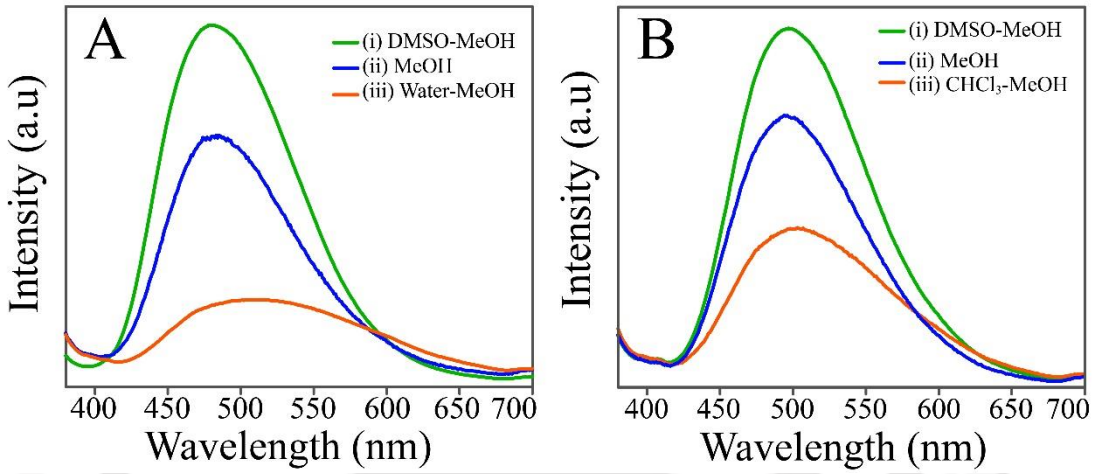

Figure 4.4. PL emission spectra (λ_{ex} – 365 nm) of dispersion of pellet to same volume of methanol obtained after magnetic separation of reaction mixture consisting of **(A)** as synthesized Fe_3O_4-ZnS nanocomposites (NCs) and ZnO-HQS QDC in (i) DMSO-MeOH 5.0/0.75 (v/v), (ii) pure MeOH and (iii) Water-MeOH 5.0/0.75 (v/v) solvent system and **(B)** as synthesized Fe_3O_4-ZnS nanocomposite and ZnO-HQ QDC in (i) DMSO-MeOH 5.0/0.75 (v/v), (ii) pure MeOH and (iii) chloroform-MeOH 5.0/0.75 (v/v) solvent system.

An important issue that needs to be addressed is to ascertain whether the ligand (HQS) or Zn-HQS complex i.e. $Zn(QS)_2$ had migrated from ZnO surface to ZnS surface. Solubility of the migrating species in a particular solvent is key to the transfer. In order to pursue this, reaction between Fe_3O_4-ZnS NCs and ZnO-HQS QDC was monitored in three different solvent systems – (i) 5.0:0.75 (v/v) DMSO - methanol, (ii) methanol or (iii) 5.0:0.75 (v/v) water - methanol, which were chosen depending on solubility of HQS and $Zn(QS)_2$. This was followed by magnetic separation of the products for further analyses. Importantly, solubility of $Zn(QS)_2$ followed the order – DMSO-MeOH > MeOH > MeOH-water, whereas for HQS the order was DMSO-MeOH ≈ MeOH-water > MeOH. Experimentally, the same amount of Fe_3O_4-ZnS NC and ZnO-HQS QDC were used for each solvent system. Following magnetic separation, pellets were collected and

redispersed separately in the same amount of methanol. It was observed that pellets obtained from DMSO-methanol, pure methanol and water-methanol solvent system exhibited decreasing order in photoluminescence emission intensity at 485 nm (Figure 4.4A) – indicating the order of the extent of migration of $Zn(QS)_2$ complex to Fe_3O_4-ZnS NC surface. This results indicated $Zn(QS)_2$ complex as migrating species, as highest PL emission intensity at 485 nm was observed in case of DMSO-MeOH solvent system, which was the best solvent for $Zn(QS)_2$ complex among those three. Mechanistically, extent of desorption of ligand from the surface of nanocrystals increased as solubility of ligand in dispersing medium increased.[7,8] Similar results were obtained when ZnO-HQ QDC was used in lieu of ZnO-HQS QDC (Figure 4.4B). For example, the product of the reaction in DMSO-MeOH exhibited the highest emission intensity whereas that from $CHCl_3$-MeOH solvent showed the lowest emission intensity at 500 nm. Additionally, the emission intensity at 500 nm of the sample from MeOH medium was in between the two (Figure 4.4B). This observation can again be attributed to the solubility of migrating species i.e., ZnQ_2 complex having the highest solubility in DMSO-MeOH among the three. The results presented above indicated zinc-quinolato complex as the migratory species.

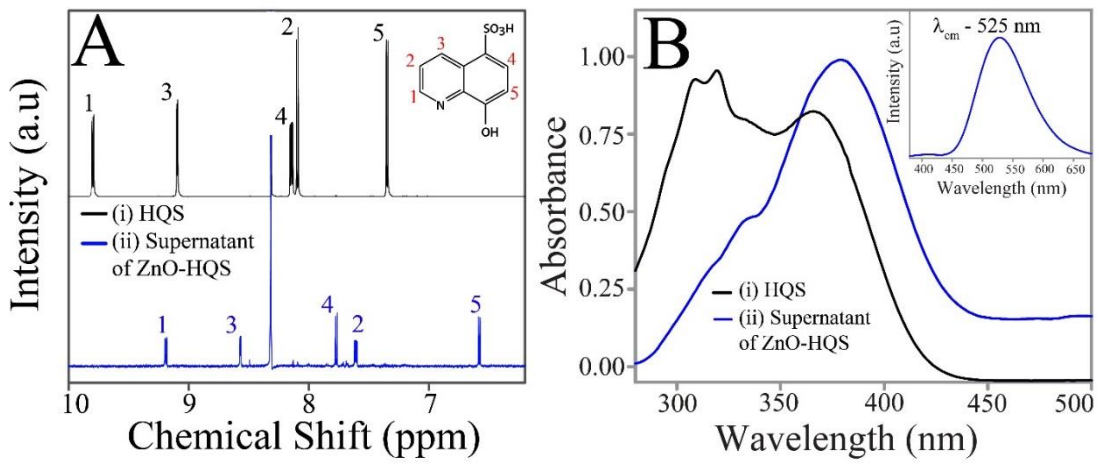

Figure 4.5. (A) Proton NMR spectra (aromatic zone) and (B) UV-vis spectra of (i) 8-hydroxyquinoline-5-sulphonic acid (HQS) and (ii) supernatant obtained after centrifugation of as prepared ZnO-HQS QDC in DMSO-d6 and (inset of B, PL emission spectrum of the supernatant mentioned in (ii)). Solvent used for UV-vis: MeOH – DMSO 30:2 v/v solvent mixture.

The results were further supported by NMR spectroscopy. For NMR analyses, solid ZnO-HQS QDC was dispersed in DMSO-d_6, which was then centrifuged. The supernatant was used for studies. The spectrum of the supernatant (Figure 4.5A) consisted of peaks, which were substantially shifted (up field) from the peaks due to HQS. From NMR spectroscopic measurements, similar up-field shift was observed when Zn^{2+} ion was added to HQS in DMSO-d_6 – leading to the formation of Zn-HQS complex (Figure A.4.14 – A4.16, Appendix). For example, NMR peak due to the proton of HQS designated as 1 in Figure 3A and having δ value 9.79 appeared at 9.19 and 9.23 in case of supernatant obtained from ZnO-HQS QDC and Zn^{2+} added HQS, respectively (Figure A.4.14 – A4.16, Appendix). Likewise, all the protons corresponding to the supernatant and Zn-HQS complex exhibited similar δ values (Figure A.4.14 – A4.16, Appendix). The results thus indicated the presence of Zn-complex of HQS (i.e., $Zn(QS)_2$) in supernatant, thus substantiating the preferential desorption of the complex from the surface of ZnO Qdots and thus subsequently binding on the surface of ZnS Qdots. The presence of complex (i.e., Zn-HQS complex) was further supported by the PL emission and UV-vis spectra of the same supernatant solution used for NMR analyses (Figure 4.5B). The solution exhibited PL emission maximum centered at 525 nm and absorption maximum at 375 nm, which resembled that of Zn^{2+} added HQS solution (Figure A.4.6, Appendix).

4.2.5 Kinetic Model of the Complex Transfer Reaction.

Time-dependent PL spectroscopic investigations revealed that kinetics of the reaction was dependent on the concentrations of both ZnO-HQS QDC and ZnS Qdots (Figure 4.6).[9] For example, the intensity of the luminescence peak at ~ 525 nm due to ZnO-HQS QDC in the alcoholic dispersion increased with time after addition of ZnS Qdots (Figure 4.6A). This was accompanied by gradual peak shift towards ~ 485 nm, which was attributed to the migration of the complex from ZnO-HQS QDC to ZnS Qdot surface. The initial rate of the reaction (calculated from the intensity of the peak at 485 nm) exhibited linear dependence on $[QDC_{ZnO}]$ and was independent of $[QD_{ZnS}]$ when $[QD_{ZnS}]$ was kept equivalent to or relatively higher than $[QDC_{ZnO}]$ (Figure 4A). Whereas, at low concentrations of ZnS Qdot, initial rate was linear with $[QD_{ZnS}]$ and independent of $[QDC_{ZnO}]$.

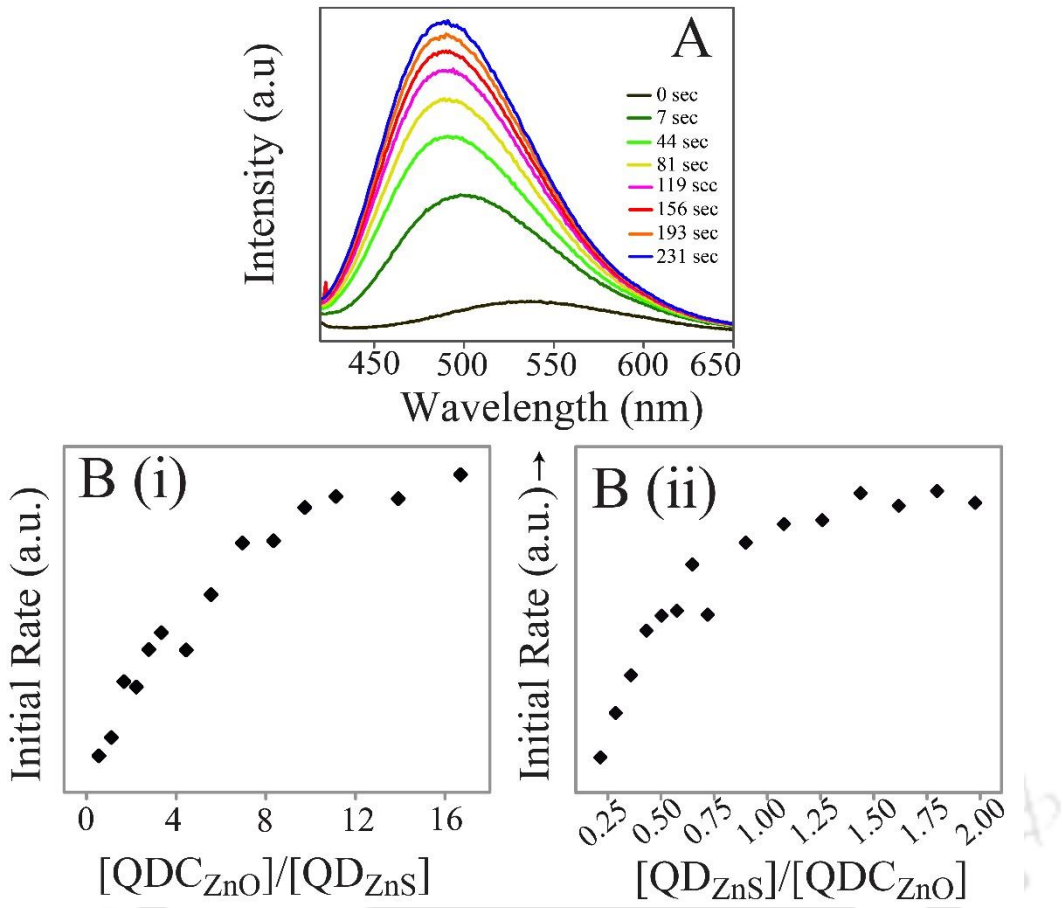

Figure 4.6. **(A)** Representative time dependent PL emission spectra of 50 µL as synthesized ZnS Qdots added to 50 µL as prepared ZnO-HQS QDC. **(B)** Initial rate vs Ratio of concentration of ZnO-HQS QDC to ZnS Qdots showing dependence of initial rate at (i) variable concentration of ZnO-HQS QDC keeping concentration of ZnS Qdot fixed and (ii) variable concentration of ZnS Qdot keeping concentration of ZnO-HQS QDC fixed.

Based on the results presented above, a model was proposed to understand the reaction between ZnO-HQS QDC and ZnS Qdot by considering adsorption equilibrium being prevalent on the surface of both the Qdots (i.e., ZnO and ZnS Qdots). It is assumed that the reaction followed two-step process: (i) desorption of complex from ZnO surface followed by (ii) adsorption of complex on ZnS surface – which can be expresses as –

$$(ZnO)_x C_p \underset{k_a}{\overset{k_d}{\rightleftharpoons}} (ZnO)_x C_{p-1} + C \qquad \text{.....(4.1)}$$

$$(ZnS)_y C_q + C \underset{k_d'}{\overset{k_a'}{\rightleftharpoons}} (ZnS)_y C_{q+1} \qquad \text{.....(4.2)}$$

Thus, overall reaction can be expressed as –

$$(ZnO)_x C_p + (ZnS)_y C_q \underset{k_{-1}}{\overset{k_1}{\rightleftharpoons}} (ZnO)_x C_{p-1} + (ZnS)_y C_{q+1} \quad \text{.....(4.3)}$$

Where, C represents migrating species i.e. Zn complex of HQS ($Zn(QS)_2$) and x, y, p, q represent the stoichiometry (as appropriate). Kinetic parameters (mentioned in equation 4.1 and 4.2) k_a, k_d are the adsorption and desorption coefficients of C on the surface of ZnO Qdot surface; likewise, parameters for ZnS surface are k_a', k_d'. Whereas, k_1 *and* k_{-1} (mentioned in equation 2.3) represent forward and backward rate constants of overall reaction.

Table 4.1. Meaning of the notations used in kinetic equation.

Parameter	Notational meaning
θ / θ′	Mean fractional coverage of single ZnO / ZnS Qdot Surface
n / n′	Average total number of surface site per ZnO / ZnS Qdot
N / N′	Total concentration of surface site of ZnO / ZnS Qdots = n (/

Now, adsorption equilibria on both the Qdot surfaces can be explained by using Langmuir model.[10] In this case, desorbed complex (C) from ZnO surface – migrates to ZnS surface – undergoes adsorption on it. Therefore, simultaneously two adsorption equilibria persist and the kinetic parameters involved control the course of the reaction. From centrifugation experiments, it was evident that attachment of HQS on the surface of ZnS Qdot was more facile than that on ZnO Qdot surface (Figure A.4.10, Appendix). Thus, the supernatant obtained after centrifugation from the dispersion of ZnS and HQS in methanol exhibited weaker PL emission intensity as compared to that obtained following re-dispersion of the pellet. On the other hand, the supernatant obtained from the dispersion of ZnO and HQS in the same solvent showed substantial PL emission intensity as compared to the redispersion of the pellet. The result signified better adsorption and thus weak desorption of HQS (in the form of $Zn(QS)_2$) on ZnS surface, which was opposite of that on the surface of ZnO Qdot. This could be possible if $k_a' > k_a$ and at the same time $k_a' >> k_d'$. Hence, steady state approximation applied for the intermediate migrating species C (i.e., $Zn(QS)_2$).

$$\frac{d}{dt}[C] = N\left[k_d\theta - k_a(1-\theta)[C]\right] + N'\left[k_d'\theta' - k_a'(1-\theta')[C]\right] = 0 \quad \text{.....(4.4)}$$

Now, the rate of attachment of $Zn(QS)_2$ on the surface of ZnS Qdot surface can be expressed as –

$$r = N'[k_a'(1-\theta')[C] - k_d'\theta'] \quad \text{.....(4.5)}$$

$$r = N'\left[k_a'(1-\theta')\frac{Nk_d\theta + N'k_d'\theta'}{Nk_a(1-\theta) + N'k_a'(1-\theta')} - k_d'\theta'\right] \quad \text{.....(4.6)}$$

As, for a particular set of synthesis of ZnO-HQS QDC and ZnS Qdot, fractional surface coverage and adsorption, desorption co-efficient are fixed, dependence of initial rate would be only on N and N′, more particularly, on $[QDC_{ZnO}]$ and $[QD_{ZnS}]$. At the initial point, at the starting of the reaction fractional surface coverage of ZnS Qdots with the complex can be set to zero. Now, rate equation would be –

$$r = \frac{N'k_a'Nk_d\theta}{Nk_a(1-\theta) + N'k_a'} \quad \text{.....(4.7)}$$

Considering all other parametric constraints, different kinetic rate laws can be obtained for different concentration regions. Finally, obtained the rate laws were,

$r = Nk_d\theta$; when $[QD_{ZnS}] > [QDC_{ZnO}]$ (i.e. N′>N) and $r = {N'k_a'k_d\theta}/{k_a(1-\theta)}$; when $[QDC_{ZnO}] >> [QD_{ZnS}]$ (i.e. N>>N′).

When amount of ZnO-HQS QDC is kept constant while varying amount of ZnS Qdots, the rate equation becomes –

$$r = \frac{C_1[QD]}{C_2[QD] + C_3} = \frac{\left({C_1}/{C_2}\right)[QD]}{[QD] + \left({C_3}/{C_2}\right)} \quad \text{.....(4.8)}$$

where constants are $C_1 = n'k_a'Nk_d\theta$, $C_2 = n'k_a'$, $C_3 = Nk_a(1-\theta)$.

When amount of ZnS Qdots is kept constant while varying amount of ZnO-HQS QDC, the rate equation becomes –

$$r = \frac{C_1'[QDC]}{C_2'[QDC] + C_3'} = \frac{\left({C_1'}/{C_2'}\right)[QDC]}{[QDC] + \left({C_3'}/{C_2'}\right)} \quad \text{.....(4.9)}$$

where, constants are : $C_1' = N'k_a'nk_d\theta$, $C_2' = nk_a(1-\theta)$, $C_3' = N'k_a'$.

Observations on initial rate (Figure 4.6B) can be related to equation 4.7 more particularly on equation 4.8 and 4.9. Experimental data of initial rate vs concentration of species(es) can be fitted with good precision to equation 4.8 and 4.9, which is again a hyperbolic equation. Interestingly, the rate of the reaction exhibited linear dependence on $[QDC_{ZnO}]$ upto much higher concentration ratio of $[QDC_{ZnO}]$ / $[QD_{ZnS}]$, whereas,

linear dependence on [QD_{ZnS}] was observed upto relatively much lower concentration ratio of [QD_{ZnS}] / [QDC_{ZnO}]. This was observed because $k_a' > k_a$, and for that reason denominator of equation 4.7 is mainly dominated by the term associated with k_a' by multiplication.

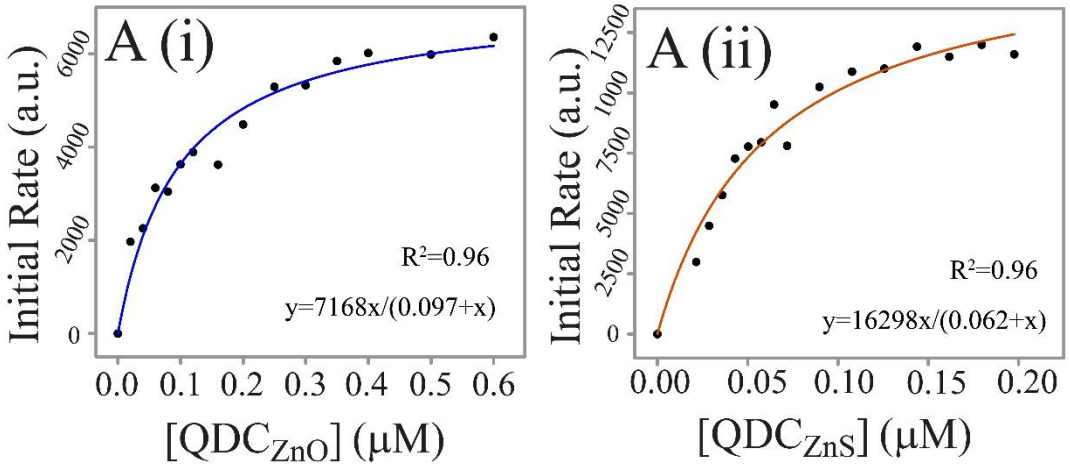

Figure 4.7. (A) Hyperbolic fitting (according to equation 4.8 and 4.9) of plot of Initial Rate versus concentration of reaction between ZnO-HQS QDC to ZnS Qdots at (i) variable concentration of ZnO-HQS QDC keeping concentration of ZnS Qdot fixed and (ii) variable concentration of ZnS Qdot keeping concentration of ZnO-HQS QDC fixed. In these fitting plots we have considered the point (0,0)

4.2.6 Plausible Mechanism of the Complex Transfer Reaction.

Thus, the overall reaction is a manifestation of competition between two parallel adsorption equilibria, which are dependent on solubility of the departing complex in a particular solvent and adsorption coefficients of the same on the Qdot surfaces (Scheme 4.1). In a dispersion of ZnO-HQS QDC, certain amount of desorbed Z-type ligand or complex – here $Zn(QS)_2$ – always exists because of dynamic adsorption equilibrium between ZnO surface and the complex in the medium, which was substantiated by NMR spectroscopic investigations.[11] For a particular amount of ZnO-HQS QDC and a solvent system, constant amount of desorbed complex persists – that initiates the reaction with ZnS Qdot and consequently equilibrium shifts towards right for reaction 1 (equation 1). Hence, the initial desorbed complex can solely account for the initial rate of the reaction. At relatively higher concentrations of ZnS Qdot, the available surface site is greater in number than that of desorbed complex molecule (Z-type ligand) – leading to linear dependence of initial rate on [QDC_{ZnO}] and independent of [QD_{ZnS}]. On the other hand, at lower concentrations of ZnS Qdots, initially all the desorbed complex molecule cannot be accommodated on ZnS surface because of lack of surface sites, leading to linear

dependence of initial rate on [QD_{ZnS}] and independent of [QDC_{ZnO}]. Except for significantly lower concentrations of ZnS Qdot, the rate of attachment of $Zn(QS)_2$ on ZnS surface depends on the rate of desorption of Z-type ligand i.e., $Zn(QS)_2$ complex from ZnO surface ($r=Nk_d\theta$).

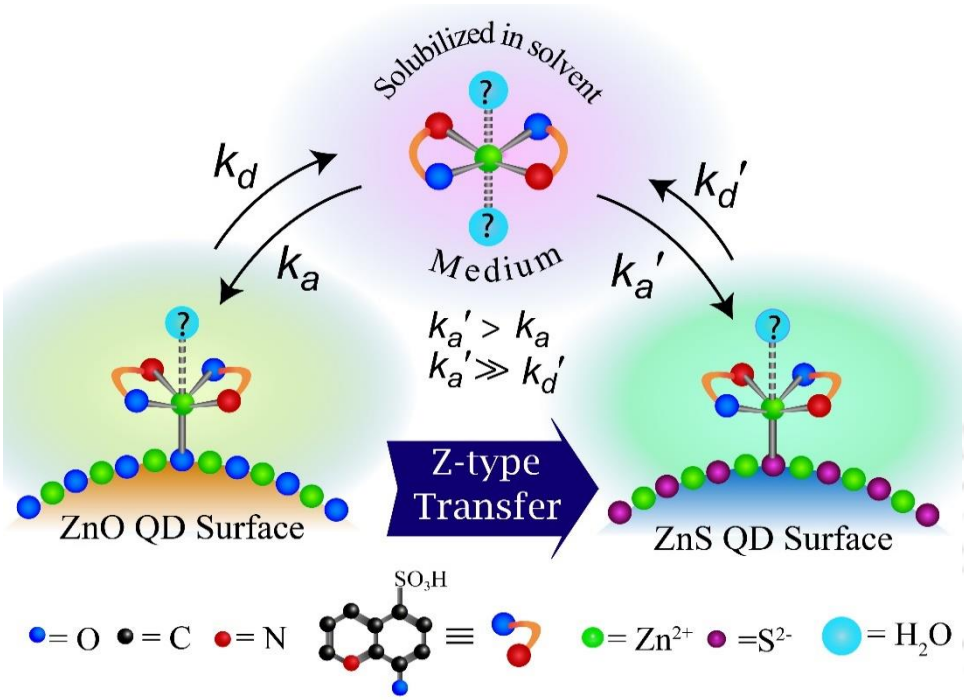

Scheme 4.1. Plausible mechanism of complex [$Zn(QS)_2$] (Z-type ligand) transfer from ZnO Qdot surface to ZnS Qdot surface considering Langmuir adsorption model.

4.3 Conclusion.

In conclusion, HQS ligand transfer reaction from ZnO Qdot surface to ZnS Qdot surface was successfully demonstrated, which was occurring by means of $Zn(QS)_2$ complex migration as opposed to conventional knowledge of 'ligand' transfer. Solubility of the migrating complex affected the reaction rate and the feasibility of the reaction significantly. The reaction pathway was successfully modelled using Langmuir adsorption model and considering steady state approximation of the intermediate complex. It was the first time report of inter Qdots Z-type ligand (or complex) transfer solely driven by the stability of the complex provided by the dangling anions through attachment. Importantly, the stability of inorganic complex on the surface of a Qdot not only provided by the cations but also by the anions thus driving the transfer of the complex from one Qdot surface to the other. This mechanistic approach to understand

the complex transfer reaction between Qdots will certainly enrich the concept of ligand binding, stability and reaction on the surface of Qdots. Further, it is our quest to know whether cation driven complex transfer reaction is possible. In addition, our future work is focused on surface ligand exchange reaction between different quantum dots.

4.4 Bibliography.

1. Roy, S.; Pramanik, S.; Bhandari, S.; Chattopadhyay, A. Surface Complexed ZnO Quantum Dot for White Light Emission with Controllable Chromaticity and Color Temperature. *Langmuir* **2017**, *33*, 4627–14633.
2. Roy, S.; Bhandari, S.; Chattopadhyay, A. Quantum Dot Surface Mediated Unprecedented Reaction of Zn^{2+} and Copper Quinolate Complex. *J. Phys. Chem. C* **2015**, *119*, 21191–21197.
3. Bhandari, S.; Khandelia, R.; Pan, U. N.; Chattopadhyay, A. Surface Complexation-Based Biocompatible Magnetofluorescent Nanoprobe for Targeted Cellular Imaging. *ACS Appl. Mater. Interfaces* **2015**, *7*, 17552–17557.
4. Bhandari, S.; Khandelia, R.; Pan, U. N.; Chattopadhyay, A. Surface Complexation-Based Biocompatible Magnetofluorescent Nanoprobe for Targeted Cellular Imaging. *ACS Appl. Mater. Interfaces* **2015**, *7*, 17552–17557.
5. Lü, X.; Yang, J.; Fu, Y.; Liu, Q.; Qi, B.; Lü, C.; Su, Z. White light emission from Mn^{2+} Doped ZnS Nanocrystals Through the Surface Chelating of 8-hydroxyquinoline-5-sulfonic Acid. *Nanotechnology* **2010**, *21*, 115702.
6. Bhandari, S.; Roy, S.; Chattopadhyay, A. Enhanced Photoluminescence and Thermal Stability of Zinc Quinolate Following Complexation on the Surface of Quantum Dots. *RSC Adv.* **2014**, *4*, 24217-24221.
7. Boles, M. A.; Ling, D.; Hyeon, T.; Talapin, D. V. The Surface Science of Nanocrystals. *Nat. Mat.* **2016**, *15*, 141–153.
8. Aruda, K. O.; Amin, V. A.; Thompson, C. M.; Lau, B.; Nepomnyashchii, A. B.; Weiss, E. A. Description of the Adsorption and Exciton Delocalizing Properties of p-Substituted Thiophenols on CdSe Quantum Dots. *Langmuir* **2016**, *32*, 3354−3364.
9. Koole, R.; Schapotschnikow, P.; Donegá, C. M.; Vlug, T. J. H.; Meijerink, A. Time-Dependent Photoluminescence Spectroscopy as a Tool to Measure the Ligand Exchange Kinetics on a Quantum Dot Surface. *ACS Nano* **2008**, *2*, 1703−1714.
10. Bullen, C.; Mulvaney, P. The Effects of Chemisorption on the Luminescence of CdSe Quantum Dots. *Langmuir* **2006,** *22*, 3007–3013.
11. Ji, X.; Copenhaver, D.; Sichmeller, C.; Peng, X. Ligand Bonding and Dynamics on Colloidal Nanocrystals at Room Temperature: The Case of Alkylamines on CdSe Nanocrystals. *J. Am. Chem. Soc.* **2008**, *130*, 5726–5735.

Chapter 5

Duality in the Photoluminescence Intermittency of Quantum Dot Complex

This chapter is a description of the concurrent photoluminescence intermittency behaviors of a blue emitting $Zn(MSA)_2$ complex and orange emitting Mn^{2+}-doped ZnS quantum dot (Qdot) with the complex being present on the surface of the Qdot. The optical properties of the Qdot complex (QDC: the complex and the Qdot together) were probed at a few particle level using confocal laser scanning microscopy under super-resolution mode. Notably, the QDC exhibited blinking characteristics similar to those of Mn^{2+}-doped ZnS Qdot and $Zn(MSA)_2$ complex when probed at the Qdot and complex emission peaks separately. The observed square wave blinking with respect to their constituent's emission peaks, indicated the dual nature of QDC at particle level consisting of a few QDC. Interestingly, $Zn(MSA)_2$ complex, when present in QDC, was more photostable than as an independent complex.

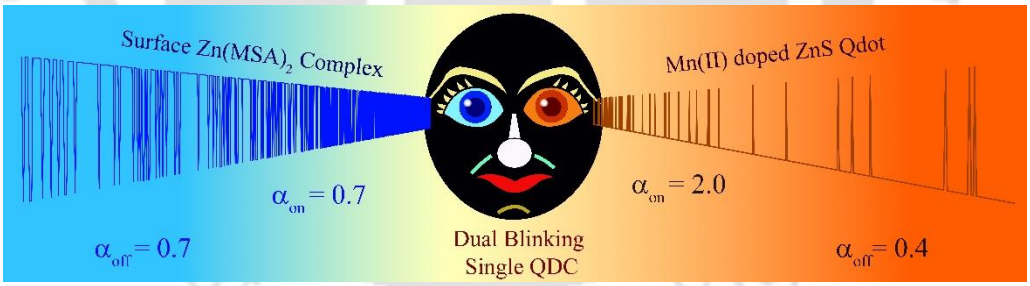

*Manuscript to be submitted.

5.1 Experimental.

5.1.1 Materials.

Manganese acetate tetrahydrate (Merck), zinc acetate dihydrate (Merck), sodium sulphide flakes (Merck), 1 M methyl amine in methanol (Sigma Aldrich), salicylaldehyde (Sigma Aldrich), and methanol (Merck), hexane (Merck), ethyl acetate (Merck), silica gel mesh (Merck), potassium bromide (Sigma aldrich) were procured and used directly without any purification. Milli-Q grade water was used for synthesis and purification of products.

5.1.2 Synthesis of Mn doped ZnS Qdots.

Synthesis of Mn^{2+} doped ZnS Qdots was carried out in aqueous environment following a reported protocol.[1-2] In brief, ~10.0 mg of manganese acetate and ~34.0 mg sodium sulfide were added to 5.0 mM 50.0 mL aqueous solution of zinc acetate taken in a round bottom flask. The resulting milky white dispersion was centrifuged with a speed of 25 000 rpm for 15 min and repeatedly washed with methanol. Lastly, the so obtained pellet was redispersed in 100 mL of methanol and used for further experiments.

5.1.3 Synthesis of N-methylsalicylaldimine (MSA).

A reported condensation reaction between salicylaldehyde and methylamine was followed to synthesize *N*-methylsalicylaldimine (MSA).[3-4] In brief, 2.0 mmol of methylamine was added dropwise to a solution of 2.0 mmol of salicylaldehyde in 20.0 mL of methanol and the reaction mixture was allowed to stir for 4 h at 25 °C. The appearance of dense yellow color in the mixture confirmed the successful formation of the MSA. Lastly, the resulting yellow color product was purified using column chromatography.

5.1.4 Synthesis of Dual Emitting QDC.

A dual emitting QDC was synthesized following room temperature reaction of 30.0 μL of 1.0 mM MSA (soluble in methanol) with 200.0 μL of as synthesized Mn^{2+} doped ZnS Qdots (having absorbance of 0.22 at 330 nm) in 3.0 mL methanol. The reaction was allowed to continue for 10.0 min. The resulting mixture was centrifuged with a speed of 25 000 rpm for 15 min and repeatedly washed with methanol. Lastly, the so obtained pellet was redispersed in the same amount of methanol and used for further

experiments. The dispersion (having absorbance of 0.22 at 330 nm) of QDC was deposited on a glass cover slip and then was dried at room temperature, which was followed by using the same for imaging and blinking analyses.

5.1.5 Confocal Microscopic Measurements and Blinking Analysis.

Zeiss LSM-880 confocal laser scanning microscope (equipped with a 355 nm diode-pumped solid-state UV laser (63 mW) for excitation and Plan-Apochromat, 63x /1.40, oil- immersion) was used to record imaging and for blinking analysis of the QDC, Qdot and complex. The samples were prepared on glass cover slips as mentioned above. The blinking profile were recorded in acquisition mode under super resolution with the frame size of 64 × 64 μm^2, binning time of 27 ms, [5-6] excitation power of 63 mW and time duration of 27 s for each particle and the so obtained images and data were analyzed using ZEN black software.

5.1.6 Calculation of Probability Density Distributions of On and Off States.

The on and off state probability distributions of QDC, Qdot and complex were calculated by using the reported method[6-10] and the following equation:

$$P_i(t) = \frac{N_i(t)}{N_{i,\,total}} \times \frac{1}{\Delta t_{i,\,av}}$$ (i= on or off).

where P_i = probability density of on or off events at time t

N_i = number of on or off events

$N_{i,total}$ = total number of events and

$\Delta t_{i,\,av}$ =average of the time intervals to the events.

These P_{on} or P_{off} distributions can be fitted to the truncated power law:

$P_i(t) = B_i\, t^{-\alpha} \exp(-\mu_i t)$, (i=on or off);

where B= amplitude, α= power law exponent, μ= saturation rate.

5.1.7 Calculation of Quantum Yield from Confocal Microscopy.

(i) Calculation of concentration of Qdot and QDC:

From TEM analysis diameter of the Mn^{2+} doped ZnS Qdot as well as QDC was found to be, d = 3.29 nm. So, radius = 1.645 nm or 16.45 Å.

Hence, for a single Qdot volume, V = 1.86 × 104 $Å^3$

From SAED and powder XRD pattern of Qdot, zinc blende lattice structure was observed.[1-2] Now, volume of single sphalerite zinc blende cell, a = 157.55 $Å^3$. So, the

number of unit wurtzite cell per Qdot = (V/a) = 118.34. So, the number of Zn per Qdot = 4 × 118.34 = 473 [as a unit sphalerite cell consists four metal ions].

Qdot was dispersed in 50.0 mL of methanol (instead of typical 100 mL for other experiments) and used for absorbance measurement. For preparing QDC for absorbance analysis, 50.0 mL of prepared Qdot added with 1.5 μL of 1.0 mM MSA was centrifuged and dispersed in 20.0 mL of methanol (instead of typical 100 mL for other experiments). From ICP-AES analysis, it was found that concentration of total Zn^{2+} ion present in stock solution of as prepared Qdot = 1.84 mM.

So, concentration of Qdot = 3.9 μM.

From ICP-AES analysis, it was found that concentration of total Zn^{2+} ion present in stock solution of as prepared QDC = 2.59 mM

So, concertation of QDC = 5.5 μM.

(ii) Calculation of molar extinction coefficient and absorption cross section:

The absorption cross section was calculated by using the following formula: [11]

absorption cross section $\sigma_{sample} = (2.303 \times 10^3 \times \varepsilon_{sample}) / N_A = (2303 \times \varepsilon_{sample}) / N_A$

where, ε_{sample} and N_A stand for molar extinction co-efficient and Avogadro number respectively.

Linear fitting of the plot of absorbance (at 355 nm) vs concentration provided the value of molar extinction coefficient, ε = slope.

From Figure A.5.1 value of molar extinction coefficient values were found to be as follows.

molar extinction coefficient of Qdot, $\varepsilon_{QD} = 3.44 \times 10^5$ $mol^{-1}.cm^2$.

molar extinction coefficient of QDC, $\varepsilon_{QDC} = 3.25 \times 10^5$ $mol^{-1}.cm^2$.

molar extinction coefficient of rhodamine-6G, $\varepsilon_{Rh\text{-}6G} = 4.0 \times 10^3$ $mol^{-1}.cm^2$.

So, absorption cross section of Qdot, $\sigma_{QD} = (2303 \times \varepsilon_{QD}) / N_A = 1.32 \times 10^{-15}$ cm^2.

So, absorption cross section of QDC, $\sigma_{QDC} = (2303 \times \varepsilon_{QDC}) / N_A = 1.25 \times 10^{-15}$ cm^2.

So, absorption cross section of rhodamine-6G, $\sigma_{Rh\text{-}6G} = (2303 \times \varepsilon_{Rh\text{-}6G}) / N_A = 1.45 \times 10^{-17}$ cm^2. s

It is to be mentioned here that the obtained value of absorption cross section of Rh6G at 355 nm was 1/13.1 times of the reported (Goldsmith et al.) absorption cross section value 1.9 x 10^{-16} cm^2 at 530 nm.[11] This may be due to the fact that Rh6G showed 14.3 times

higher absorbance at 530 nm compared to that at 355 nm (which is reflected in Figure A.5.2).

(iii) Calculation of quantum yield (QY)

Upper limit of Quantum yield (QY) of Qdot, $QY_{QD} = (I_{QD} / I_{Rh\text{-}6G}) \times (\sigma_{Rh\text{-}6G} / \sigma_{QD}) \times 0.95 = 0.0094$.

Upper limit of Quantum yield (QY) of QDC, $QY_{QDC} = (I_{QDC} / I_{Rh\text{-}6G}) \times (\sigma_{Rh\text{-}6G} / \sigma_{QDC}) \times 0.95 = 0.0089$.

[N_A = Avogadro number; I = intensity calculated from each single particle image using image-J software].

5.1.8 Characterization Techniques:

(i) 600 MHz nuclear magnetic resonance (NMR) spectrometer (Bruker) (ii) Agilent Accurate Mass (LC/MS Q-TOF 6520) spectrometer (iii) Perkin Elmer LAMBDA 750 UV/Vis/NIR spectrophotometer and (iv) HORIBA Jobin Yvon FluoroMax-4 spectrofluorimeter, (v) JEOL JEM-2100 transmission electron microscope (maximum accelerating voltage 200 kV), (vi) Rigaku TTRAX III X-ray diffractometer (with Cu-Kα radiation, λ = 1.54056 Å), (vii) Perkin-Elmer (Model: Spectrum Two) FTIR spectrophotometer, (viiii) Life-Spec-II spectrofluorimeter (Edinburgh Instrument, using Pico Quant 375 nm LASER source) for time-resolved photoluminescence measurement and (ix) CIE-1931 color space of the OSRAM color calculator were used to measure (i) chemical shifts, (ii) molecular mass, (iii) absorption and (iv) photoluminescence (emission, excitation and quantum yield), (v) particle size and lattice fringes, (vi) morphology, (vii) functional groups detection, (viii) life-time and (ix) chromaticity color coordinates, color rending indices and correlated color temperatures of the samples, respectively.

5.2 Results and Discussion:

5.2.1 Characterization of MSA treated Mn doped ZnS Qdot i.e. QDC:

Upon complexation of Mn doped ZnS Qdot with MSA, and then excitation with 355 nm light a new emission peak at 440 nm, due to formation of blue emitting surface $Zn(MSA)_2$ complex was observed (Figure 5.1A). [3,12-13] This was in addition to the original orange emission at 595 nm of Mn^{2+}-doped ZnS Qdots (due to $^6A_1 - {}^4T_1$ transition of Mn^{2+} dopants).[1-2] Additionally, no significant change occurred in the absorption spectrum of Mn^{2+}-doped ZnS Qdots following MSA addition (Figure A.5.3, Appendix). On the other hand, MSA treated Mn^{2+}-doped ZnS Qdots showed two separate excitation peaks at 320 and 365 nm, when emission maxima were probed at 588 and 440 nm, respectively (Figure A.5.4, Appendix). Alternatively, $Zn(MSA)_2$ complex exhibited blue emission (λ_{em}-440 nm), which originates from the highest occupied molecular orbital (HOMO) to the lowest occupied molecular orbital (LUMO) transition, [3-4] while negligible luminescence was observed for $Mn(MSA)_2$ complex at an excitation wavelength of 355 nm (Figure A.5.5, Appendix). The combined blue emitting surface $Zn(MSA)_2$ complex and Mn^{2+}-doped ZnS Qdot is called hereafter as QDC. Further, the average emission life times of the QDC were found to be 2.07 ms and 10.36 ns when probed with the emission peaks of Qdot (excited by 330 nm light) and complex (excited by 375 nm laser), respectively (Figure A.5.6 and Table A.5.1, Appendix). Alternatively, only Mn^{2+} doped ZnS Qdots and $Zn(MSA)_2$ complex exhibited average emission life times of 2.17 ms and 5.44 ns, respectively (Figure A.5.6 and Table A.5.1, Appendix). The similarity in the emission life times of QDC with those of Mn^{2+} doped ZnS Qdot and $Zn(MSA)_2$ complex, clearly supported the duality in the luminescence characteristics of Mn^{2+} doped ZnS Qdot and $Zn(MSA)_2$ complex in a QDC. The successful formation of $M(MSA)_2$ (M = Zn / Mn) complex on the surface of Mn^{2+}-doped ZnS Qdots was further confirmed by observing the presence of M-O and M-N stretching frequencies [3-4] in the fourier transform infrared spectroscopic (FTIR) analysis of QDC, the details of which are described in the appendix (Figure A.5.7, Appendix). Additionally, the structural integrity, especially particle size, lattice fringe and selected area diffraction pattern of cubic Mn^{2+}-doped ZnS Qdots, [1-2] following reaction with MSA, remained unaltered (Figure A.5.8, Appendix). These clearly indicated the successful formation of dual emitting QDC.

5.2.2 Duality in Blinking Characteristics of QDC:

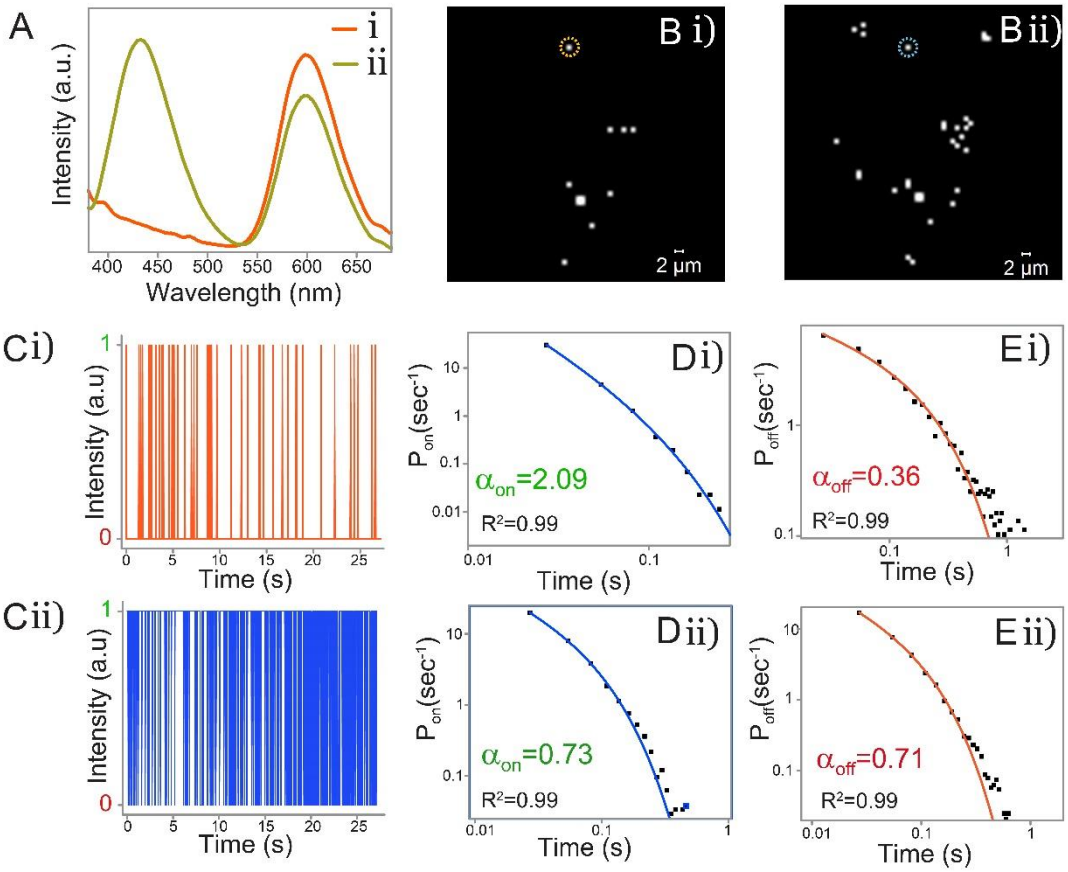

Figure 5.1. **(A)** Emission spectra (λex – 355 nm) of (i) Mn^{2+}-doped ZnS Qdots and (ii) QDC. **(B)** Superresolution confocal laser scanning microscopic (CLSM) images (scale bar-2.0 μm) and **(C)** representative time-dependent blinking profile (related to the particle marked in Figure 1B) of QDC recorded with regard to emission peaks of (i) Qdot (emission range: 570-650 nm) and (ii) complex (emission range: 465-525 nm). Probability densities of **(D)** on-states (P_{on}) and (E) off-states (P_{off}) of QDC when probed with emission peaks of (i) Qdot (emission range: 570-650 nm) and (ii) complex (emission range: 465-525 nm).

We were further interested in pursuing the optical properties of the QDC at the level of a few particles. This was attempted by following blinking characteristics and quantum yield measurement using confocal laser scanning microscopy (CLSM) under super resolution mode [13] (with 355 nm laser). Figures 5.1B (i) and (ii) display the representative super resolution CLSM images of the QDC, acquired with respect to two different emission channels: (i) Qdot channel: in the range of 570-650 nm and (ii) complex channel: in the range of 465-525 nm, respectively. The representative blinking profiles, with respect to two different emission channels (Qdot and complex), of the QDC were recorded against the marked particles in Figures 5.1B(i) and 5.1B(ii). Interestingly, the difference in the square wave blinking profiles and corresponding blinking activities,

of particle consisting of a few QDC, were noticed when probed with two different emission channels for a single wavelength excitation (Figure 5.1C(i) and (ii)). The square wave blinking profiles indicated dual nature of QDC with regard to two different emission channels at a level of particle consisting of a few QDC. Notably, the on and off time probability distributions of QDC, with respect to two different emission peaks, could be fitted with a truncated power law [7-10] through a log-log plot as also with the Qdot. That means the rates of trapping and de-trapping of photo-excited electrons in Qdots and QDC follow distributed kinetics, accompanied with an exponential cut off. The frame size of 64 × 64 μm^2, binning time of 27 ms, [5-10] excitation power of 63 mW and time duration of 27 s were used to record the blinking statistics of 50 particles - each consisting of a few QDC. The value of the exponent (α_{on} =2.09) of the on time probability distribution was found to be higher compared to the exponent (α_{off} =0.36) of the off time probability distribution of particle (consisting of a few QDC), when probed with Qdot channel (Figure 5.1D(i) and Figure 5.1E(i) and Table 5.1). On the other hand, probing with complex channel, particle (consisting of a few QDC) exhibited equal exponent values (α_{off}=α_{on}=0.7) for both the on and off time probability distributions (Figure 5.1D(ii) and Figure 5.1E(ii) and Table 5.1). The difference in the exponents of blinking statistics of QDC, probing with two different emission channels, clearly demonstrated the presence of duality in photoluminescence intermittency at particle level – that might be consisted of a few QDCs. On the other hand, as such particle consisting of a few Mn^{2+}-doped ZnS Qdots exhibited square wave blinking, with α_{off} =0.57 and α_{on}=1.73, which are close to the observed exponents values of off and on time distributions when QDC probed with Qdot emission channel (Figure A.5.9 and Table 5.1, Appendix). Likewise, particle consisting of a few MSA treated undoped ZnS Qdots (having possibility of forming only $Zn(MSA)_2$) exhibited the off and on time exponent values of 0.96 and 0.45 - which are close to the observed exponents values of off and on time distributions when QDC was probed with complex emission channel (Figure A.5.10 and Table 5.1, Appendix). The closeness of the exponents of the MSA treated ZnS Qdots with that of dual emitting QDC, probing with complex and Qdot peaks, respectively, clearly supported the presence of the similar type of $Zn(MSA)_2$ complex in QDC as well as in MSA treated ZnS Qdots. However, the observed deviation in the exponent values may be either due to the difference in size and composition of the Mn doped ZnS Qdots,

compared to only ZnS Qdots or due to the presence of nonfluorescent $Mn(MSA)_2$ complex in the case of QDC formed out of reaction between Mn^{2+}-doped ZnS Qdots and MSA, in comparison to only MSA treated ZnS Qdots.

Table 5.1. Fitting parameters for probability density of on and off-states for **(A)** QDC (MSA treated Mn^{2+} doped ZnS Qdots) at two different emission peaks (Qdot and complex), **(B)** Only Mn^{2+} doped ZnS Qdots **(C)** QDC (MSA treated undoped ZnS Qdots) and (D) $Zn(MSA)_2$ complex at a few particle level.

Samples	Emission Peak	Excitation	α_{on}	α_{off}
(A) QDC (MSA treated Mn^{2+} doped ZnS Qdots)	Qdot	355 nm laser	2.09 ± 0.06	0.36 ± 0.02
	Complex		0.74 ± 0.03	0.71 ± 0.02
(B) Mn^{2+} doped ZnS Qdots	Qdot		1.74 ± 0.21	0.58 ± 0.02
(C) MSA treated ZnS Qdots	Complex		0.96 ± 0.03	0.45 ± 0.02
(D) $Zn(MSA)_2$ Complex	Complex		1.04 ± 0.12	0.37 ± 0.05

5.2.3 Quantum Yield at Particle Level:

Importantly, presence of the two different emissions within a particle consisting of a few QDC; one at 440 nm and another at 595 nm – of QDC, for a single wavelength of excitation (recorded by using CLSM) clearly demonstrated the dual nature of QDC at particle level. (Figure A.5.11, Appendix). Interestingly, upper limit of the quantum yields (QYs; measured using rhodamine 6G as a standard dye) of QDC and Mn^{2+} doped ZnS Qdot, at particle level (consisting of a few QDC/Qdots) were found to be 0.9 and 0.9 %, respectively (Table A.5.2, Appendix). These were calculated based on the emission intensity of particles (consisting of a few QDC) and the absorption cross section.[14] The details of the calculation have been described in section 3.1.7 (Figure A.5.1 and Table A.5.2, Appendix). On the other hand, 1.0 and 0.8 % of QYs were obtained for QDC and Mn^{2+} doped ZnS Qdot dispersions (Table A.5.2, Appendix). The closeness of the results supported the possibly single particle nature of the QDC as measured using CLSM.

5.2.4 Probing Enhanced Photostability of Complex on Qdot Surface by Blinking Profile:

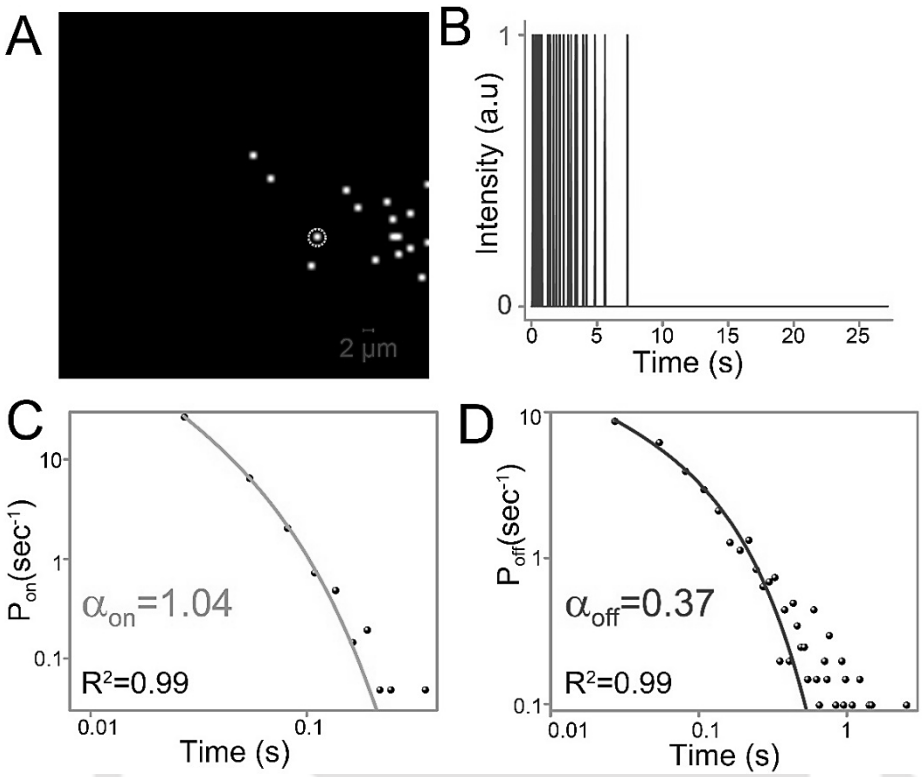

Figure 5.2. (A) Superresolution confocal laser scanning microscopic (CLSM) image (scale bar-2.0 μm) and **(B)** representative time-dependent blinking profile (related to the particle marked in Figure 3A) and corresponding probability densities of **(C)** on-states (P_{on}) and **(D)** off-states (P_{off}) of $Zn(MSA)_2$ when probed with emission channel of the complex (emission range: 465-525 nm).

An important aspect of the QDC was the enhanced photostability of the complex present on the surface of the Qdto. Thus $Zn(MSA)_2$ complex exhibited square wave blinking, with α_{off} =0.5 and α_{on} =1.0 and subsequent photo bleaching after 5 s when subjected to analysis under CLSM (λ_{ex}- 355 laser; Figure 5.2 and Table 5.1). On the other hand, no blinking studies could be performed for $Mn(MSA)_2$ as they are nonfluorescent in nature. Furthermore, the presence of blinking characteristics of the QDC (with regard to emission peak of the complex) for 140 s clearly supported the extraordinary stability against the photobleaching of the $Zn(MSA)_2$ complex, present in QDC compared to only $Zn(MSA)_2$ complex at particle level (consisting of a few QDC) and consequently ruling out the possibility of the presence of the longer off times in QDC (Figure 5.1 and Figure 5.3). The enhanced photostability of the inorganic complex, being attached to the surface

of Qdot might have occurred via involvement of dangling chalcogenide bond, as is the case of our earlier observations.[1-2, 15-16]

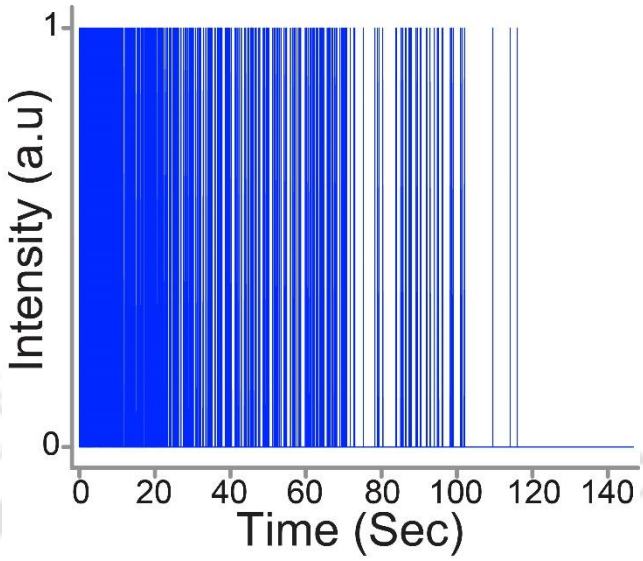

Figure 5.3. A representative time-dependent blinking profile of QDC, formed out of a complexation between MSA and undoped ZnS Qdot and recorded with regard to emission peak of complex (465 - 525 nm) for a longer time (150 s) compared to only $Zn(MSA)_2$ complex. This is in support of the extraordinary photostablity of the $Zn(MSA)_2$ complex, present in QDC, compared to only $Zn(MSA)_2$ complex.

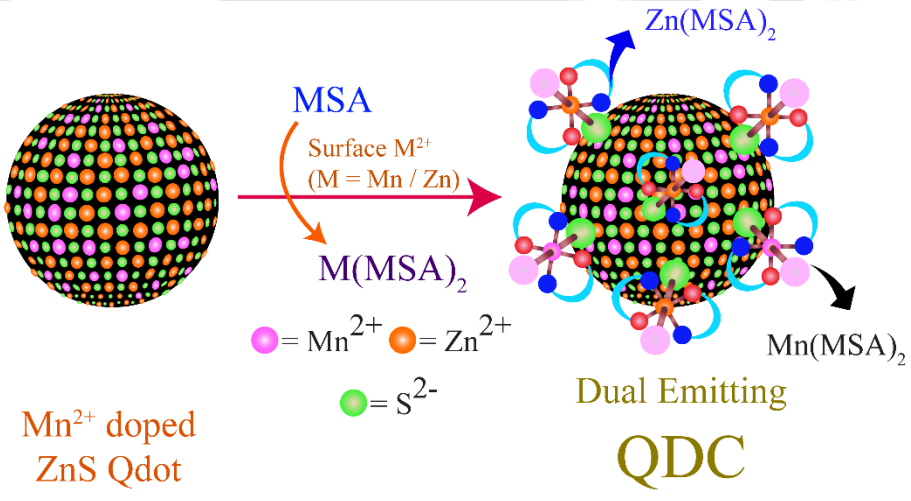

Scheme 5.1. Schematic representation of the formation of dual emitting QDC from Mn^{2+}-doped ZnS Qdot, following complexation with MSA.

Schematically, the formation of QDC, consisting of two differently emitting species – i.e., orange emitting Mn^{2+}-doped ZnS Qdots and blue emitting $M(MSA)_2$ complex, is shown in Scheme 5.1. Notably, QDC exhibited two different independent emissive pathways due to the presence of two different luminescent species – orange emitting Mn^{2+} dopant ($^6A_1$–$^4T_1$ transition) and blue emitting $M(MSA)_2$ complex

(HOMO-LUMO transition) with different blinking profiles and enhanced photostability of the complex while on the surface of the Qdot.

5.3 Conclusions:

In conclusion, the concurrent particle level (consisting of few QDC) photoluminescence intermittency behaviors of blue emitting $Zn(MSA)_2$ complex (λ_{em}-440 nm) and orange emitting Mn^{2+}-doped ZnS Qdot (λ_{em}-590 nm) present in quantum dot complex (QDC) have been reported. This is based on the square wave and independent blinking characteristics of the Qdot and the complex as observed through their corresponding emission peaks and upper limit of particle level QY measurements, using confocal laser scanning microscopy under super resolution mode. The QDC showed the blinking statistics and upper limit of particle level quantum yields akin to those of only Mn^{2+}-doped ZnS Qdot and $Zn(MSA)_2$ complex. Remarkably, the particle level enhanced photostability of the $Zn(MSA)_2$ complex when bonded to the surface of a Qdot provided a new opportunity for their probe and possible use. The presence of two independent emitting species on a QDC with different intermittency behaviors provides an opportunity for systematic design of multifunctional nanomaterials possibly at a few particle resolution. Our future work will aim towards finding out possible presence of different types of emitting complexes on the surface of a single quantum dot.

5.4 Bibliography.

1. Pramanik, S.; Bhandari, S.; Roy, S.; Chattopadhyay, A. Synchronous Tricolor Emission-Based White Light from Quantum Dot Complex. *J. Phys. Chem. Lett*. **2015**, *6*, 1270– 1274.
2. Bhandari, S.; Roy, S.; Pramanik, S.; Chattopadhyay, A. Double Channel Emission from a Redox Active Single Component Quantum Dot Complex. *Langmuir*, **2015**, *31*, 551-561.
3. Komiya, N.; Okada, M.; Fukumoto, K.; Jomori, D.; Naota, T. Highly Phosphorescent Crystals of Vaulted trans-Bis- (salicylaldiminato)platinum(II) Complexes. *J. Am. Chem. Soc*. **2011**, *133*, 6493−6496.
4. Roy, S.; Pramanik, S.; Bhandari, S.; Chattopadhyay, A. Surface Complexed ZnO Quantum Dot for White Light Emission with Controllable Chromaticity and Color Temperature. *Langmuir* **2017**, *33*, 14627–14633.
5. Zhou, J.; Zhu, M.; Meng, R.; Qin, H; Peng, X. Ideal CdSe/CdS Core/Shell Nanocrystals Enabled by Entropic Ligands and Their Core Size-, Shell Thickness-, and Ligand-Dependent Photoluminescence Properties. *J. Am. Chem. Soc.* **2017**, *139*, 16556–16567.
6. Zhang, A.; Dong, C.; Liu, H.; Ren, J. Blinking Behavior of CdSe/CdS Quantum Dots Controlled by Alkylthiols as Surface Trap Modifiers. *J. Phys. Chem. C* **2013**, *117*, 24592−24600.
7. Li, B.; Zhang, G. F.; Wang, Z.; Li, Z. J.; Chen, R. Y.; Qin, C. B.; Gao, Y.; Xiao, L. T.; Jia, S. T. Suppressing the Fluorescence Blinking of Single Quantum Dots Encased in N-type Semiconductor Nanoparticles. *Sci. Rep*. **2016**, *6*, 32662.
8. Xu, W.; Liu, W.; Schmidt, J. F.; Zhao, W.; Lu, X.; Raab, T.; Diederichs, C.; Gao, W.; Seletskiy, D. V.; Xiong, Q. Correlated Fluorescence Blinking in Two-Dimensional Semiconductor Heterostructures. *Nature* **2016**, *541*, 62– 67.
9. Bae, Y. J.; Gibson, N. A.; Ding, T. X.; Alivisatos, A. P.; Leone, S. R. Understanding the Bias Introduced in Quantum Dot Blinking Using Change Point Analysis. *J. Phys. Chem. C* **2016**, *120*, 29484– 29490.
10. Crouch, C. H.; Sauter, O.; Wu, X.; Purcell, R.; Querner, C.; Drndic, M.; Pelton, M. Facts and Artifacts in the Blinking Statistics of Semiconductor Nanocrystals. *Nano Lett*. **2010**, *10*, 1692– 1698.
11. Dolan, G.; Goldschmidt. C. R. A new method for absolute absorption cross-section measurements: rhodamine-6G excited singlet-singlet absorption spectrum *Chem. Phys. Lett*. **1976**, *39*, 320-322.
12. Pramanik, S.; Bhandari, S.; Pan, U. N.; Roy, S.; Chattopadhyay, A. A White Light-Emitting Quantum Dot Complex for Single Particle Level Interaction with Dopamine Leading to Changes in Color and Blinking Profile. *Small* **2018**, *14*, 1800323.
13. Schermelleh, L.; Heintzmann, R.; Leonhardt, H. A guide to super-resolution fluorescence microscopy. *J. Cell Biology* **2010**, *190*, 165-175.
14. Hu, J.; Zhang, C. Y. Simple and Accurate Quantification of Quantum Yield at the Single-Molecule/Particle Level. *Anal. Chem.* **2013**, *85*, 2000– 2004.
15. Bhandari, S.; Roy, S.; Chattopadhyay, A. Enhanced Photoluminescence and Thermal Stability of Zinc Quinolate Following Complexation on the Surface of Quantum Dot *RSC Adv.* **2014**, 4, 24217–24221.
16. Roy, S.; Bhandari, S.; Chattopadhyay, A. Quantum Dot Surface Mediated Unprecedented Reaction of $Zn^{2+}$and Copper Quinolate Complex. *J. Phys. Chem. C* **2015**, *119*, 21191– 21197.

Chapter 6A

Surface Complexed ZnO Quantum Dot for White Light Emission with Controllable Chromaticity and Color Temperature

Herein, it is reported that the blue emitting $Zn(MSA)_2$ complex can be formed on the surface of a yellow emitting ZnO quantum dot (Qdot) – out of a complexation reaction between N-methylsalicylaldimine (MSA) and ZnO Qdot. This led to formation of a highly luminescent, photostable, single component nanocomposite that emit bright natural white light, with (i) chromaticities of (0.31, 0.38) and (0.31, 0.36), (ii) color rendering indices (CRI) of 74 and 82 and (iii) correlated color temperatures (CCT) of 6505 K and 6517 K, in their solution and solid phases, respectively. Importantly, the control over the chromaticity and CCT – depending upon the degree of complexation – makes the reported nanocomposite a potential new advanced material in fabricating cost-effective single component white light emitting devices (WLED) of choice and design in near future.

*[Roy et al. *Langmuir*, 2017, 33, 14627-14633.] - Reproduced with permission from The American Chemical Society.

6.1 Experimental.

6.1.1 Materials.

Zinc acetate dihydrate (Merck), potassium hydroxide (KOH, Merck), salicylaldehyde (Sigma Aldrich), 1 M methyl amine in methanol (Sigma Aldrich), quinine sulfate (Fluka, USA), sulphuric acid (Merck, India) and ethanol (Tedia) were purchased and used directly without any purification.

6.1.2 Synthesis of ZnO Qdots.

ZnO quantum dots were prepared – following an earlier reported method – in ethanolic medium under basic condition.[1-2] In brief, 2.0 mL 0.5 M ethanolic KOH solution was added to 5.0 mM 50.0 mL ethanolic zinc acetate solution under vigorous stirring at room temperature (at 25 ºC) and the reaction mixture was allowed to stir for ~1 h maintaining same experimental conditions. Then, the so obtained milky white reaction mixture was centrifuged at 25,000 rpm speed for 15 min and the resulting pellet was washed with ethanol. This cycle was repeated for two times in order to remove excess salts that were used during synthesis. Then, the final pellet was dispersed in 100 mL of ethanol, which was used for further experiments.

6.1.3 Synthesis of N-methylsalicylaldimine (MSA).

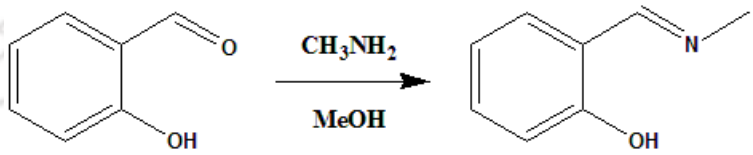

Scheme 6.1. Schematic representation of the formation of N-methylsalicylaldimine **(**MSA) out of a condensation reaction between salicylaldehyde and methyl amine.

The Schiff base, N-methylsalicylaldimine (MSA) was synthesized following an earlier reported condensation reaction between salicylaldehyde and methylamine (Scheme 6.1).[3-6] Then, the so obtained product was purified using column chromatographic technique. Briefly, 2.0 milli mole of salicylaldehyde in 20.0 mL methanol was taken in a round bottom flask. To that solution, 2 milli mole of methyl amine was added dropwise and the reaction mixture was allowed to stir for 4 h at room temperature (at 25 ºC). The complete formation of the MSA was confirmed by observing

the appearance of dense yellow color in the solution mixture. Finally, the product (MSA) obtained from the reaction mixture was purified using column chromatography. The purified MSA was characterized by using high resolution mass spectrometric, NMR, FTIR, UV-vis and photoluminescence (PL) spectroscopic techniques.

6.1.4 Synthesis of white light emitting (WLE) QDC nanocomposite.

At first, the absorbance of ZnO Qdots was fixed to be 0.8 at 350 nm. Then, 1.0 mM MSA (soluble in ethanol) was added sequentially into the ethanolic dispersion of ZnO Qdots at room temperature (25 ^{o}C).The emission and white light parameters such as chromaticity, CRI and CCT were monitored to choose the best condition for the fabrication of white light QDC (Table 6.1). It was found that treatment of 33.2 μM MSA to 3.0 mL ZnO Qdots (having absorbance of 0.8 at an excitation wavelength of 350 nm) was the best condition for synthesizing WLE QDC nanocomposite. The resulting dispersion of the QDC was centrifuged (at a speed of 25000 rpm for 15 min) and repeatedly washed with ethanol. Finally, the pellet was redispersed in same amount of ethanol, which was used for further experiments. The solid form of the QDC was obtained by depositing the dispersion on a quartz substrate and drying at room temperature. The same was used for further experiments.

6.1.5 Characterization Techniques.

(i) 600 MHz nuclear magnetic resonance (NMR) spectrometer (Bruker), (ii) Agilent Accurate Mass (LC/MS Q-TOF 6520) spectrometer, (iii) Perkin Elmer LAMBDA 750 UV/Vis/NIR spectrophotometer, (iv) HORIBA Jobin Yvon FluoroMax-4 spectrofluorimeter, (v) JEOL JEM-2100 transmission electron microscope (maximum accelerating voltage 200 kV), (vi) Rigaku TTRAX III X-ray diffractometer (with Cu-Kα radiation, λ = 1.54056 Å), (vii) Perkin-Elmer (Model: Spectrum Two) FTIR spectrophotometer, (viiii) Life-Spec-II spectrofluorimeter (Edinburgh Instrument, using Pico Quant 336 nm LED source) and (ix) CIE-1931 color space of the OSRAM color calculator were used respectively to measure (i) chemical shifts, (ii) molecular mass, (iii) absorption and (iv) photoluminescence (emission, excitation and quantum yield), (v) particle size and lattice fringes, (vi) morphology, (vii) functional groups detection, (viii) life-time and (ix) chromaticity color coordinates, color rendering indices and correlated color temperatures of the samples, respectively.

6.2 Results and Discussion.

6.2.1 Characterization of ZnO Qdot.

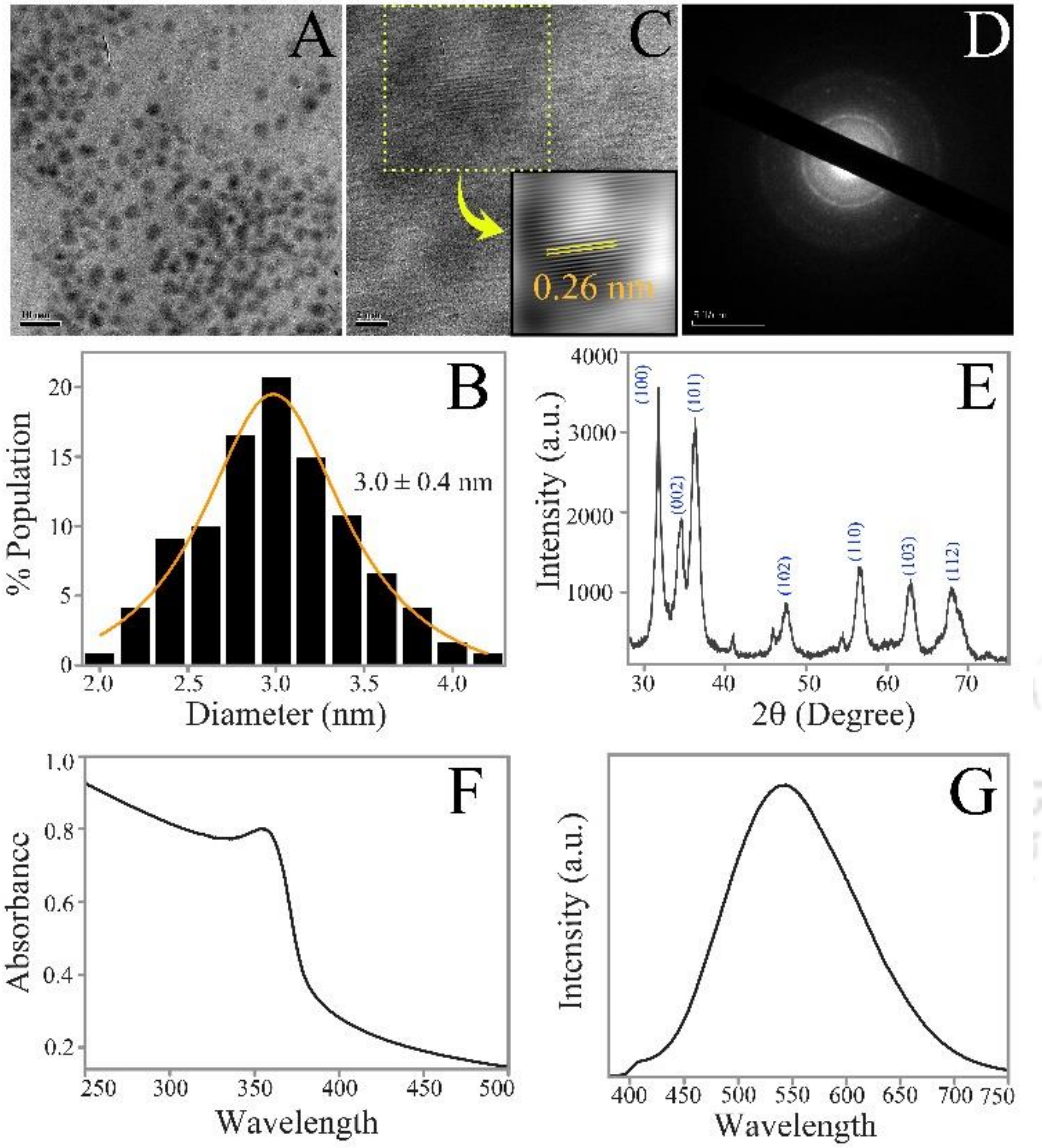

Figure 6.1. (A) Transmission electron microscopic (TEM) image (scale bar-10 nm), **(B)** corresponding particle size distribution, **(C)** high resolution TEM image (scale bar-2 nm) and corresponding inverse fast Fourier transform (IFFT; inset square box) image, **(D)** selected area electron diffraction (SAED) pattern (scale bar-5 nm-1) **(E)** powder x-ray diffraction (XRD) pattern, **(F)** UV-vis and **(G)** emission spectra (λ_{ex}–350 nm) of ligand free ZnO Qdots (in ethanol).

The transmission electron microscopic (TEM) image showed that the average particle size of the synthesized ligand free ZnO Qdots was 3.0 ± 0.4 nm (Figure 6.1A-B). Importantly, the observed 0.26 nm lattice fringe (due to the 002 plane of wurtzite ZnO) in the high resolution TEM confirmed the formation of ZnO Qdots (Figure 6.1C).[1-2] In addition, selected area electron diffraction (SAED) pattern indicated the crystallinity

of the as-synthesized Qdots (Figure 6.1D). Further, the presence of the main characteristics peaks of wurtzite ZnO in the x-ray diffraction pattern is in support of the successful formation of wurtzite ZnO Qdots (Figure 6.1E).[1-2] The as synthesized ligand free ZnO Qdots exhibited an absorption peak at 350 nm and a broad yellow colored emission centered at 545 nm (upon excitation at 350 nm; Figure 6.1F-G). It is to be mentioned here that the literature reports suggest that the source of the broad yellow emission (λ_{max}- 545 nm) of ZnO Qdots is solely from the surface traps created during the synthesis and the control over the surface defects – depending upon the synthesis procedure – decides the emission characteristics, such as the wavelength of emission maximum and photoluminescence quantum yield (PLQY) of ZnO Qdots. [7-10, 1-2, 11-12]

6.2.2 Characterization of MSA Ligand and Zn-MSA Complex.

The successful synthesis of the MSA ligand was confirmed through nuclear magnetic resonance (NMR) and mass spectroscopic techniques (Figure A.6.1 and Figure A.6.2, Appendix). [3-6] The MSA ligand showed an absorption maximum at 316 nm while negligible photoluminescence (at 440 nm) was observed upon excitation with 350 nm light (Figure A.6.3**,** Appendix). Interestingly, upon addition of Zn^{2+} ions into the solution of MSA, the absorbance maximum of MSA was shifted from 316 to 360 nm, while the very weak emission at 440 nm was enhanced (Figure A.6.3, Appendix). The observed changes in absorption maximum and enhancement in emission are possibly due to the electronic transition from the highest occupied molecular orbital (HOMO) to the lowest unoccupied molecular orbital (LUMO) transition in $Zn(MSA)_2$ complex. [3-6] This clearly demonstrated the ability to form highly luminescent metal chelate complexes as reported earlier. [3-6]

6.2.3 Formation and Characterization of QDC out of Reaction between MSA and ZnO Qdot.

On the other hand, following complexation reaction of MSA ligands with the Zn^{2+} ions, being present on the surface of ZnO Qdots, a new emission peak at 440 nm (due to formation of surface $Zn(MSA)_2$ complex) – in addition to the original emission peak at 545 nm due to the Qdots – appeared (Figure 6.2A). Also, no significant change was observed in the absorption peak (at 350 nm) of Qdots upon complexation (Figure A.6.4). The $Zn(MSA)_2$ surface complex incorporated ZnO Qdot is termed here as quantum dot complex (QDC) nanocomposite. The formation of surface $Zn(MSA)_2$

complex was confirmed through observing the main characteristic functional groups of MSA (when coordinated to Zn^{2+}) in the Fourier transformed infrared (FTIR) spectrum of the solid nanocomposite (Figure A.6.5 and Table A.6.1, Appendix).[3-6] Notably, when the ZnO Qdots were treated with MSA, two new peaks at 490 and 545 cm^{-1} – which are due to the formation of Zn-N and Zn-O bonds and generally absent in only MSA – appeared. This clearly indicated the successful formation of $Zn(MSA)_2$ complex on the surface of ZnO Qdots (Figure A.6.5 and Table A.6.1, Appendix). Additionally, the presence of other peaks, due to N-H, C=N, phenolic C-O bonds, with slight shifts, also confirmed the presence of MSA in the form of $Zn(MSA)_2$ complex on the surface of ZnO Qdots (Figure A.6.5 and Table A.6.1, Appendix).

Scheme 6.2. Schematic illustration of the fabrication of white light emitting (WLE) quantum dot complex (QDC) nanocomposite.

Importantly, the TEM and HRTEM analyses of the nanocomposite revealed that there was no significant change in terms of their average particle size (of 3.0 ± 0.4 nm) and lattice fringe of 0.26 nm (due to (002) plane) of the wurtzite ZnO Qdots - following complexation with MSA ligand (Figure A.6.6, Appendix).[1-2] Further, the XRD of the solid WLE QDC nanocomposite supported the preservation of structural integrity (as revealed by the same diffraction pattern) of the wurtzite ZnO Qdots in QDC nanocomposite (Figure A.6.7, Appendix).[1-2] These results clearly demonstrated the successful formation of $Zn(MSA)_2$ complex on the surface of ZnO Qdots, without affecting the structural integrity of wurtzite ZnO Qdots and thus the formation of QDC

nanocomposite – having ZnO Qdot and surface $Zn(MSA)_2$ complex. The role of dangling sulphide ions of the Qdot in the formation and stabilization of the complex on the surface could be conjectured based on current and earlier observations.[13-16] A schematic representation of the formation of the nanocomposite – formed out of a complexation reaction between the presynthesized ligand free ZnO Qdots and an external organic ligand MSA – is shown in Scheme 6.2. The presented nanocomposite consisted of yellow emitting ZnO Qdot and blue emitting surface $Zn(MSA)_2$ complex.

6.2.4 Tunable Color Chromaticity of MSA added ZnO Qdot.

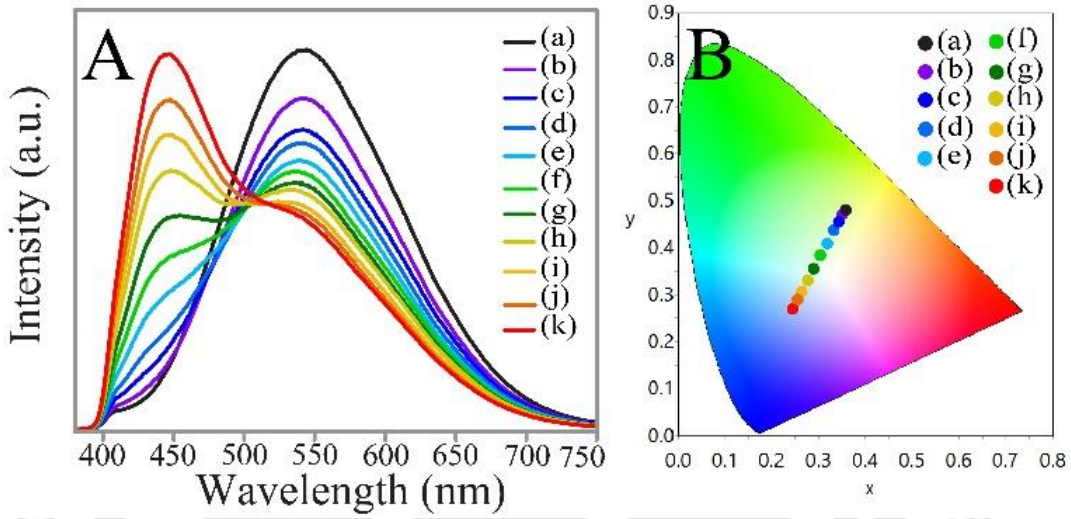

Figure 6.2. **(A)** Emission spectra (λ_{ex}– 350 nm) and **(B)** chromaticity color coordinates in CIE diagram of (a) 0.0, (b) 6.7, (c) 13.3, (d) 19.9, (e) 26.6, (f) 33.2, (g) 39.8, (h) 46.4, (i) 53.0, (j) 59.6, (k) 66.2 μM MSA treated ZnO Qdot dispersion (absorbance of 0.8 fixed at 350 nm).

Further, as shown in Figure 6.2A**,** with increasing concentration of MSA, the emission intensity at 440 nm (due to surface $Zn(MSA)_2$ complex) increased while the emission intensity of the peak at 545 nm (due to ZnO Qdots) decreased simultaneously. It is to be mentioned here that we have particularly used concentration of MSA in the range of 6.7 - 66.2 μM so as to achieve the best conditions for near perfect and high quality white light emission with respect to conventional WLE parameters such as chromaticity, CRI and CCT. As a result, the tunability in chromaticity, CRI and CCT were observed with the concentration of MSA, keeping the concentration of ZnO Qdots constant (absorbance of 0.8 fixed at 350 nm; Figure 6.2B, Table 6.1). For example, QDC, obtained by using 33.2 μM MSA, exhibited chromaticity of (0.31, 0.38), CRI and CCT values of 74 and 6505 K while chromaticity, CRI and CCT values of (0.27, 0.31), 81 and 10524 K, respectively, were measured when 53.0 μM MSA was used for the synthesis

of QDC. The as-synthesized ZnO Qdots exhibited chromaticity of (0.36, 0.48), CRI and CCT values of 63 and 4958 K, respectively. It is important to mention here that ability to control emission parameters – especially CCT – from warm white (5078 K) to cold white (10524 K), based on the presented strategy (without changing the size and morphology of the Qdots), not only would help make fabrication process of WLED simpler and cost effective but also provide a new way for solid state lighting choice. Similarly, upon varying the absorbance at 350 nm (with the value in the range of 0.2-1.2) of ZnO Qdots, for a fixed concentration of MSA (here 33.2 μM was used), the tunability in emission and corresponding color chromaticity, CRI and CCT were also noticed (Figure A.6.8 and Table A.6.2, Appendix). This clearly indicated that the concentration of MSA and the absorbance (which is related to concentration) of Qdots play the key role in deciding the WLE properties of the QDC.

Table 6.1. Tabulated form of chromaticity color coordinates (x,y), color rendering indices (CRI) and correlated color temperatures (CCT) of (a) 0.0, (b) 6.7, (c) 13.3, (d) 19.9, (e) 26.6, (f) 33.2, (g) 39.8, (h) 46.4, (i) 53.0, (j) 59.6, (k) 66.2 μM MSA treated ZnO Qdots (having absorbance of 0.8 at 350 nm) and (c) solid WLE emitting QDC nanocomposite. These parameters were calculated based on the emission spectra in Figure 6.2A (for solution phase) and Figure 6.3C (for solid phase).

Sl No.	Conc. of MSA (μM)	Phase	Chromaticity	CRI	CCT (K)
(a)	0.0	Liquid	(0.36, 0.48)	63	4958
(b)	6.7	Liquid	(0.35, 0.47)	65	5078
(c)	13.3	Liquid	(0.34, 0.45)	67	5233
(d)	19.9	Liquid	(0.33, 0.44)	68	5479
(e)	26.6	Liquid	(0.32, 0.41)	71	5915
(f)	33.2	Liquid	(0.31, 0.38)	74	6505
(g)	39.8	Liquid	(0.29, 0.35)	76	7339
(h)	46.4	Liquid	(0.28, 0.33)	79	8595
(i)	53.0	Liquid	(0.27, 0.31)	81	10524
(j)	59.6	Liquid	(0.26, 0.29)	82	13178
(k)	66.2	Liquid	(0.25, 0.27)	84	19263
Best Condition: 33.2 μM MSA treated ZnO Qdots		Liquid	(0.31, 0.38)	74	6505
		Solid	(0.31, 0.36)	82	6517

6.2.5 White Light Emission from QDC.

The QDC nanocomposite obtained from the treatment of 33.2 μM of MSA with 3.0 mL of ZnO Qdots (dispersion in ethanol; with absorbance of 0.8 at 350 nm) was found to be the optimum condition for achieving the best white light emission as judged by chromaticity, CRI and CCT values (Figure 6.2A-B, Table 6.1 and Figure A.6.8, Table A.6.2, Appendix). This was chosen considering the closeness of three parameters, namely, chromaticity, CRI and CCT of a perfect bright cool white light emitter – which usually exhibits chromaticity of (0.33, 0.33), CRI $\geq$ 80 (as is the case for excellent bright material) and CCT near to 6500 K (as is the case for cool daylight).[17] Furthermore, the absorbance (at 350 nm) of WLE QDC was varied in order to test the concentration dependent emission and WLE properties of the QDC. It was found that the QDC, with absorbance value near about 0.8 at 350 nm, exhibited excellent WLE properties (with respect to chromaticity, CRI and CCT) and was thus chosen for demonstrating its application potential in the solid state (Figure A.6.9, Table A.6.3, Appendix).

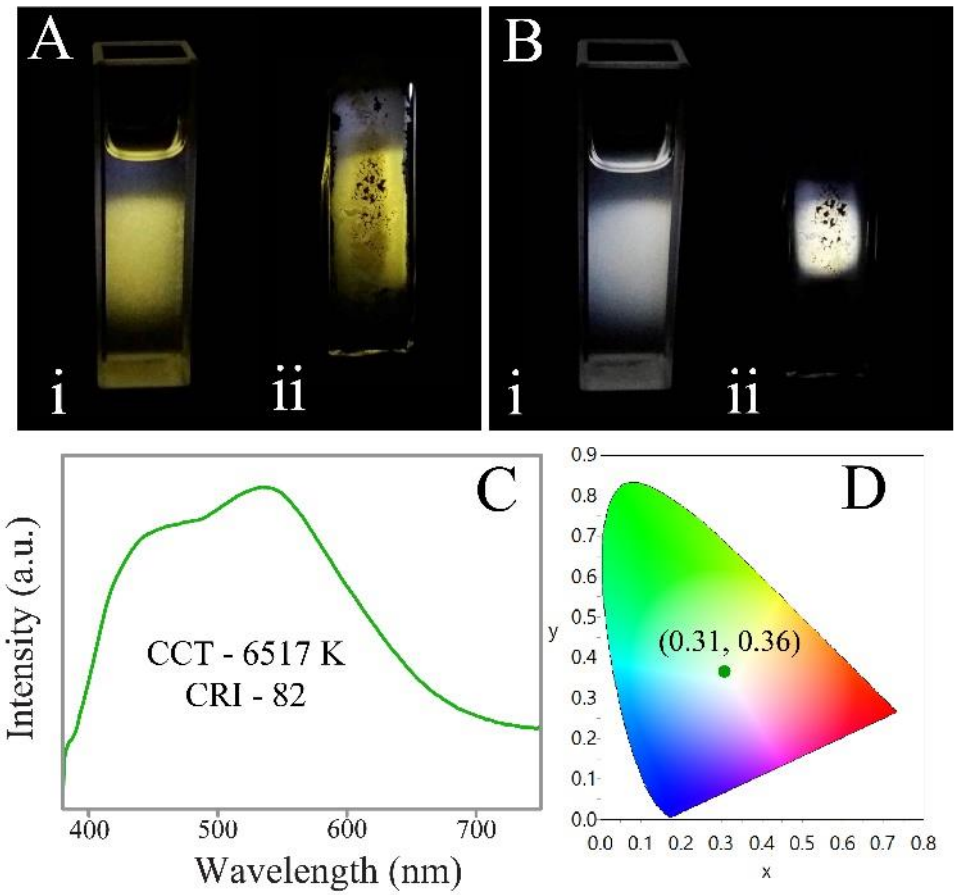

Figure 6.3. Digital photographs of the **(A)** ZnO Qdots and **(B)** WLE nanocomposite (i) in liquid phase (in ethanol) and (ii) in solid phase captured under 350 nm light from a spectrofluorimeter. **(C)** Emission spectrum (λ_{ex}–350 nm); and **(D)** corresponding chromaticity in CIE diagram of

solid WLE QDC nanocomposite. The solid form of the samples was obtained by depositing the dispersion on a quartz substrate and then drying at room temperature.

The digital photographs showed that solution and solid phases of ZnO Qdots and QDC nanocomposite (recorded under the irradiation of 350 nm light from a spectrofluorimeter) exhibited yellow and white light (Figure 6.3A-B), respectively, while both of them (in solution) were light milky white in color in presence of daylight (Figure A.6.10, Appendix). The photoluminescence quantum yield (PLQY) of WLE QDC nanocomposite was found to be 2.4% while ZnO Qdots showed PLQY of 1.3% (Table A.6.4, Appendix). It is to be mentioned here that the observed difference in PLQY between WLE QDC and only ZnO Qdots may be due to the additional emission owing to an extra blue emission peak of surface $Zn(MSA)_2$ complex compared to only ZnO Qdots. In addition, the observed relatively low PLQY of ZnO Qdots and the composite may be due to the presence of larger number of surface defects. [1-2, 10, 11-12] This may be a consequence of synthesis at low temperatures, which is essential for the experiments pursued herein. Additionally, the WLE QDC exhibited average emission life times of 35.9 ns (measured with excitation at λ_{em} - 545 nm using 336 nm LED source) and 4.2 ns (measured with excitation at λ_{em} - 440 nm using 375 nm laser source; Figure A.6.11 and Table A.6.5, Appendix). On the other hand, as such ZnO Qdots showed average emission life times of 44.1 ns (measured with excitation at λ_{em} - 545 nm using 336 nm LED source, Figure A.6.11 and Table A.6.5, Appendix). It is to be mentioned here that the decrease in emission intensity as well as average life time for the emission peak at 545 nm (Figure 6.2B and Figure A.6.11 and Table A.6.5, Appendix) of ZnO Qdots, upon complexation with MSA, may be either due to the quenching action by the newly formed $Zn(MSA)_2$ complex – which is commensurate with our earlier observations[13-16] - or due to competitive absorptions of both the luminescent species (here ZnO Qdots and $Zn(MSA)_2$ complex; as both of them absorb at 350 nm). Additionally, the narrow overlap between the broad absorption spectrum of ZnO Qdots and emission spectrum of $Zn(MSA)_2$ complex (being present on the surface of ZnO Qdots) may have led to energy transfer from the surface $Zn(MSA)_2$ complex to ZnO Qdots (Figure A.6.12, Appendix). Interestingly, the WLE QDC (in solution) was found to be photo-stable under continuous irradiation of UV light for half an hour. This was pursued by probing the time-dependent changes in the intensities of the emission maxima of the both $Zn(MSA)_2$ complex and ZnO Qdots (Figure 6.4). The experiments were performed with excitation at 350 nm,

using a spectrofluorimeter fitted with 150-W ozone-free xenon arc-lamp as the light source. Additionally, no significant change was observed in the emission spectrum (λ_{ex}- 350 nm) of the WLE QDC nanocomposite following irradiation (Figure 6.4). This could possibly rule out of the degradation of the $Zn(MSA)_2$ complex in presence of UV light and thus indicated the long term photo-stability of the QDC WLE nanocomposite. It is to be mentioned here that although ZnO Qdots have been widely used as photo oxidants[35-37]; however, the photo oxidation property of ZnO Qdots did not affect the luminescence of $Zn(MSA)_2$ complex. This indicated the stability of the complex even in the presence of oxidizing environment.

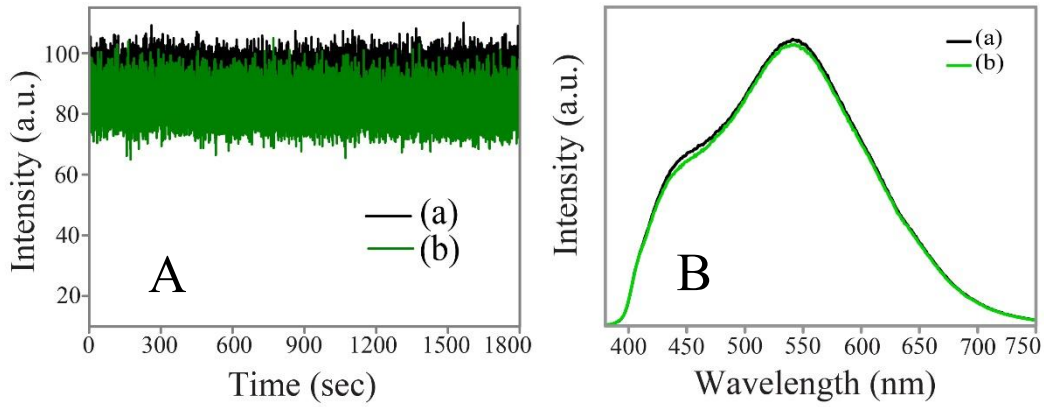

Figure 6.4. (A) Change in emission intensity vs time (a) at 545 nm and (b) at 440 nm of WLE QDC nanocomposite (in dispersion), following continuous irradiation with 350 nm light for half an hour (using a spectrofluorimeter fitted with 150-W ozone-free xenon arc-lamp as the light source and recorded with 0.1 s interval). **(B)** Emission spectra (λ_{ex}–350 nm) of WLE QDC nanocomposite (a) before and (b) after photo irradiation of with 350 nm light for half an hour.

6.2.6 Stability of White Light Emitting QDC in Solid Form.

Importantly, the solid form obtained from the WLE dispersion of the QDC nanocomposite (measured following deposition on a quartz substrate with drying at room temperature) emitted white light (Figure 3B; under the irradiation of 350 nm light from a spectrofluorimeter) with chromaticity of (0.31, 0.36), and CRI and CCT values of 82 and 6517 k, respectively (Figure 6.3C-D and Table 6.1), thus indicating stability in solid form. In addition, the long term stability (as measured using luminescence and from corresponding chromaticity color coordinates) and the luminescence stability (with respect to continuous irradiation of light with λ_{ex}- 350 nm) of the solid QDC clearly demonstrated its potential utility (Figure 6.5 and Figure A.6.13, Appendix). The near to perfect white light chromaticity and day light CCT with average CRI values of the

dispersion and the solid form (combined with long term chemical, physical and photo-stability) of the presented highly luminescent QDC nanocomposite clearly demonstrated its future practical use in fabricating LEDs.

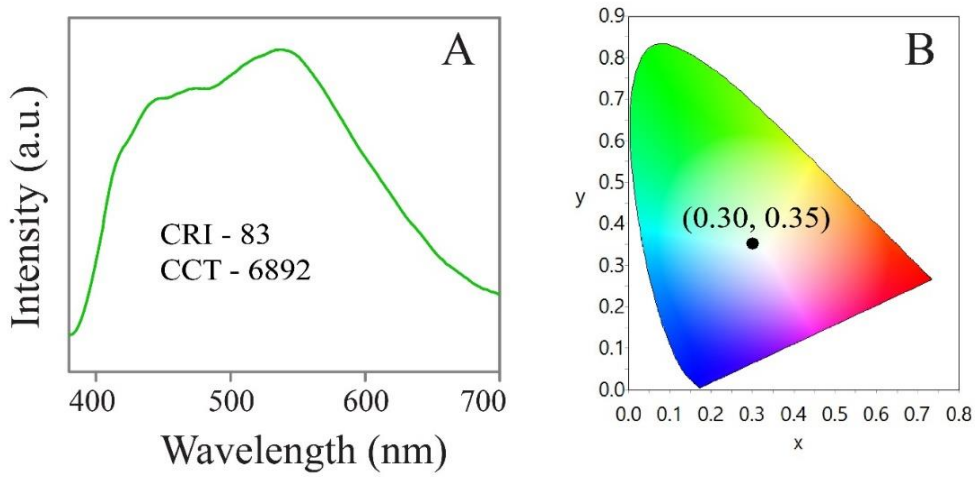

Figure 6.5. (A) Emission spectrum (λ_{ex}-350 nm) and corresponding **(B)** chromaticity, CRI and CCT in CIE diagram of the solid films of WLE QDC nanocomposite, deposited on a quartz glass and recorded after 15 days.

6.3 Conclusions.

In conclusion, the complexation reaction involving N-methylsalicylaldimine (MSA) and surface Zn^{2+} ions of a yellow emitting ZnO quantum dot (Qdot), led to the formation of blue emitting $Zn(MSA)_2$ complex on the surface of the Qdot and thus to a single component white light emitting (WLE) nanocomposite. Importantly, the tunability in chromaticity, CRI and CCT of the reported nanocomposite - depending upon the variation in concentration of complexing ligand – makes the composite a versatile emitter of choice. Under the best reaction condition, the dispersion and corresponding solid form of the nanocomposite (with 2.4% quantum yield) displayed bright natural cool white light with (i) chromaticity color coordinates of (0.31, 0.38) and (0.31, 0.36), (ii) CRI values of 74 and 82 and (iii) CCT values of 6505 K and 6517 K, respectively. The new strategy in fabricating LED emitting source material could pave the way for better solid state lighting devices. In addition, the knowledge accrued herein may be useful for development of other highly emitting LED materials. Apart from light emitting applications, the present WLE nanocomposite may have important applications in sensing, based on the specific chemical interaction of one of the emitting species, present

in WLE nanocomposite (here ZnO Qdots or $Zn(MSA)_2$ complex) with the external analyte. That this is a new way of developing photoresponsive materials for the development of novel Qdot based device fabrication. For making the material more appealing towards practical application, increment of quantum yield and electroluminescence measurement will be of our primary focus.

6.4 Bibliography.

1. Abhilash, S.; Parwathy, C.; Deepthy, M.; Sreerekha, R.; Nair, S. V.; Manzoor, K. Rapid Dissolution of ZnO Nanocrystals in Acidic Cancer Microenvironment Leading to Preferential Apoptosis. *Nanoscale* **2011**, *3*, 3657– 3669.
2. Patra, M. K.; Manoth, M.; Singh, V. K.; Siddaramana Gowd, G.; Choudhry, V. S.; Vadera, S. R.; Kumar, N. Synthesis of Stable Dispersion of ZnO Quantum Dots in Aqueous Medium Showing Visible Emission from Bluish Green to Yellow. *J. Lumin*. **2009**, *129*, 320– 324.
3. Nikitina, P. A.; Peregudov, A. S.; Koldaeva, T. Y.; Kuz'mina, L. G.; Adiulin, E. I.; Tkach, I. I.; Perevalov, V. P. Synthesis and Study of Prototropic Tautomerism of 2-(2-hydroxyphenyl)-1-hydroxyimidazoles. *Tetrahedron* **2015**, *71*, 5217– 5228.
4. Komiya, N.; Okada, M.; Fukumoto, K.; Jomori, D.; Naota, T. Highly Phosphorescent Crystals of Vaulted trans-Bis(salicylaldiminato)platinum(II) Complexes. *J. Am. Chem. Soc*. **2011**, *133*, 6493– 6496.
5. Garnovskii, A. D.; Burlov, A. S.; Lysenko, K. A.; Garnovskii, D. A.; Borodkina, I. G.; Ponomarenko, A. G.; Chigarenko, G. G.; Nikolaevskii, S. A.; Minkin, V. I. Tribochemically Active Chelate Complexes of Salicylideneimines. *Russ. J. Coord. Chem*. **2009**, *35*, 120– 127.
6. Jeevan, T. S. M. A.; Johnson, M. F. G.; Assefa1, A. G.; Arockiasamy, S.; Nagaraja, K. S. Characterization and Evaluation of Standard Enthalpy of Vaporization and Kinetic Studies of Volatile bis(N-ethyl-5-methyl-salicylaldimine)nickel (II) Complex. *Am J Analyt Chem*. **2015**, *6*, 156– 163.
7. Son, D. I.; Kwon, B. W.; Park, D. H.; Seo, W.-S.; Yi, Y.; Angadi, B.; Lee, C.-L.; Choi, W. K.Emissive ZnO–Graphene Quantum Dots for White-Light-Emitting Diodes. *Nat. Nanotechnol*. **2012**, *7*, 465– 471.
8. Layek, A.; Stanish, P. C.; Chirmanov, V.; Radovanovic, P. V. Hybrid ZnO-Based Nanoconjugate for Efficient and Sustainable White Light Generation. *Chem. Mater*. **2015**, *27*, 1021– 1030.
9. Guo, H.; Lin, Z.; Feng, Z.; Lin, L.; Zhou, J. White-Light-Emitting Diode Based on ZnO Nanotubes. *J. Phys. Chem. C* **2009**, *113*, 12546– 12550.
10. Kar, A.; Kundu, S.; Patra, A. A Simple Approach to Generate Efficient White Light Emission from a ZnO-Ionic Liquid Complex. *RSC Adv*. **2012**, *2*, 4879– 4885.
11. Zeng, H.; Duan, G.; Li, Y.; Yang, S.; Xu, X.; Cai, W. Blue Luminescence of ZnO Nanoparticles Based on Non-Equilibrium Processes: Defect Origins and Emission Controls. *Adv. Funct. Mater*. **2010**, *20*, 561– 572.

12. Nie, B.; Hu, J.; Luo, L.; Xie, C.; Zeng, L.; Lv, P.; Li, F.; Jie, J.; Feng, M.; Wu, C.; Yu, Y.; Yu, S. Monolayer Graphene Film on ZnO Nanorod Array for High-Performance Schottky Junction Ultraviolet Photodetectors. *Small* **2013**, *9*, 2872–2879.
13. Pramanik, S.; Bhandari, S.; Roy, S.; Chattopadhyay, A. Synchronous Tricolor Emission-Based White Light from Quantum Dot Complex. *J. Phys. Chem. Lett*. **2015**, *6*, 1270– 1274.
14. Bhandari, S.; Pramanik, S.; Khandelia, R.; Chattopadhyay, A. Gold Nanocluster and Quantum Dot Complex in Protein for Biofriendly White-Light-Emitting Material. *ACS Appl. Mater. Interfaces* **2016**, *8*, 1600−1605
15. Bhandari, S.; Roy, S.; Pramanik, S.; Chattopadhyay, A. Double Channel Emission from a Redox Active Single Component Quantum Dot Complex. *Langmuir* **2015**, *31*, 551– 561.
16. Bhandari, S.; Roy, S.; Chattopadhyay, A. Enhanced Photoluminescence and Thermal Stability of Zinc Quinolate Following Complexation on the Surface of Quantum Dot. *RSC Adv*. **2014**, *4*, 24217– 24221.
17. Zhang, Q.; Wang, C.F.; Ling, L. T.; Chen, S. Fluorescent Nanomaterial-Derived White Light-Emitting Diodes: What's Going On. *J. Mater. Chem. C* **2014**, *2*, 4358– 4373.

Chapter 6B

Broad - Spectrum Sun Protection Formula from ZnO Qdot-Herbal (Holy Basil and Rosemary) Nanocomposite

Herein, it is reported that broad-spectrum sun protection formula (SPF) can be formulated using ZnO Qdot and herbal extract from holy basil leaf or rosemary leaf. Utilizing the molecules with ligating capability – extracted from holy basil leaf – as a binding moiety to the surface of ZnO Qdot, efficient UV absorbing material was prepared. The naturally synthesized molecules with extended conjugation was the key to design the material with more efficient UV absorbing capability. The advantage of the nanocomposite compared to ZnO Qdot is its enhanced absorption capability in the range of 355 nm - 400 nm, in addition to absorption in the zone of 290 nm - 355 nm – primarily contributed by ZnO itself. In other words, ZnO-basil (or ZnO-rosemary) nanocomposite is an efficient UV-A as well as UV-B absorbing material; thus, making it broad spectrum SPF. As, mainly the polyols with catechol moiety would attach on the surface of ZnO Qdot; the attached molecule may be preferably separated from the blend of natural products from leaf (basil or rosemary) extract.

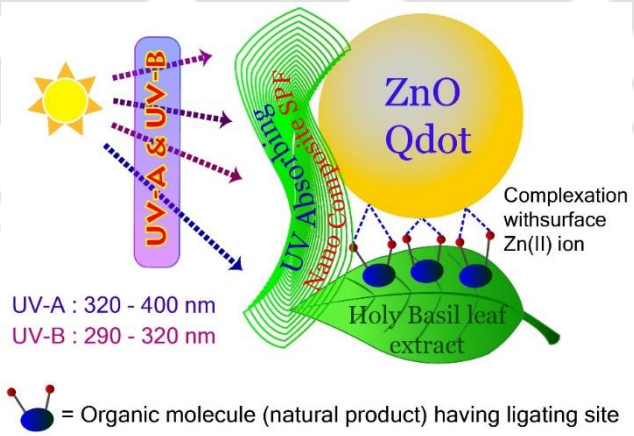

*Manuscript under preparation.

6.4 Experimental.

6.4.1 Materials:

Zinc acetate dihydrate (Merck), potassium hydroxide (KOH, Merck), ethanol (Tedia) were purchased and used directly without any purification. Holy basil leaves were collected from Holy Basil (osmium sanctum) herbs inside IIT Guwahati and Rosemary dry leaves were bought from amazon.in.

6.4.2 Synthesis of ZnO Qdots.

ZnO Qdot was synthesized using protocol similar to that, which has been described in chapter 6A.[1]

6.4.3 Extraction of Holy Basil Leaf and Rosemary Leaf.

After collecting the Holy Basil leaves, they were thoroughly washed under water flow. Finally, they were washed with Milli-Q grade water. Following this, the leaves were dried to remove water from the leaves. Then, the dried leaves (weight ~ 10 g) were taken in 100 mL of ethanol and the mixture was heated at 60 ºC for overnight and it was filtered and the filtrate was collected. The filtrate was used as extract of the leaf and was used for further experiment.

The same method was followed to extract rosemary leaf.

6.4.4 Preparation of ZnO Qdot - Herbal Nanocomposite.

ZnO Qdot (as synthesized in 5 mM scale) was dispersed in 100 mL of methanol. To that ZnO Qdot dispersion, 10 mL of leaf extract (holy basil or rosemary) was added and was stirred under sonication for ~15 min. The resulting reaction mixture was centrifuged and so obtained pellet was washed with methanol followed by water. After washing, the pellet was collected and dried for use as Qdot herbal nanocomposite.

6.4.5 Characterization Techniques.

(i) Perkin Elmer LAMBDA 750 UV/Vis/NIR spectrophotometer and (ii) HORIBA Jobin Yvon FluoroMax-4 spectrofluorimeter, (iii) JEOL JEM-2100 transmission electron microscope (maximum accelerating voltage 200 kV), were used to measure (iii) absorption, (iv) photoluminescence, (v) particle size and lattice fringes and morphology.

6.5 Results and Discussion.

6.5.1 Characterization of ZnO Qdot.

As synthesized ZnO Qdot exhibited absorbance maximum at ~355 nm and photoluminescence emission was centered at ~550 nm (Figure 6.6A and B). Upon reaction of ZnO Qdot with holy basil extract, the so obtained herbal composite – herein called as ZnO-OS QDC – exhibited absorbance maximum 350 nm and was non fluorescent in nature (Figure 6.6A and B). Likewise, treating ZnO Qdot with rosemary extract resulted in the formation of ZnO-RM QDC, which had absorption maximum at ~350 nm and also it was non fluorescent in nature. Interestingly, in case of ZnO-herbal nanocomposites (i.e., ZnO-OS QDC and ZnO-RM QDC), absorbance in total UV region (290-400 nm) was significantly increased in comparison to ZnO Qdot itself. In addition, the size and shape of ZnO Qdots remained same after reaction with both the herbal extract, which is evident from transmission electron microscopic (TEM) analysis (Figure A.6.14, Appendix). Also, HRTEM analysis and SAED pattern indicated the intact nature of morphology of ZnO Qdot following composite (QDC) formation with herbal extract (Figure A.6.15, Appendix).

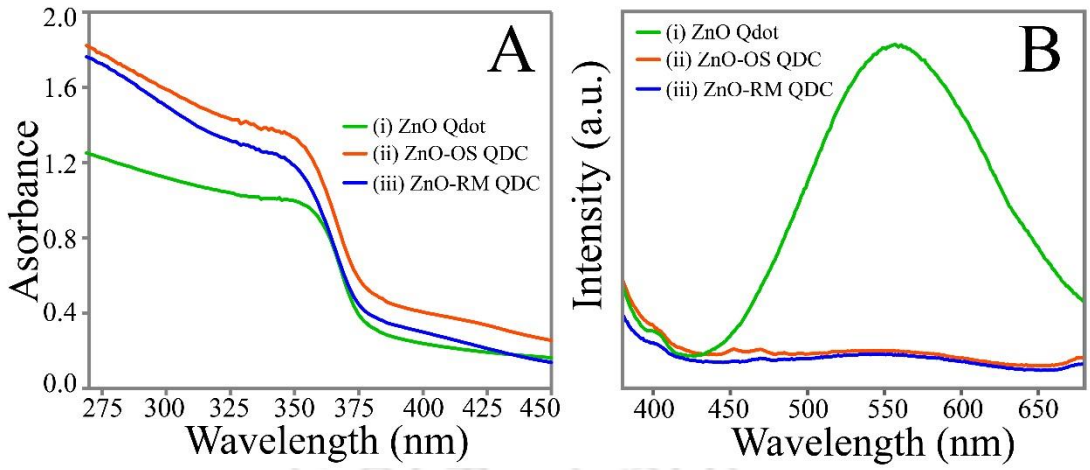

Figure 6.6. (A) UV-vis spectra and **(B)** photoluminescence spectra (λ_{ex}= 350 nm) of **(i)** ZnO Qdot (0.2 mg/mL), **(ii)** ZnO-OS QDC composite (0.2 mg/mL) and **(iii)** ZnO-RM QDC composite (0.2 mg/mL).

Sun Protection Factor (SPF) was determined using spectrophotometric technique. Calculation of SPF value was performed using Mansur equation (Figure 6.6A).[2]

$$SPF_{spectrophotometric} = CF \times \sum_{290}^{320} EE(\lambda) \times I(\lambda) \times Abs(\lambda)$$

Where, *EE (λ)* - erythemal effect spectrum*; I (λ)* - solar intensity spectrum*; Abs (λ)*-absorbance of sunscreen*; CF* - correction factor (= 10).

Calculated SPF value for ZnO Qdot was 11, whereas SPF values for ZnO-OS QDC and ZnO-RM QDC were 15 and 14 respectively (SPF values were rounded off to closest integer). It is to be mentioned here that the dispersion with same amount (i.e., 02 mg/mL) of each nanomaterials (i.e., ZnO Qdot, ZnO-OS QDC and ZnO-RM QDC) were taken for SPF calculation. Importantly, SPF value is applicable for the UV-B region. It is important to mention here that, UV-B (290 – 320 nm) is responsible for skin-burn and may cause skin cancer.[20] Whereas, UV-A (320 – 400 nm) radiation can penetrate the skin more extensively than UV-B radiation from sun. UV-A is responsible for skin aging and also for wrinkling.[20] In addition, UV-A can severely damage the keratinocytes or skin cell in the epidermis basal layer. Recent research has also revealed that UV-A may be one of the reasons for skin cancer.[3] Therefore, it is important to shield UV-A along with UV-B radiation to protect the skin from damage by sunrays.

In this aspect, ZnO is a well known SPF material; whereas nanostructured ZnO or ZnO Qdot is more efficient SPF material. [4] But, ZnO Qdot has absorption band edge at 355 nm; beyond that, UV radiation in the region from 355 – 400 nm is not absorbed significantly by ZnO Qdot itself. The so formed ZnO herbal nanocomposite (i.e., ZnO-OS QDC and ZnO-RM QDC) exhibited considerable enhancement in absorbance in the particular UV region from 345 – 400 nm along with significant increase in the region of 290 – 350 nm. Thus, the ZnO herbal nanocomposite can be regarded as broad-spectrum sun protection agent as it covers UV-A as well as UV-B region.

The organic moieties – more precisely the natural products – extracted from holy basil or rosemary leaves may react with surface Zn^{2+} ions of ZnO Qdot to form surface complex (i.e., QDC), in case the moieties possess ligating site. As for example, rosmarinic acid or eugenols – those are present in herbal extract – may be attached on the surface by means of complexation reaction.[5-6] Interestingly, these molecules also possess extensive conjugation – that makes the molecules a good absorber in the entire UV region; thus, making the composite a better SPF (broad spectrum) material than ZnO Qdot itself. Hence, the composite may be considered as ZnO based environmentally benign broad spectrum SPF.

6.6 Conclusions.

In conclusion, using complexation strategy, efficient broad specrun SPF material can be formulated from ZnO herbal nanocomposite. As, the complexing agents are obtained form herbal source like holy basil or rosemary; thus, the QDC nanocomposites may be thought to be non-toxic and environment friendly. Next, it is our aim to identify the attached herbal components on the surface of quantum dots following treatment with ZnO quantum dots. Additionally, we are interested to formulate a cream using the nanocomposite as an active ingredient and to check the healing property of the herbal nanocomposite.

6.7 Bibliography.

1. Roy, S.; Pramanik, S.; Bhandari, S.; Chattopadhyay, A. Surface Complexed ZnO Quantum Dot for White Light Emission with Controllable Chromaticity and Color Temperature. *Langmuir* **2017**, *33*, 4627–14633.
2. Mansur, J. S.; Breder, M. N. R.; Mansur, M. C. A.; Azulay, R. D. *An. Bras. Dermatol.***1986,** *61*, 121-124.
3. Bens, G. Sunscreens. In Sunlight, Vitamin D and Skin Cancer, 2nd ed.; Reichrath, J., Ed.; Advances in Experimental Medicine and Biology Series; Landes Bioscience and Springer Science + Business: Austin, TX, and New York, **2014**; Vol 810, Chapter 25, pp 429−463.
4. Guedens, W. J.; Reynders, M.; de Rul, H. V.; Elen, K.; Hardy, A.; Bael, M. K. V.; ZnO-Based Sunscreen: The Perfect Example To Introduce Nanoparticles in an Undergraduate or High School Chemistry Lab. *J. Chem. Educ.* **2014**, *91*, 259−263.
5. Hakkim, F. L.; Shankar, C. G.; Girija, S. Chemical composition and antioxidant property of holy basil (*Ocimum sanctum L.*) leaves, stems, and inflorescence and their *in vitro* callus cultures. *J. Agric. Food Chem*. **2007**, *55*, 9109– 9117
6. Angioni, A.; Barra, A.; Cereti, E.; Barile, D.; Coisson, J. D.; Arlorio, M.; Dessi, S.; Coroneo, V.; Cabras, P. Chemical composition, plant genetic of essential oil of *Rosmarinus officinalis* L. *J. Agric. Food Chem.* **2004**, *52*, 3530– 3535.

Chapter 7

Summary and Future Prospects

7.1 Summary.

As a whole, the thesis is an effort to unveil the physical and chemical aspect of surface complexation reactions and to demonstrate the fabrication of environment-friendly material for white light generation and broad-spectrum sun protection formula. Discussions on probable Z-type binding fashion of 8-hydroxyquinoline on the surface of ZnS Qdot – coupled with the coordination chemistry – helped explain the extraordinary stability attained by the complex while attached to the surface via dangling anion – which was also reflected in the unusual reaction between surface Zn^{2+} ion and copper quinolato complex that resulted in formation of surface zinc quinolato complex. Furthermore, role of dangling anions in providing the stability to the surface zinc quinolato complex was revealed in the demonstration of complex transfer reaction from the surface of ZnO Qdot to ZnS Qdot. In addition, kinetic approach to study the complexation reaction and complex migration reaction seems useful for fundamental understanding of adsorption and binding phenomenon of ligand related to surface chemistry of Qdots. Notably, the complexation on the surface of Qdot was also probed at few particle level using dual photoluminescence intermittency of QDC (MSA treated Mn(II) doped ZnS Qdot) – which further validated the concept of coexistence of fluorescent complex and Qdot within a single entity i.e., QDC. Practically, the principle of 'surface complexation' was successfully implemented in worthwhile applications like – (i) fabrication of environment-friendly white light emission from QDC (out of reaction between ZnO Qdot and N-methylsalicyldimine) and (ii) formulation of broad spectrum sun protection formula from nanocomposite – formed as a result of reaction between ZnO Qdot and alcoholic extract of holy basil as well as rosemary leaves.

7.2 Future Prospects.

Through the reported studies, Qdot surface complexation reactions were explored. The concept might be useful not only for understanding the fundamentals of surface complexation but also for practical application. These studies may help open up a new area of nanoscience involving typical inorganic and physical chemistry concepts – that may help generate a new sub-field of organometallic chemistry and related catalytic reactions. Additionally, the principle of complexation might be useful in fabricating self-assembled structure of Qdots – which is being considered as an exceptional material for the next generation photovoltaics and electronics. Also, by using the principle of relative stability of complexes on the surface of different Qdots, preferential extraction of particular chemicals like eugenols, rosmarinic acid, having binding capability, from the extract of herbal plant is possible – which may be beneficial for biomedical applications. Essentially, dual photoluminescence intermittency from QDC may achieve its novelty in studying the energy related issues, detection of biologically or environmentally important molecules at few particle level. As for example, energy transfer between quantum dot and surface complex following non radiative pathway can be determined using photoluminescence intermittency. On the other hand, interacting biomolecules particularly with anyone of the emitting components can be detected at almost single particle level by observing changes in photoluminescence intermittency behavior. Moreover, the principle of 'complexation on the surface of Qdots' may find its importance as a foundation concept amidst plethora of applications related to energy, environment and biomedicine.

Appendix

A.2. Chapter2.

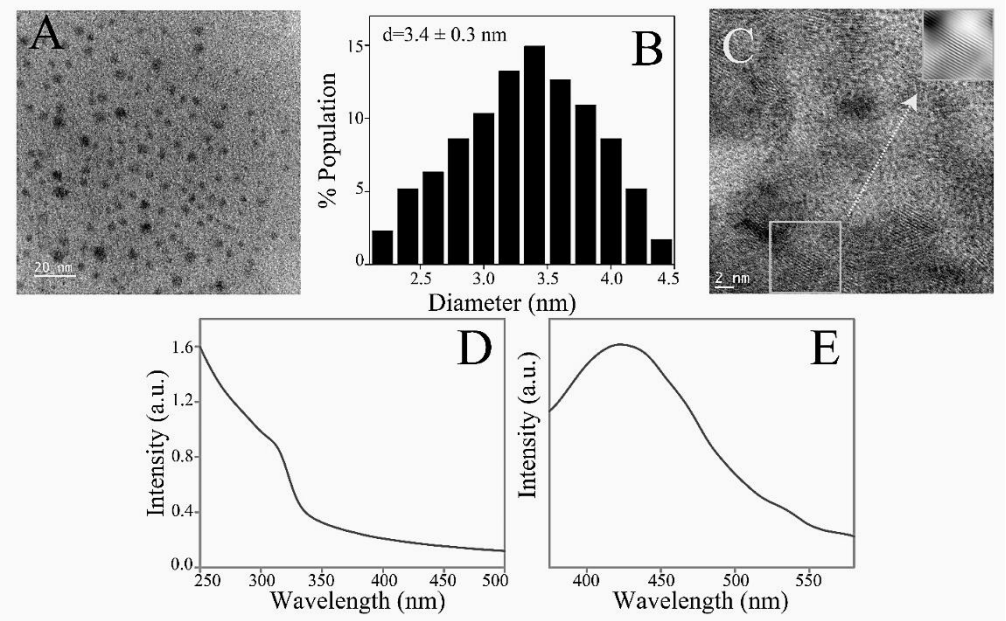

Figure A.2.1. **(A)** Transmission electron microscopic (TEM) image, **(B)** corresponding particle size distribution, **(C)** high resolution TEM image, **(D)** UV-vis spectrum and **(E)** photoluminescence emission spectrum (λ_{ex} – 325 nm) (aqueous dispersion) of as-synthesized ZnS quantum dots.

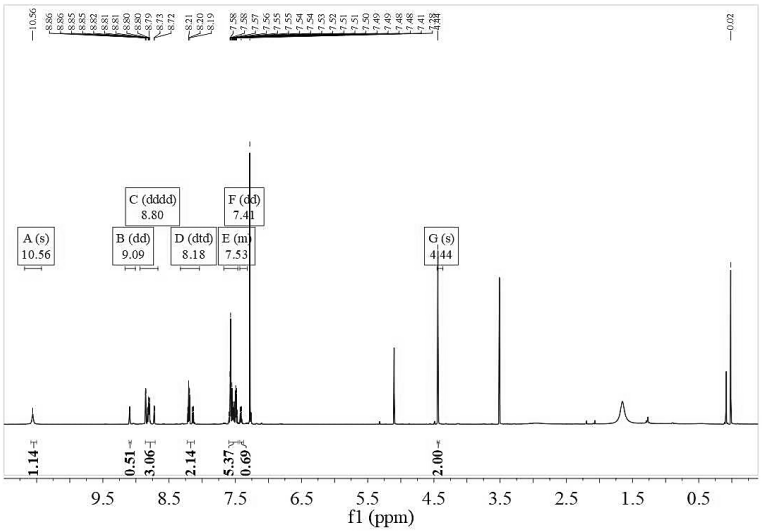

Figure A.2.2. Proton NMR spectrum of N-(quinolin-8-yl)-2-(quinolin-8-yloxy)acetamide (L1). ^{1}H NMR (600 MHz, $CDCl_3$) δ 10.56 (s, 1H), 9.09 (dd, *J* = 4.2, 1.7 Hz, 1H), 8.80 (dddd, *J* = 48.2, 45.0, 4.2, 1.6 Hz, 2H), 8.18 (dtd, *J* = 9.8, 8.0, 1.6 Hz, 2H), 7.67 – 7.46 (m, 3H), 7.41 (dd, *J* = 8.3, 4.2 Hz, 1H), 4.44 (s, 1H).

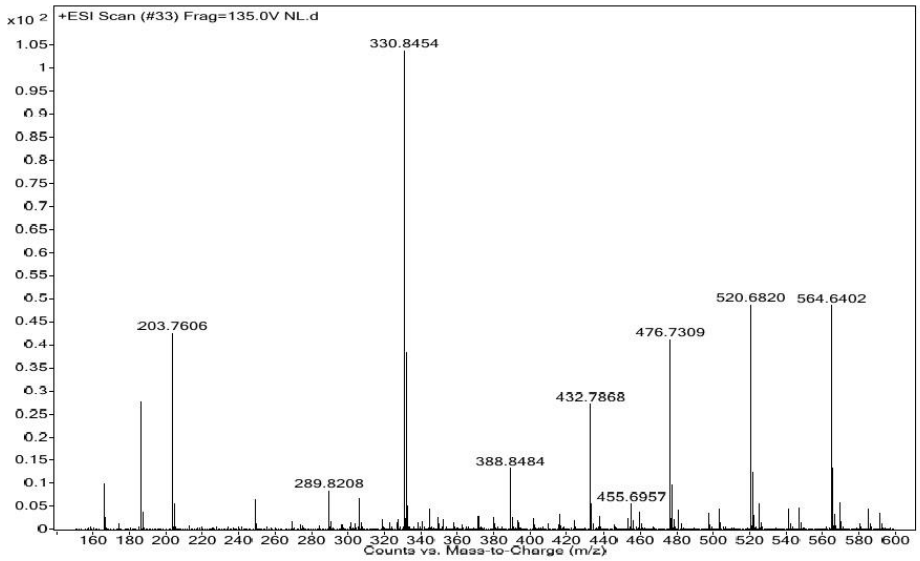

Figure A.2.3. ESI-MS spectrum of L1.

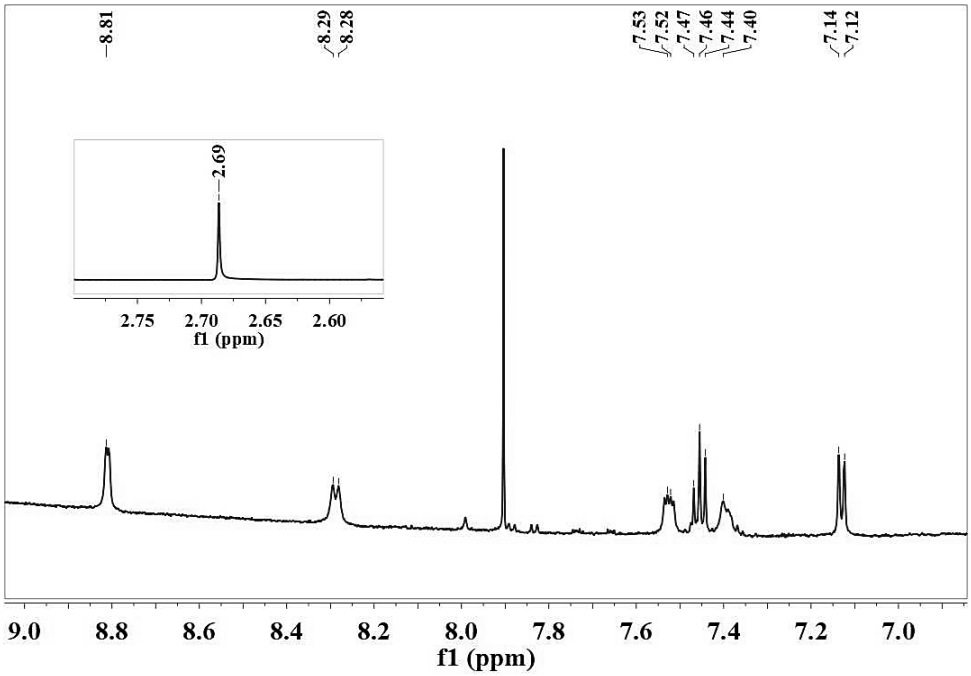

Figure A.2.4. Proton NMR spectrum of reaction mixture consisting of 30.0 μL 50.0 mM HQ and ZnS Qdot in methanol-d_4. (inset) NMR spectra of DMSO used as internal standard.

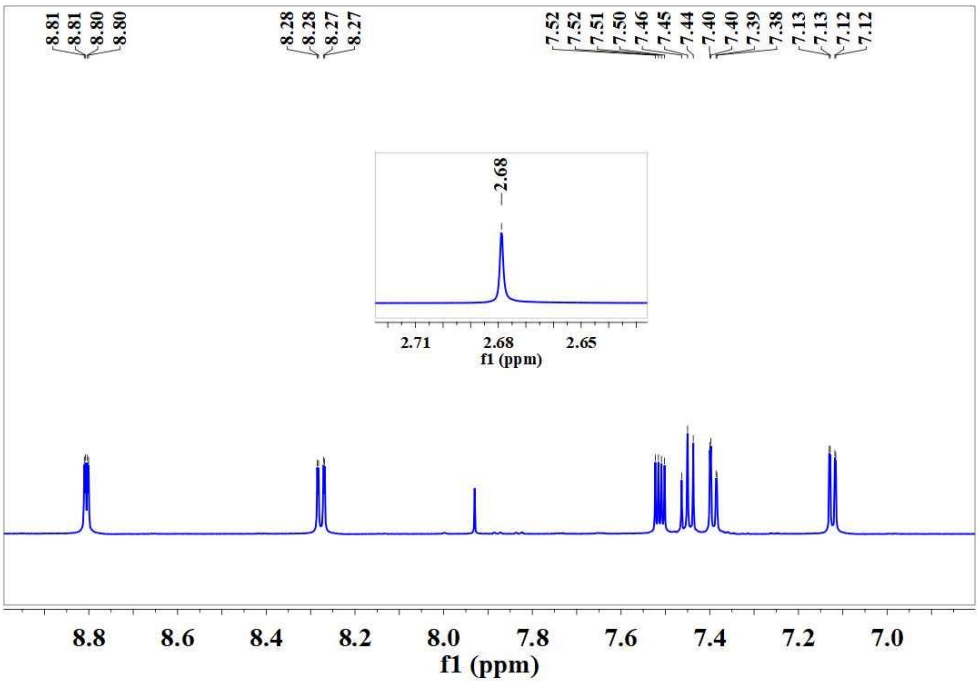

Figure A.2.5. Proton NMR spectrum of 500 μL 1 mM HQ in methanol-d_4. (inset) NMR spectra of DMSO used as internal standard.

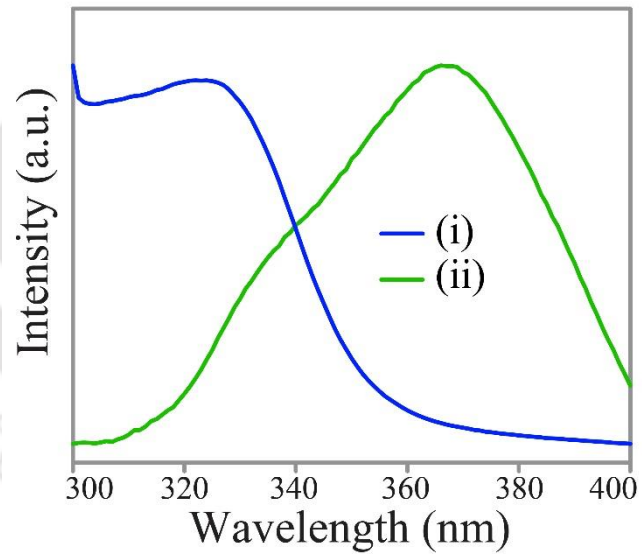

Figure A.2.6. Photoluminescence excitation spectra of (i) as synthesized ZnS Qdots (λ_{em}= 440 nm) in aqueous solution and (ii) QDC (λ_{em}= 500 nm) in DMSO.

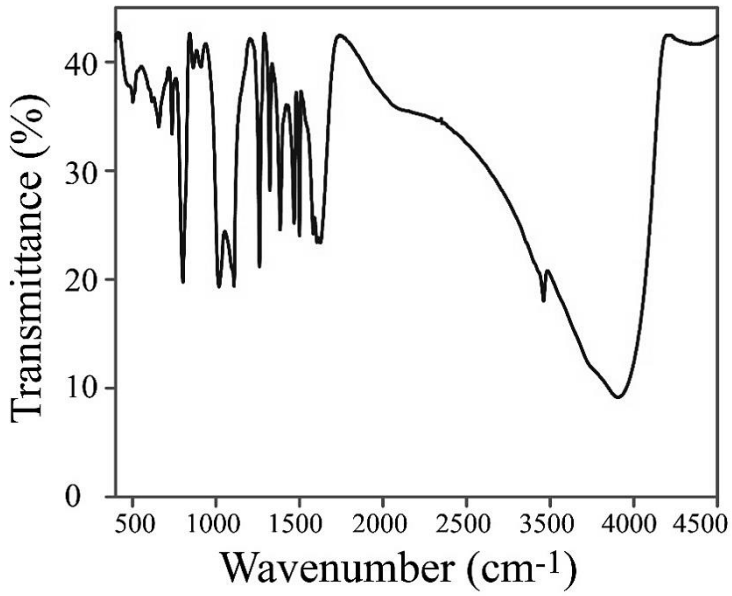

Figure A.2.7. Fourier transform infrared (FTIR) spectrum of the solid sample (KBr pellet) of ZnS-Q QDC.

Table A.2.1. FTIR peak assignment corresponding to Figure A.2.7.

FTIR peak (wavenumber, cm^{-1})	**Band assignment (functional group)**
1604	C–N/ C–C stretching
1582	C–N/ C–C stretching
1500	C–H bending of pyridyl ring
1468	C–H bending of pyridyl ring
1322	C–H bending of pyridyl ring
1108	Zn–O–C– stretching
820	C–H wagging (out of plane)
803	C–H wagging (out of plane)
737	Ring deformation (in plane), C–H wagging (out of plane)
655	Ring deformation (in plane)
615	Ring deformation (in plane)

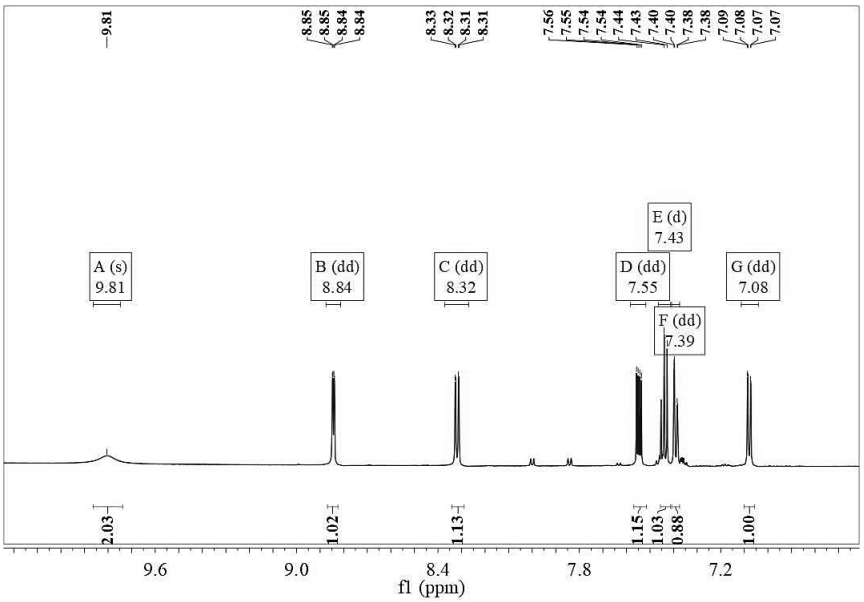

Figure A.2.8. Proton NMR spectrum of 8-hydroxyquinoline (HQ). ^{1}H NMR (600 MHz, DMSO) δ 9.81 (s, 1H), 8.84 (dd, *J* = 4.1, 1.6 Hz, 1H), 8.32 (dd, *J* = 8.3, 1.6 Hz, 1H), 7.55 (dd, *J* = 8.3, 4.1 Hz, 1H), 7.43 (d, *J* = 7.6 Hz, 1H), 7.39 (dd, *J* = 8.2, 1.2 Hz, 1H), 7.08 (dd, *J* = 7.5, 1.3 Hz, 1H).

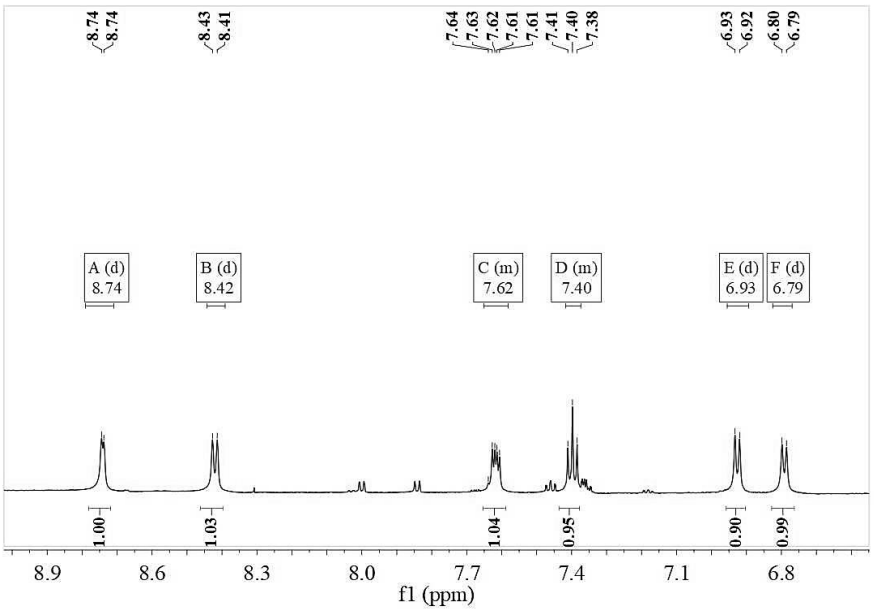

Figure A.2.9. Proton NMR spectrum of ZnQ_2. ^{1}H NMR (600 MHz, DMSO) δ 8.74 (d, *J* = 3.7 Hz, 1H), 8.42 (d, *J* = 8.1 Hz, 1H), 7.65 – 7.58 (m, 1H), 7.42 – 7.37 (m, 1H), 6.93 (d, *J* = 7.9 Hz, 1H), 6.79 (d, *J* = 7.7 Hz, 1H).

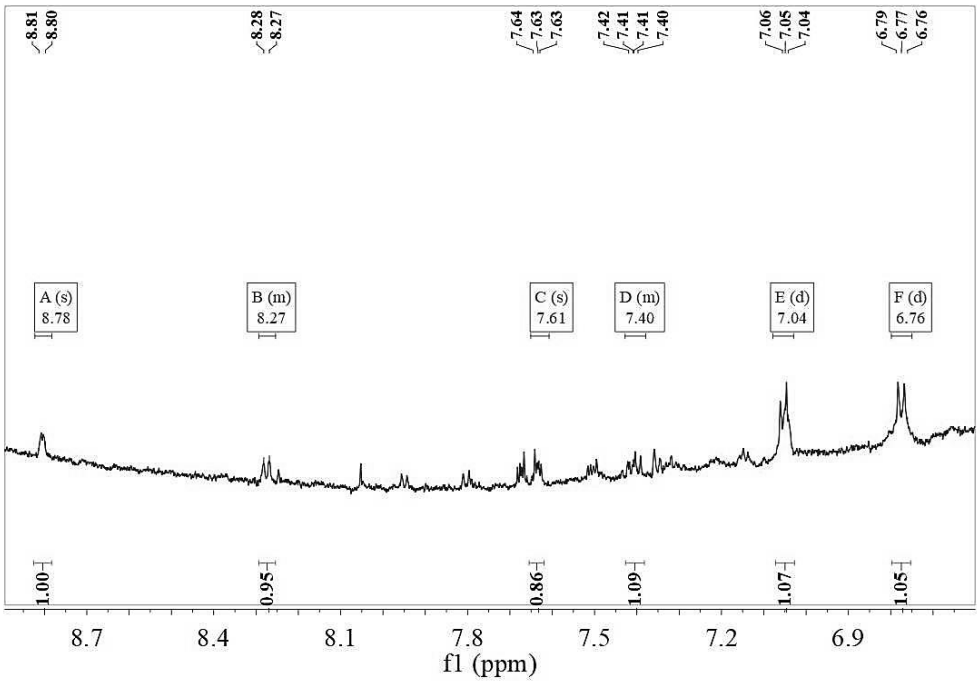

Figure A.2.10. Proton NMR spectrum of supernatant obtained after centrifugation of as prepared ZnS-HQ QDC. ^{1}H NMR (600 MHz, DMSO) δ 8.78 (s, 1H), 8.29 – 8.25 (m, 1H), 7.61 (s, 1H), 7.43 – 7.38 (m, 1H), 7.04 (d, J = 15.2 Hz, 1H), 6.76 (d, J = 13.5 Hz, 1H).

A.3. Chapter3.

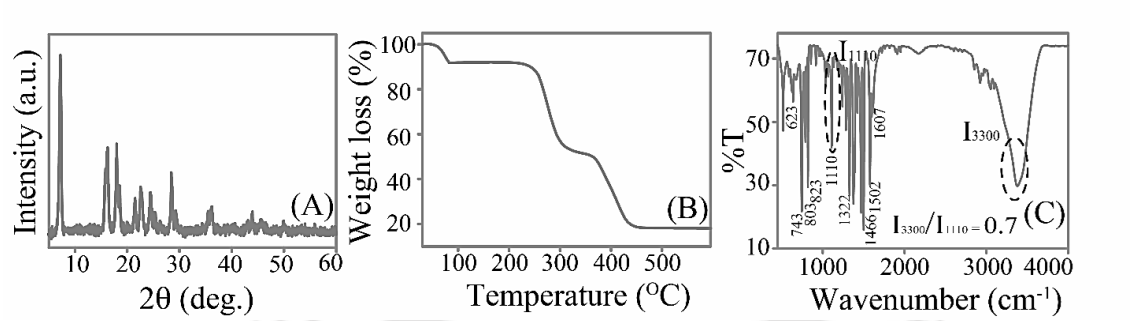

Figure A.3.1. (A) Powder X-ray diffraction pattern, **(B)** thermo-gravimetric analysis (TGA) and **(C)** FTIR spectrum of solid $CuQ_2.2H_2O$ complex.[1]

The presence of two strong peaks at 6.9° and 20.8° in powder XRD pattern indicated the formation of $CuQ_2.2H_2O$ complex (Figure A.3.1A). The presence of two water molecules were confirmed through the first weight loss in TGA (Figure A.3.1B), while the second and third weight losses in TGA curve are attributed to the partial and complete decomposition of the complex. Importantly, the obtained ratio of 0.7 of the two bands at 3300 and 1110 cm^{-1} in FTIR spectrum also supported the octahedral nature of the complex (refer to Figure A.3.1C).

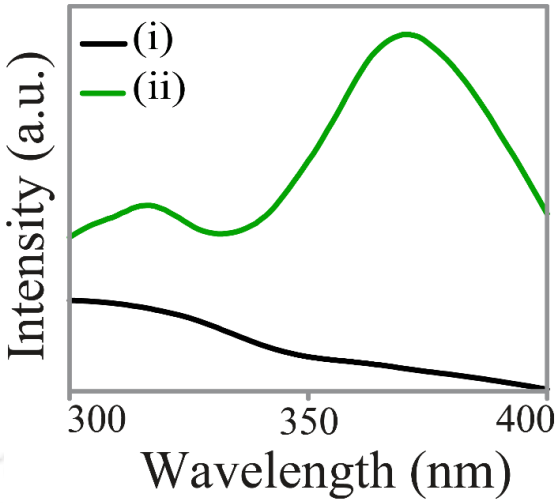

Figure A.3.2. Excitation spectra of the ethanolic dispersion of (i) en-capped ZnS Qdots (at λ_{em}= 440 nm) and (ii) CuQ_2 added ZnS Qdots (at λ_{em}= 497 nm).

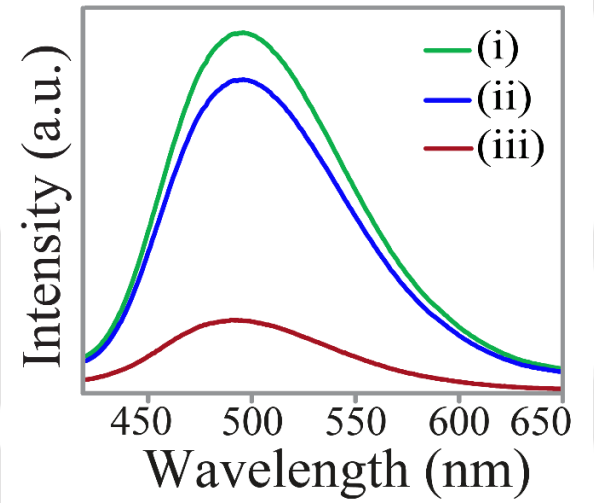

Figure A.3.3. Emission spectra (λ_{ex}-361 nm) of CuQ_2 added *en*-capped ZnS Qdots (i) before centrifugation, (ii) of the pellet obtained after centrifugation and following redispersion into same amount of ethanol and (iii) of the supernatant after centrifugation.

Table A.3.1. Quantum yield (%) (λ_{ex}= 361 nm) w.r.t. quinine sulphate (in 0.1 M H_2SO_4) of the ethanolic dispersion of (a) CuQ_2 added *en*-capped ZnS Qdots and (b) HQ added *en*-capped ZnS Qdots.

Samples	QY (%)
(i) CuQ_2 added *en*-capped ZnS Qdots	2.1
(ii) HQ added *en*-capped ZnS Qdots	2.9

Quantum yield calculation. The following equation was used to calculate the quantum yield of the samples,

$$Q_s = Q_R \times \frac{I_s}{I_R} \times \frac{A_R}{A_S} \times \frac{\eta_S^2}{\eta_R^2} \qquad (1)$$

Here, Q_S and Q_R are quantum yields of sample and reference (quinine sulphate), respectively; I_S and I_R are the areas under emission curve of sample and reference, respectively; A_S and A_R are the absorbance of the sample and reference, respectively; η_S and η_R are the refractive indices of the solvent in which sample and reference were dissolved; Q_R is the Q.Y. of reference (here quinine sulphate) which is 0.54 (54 %). It may be noted here that absorbance of all the samples were fixed at 0.10 ± 0.01 at their individual excitation wavelength (as mentioned in the table A.3.1).

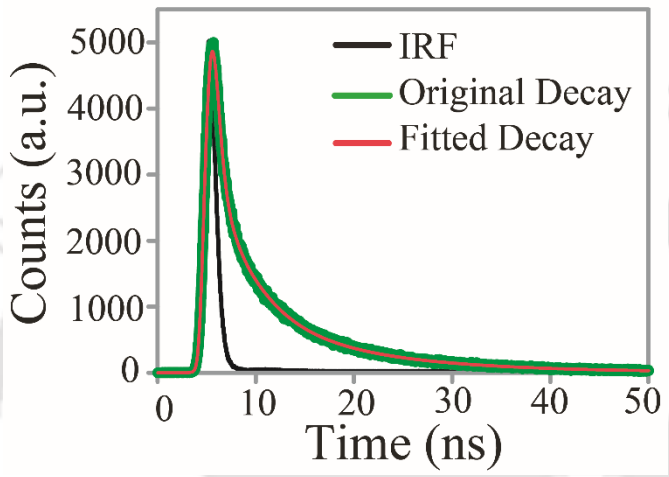

Figure A.3.4. Decay profiles (using 340 nm LASER) of the ethanolic dispersion of CuQ_2 added en-capped ZnS Qdots (λ_{em}=497 nm) and the graph fitted with a tri-exponential function. Here IRF stands for instrument response function.

Table A.3.2. Decay parameters (using 340 nm LASER) obtained following by tri-exponential fitting of the emission curve of the ethanolic dispersion of CuQ_2 added en-capped ZnS Qdots (λ_{em}=497 nm).

Samples	α_i (%)	τ_i (ns)	τ_{av} (ns)	χ^2
CuQ_2 added en-capped ZnS Qdots	32.49	3.72	10.52	1.07
	19.00	0.35		
	48.51	12.04		

Life time calculation. The decay profile was fitted to a multi-exponential model using following equation

$$I(t) = \sum_i \alpha_i \exp\left(-t/\tau_i\right) \qquad (2)$$

Where, single, bi and tri exponential functions were used to fit respective emission with obtaining χ^2 close to 1.0. The averaged life times (τ_{av}) in Table A.3.2, determined from the results of three exponential model using

$$\tau_{av} = \frac{\sum_i \alpha_i \tau_i^2}{\sum_i \alpha_i \tau_i} \qquad (3)$$

Where, α_i and τ_i are the pre-exponential factors and excited-state luminescence decay time associated with the *i*-th component, respectively.

Table A.3.3. Zeta potential values of the ethanolic dispersion of (a) en-capped ZnS Qdots and (b) CuQ_2 added en-capped ZnS Qdots.

Samples	Zeta potential (mV)
(i) en-capped ZnS Qdots	18.9 ± 0.36
(ii) CuQ_2 added en-capped ZnS Qdots	25.3 ± 0.98

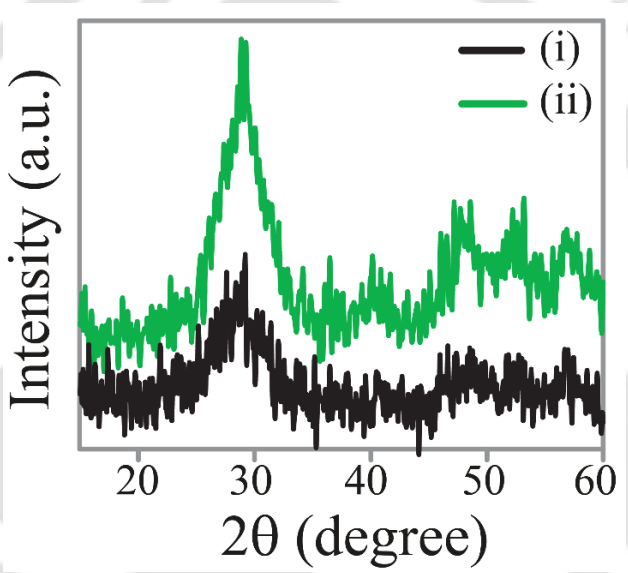

Figure A.3.5. Powder x-ray diffraction (XRD) pattern of the solid particles of (i) en-capped ZnS Qdots and (ii) CuQ_2 added en-capped ZnS Qdots.

It has been demonstrated that the wurtzite phase of the ZnS nanocrystals are preferably formed over cubic one when ethylene diamine is used as capping ligand and the synthesis is carried out at an above 100 °C. The emergence of six peaks at 2θ = 26.2º, 28.9º, 32.7º, 40.2º, 47.6º, 52.5º and 56.9º due to (100), (002), (101), (102), (110), (103), and (112) characteristic planes clearly indicated the formation of the wurtzite phase of ZnS. The morphology of the wurtzite remained unaltered following complexation/reaction with CuQ_2.

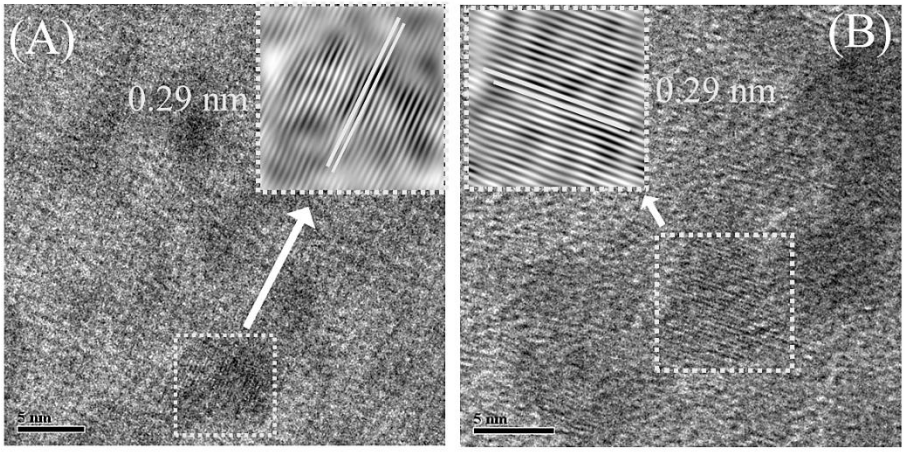

Figure A.3.6. High resolution TEM (HRTEM) and corresponding inverse fast Fourier transform (IFFT) images of the ethanolic dispersion of **(A)** en-capped ZnS Qdots and **(B)** CuQ_2 added en-capped ZnS Qdots. The lattice spacing (0.29 nm) is due to the (002) plane of wurtzite ZnS – which was preserved following complexation/reaction with CuQ_2.

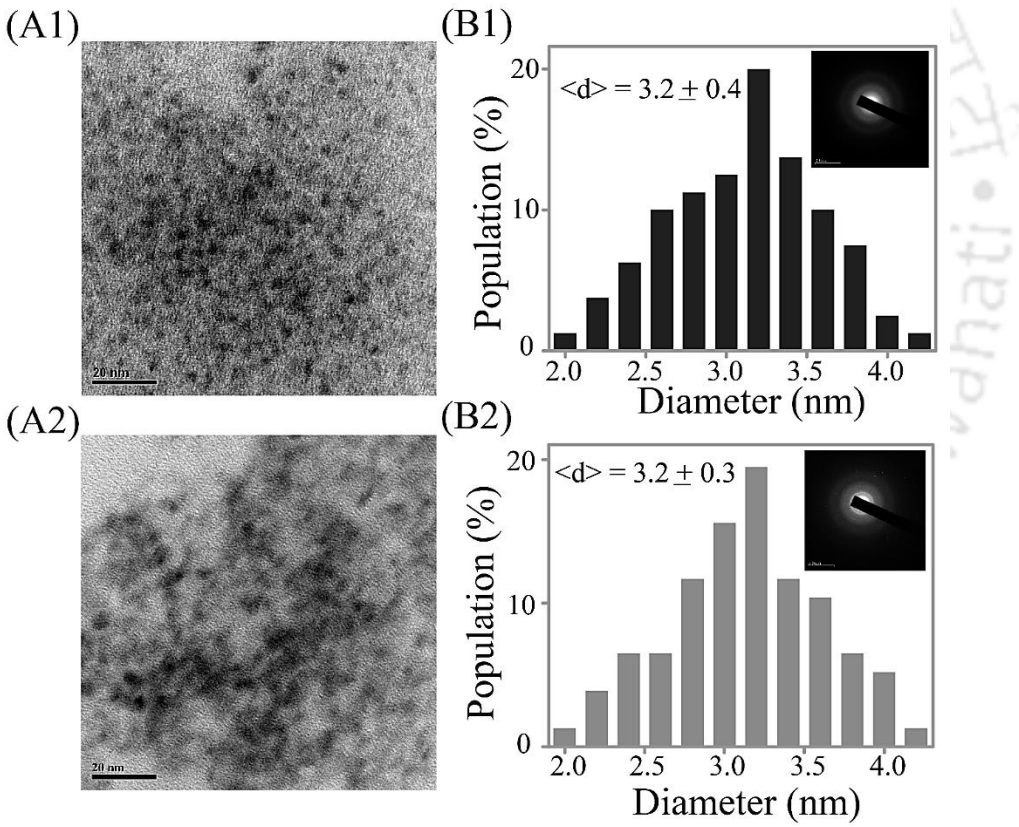

Figure A.3.7. (A) TEM (scale bar-20 nm) image, **(B)** corresponding particle size distribution (inset: selected area diffraction pattern; scale bar 5 nm^{-1}) of the ethanolic dispersion of (1) en-capped ZnS Qdots and (2) CuQ_2 added en-capped ZnS Qdots.

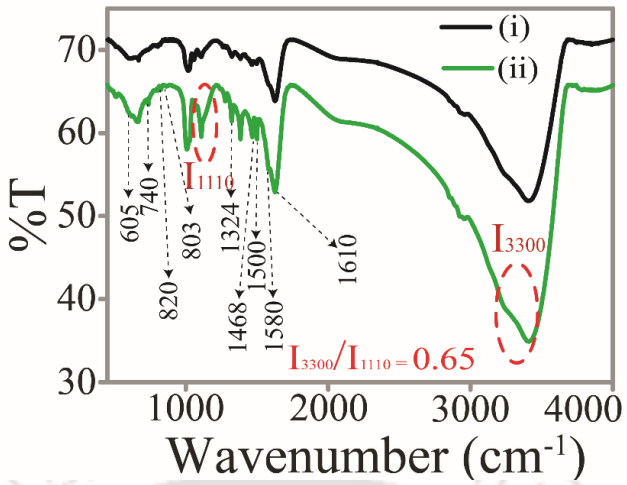

Figure A.3.8. Fourier transform infrared (FTIR) spectra of the solid particles of (i) en-capped ZnS Qdots and (ii) CuQ_2 added en-capped ZnS Qdots.

The characteristic peaks at 1605 and 1577 cm^{-1} (C-C/C-N stretching), 1500 and 1468 cm^{-1} (pyridyl and phenyl rings), at 1328 cm^{-1} (C-H bending peaks), 822, 800 and 742 cm^{1} (C-H out plane wagging) and 742, 642 and 605 cm^{-1} (in-plane ring deformation) revealed the presence metal-HQ complexes – which are absent in as synthesized Qdots – in CuQ_2 treated Qdots (Figure A.3.8).

Table A.3.4. Tabulated metal ion concentration of the (i) as synthesized en-capped ZnS Qdots and (ii) CuQ_2 added en-capped ZnS Qdots (following centrifugation and redispersion into same amount of solvent). The measurements were made using an atomic absorption spectrometer.

Samples	[Zn] (ppm)	[Cu] (ppm)
(i) en-capped ZnS Qdots	46.8	-
(ii) CuQ_2 added en-capped ZnS Qdots	43.2	0.967

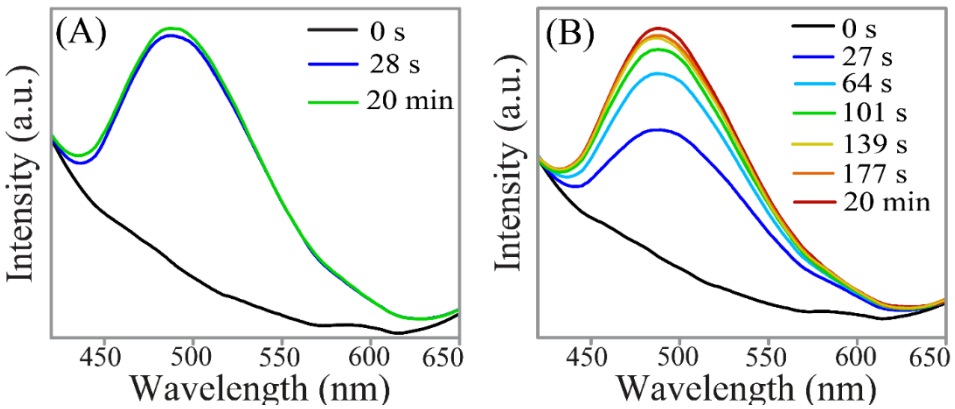

Figure A.3.9. Time dependent changes (at T= 20 °C) in emission (λ_{ex}-361 nm) intensity following addition of **(A)** 10.0 µL 0.02 mM of HQ and **(B)** 10.0 µL 0.01 mM of MnQ_2 (in ethanol) to a solution containing 200.0 µL of as prepared Qdots (in ethanol) and 2.8 mL ethanol.

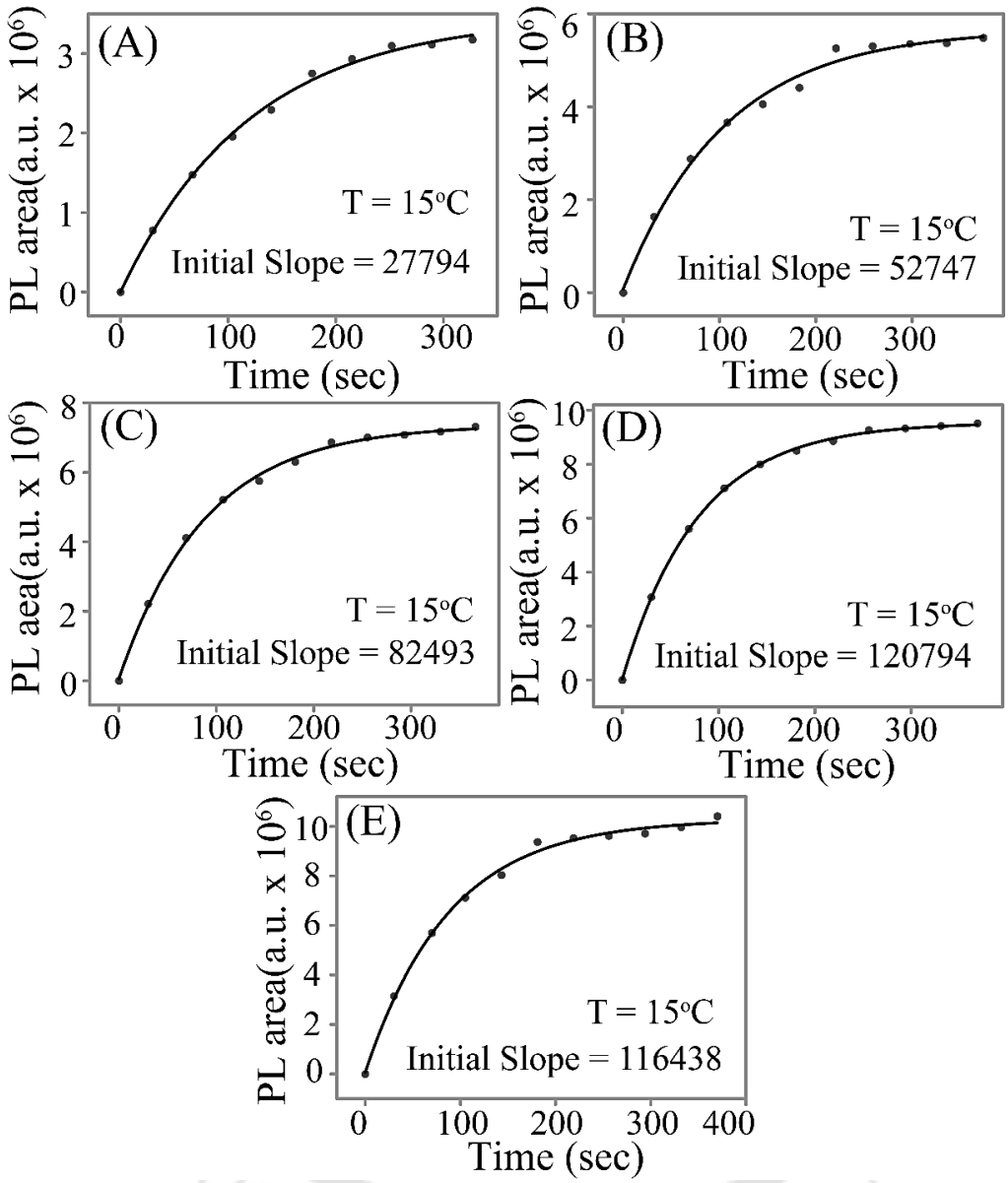

Figure A.3.10. Exponential fittings of PL Area (area under the emission curve) vs time plot at T= 15 °C obtained from time-dependent PL emission spectra of **(A)** 2.0 µL, **(B)** 4.0 µL, **(C)** 6.0 µL, **(D)** 8.0 µL and **(E)** 10.0 µL 0.1 mM of CuQ_2 (in ethanol) added Qdots dispersion (which contained 200.0 µL ethanolic solution of as synthesized Qdots and 2.8 mL ethanol). Data points were fitted to exponential functions and the slopes were considered as initial rates of the reaction.

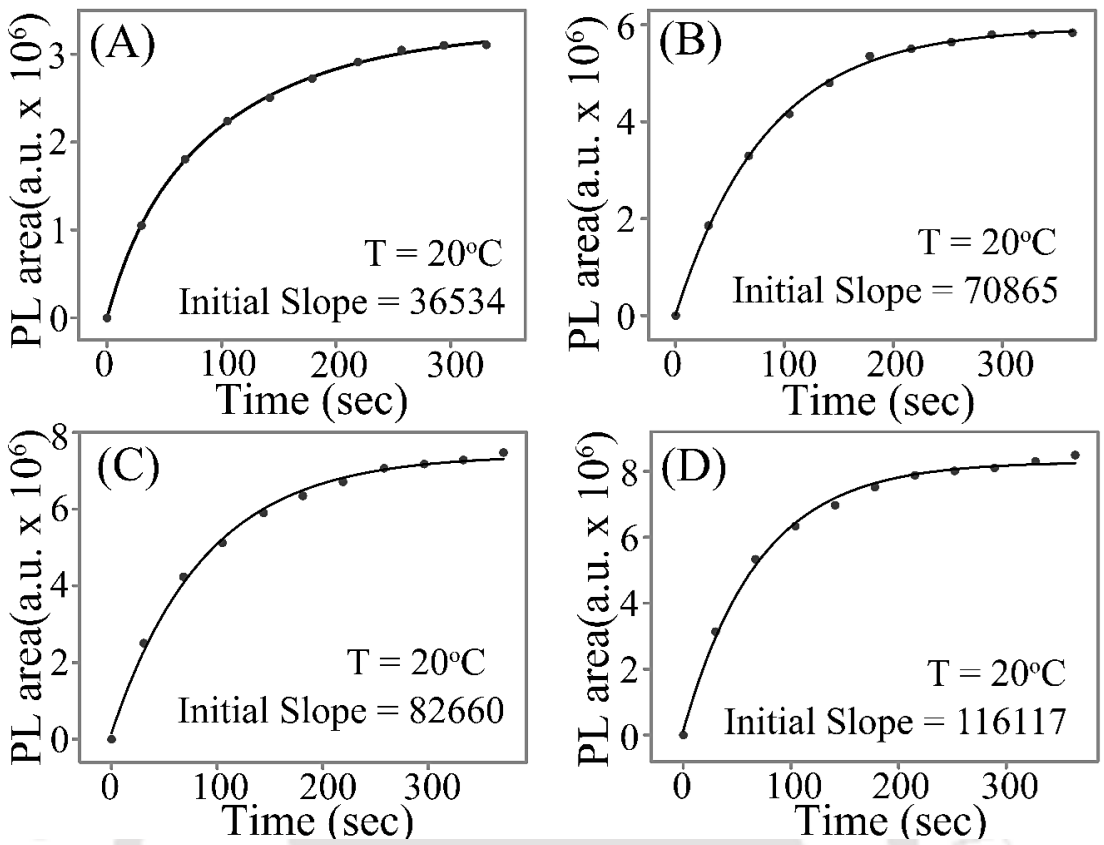

Figure A.3.11. Exponential fittings of PL area (area under the emission curve) vs time plot at T= 20 °C obtained from time dependent PL emission spectra of **(A)** 2.0 µL, **(B)** 4.0 µL, **(C)** 6.0 µL and **(D)** 8.0 µL 0.1 mM of CuQ_2 (in ethanol) added Qdots dispersion (which contained 200.0 µL ethanolic solution of as synthesized Qdots and 2.8 mL ethanol). Data points were fitted to exponential functions and the slopes were considered as initial rates of the reaction.

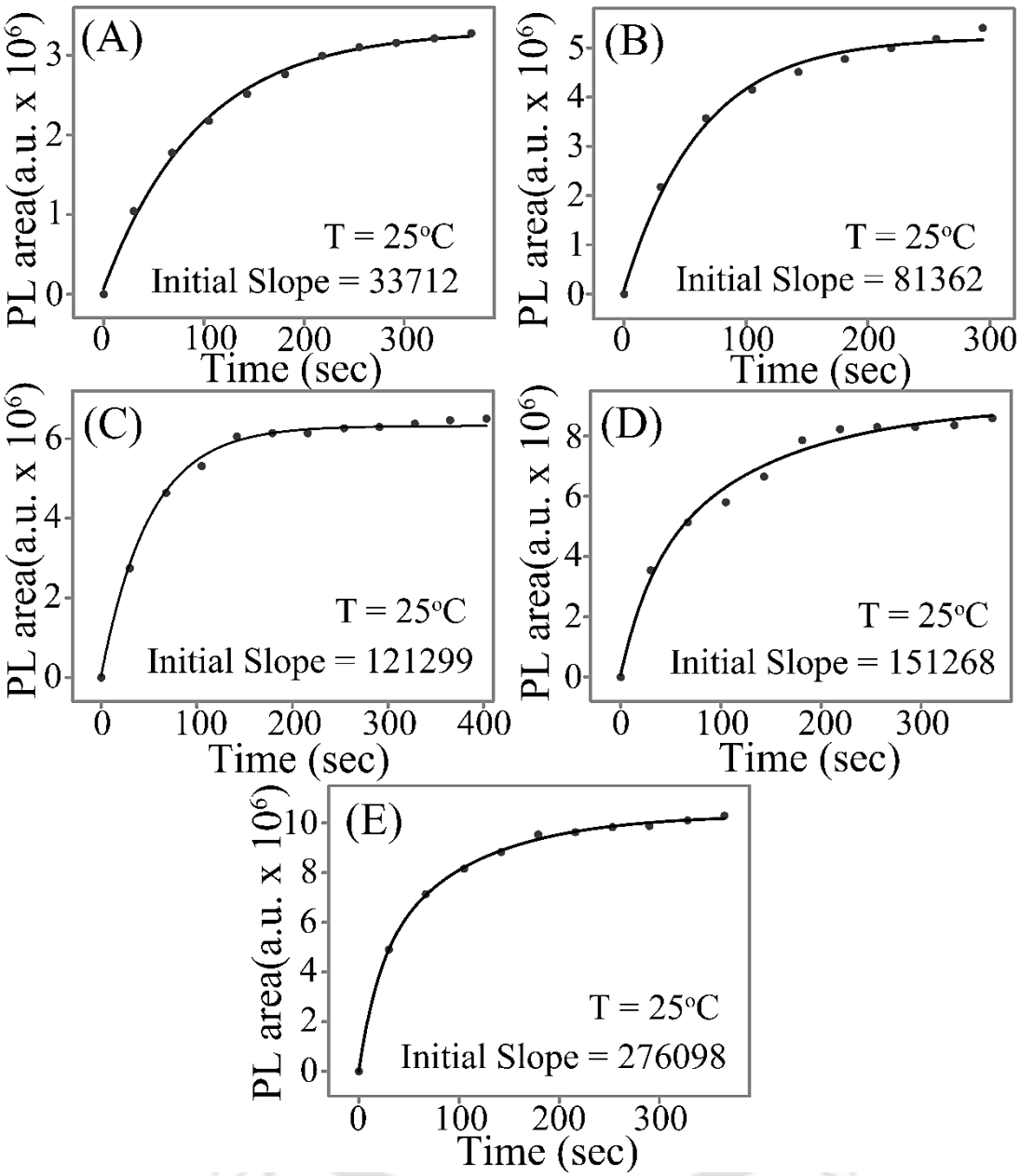

Figure A.3.12. Exponential fittings of PL area (area under the emission curve) vs time plot at T= 25 ºC obtained from time dependent PL emission spectra of **(A)** 2.0 µL, **(B)** 4.0 µL, **(C)** 6.0 µL and **(D)** 8.0 µL, and **(E)** 10.0 µL 0.1 mM of CuQ_2 (in ethanol) added Qdot dispersion (which contained 200.0 µL ethanolic solution of as synthesized Qdots and 2.8 mL ethanol). Data points were fitted to exponential functions and the slopes were considered as initial rates of the reaction.

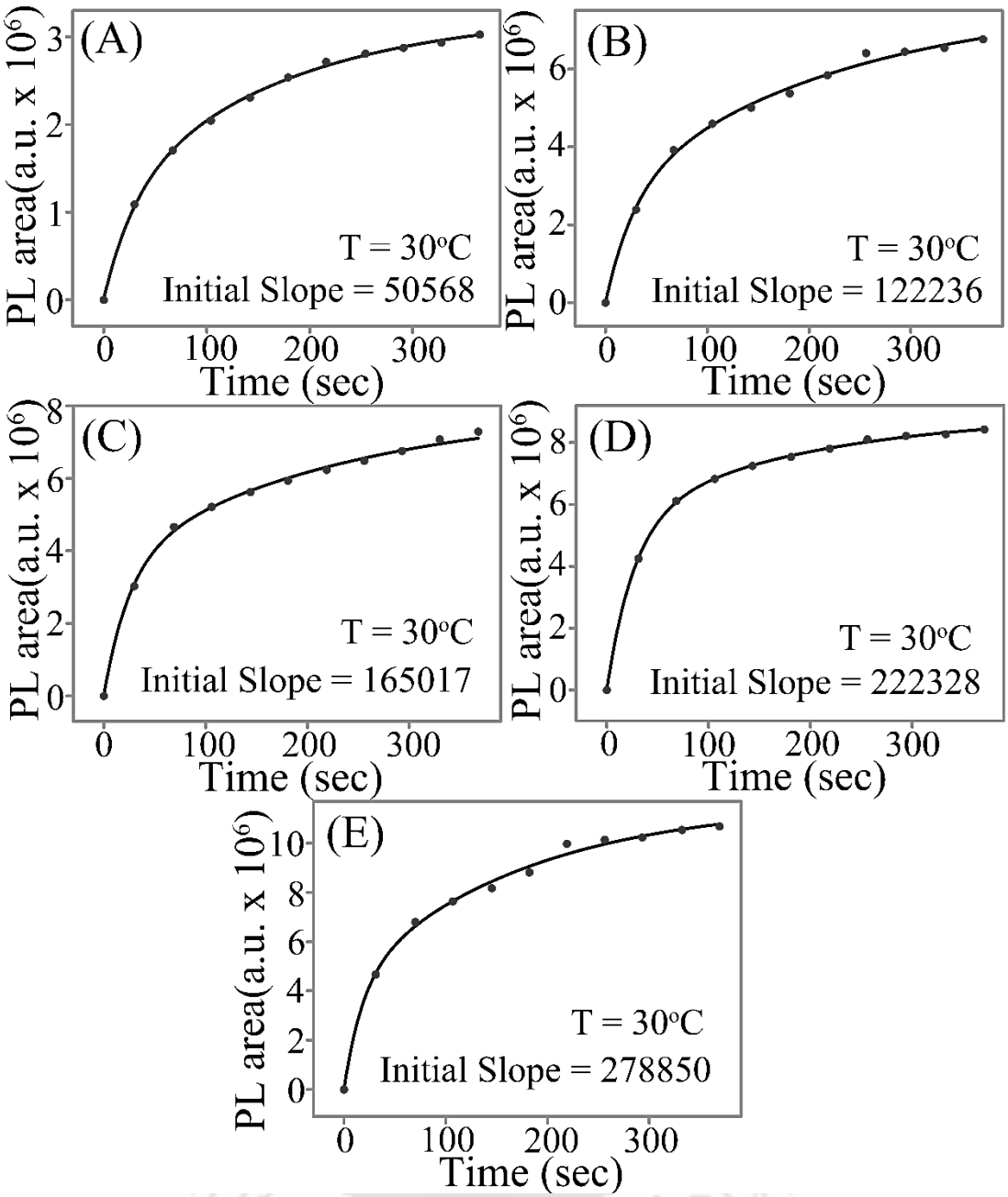

Figure A.3.13. Exponential fittings of PL area (area under the emission curve) vs time plot at T= 30 ºC obtained from time dependent PL emission spectra of **(A)** 2.0 µL, **(B)** 4.0 µL, **(C)** 6.0 µL, **(D)** 8.0 µL and **(E)** 10.0 µL 0.1 mM of CuQ_2 (in ethanol) added Qdot dispersion (which contained 200.0 µL ethanolic solution of as synthesized Qdots and 2.8 mL ethanol). Data points were fitted to exponential functions and the slopes were considered as initial rate of the reaction.

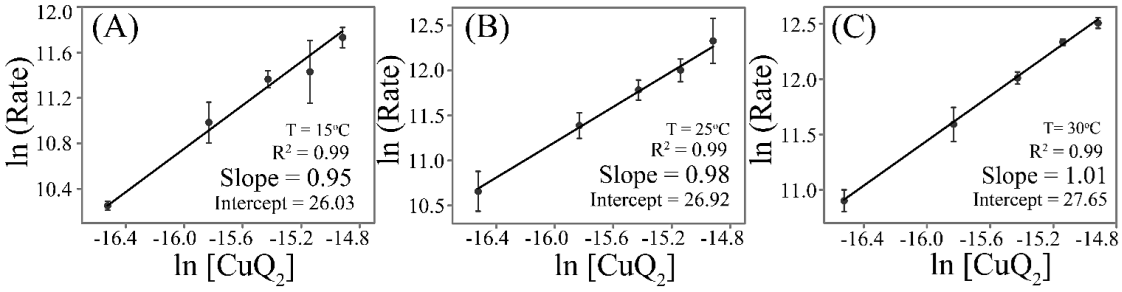

Figure A.3.14. Plot of ln (Rate) Vs ln [CuQ_2] at different temperatures: **(A)** T= 15 ºC, **(B)** T= 25 ˚C and **(C)** T= 30 ˚C. Data points were fitted to linear functions and the slopes were considered equal to order of the reaction (i.e., 1).

Table A.3.5: Tabulated form of the solutions, which were used for measuring order and activation energy of the formation of QDC with respect to CuQ_2.

Amount of 0.1 mM CuQ_2 used (µL)	Amount of as synthesized Qdots used (µL)	Amount of ethanol used (µL)	Total volume (µL)	Final concentration of CuQ_2 (µM)
2.0	200.0	2800.0	3002.0	0.07
4.0	200.0	2800.0	3004.0	0.13
6.0	200.0	2800.0	3006.0	0.20
8.0	200.0	2800.0	3008.0	0.26
10.0	200.0	2800.0	3010.0	0.33

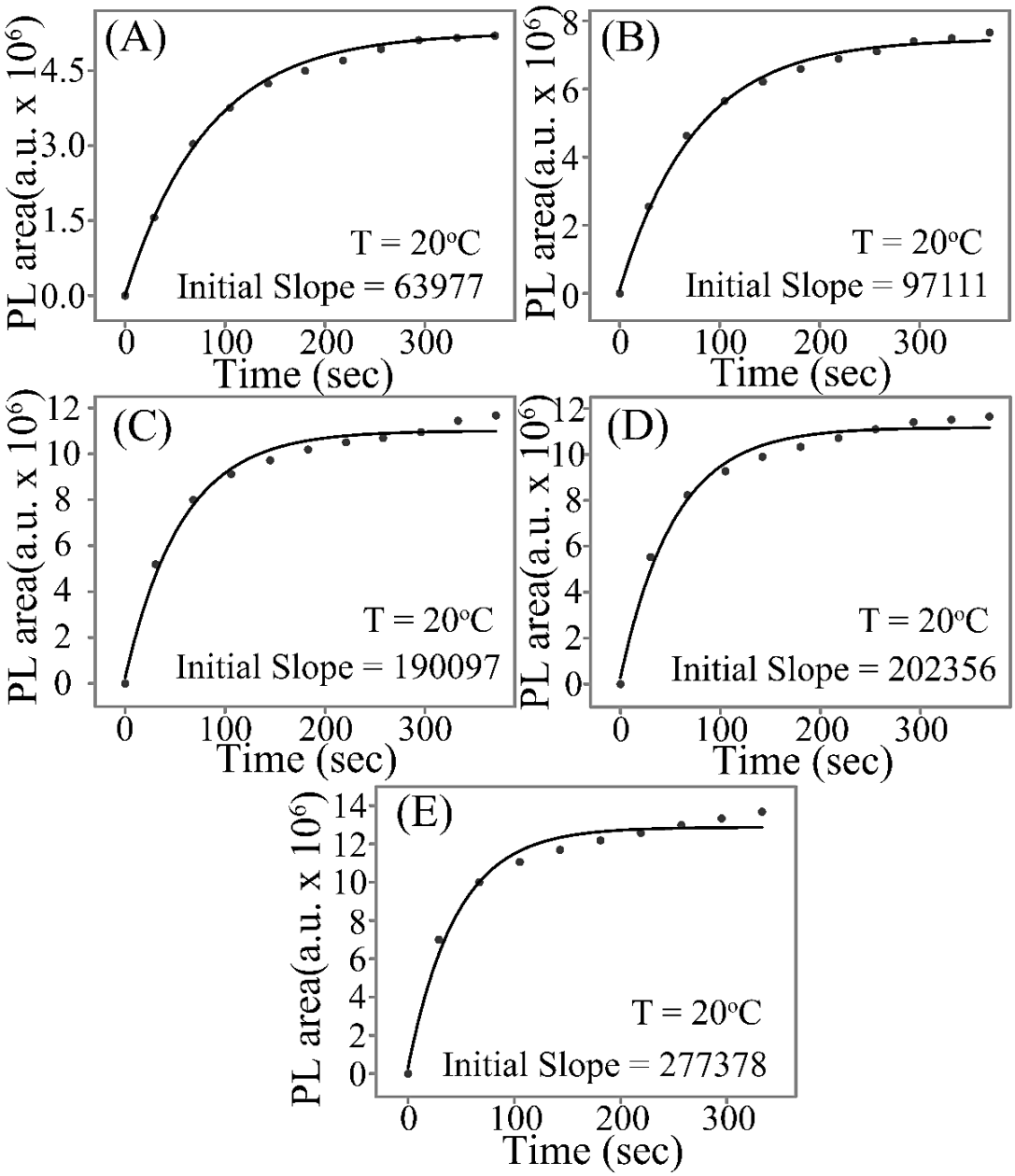

Figure A.3.15. Exponential fittings of PL area (area under the emission curve) vs time plot at T= 20 °C obtained from time dependent PL emission spectra of 10.0 µL 0.1 mM of CuQ_2 (in ethanol) added to a solution which contained different volumes of as synthesized Qdots (in ethanol): **(A)** 50.0 µL, **(B)** 100.0 µL, **(C)** 150.0 µL, **(D)** 200.0 µL and **(E)** 250 µL Qdot dispersion. The total volume of each solution was adjusted to 3.0 mL by adding ethanol Data points were fitted to exponential functions and the slopes were considered as initial rate of the reaction.

A.4. Chapter4.

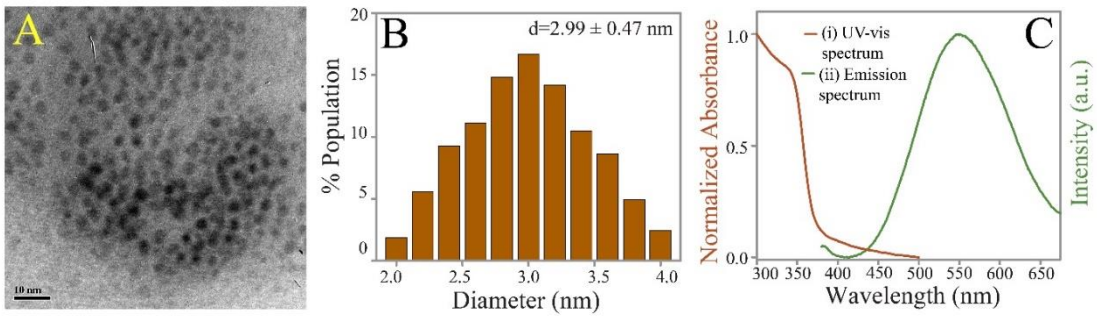

Figure A.4.1. (A) Representative transmission electron microscopic (TEM) image, (B) corresponding particle size distribution, (C) (i) UV-vis spectrum and (ii) photoluminescence (PL) emission spectrum of as-synthesized ZnO quantum dots.

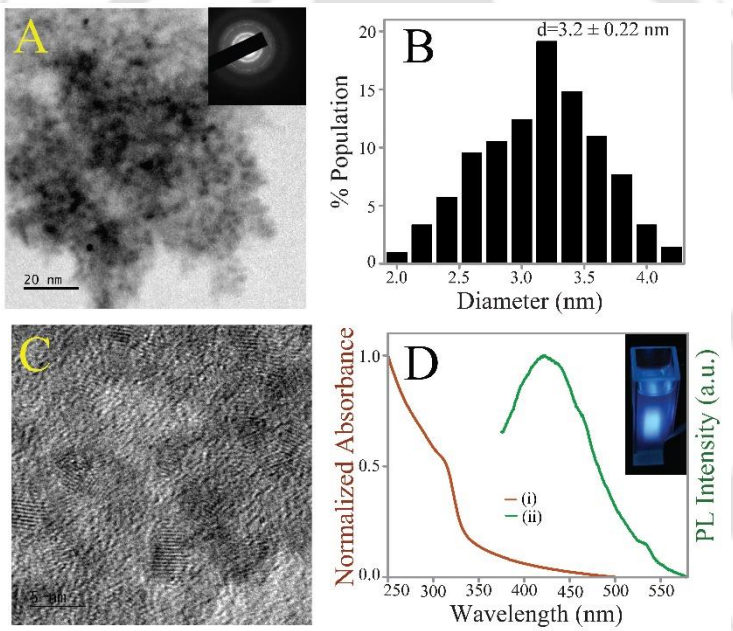

Figure A.4.2. (A) Representative transmission electron microscopic (TEM) image and (inset) SAED pattern, (B) corresponding particle size distribution, (C) high resolution TEM image, (D) (i) UV-vis spectrum, (ii) photoluminescence emission spectrum and (inset) photograph under UV radiation (λ_{ex} – 325 nm) of as-synthesized ZnS quantum dots (aqueous dispersion).

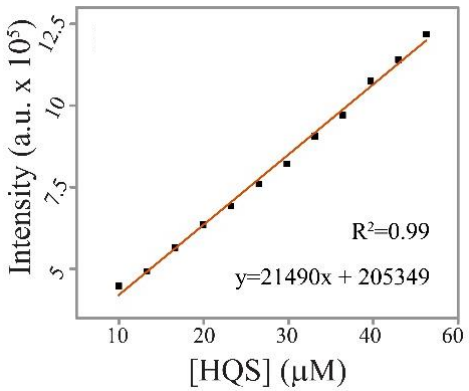

Figure A.4.3 Dependence of PL emission intensity of HQS added ZnO with concentration of HQS corresponding to Figure 4.1A (Chapter 4).

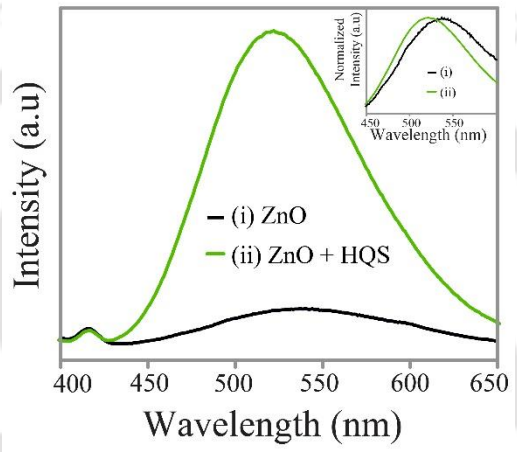

Figure A.4.4. Photoluminescence emission spectra (λ_{ex} – 365 nm) of (i) as synthesized ZnO quantum dots dispersed in phosphate buffer (resulting pH ~ 6.83) and (ii) that after addition of 5 mM 50 μL HQS solution (water-methanol mixture) (resulting pH ~ 6.80) and (inset) corresponding normalized spectra indicating blue shift after addition of HQS.

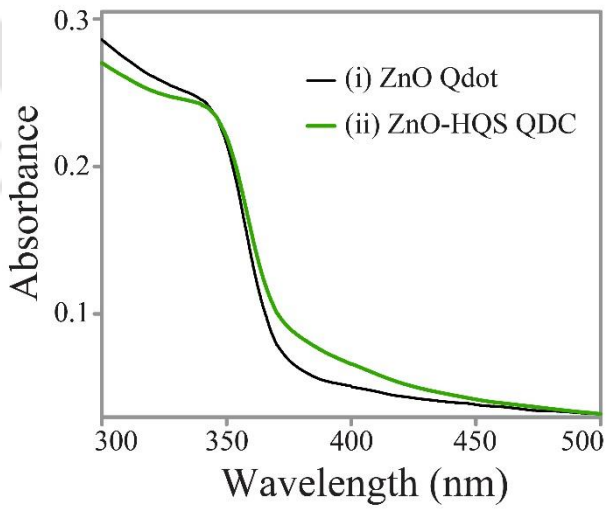

Figure A.4.5. UV-vis spectra of (i) as synthesized ZnO Qdots and (ii) ZnO-HQS QDC in methanolic dispersion.

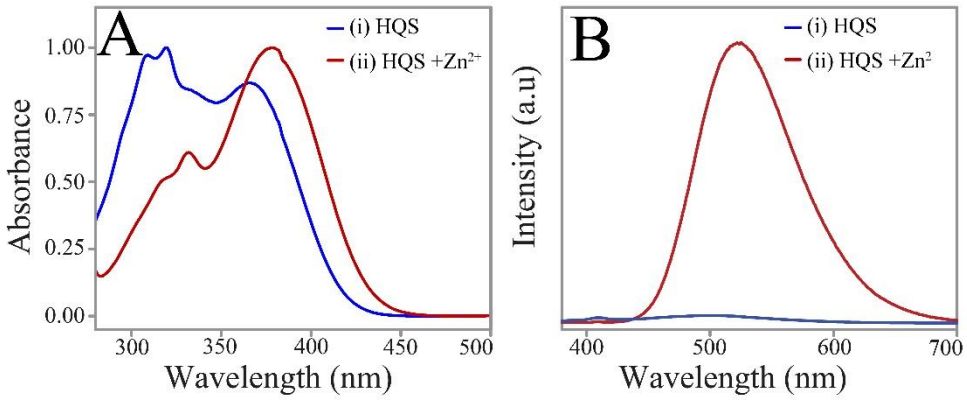

Figure A.4.6. (A) UV-vis spectra and (B) photoluminescence emission spectra (λ_{ex} – 365 nm) of (i) 8-hydroxyquinoline-5-sulphonic acid (HQS) and (ii) Zn^{2+} added with HQS in MeOH.

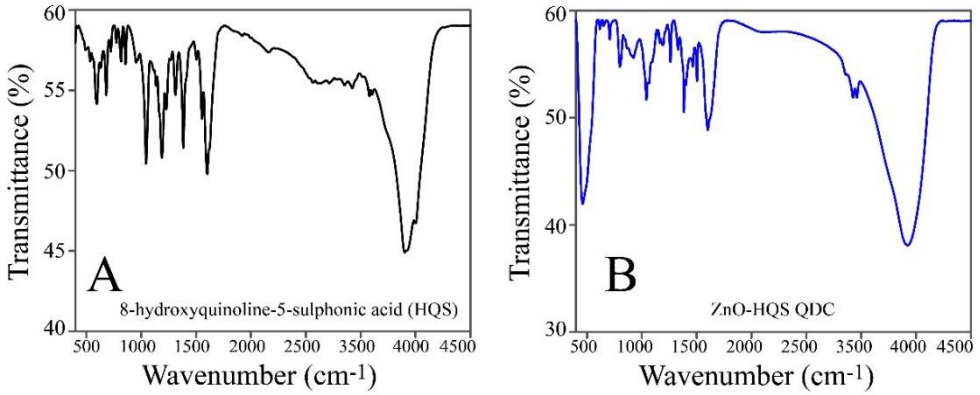

Figure A.4.7. Fourier transformed infrared (FTIR) spectra of the solid sample (KBr pellet) of (A) 8-hydroxyquinoline-5-sulphonic acid (HQS) and (B) ZnO-HQS QDC solid obtained after centrifugation of mixture of HQS and ZnO Qdot followed by drying in vacuum.

The characteristic peaks are at 1603 and 1570 cm^{-1} (C-C/C-N stretching), 1495 and 1464 cm^{-1} (pyridyl and phenyl rings), at 1325 cm^{-1} (C-H bending peaks), 825, 804 and 740 cm^{-1} (C-H out plane wagging), 645 cm^{-1} (in-plane ring deformation). Presence of these peaks in FTIR spectrum of ZnO-HQS QDC confirmed the presence of HQS on surface of ZnO Qdot.

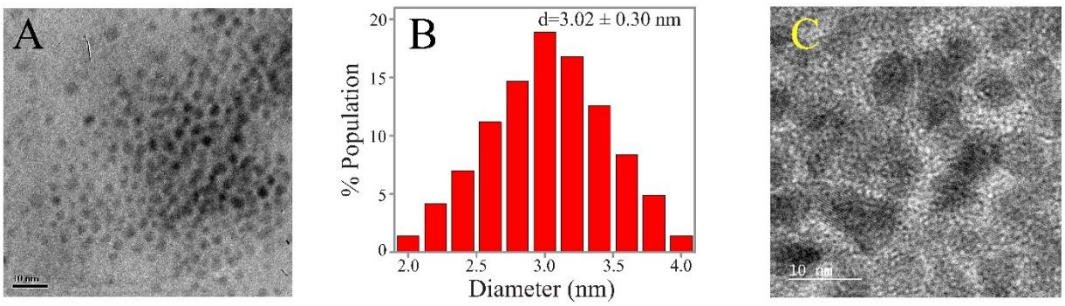

Figure A.4.8. (A) Transmission electron microscopic (TEM) image, (B) corresponding particle size distribution, and (C) high resolution TEM image of ZnO-HQS QDC.

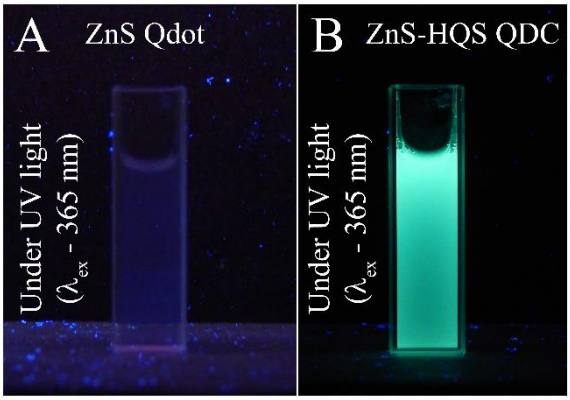

Figure A.4.9. Photographic images of (A) ZnS Qdot methanolic disperison and (B) ZnS-HQS QDC dispersion in methanol under UV light (λ_{ex} – 365 nm).

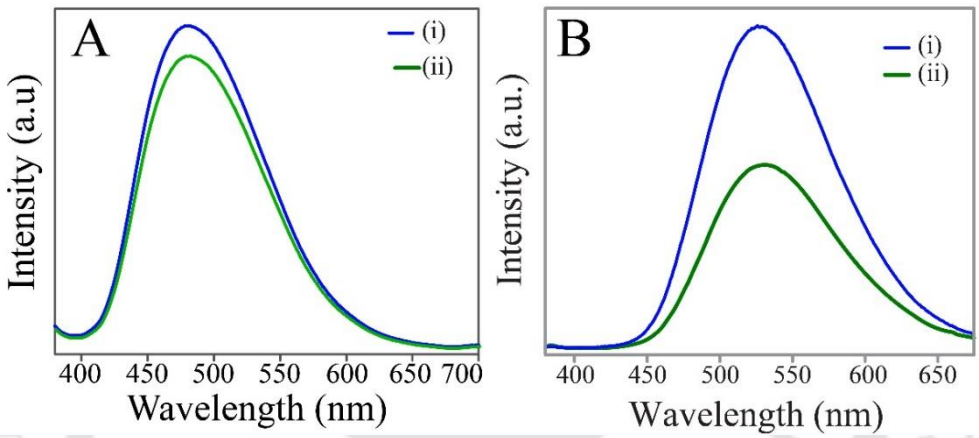

Figure A.4.10. PL emission spectra (λ_{ex} – 365 nm) of (A) en-capped ZnS Qdots treated with HQS and (B) ZnO Qdots treated with HQS both in methanolic medium (i) before centrifugation and (ii) dispersion of pellet to same volume of methanol after centrifugation.

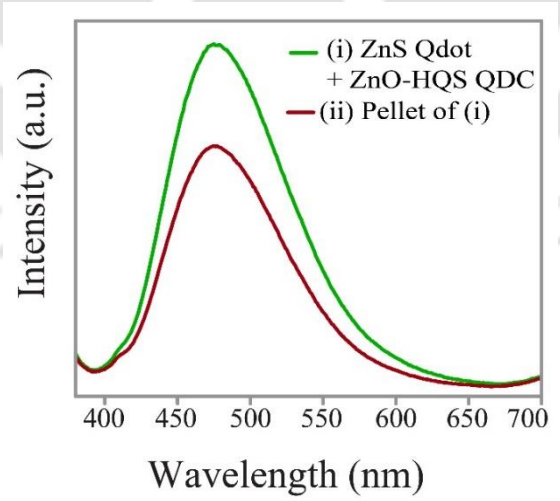

Figure A.4.11. PL emission spectra (λ_{ex} – 365 nm) of (i) en-capped ZnS added with ZnO-HQS QDC (both in methanolic dispersion) and (ii) dispersion of the pellet (obtained after centrifugation of the mixture) in same volume of methanol.

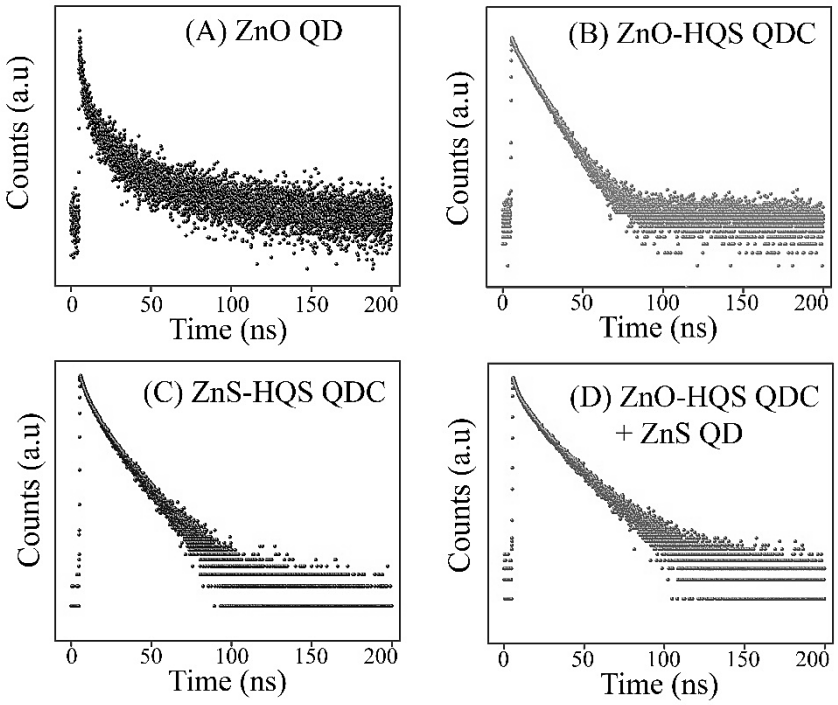

Figure A.4.12. Time resolved photoluminescence spectra (λ_{ex} – 375 nm, laser source) of (A) ZnO QD (λ_{em} – 550 nm), (B) ZnO-HQS QDC (ZnO Qdot + HQS) (λ_{em} – 530 nm), (C) ZnS-HQS QDC (ZnS Qdot + HQS) (λ_{em} – 490 nm), and (D) ZnO-QDC (ZnO Qdot + HQS) added with en-capped ZnS Qdot (λ_{em} – 490 nm).

Table A.4.1. Decay parameters (from experiments carried out using 375 nm laser) obtained following multi-exponential fitting of the emission curve of different samples corresponding to Figure A.4.12.

Samples	λ_{em} (nm)	α_i (%)	τ_i (ns)	τ_{av} (ns)	χ^2
ZnO QD	550	21.24	5.14	40.69	0.99
		78.76	41.86		
ZnO-QDC (ZnO+HQS)	530	4.52	1.78	11.59	1.05
		95.48	11.66		
ZnS-QDC (ZnS+HQS)	490	9.41	2.09	13.52	1.03
		39.47	7.32		
		51.12	15.99		
ZnO-HQS QDC + en-ZnS Qdot	490	6.89	1.67	16.69	1.17
		28.80	7.28		
		64.31	18.47		

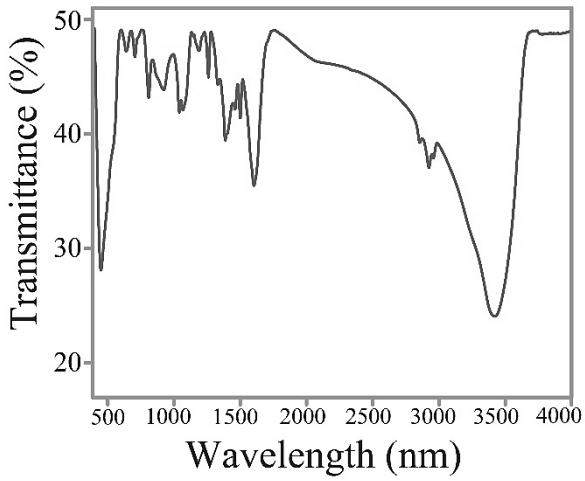

Figure A.4.13. Fourier transform infrared (FTIR) spectrum of the solid sample (KBr pellet) of pellet obtained after magnetic separation of Fe_3O_4@ZnS and ZnO-HQS QDC mixture.

The characteristic peaks are at 1600 cm^{-1} (C-C/C-N stretching), 1500 and 1461 cm^{-1} (pyridyl and phenyl rings), at 1329 cm^{-1} (C-H bending peaks), 809 and 733 cm^{-1} (C-H out plane wagging), 641 cm^{-1} (in-plane ring deformation). Presence of these peaks in FTIR spectrum of solid pellet obtained after magnetic separation of Fe_3O_4@ZnS and ZnO-HQS QDC mixture confirmed the attachment of HQS on Fe_3O_4-ZnS NCs.

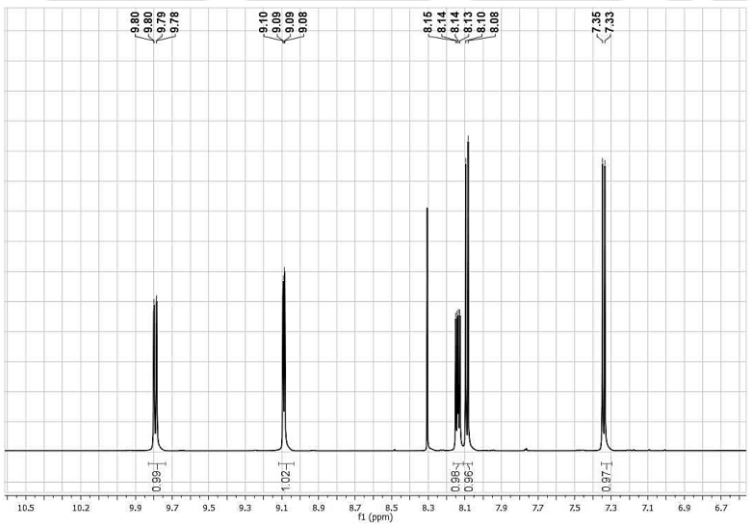

Figure A.4.14. Proton NMR spectra of 8-hydroxyquinoline-5-sulphonic acid (HQS). ^{1}H NMR (600 MHz, DMSO-d_6) 9.79 (dd, J = 8.7, 1.3 Hz, 1H), 9.09 (dd, J = 5.2, 1.4 Hz, 1H), 8.14 (dd, J = 8.7, 5.2 Hz, 1H), 8.09 (d, J = 8.1 Hz, 1H), 7.34 (d, J = 8.1 Hz, 1H).

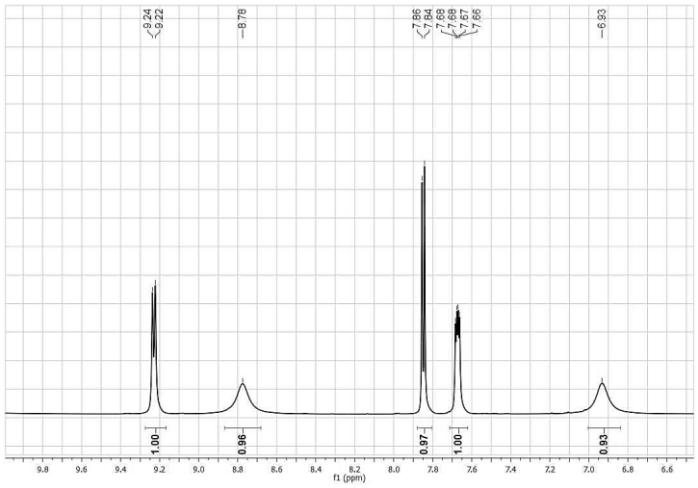

Figure A.4.15. Proton NMR spectra of Zn^{2+} added 8-hydroxyquinoline-5-sulphonic acid (HQS) (molar ratio of addition 1:2). ^{1}H NMR (600 MHz, DMSO-d_6) δ 9.23 (d, J = 8.5 Hz, 1H), 8.78 (s, 1H), 7.85 (d, J = 8.0 Hz, 1H), 7.67 (dd, J = 8.5, 4.2 Hz, 1H), 6.93 (s, 1H).

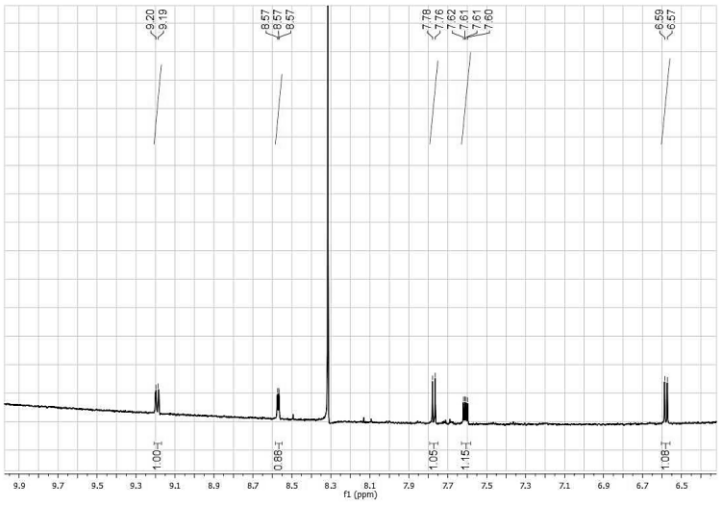

Figure A.4.16. Proton NMR spectra of supernatant obtained after centrifugation of as prepared ZnO-HQS QDC. ^{1}H NMR (600 MHz, DMSO-d_6) δ 9.19 (d, J = 7.2 Hz, 1H), 8.66 – 8.50 (m, 1H), 7.77 (d, J = 8.2 Hz, 1H), 7.61 (dd, J = 8.6, 4.4 Hz, 1H), 6.58 (d, J = 8.2 Hz, 1H).

Proton NMR spectra of HQS, Zn^{2+} added HQS (Figure A.4.14 and 15) revealed that Zn^{2+} metal coordination to the ligand, HQS results in upfield chemical shift in NMR signal. As the ligand tranfer electron density to metal centre while complexation, the aromatic protons become more shielded as a result of reducing aromatic anisotropy. Like complex ($Zn(QS)_2$), we observe same trend in proton NMR in case of supernatant obtained after centrifuging as prepared ZnO-HQS QDC. These results certainly indicate the presence of complex (i.e., $Zn(QS)_2$) in the supernatant.

A.5. Chapter 5.

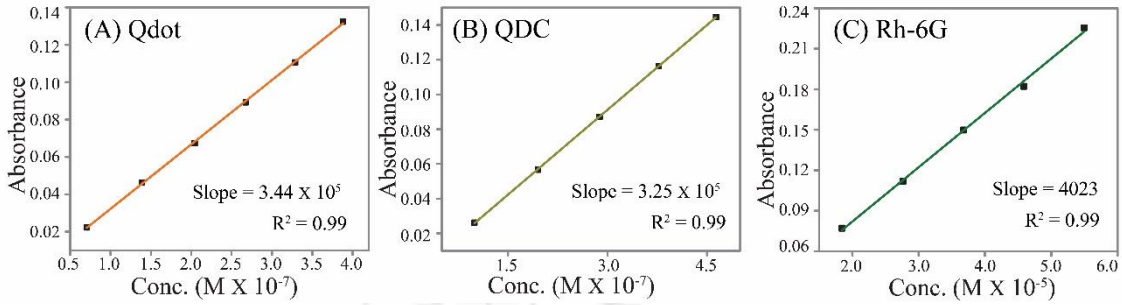

Figure A.5.1. Absorbance vs concentration plots of methanolic solution of **(A)** Mn^{2+} doped ZnS Qdot, **(B)** QDC and **(C)** rhodamine-6G.

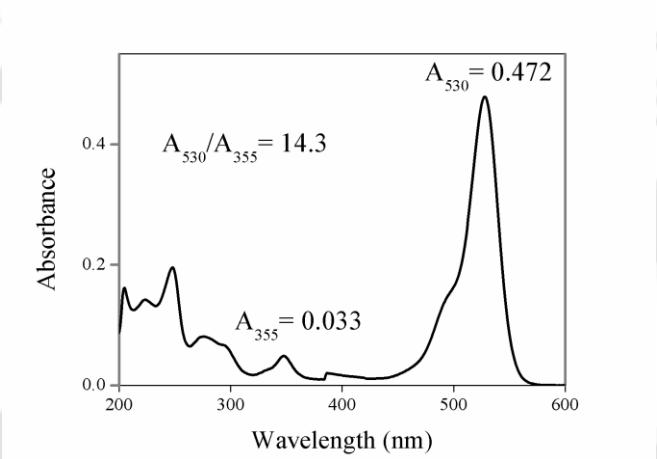

Figure A.5.2. Absorption spectrum of methanolic solution of rhodamine-6G.

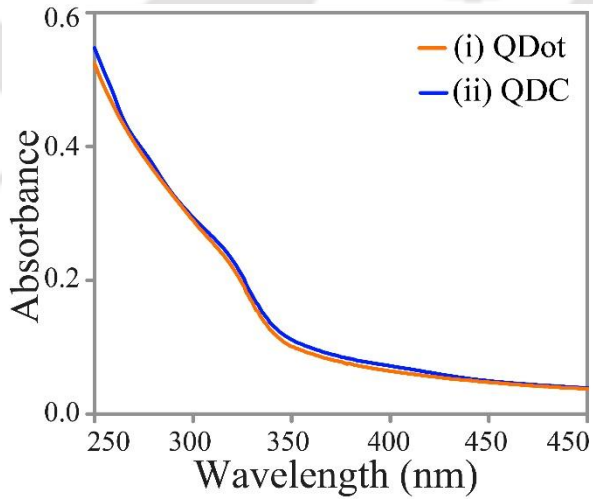

Figure A.5.3. UV-vis spectra of as-synthesized (i) Mn^{2+} doped ZnS Qdots and (ii) QDC.

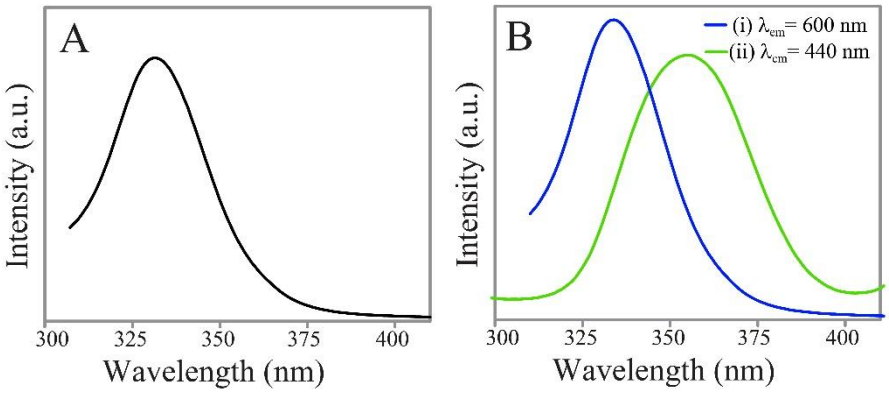

Figure A.5.4. Excitation spectra of **(A)** as-synthesized Mn^{2+} doped ZnS Qdots and **(B)** QDC with probing emission maxima at (i) 595 and (ii) 440 nm, respectively.

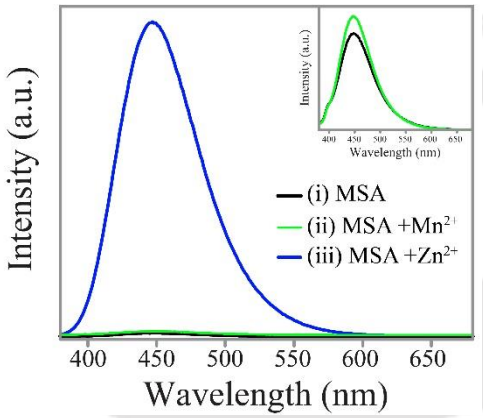

Figure A.5.5. Emission spectra (λ_{ex}-355 nm) of (i) MSA, (ii) Zn^{2+} added MSA (1:1) and (iii) Mn^{2+} added MSA (1:1) in methanol. Inset represents zoom-in spectra corresponding to (i) and (ii).

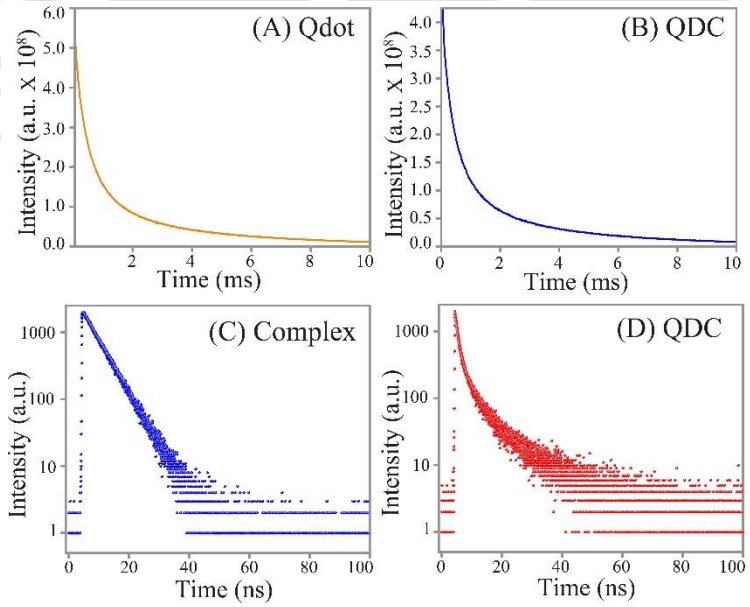

Figure A.5.6. Phosphorescence decay profile of (**A**) Mn^{2+} doped ZnS Qdots and (**B**) QDC ((λ_{em}-595 nm and λ_{ex}-330 nm). Time resolved photoluminescence decay profile (using 375 nm laser and emission monitored at 440 nm) of (**C**) Zn-MSA complex and (**D**) QDC.

Table A.5.1. Tabulated representation of luminescence lifetime corresponding to Figure A.5.6.

Sample	λ_{ex} (nm)	λ_{em} (nm)	α_i (%)	τ_i	τ_{av}	χ^2
(A) Qdot	330	595	25.5	0.13 ms	2.17 ms	0.99
			53.2	0.56 ms		
			21.3	3.03 ms		
(B) QDC	330	595	52.1	0.52 ms	2.07 ms	0.99
			21.5	2.84 ms		
			26.4	0.10 ms		
(C) Complex	375	440	100	5.44 ns	5.44 ns	1.03
(D) QDC	375	440	41.58	0.89 ns	10.35 ns	1.22
			35.07	3.49 ns		
			23.35	13.96 ns		

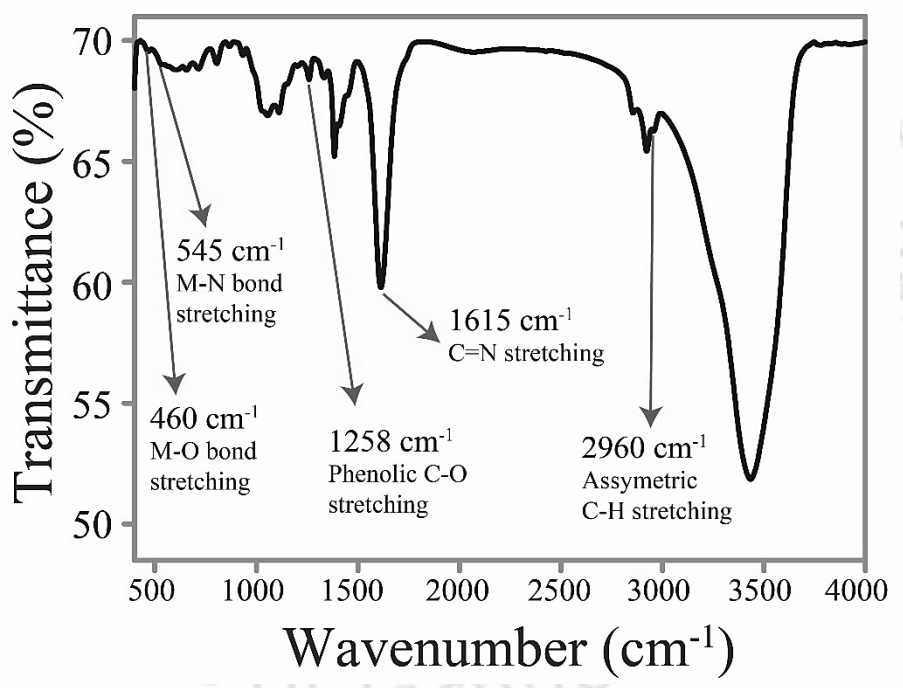

Figure A.5.7. FTIR spectrum of QDC. (where, M = Mn or Zn)

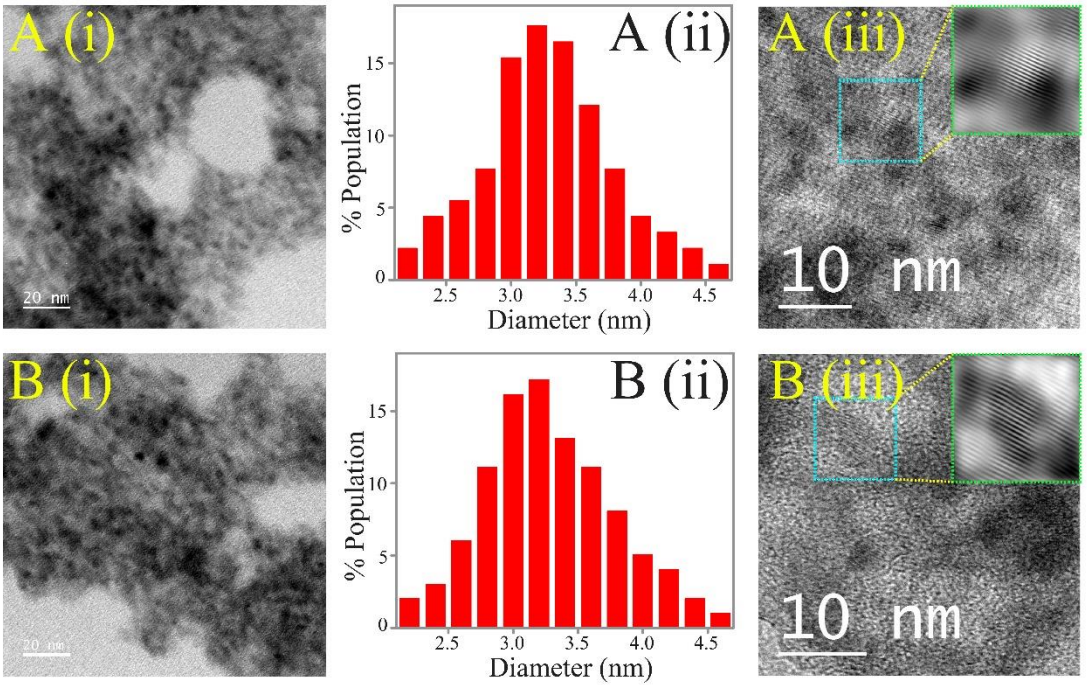

Figure A.5.8. (i) Transmission electron microscopy (TEM) images and (ii) corresponding particle size distributions and (iii) high resolution TEM images of **(A)** as-synthesized Mn^{2+} doped ZnS Qdots and **(B)** QDC.

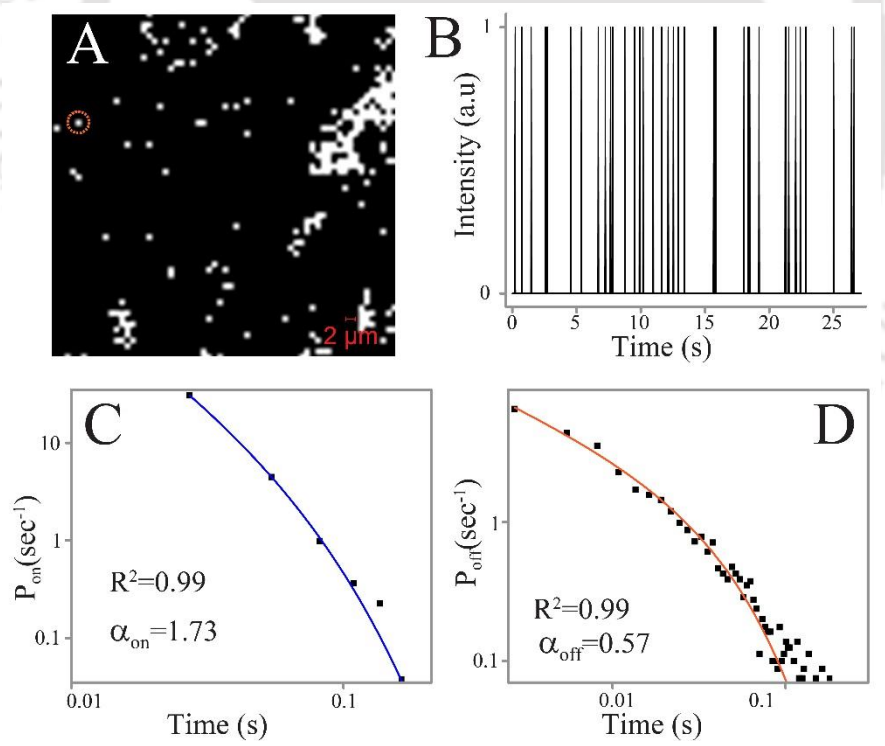

Figure A.5.9. (A) Superresolution confocal laser scanning microscopic (CLSM) images (scale bar-2.0 μm) and **(B)** representative time-dependent blinking profile (related to the particle marked in Figure A.5.9A) of Mn^{2+} doped ZnS Qdot at a few particle level recorded with regard to emission peak having range 570-650 nm. Probability densities of **(C)** on-states (P_{on}) and **(D)** off-

states (P_{off}) of Qdot. The 355 nm laser was used to excite the Qdot. The data were acquired for 50 particles (consisting of a few Qdot) by using binning time of 27 ms, frame size of 64 × 64 μm^2, excitation power of 63 mW, and for a time duration of 27 s.

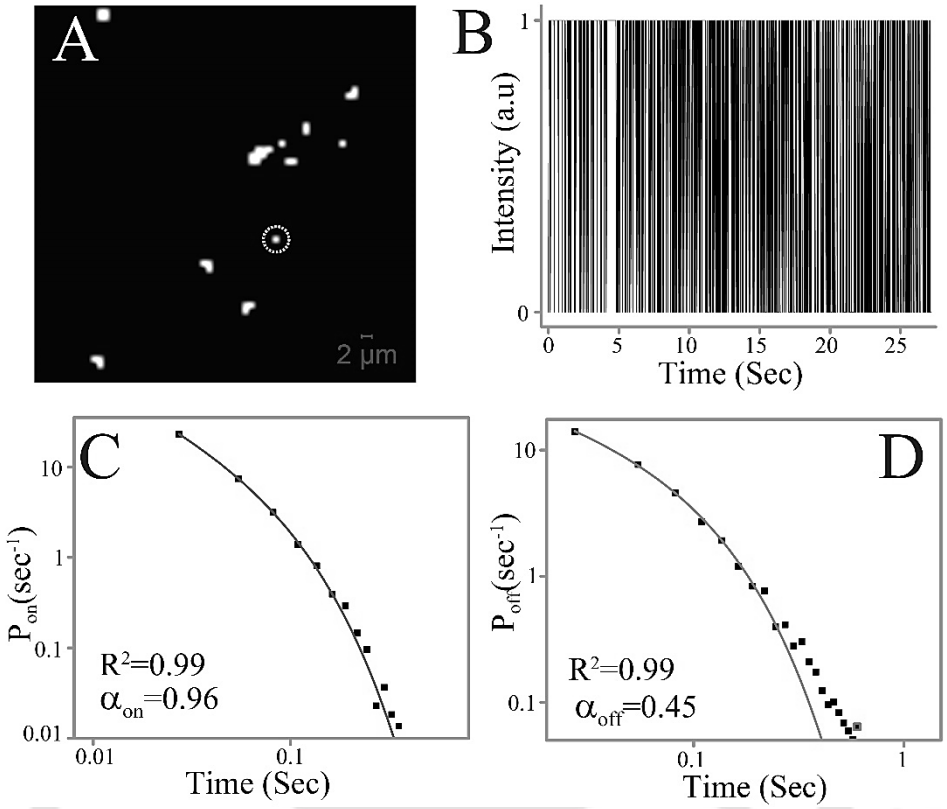

Figure A.5.10. (A) Superresolution confocal laser scanning microscopic (CLSM) images (scale bar-2.0 µm) and **(B)** representative time-dependent blinking profile (related to the particle marked in Figure A.5.10) of QDC (at a few particle level), formed out of a complexation between MSA and undoped ZnS Qdot recorded with regard to emission peak of complex (emission range: 465-525 nm). Probability densities of **(C)** on-states (P_{on}) and **(D)** off-states (P_{off}) of QDC when probed with emission peak of complex (emission range: 465-525 nm). The 355 nm laser was used to excite the QDC. The data were acquired for 50 particles (consisting few QDC) by using binning time = 27 ms, frame size of 64 × 64 μm^2, excitation power of 63 mW, and for a time duration of 27 s.

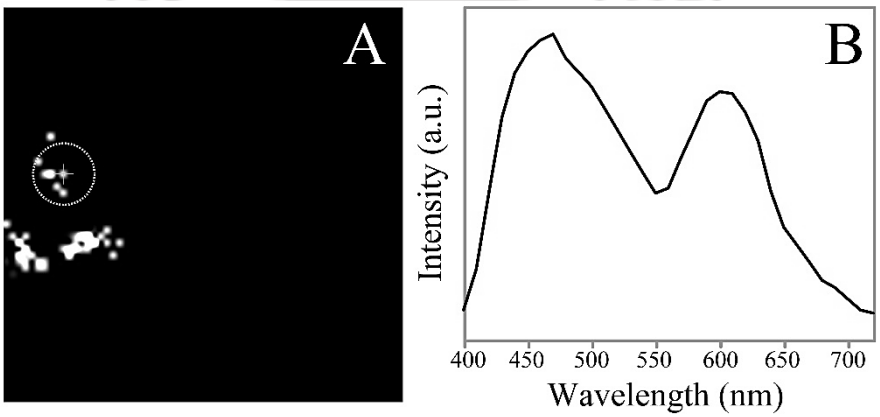

Figure A.5.11. (A) Superresolution confocal laser scanning microscopic (CLSM) image (scale bar-2.0 µm) and **(B)** a few particle level emission spectrum of QDC at laser excitation of 355 nm.

Table A.5.2. Tabulated form of quantum yield of Qdot and QDC at a few particle (Qdot) level and in ensemble.

Samples	Ensemble QY(%)	Particle QY (%)
Mn^{2+} doped ZnS Qdot	0.8	0.9
QDC	1.0	0.9

A.6.A. Chapter 6A

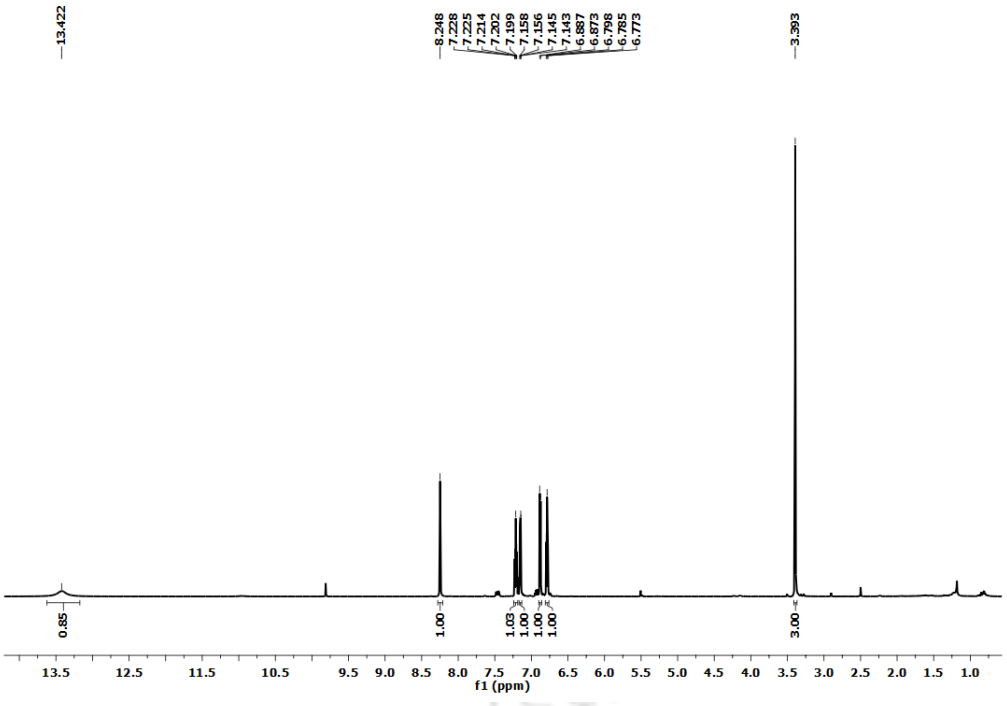

Figure A.6.1. ^{1}H - nuclear magnetic resonance (NMR) spectrum of as-synthesized MSA (purified through column chromatographic techniques).

^{1}H NMR (600 MHz, $CDCl_3$) δ (ppm): 13.42 (s, 1H), 8.25 (s, 1H), 7.24 – 7.19 (m, 1H), 7.15 (dd, *J* = 7.6, 1.3 Hz, 1H), 6.88 (d, *J* = 8.3 Hz, 1H), 6.79 (t, *J* = 7.4 Hz, 1H), 3.39 (s, 3H). The observed chemical shifts in ^{1}H NMR match with the earlier reported results, which indicated the successful formation of MSA.

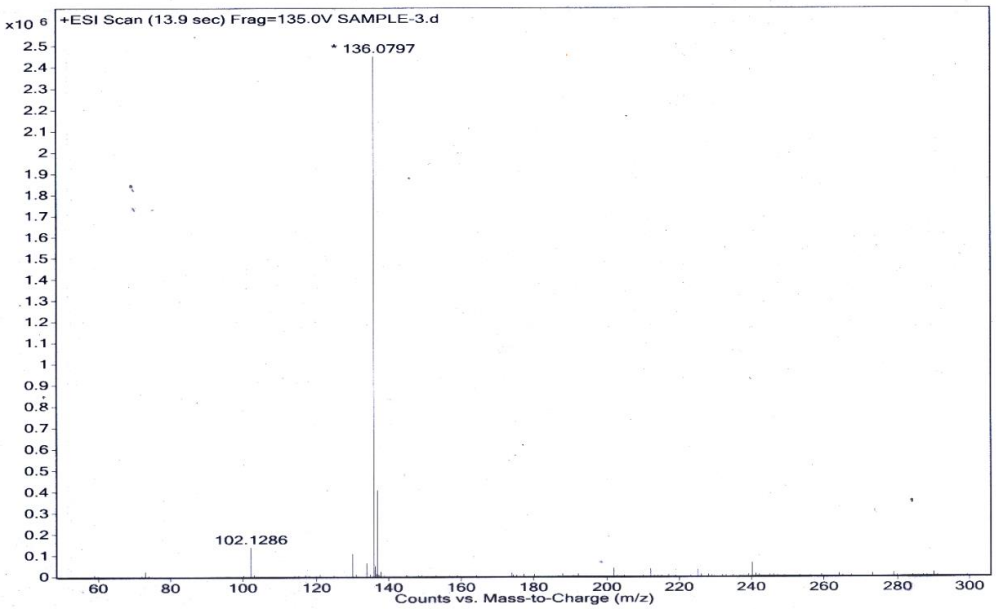

Figure A.6.2. Electrospray ionization (ESI) - mass spectrum of as-synthesized MSA (purified through column chromatographic techniques). Calculated mass M+1 was 136.0762 and experimental mass M+1 was 136.0797.

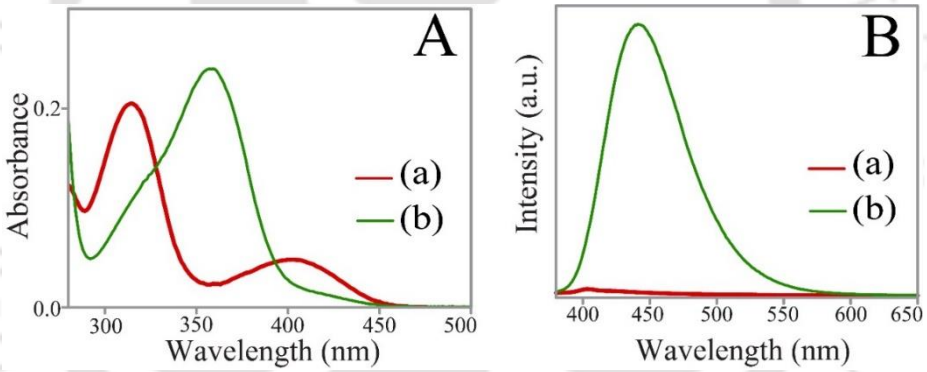

Figure A.6.3. (A) UV-vis absorption and **(B)** emission (λ_{ex}-350 nm) spectra of (a) only 10.0 µL of 5.0 mM MSA added to 3.0 mL of ethanol and (b) 10.0 µL Zn^{2+} salts added to that solution.

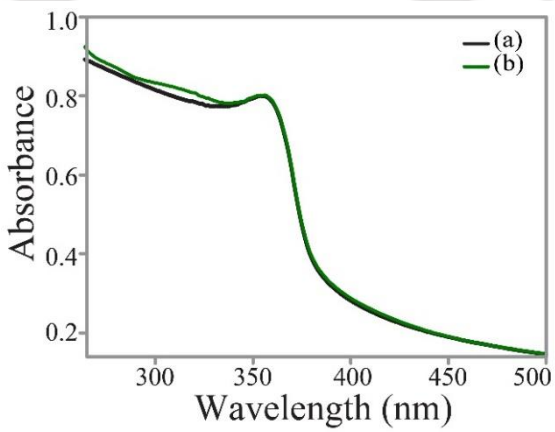

Figure A.6.4. UV-vis spectra of (a) ligand free ZnO Qdots and (b) MSA treated ZnO Qdots.

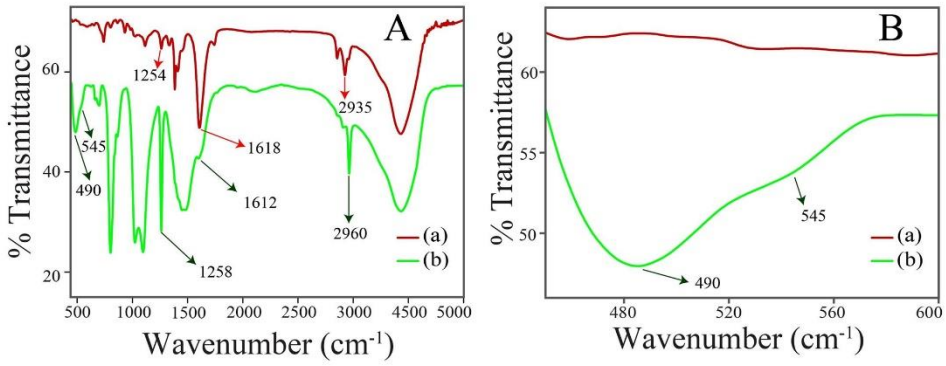

Figure A.6.5. (A) Fourier transformed infrared (FTIR) spectra and **(B)** the same spectra shown with expansion in the range of 450- 600 cm^{-1} of solid (a) only MSA and (b) WLE QDC nanocomposite.

Table A.6.1. Band assignments of the stretching frequencies - obtained from FTIR spectral data of solid MSA and WLE QDC nanocomposite - in tabular form.

Vibrational Frequency(Cm^{-1})	Assigned Bands	Only MSA	QDC
2960	Asymmetric N-H stretching	Present	Present
1612	C=N stretch	Present	Present
1258	Phenolic C-O stretching	Present	Present
545	Zn-N bond stretching	Absent	Present
490	Zn-O bond stretching	Absent	Present

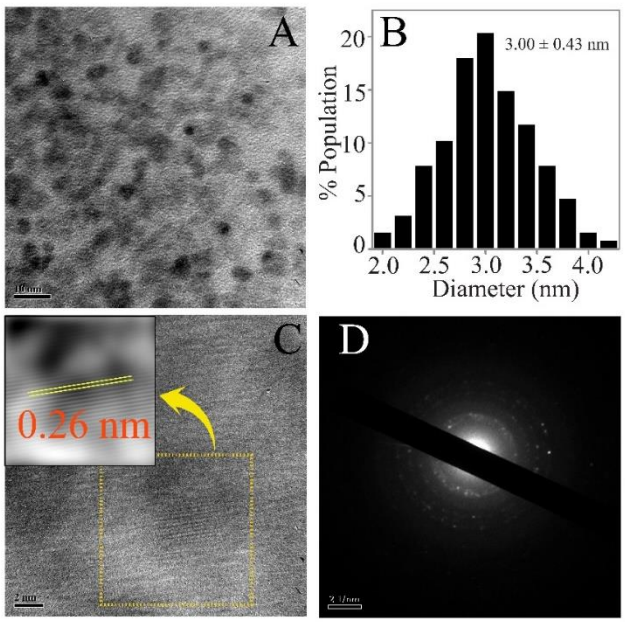

Figure A.6.6. (A) Transmission electron microscopic (TEM) image, **(B)** corresponding particle size distribution, **(C)** high resolution TEM image (scale bar- 5 nm) and corresponding inverse fast Fourier transform (IFFT; inset square box) image and **(D)** selected area electron diffraction pattern (scale bar – 5 nm^{-1}) of the WLE QDC nanocomposite.

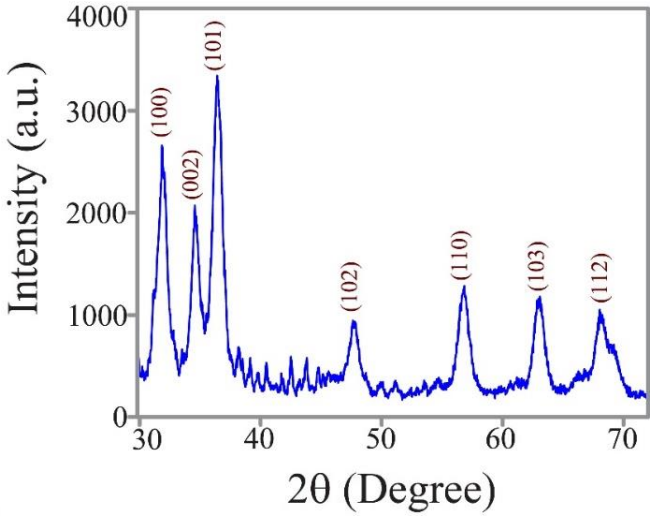

Figure A.6.7. Powder X-ray diffraction (XRD) pattern of solid WLE QDC nanocomposite. The diffraction planes corresponding to wurtzite ZnO crystal structure are identified.

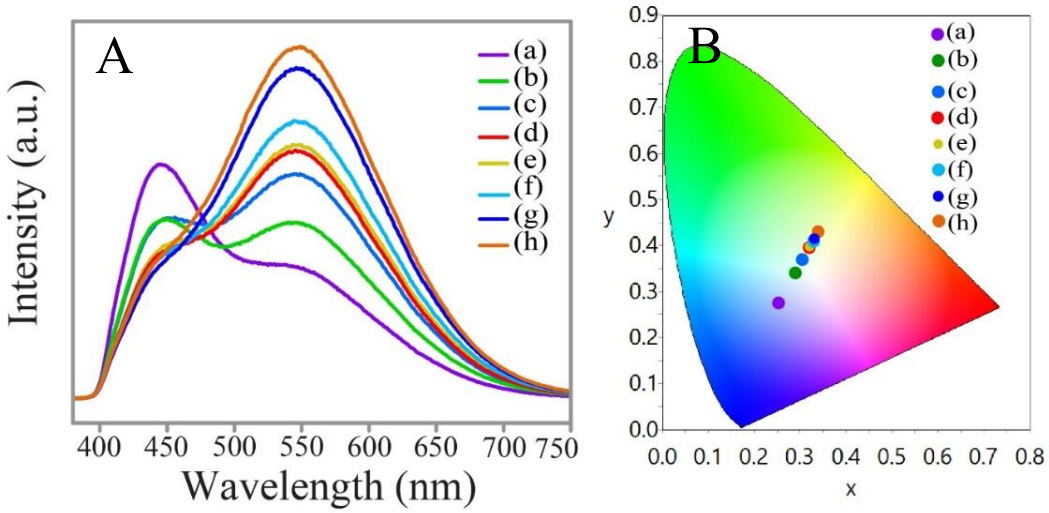

Figure A.6.8. **(A)** Emission spectra (λ_{ex}-350 nm) and **(B)** chromaticity color coordinates in CIE diagram of 33.2 μM MSA treated ZnO Qdots with absorbance values of (a) 0.2, (b) 0.4, (c) 0.6, (d) 0.8, (e) 0.9, (f) 1.0, (g) 1.1 at 350 nm.

Table A.6.2. Tabulated form of chromaticity color coordinates (x,y), color rendering indices (CRI) and correlated color temperatures (CCT) of 33.2 μM MSA treated ZnO Qdots with absorbance values of (a) 0.2, (b) 0.4, (c) 0.6, (d) 0.8, (e) 0.9, (f) 1.0, (g) 1.1 (h) 1.2 at 350 nm. These parameters were calculated based on the emission spectra in Figure A.6.8.

Sl. No.	Absorbance	Chromaticity (x,y)	CCT (K)	CRI
(a)	0.2	(0.25, 0.27)	15891	85
(b)	0.4	(0.29, 0.34)	7553	78
(c)	0.6	(0.30, 0.37)	6550	75
(d)	0.8	(0.32, 0.39)	5893	72
(e)	0.9	(0.32, 0.39)	5848	73
(f)	1.0	(0.33, 0.40)	5596	72
(g)	1.1	(0.34, 0.43)	5332	69
(h)	1.2	(0.34, 0.43)	5327	70

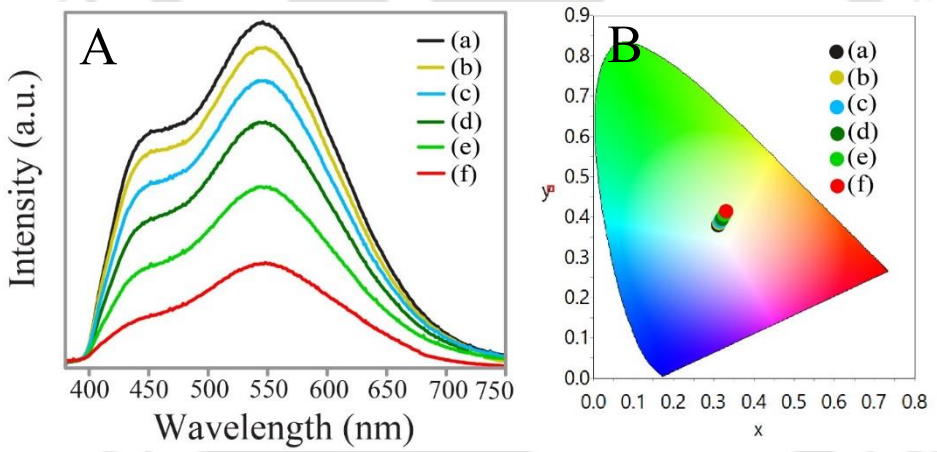

Figure A.6.9. **(A)** Emission spectra (λ_{ex}-350 nm) and **(B)** chromaticity color coordinates in CIE diagram of WLE QDC with absorbance values of (a) 1.1, (b) 0.9, (c) 0.7, (d) 0.5, (e) 0.4, (f) 0.2 at 350 nm.

Table A.6.3. Tabulated form of chromaticity color coordinates (x,y), color rendering indices (CRI) and correlated color temperatures (CCT) of WLE QDC with absorbance values of (a) 1.1, (b) 0.9, (c) 0.7, (d) 0.5, (e) 0.4, (f) 0.2 at 350 nm. These parameters were calculated based on the emission spectra in Figure A.6.9.

Sl. No.	Absorbance	Chromaticity (x,y)	CCT (K)	CRI
(a)	1.1	(0.32, 0.38)	6052	75
(b)	0.9	(0.32, 0.38)	6051	74
(c)	0.7	(0.32, 0.39)	5940	74
(d)	0.5	(0.32, 0.40)	5825	73
(e)	0.4	(0.33, 0.40)	5685	73
(f)	0.2	(0.33, 0.41)	5474	72

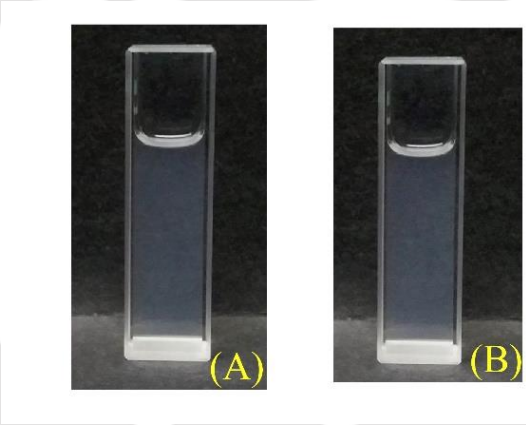

Figure A.6.10. Digital photographs of the dispersions of **(A)** ZnO Qdots and **(B)** WLE nanocomposite in the presence of day light.

Table A.6.4. Quantum yield (λ_{ex}-350 nm; using quinine sulphate (QY-54% in 0.1 M H_2SO_4) as reference of (i) as-synthesized ZnO Qdots (λ_{em}-545 nm; in ethanol), (ii) WLE QDC nanocomposite (in ethanol; obtained from the treatment of 33.2 µL of MSA to 3.0 mL ZnO Qdot (having absorbance of 0.1 at 350 nm)).

Sample	Quantum Yield (%)
(i) ZnO Qdots	1.3
(ii) QDC nanocomposite	2.4

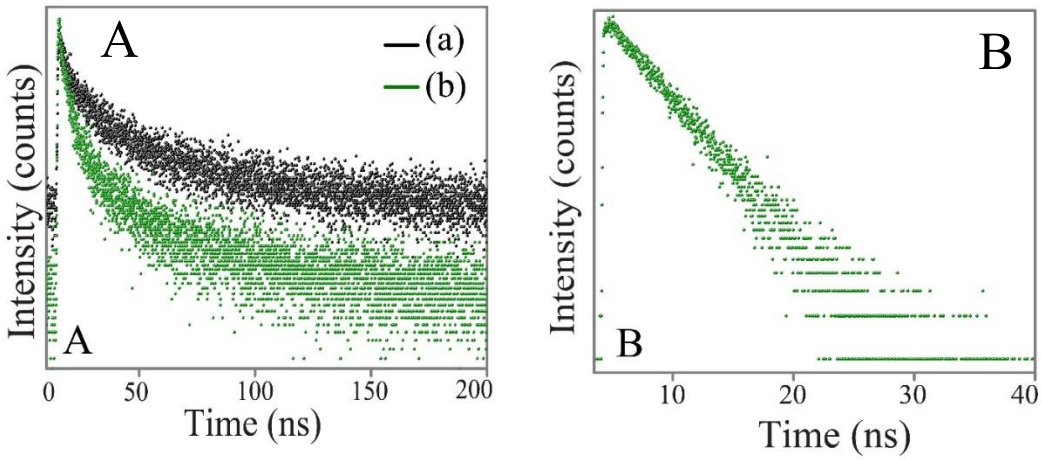

Figure A.6.11. **(A)** Time resolved PL spectra, at an excitation wavelength of 336 nm, of (a) as synthesized ZnO Qdots (λ_{em}-545 nm; in ethanol) and (b) WLE QDC nanocomposite (λ_{em}-545 nm; in ethanol). **(B)** Time resolved PL spectrum at an excitation wavelength of 375 nm of WLE QDC nanocomposite (λ_{em}-440 nm; in ethanol).

Table A.6.5. PL lifetime decay parameters obtained by analyzing the PL decay curves from Figure A.6.11.

Figure A.6.11	Sample	λ_{em} (nm)	λ_{em} (nm)	α_i (%)	τ_i (ns)	τ_{av} (ns)	χ^2
(A)	(a) ZnO Qdots	336	545	19.7 80.3	6.7 45.5	**44.1**	0.99
	(b) WLE QDC nanocomposite	336	545	28.5 71.5	4.3 37.4	**35.9**	1.05
(B)	WLE QDC nanocomposite	375	440	100	4.2	**4.2**	0.97

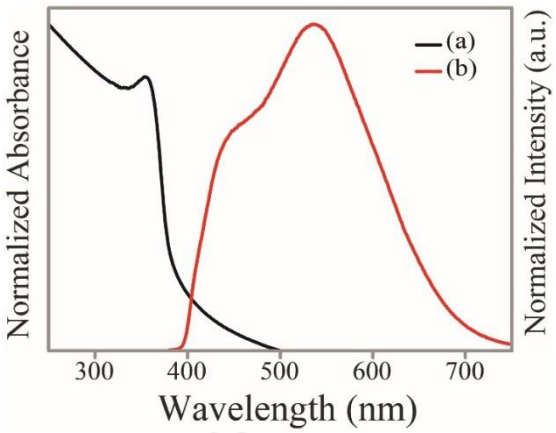

Figure A.6.12. (a) UV-vis spectrum of ZnO Qdots and (b) the emission spectrum (λ_{ex}-350 nm) of WLE QDC with a peak at 440 nm due to $Zn(MSA)_2$.

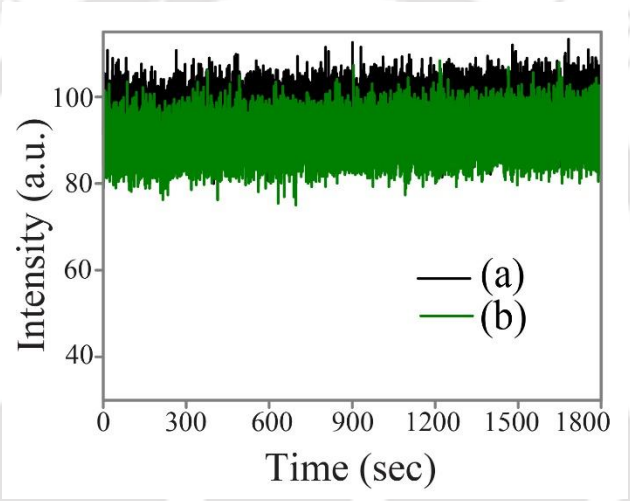

Figure A.6.13. Change in emission intensity vs time (a) at 545 nm and (b) at 440 nm of solid WLE QDC nanocomposite (deposited on a quartz glass), following continuous irradiation with 350 nm light for half an hour (using a spectrofluorimeter with light source, 150-W ozone-free xenon arc-lamp as the light source and recorded with 0.1 sec interval).

A.6.B. Chapter 6B

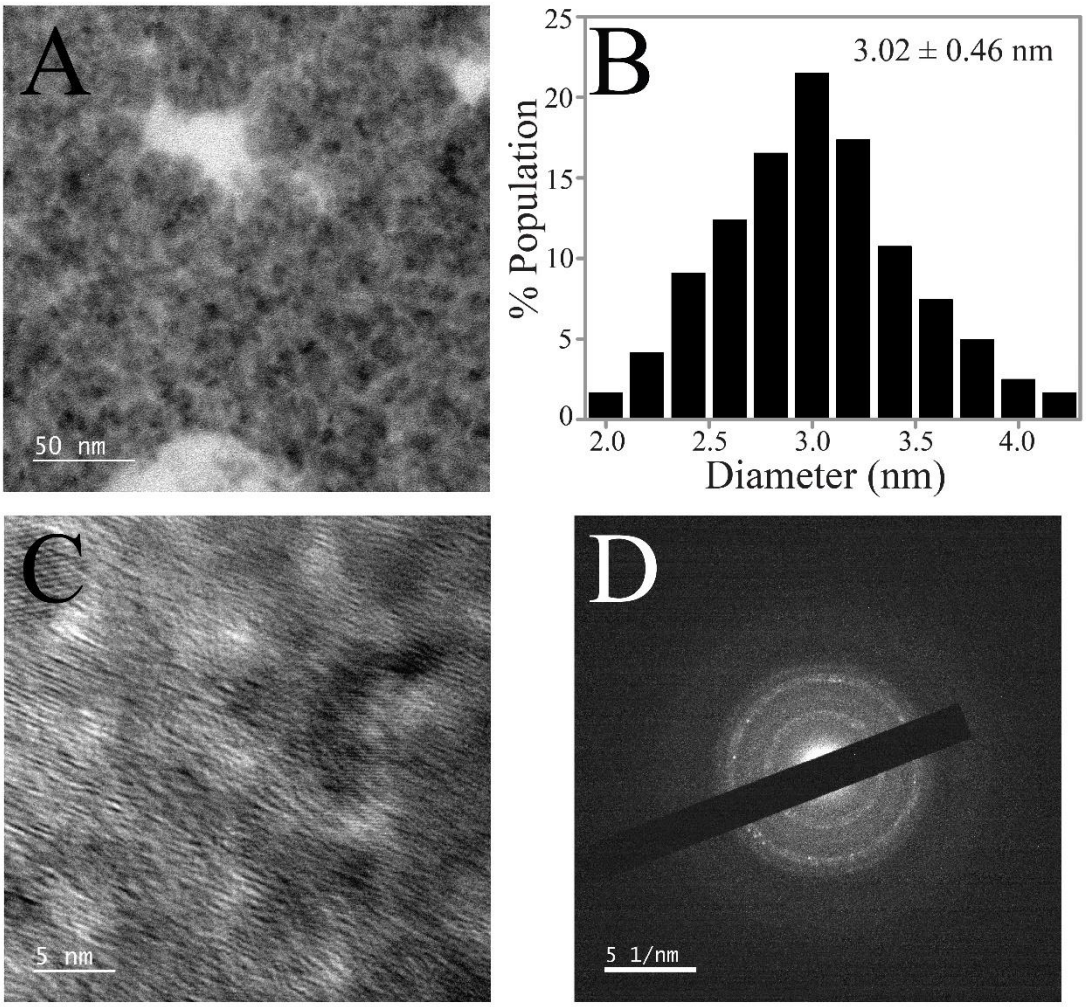

Figure A.6.14. (A) Transmission electron microscopic (TEM) image, **(B)** corresponding particle size distribution, **(C)** high resolution image (HRTEM) and **(D)** selected area electron diffraction (SAED) pattern of ZnO-OS herbal nanocomposite.

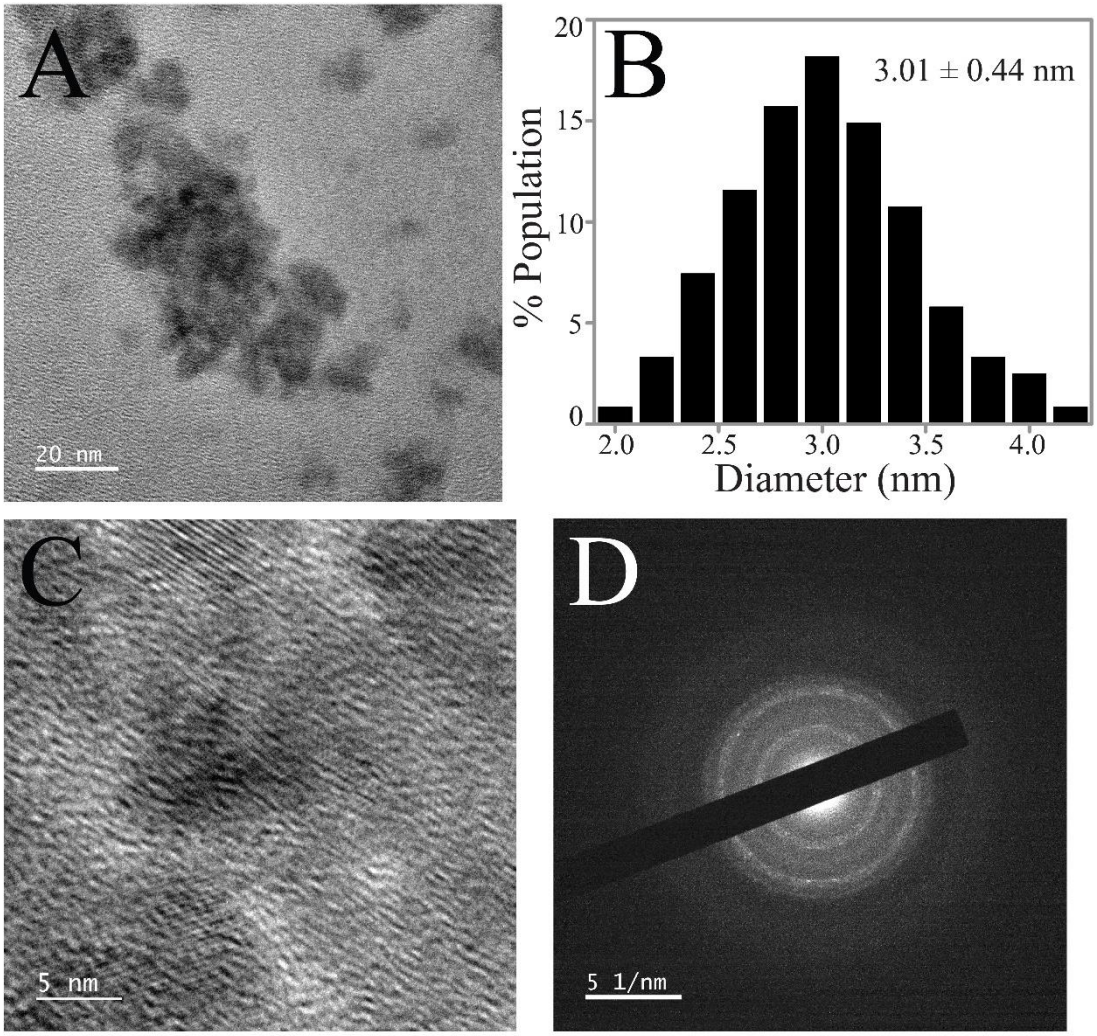

Figure A.6.15. (A) Transmission electron microscopic (TEM) image, **(B)** corresponding particle size distribution, **(C)** high resolution image (HRTEM) and **(D)** selected area electron diffraction (SAED) pattern of ZnO-RM herbal nanocomposite.

List of Publications

In Peer Reviewed Journals.

1. **Roy, S.;** Manna, M.; Chattopadhyay, A. Complex Transfer Reaction from ZnO to ZnS Quantum Dot Driven by Surface Anion. *J. Phys. Chem. C* **2018**, *122*, 9939–9946.
2. Pramanik, S.; Bhandari, S.; Pan, U. N.; **Roy, S.;** Chattopadhyay, A. A White Light Emitting Quantum Dot Complex for Single Particle Level Interaction with Dopamine Leading to Changes in Color and Blinking Profile. *Small* **2018**, *DOI: 10.1002/smll.201800323*.
3. **Roy, S.;** Pramanik, S.; Bhandari, S.; Chattopadhyay, A. Surface Complexed ZnO Quantum Dot for White Light Emission with Controllable Chromaticity and Color Temperature. *Langmuir* **2017**, *33*, 14627–14633.
4. **Roy, S.;** Bhandari, S.; Chattopadhyay, A. Quantum Dot Surface mediated Unprecedented Reaction of Zn^{2+} and Copper Quinolate Complex. *J. Phys. Chem. C* **2015**, *119*, 21191–21197.
5. Pramanik, S.; Bhandari, S.; **Roy, S.;** Chattopadhyay, A. Synchronous Tricolor Emission-Based White Light from Quantum Dot Complex. *J. Phys. Chem. Lett.* **2015**, *6*, 1270–1274. (*This article has been featured in C&E News and ACS Live Slides presentation*).
6. Bhandari, S.; **Roy, S.;** Pramanik, S.; Chattopadhyay, A. Double Channel Emission from a Redox Active Single Component Quantum Dot Complex. *Langmuir* **2015**, *31*, 551–561.
7. Bhandari, S.; **Roy, S.;** Pramanik, S.; Chattopadhyay, A. Surface Complexation Reaction for Phase Transfer of Hydrophobic Quantum Dot from Nonpolar to Polar Medium. *Langmuir* **2014**, *30*, 10760–10765.
8. Bhandari, S.; **Roy, S.;** Chattopadhyay, A. Enhanced Photoluminescence and Thermal Stability of Zinc Quinolate Following Complexation on the Surface of Quantum Dot. *RSC Adv.* **2014**, *4*, 24217–242211.
9. **Roy, S.;** Bhandari, S.; De, S.; Manna, M.; Chattopadhyay, A. Unravelling the Binding Chemistry of Zinc Quinolato Complex on the Surface of ZnS Quantum Dots. (*To be Submitted*)
10. **Roy, S.;** Bhandari, S.; Pramanik, S.; Pan, U.; Chattopadhyay, A. Dual Fluorescence Intermittency in a Single Quantum Dot Complex. (*To be Submitted*)
11. Bhandari, S; **Roy, S.;** Pramanik, S; Chattopadhyay, A. Consequences of Chemical Reactions on the Surface of Quantum Dots (*Invited Article at Langmuir: to be communicated*)

Conferences attended.

1. Presented paper at DAE-BRNS 5th Interdisciplinary Symposium on Materials Chemistry (ISMC-2014) held at BARC, Mumbai, India.
2. Presented poster at New Advances and Horizons in Nanoscience and Nanotechnology (NanoSci-2014) held at IASST, Guwahati, India. (national conference)
3. Presented poster at 6th MRS Singapore India China Trilateral Symposium on Advances of Nanomaterials: Energy, Water and Healthcare (November 2015) held at IISER, Mohali, Mohali, India organized by INST, Mohali.
4. Presented poster at Australia India Strategic Research Fund Meeting (AISRF – 2015) held at IISER, Mohali, Mohali, India organized by INST, Mohali.
5. Presented poster at 4th International Conference on Advanced Nanomaterials and Nanotechnology (ICANN-2015) held at IIT Guwahati, India.
6. Presented poster at International Conference on Nano Science and Technology (ICONSAT-2016) held at IISER Pune, India.

Permissions

- **Figure 1.2.** has been adapted with permission from (*J. Chem. Educ.* **2014**, *91*, 807–816). Copyright (2014) American Chemical Society.
- **Figure 1.3.** has been Republished (adapted) with permission of The Royal Scoiety of Chemistry, from [From ligands to binding motifs and beyond; the enhanced versatility of nanocrystal surfaces. De Roo, J.; De Keukeleere, K.; Hens, Z.; Van Driessche, I. *Dalton Trans.* **2016**, *45*, 13277-13283.]; permission conveyed through Copyright Clearance Center, Inc.
- **Figure 1.4.** has been adapted by permission from Springer Nature [Nature Material] (Boles, M. A.; Ling, D.; Hyeon, T.; Talapin, D. V. The surface science of nanocrystals. *Nature Materials* 2016, *15*, 141–153), Copyright 2016.
- **Figure 1.5A.** has been reprinted with permission from (*Langmuir* **2012***, 28,* 9722-9728). Copyright (2012) American Chemical Society.
- **Figure 1.5B.** has been reprinted with permission from (*Langmuir* **2011***, 27,* 6433– 6439). Copyright (2011) American Chemical Society.
- **Figure 1.6.** has been adapted with permission from (*J. Am. Chem. Soc.* **2013***, 135,* 18536–18548). Copyright (2013) American Chemical Society.
- **Figure 1.7A.** has been reprinted with permission from (*Langmuir* **2015**, *31*, 551-561). Copyright (2015) American Chemical Society.
- **Figure 1.7B.** has been reprinted with permission from (*Langmuir* **2014**, *30*, 10760–10765). Copyright (2014) American Chemical Society.
- **Figure 1.7C.** has been reprinted with permission from (. *J. Phys. Chem. Lett*. **2015***, 6,* 1270- 1274). Copyright (2015) American Chemical Society.
- **Figure 1.7D.** has been republished with permission of The Royal Scoiety of Chemistry, from [Zinc quinolate complex decorated CuInS2/ZnS core/shell quantum dots for white light emission. Pramanik, S.; Bhandari, S.; Chattopadhyay, A. *J. Mater. Chem. C*, **2017**, *5*, 7291-7296]; permission conveyed through Copyright Clearance Center, Inc.
- **Chapter 3** has been reprinted (adapted) with permission from (*J. Phys. Chem. C*, **2015**, *119*, 21191–21197). Copyright (2015) American Chemical Society.
- **Chapter 4** has been reprinted (adapted) with permission from (*J. Phys. Chem. C*, **2018**, *122*, 9939–9946). Copyright (2018) American Chemical Society.
- **Chapter 6A** has been reprinted (adapted) with permission from (*Langmuir*, **2017**, *33*, 14627–14633). Copyright (2015) American Chemical Society.

Title: Application of the Covalent Bond Classification Method for the Teaching of Inorganic Chemistry

Author: Malcolm L. H. Green, Gerard Parkin

Publication: Journal of Chemical Education

Publisher: American Chemical Society

Date: Jun 1, 2014

PERMISSION/LICENSE IS GRANTED FOR YOUR ORDER AT NO CHARGE

This type of permission/license, instead of the standard Terms & Conditions, is sent to you because no fee is being charged for your order. Please note the following:

- Permission is granted for your request in both print and electronic formats, and translations.
- If figures and/or tables were requested, they may be adapted or used in part.
- Please print this page for your records and send a copy of it to your publisher/graduate school.
- Appropriate credit for the requested material should be given as follows: "Reprinted (adapted) with permission from (COMPLETE REFERENCE CITATION). Copyright (YEAR) American Chemical Society." Insert appropriate information in place of the capitalized words.
- One-time permission is granted only for the use specified in your request. No additional uses are granted (such as derivative works or other editions). For any other uses, please submit a new request.

If credit is given to another source for the material you requested, permission must be obtained from that source.

Royal Society of Chemistry LICENSE TERMS AND CONDITIONS

Aug 11, 2018

This is a License Agreement between Mr. SHILAJ ROY ("You") and Royal Society of Chemistry ("Royal Society of Chemistry") provided by Copyright Clearance Center ("CCC"). The license consists of your order details, the terms and conditions provided by Royal Society of Chemistry, and the payment terms and conditions.

All payments must be made in full to CCC. For payment instructions, please see information listed at the bottom of this form.

License Number	4405990196070
License date	Aug 11, 2018
Licensed content publisher	Royal Society of Chemistry
Licensed content title	Dalton transactions
Licensed content date	Jan 1, 2003
Type of Use	Thesis/Dissertation
Requestor type	Academic institution
Format	Print, Electronic
Portion	chart/graph/table/figure
Number of charts/graphs/tables/figures	1
The requesting person/organization is:	Shilaj Roy
Title or numeric reference of the portion(s)	Fig. 1
Title of the article or chapter the portion is from	N/A
Editor of portion(s)	N/A
Author of portion(s)	N/A
Volume of serial or monograph.	N/A
Page range of the portion	13278
Publication date of portion	20 Jul 2016
Rights for	Main product
Duration of use	Life of current edition
Creation of copies for the disabled	no
With minor editing privileges	no
For distribution to	Worldwide
In the following language(s)	Original language of publication
With incidental promotional use	no
The lifetime unit quantity of new product	Up to 499
Title	Complexation on the Surface of Zinc Chalcogenide Quantum Dots:Binding, Kinetics and Application
Instructor name	Prof. Arun Chattopadhyay

TH-1971_126122025

Institution name	Indian Institute of Technology Guwahati
Expected presentation date	Aug 2018
Billing Type	Invoice
Billing Address	Mr. SHILAJ ROY Department of Chemistry INDIAN INSTITUTE OF TECHNOLOGY GUWAHATI INDIA GUWAHATI, India 781039 Attn: Mr. SHILAJ ROY
Total (may include CCC user fee)	0.00 USD

Terms and Conditions

TERMS AND CONDITIONS
The following terms are individual to this publisher:

None

Other Terms and Conditions:
STANDARD TERMS AND CONDITIONS

1. Description of Service; Defined Terms. This Republication License enables the User to obtain licenses for republication of one or more copyrighted works as described in detail on the relevant Order Confirmation (the "Work(s)"). Copyright Clearance Center, Inc. ("CCC") grants licenses through the Service on behalf of the rightsholder identified on the Order Confirmation (the "Rightsholder"). "Republication", as used herein, generally means the inclusion of a Work, in whole or in part, in a new work or works, also as described on the Order Confirmation. "User", as used herein, means the person or entity making such republication.
2. The terms set forth in the relevant Order Confirmation, and any terms set by the Rightsholder with respect to a particular Work, govern the terms of use of Works in connection with the Service. By using the Service, the person transacting for a republication license on behalf of the User represents and warrants that he/she/it (a) has been duly authorized by the User to accept, and hereby does accept, all such terms and conditions on behalf of User, and (b) shall inform User of all such terms and conditions. In the event such person is a "freelancer" or other third party independent of User and CCC, such party shall be deemed jointly a "User" for purposes of these terms and conditions. In any event, User shall be deemed to have accepted and agreed to all such terms and conditions if User republishes the Work in any fashion.
3. Scope of License; Limitations and Obligations.
3.1 All Works and all rights therein, including copyright rights, remain the sole and exclusive property of the Rightsholder. The license created by the exchange of an Order Confirmation (and/or any invoice) and payment by User of the full amount set forth on that document includes only those rights expressly set forth in the Order Confirmation and in these terms and conditions, and conveys no other rights in the Work(s) to User. All rights not expressly granted are hereby reserved.
3.2 General Payment Terms: You may pay by credit card or through an account with us payable at the end of the month. If you and we agree that you may establish a standing account with CCC, then the following terms apply: Remit Payment to: Copyright Clearance Center, 29118 Network Place, Chicago, IL 60673-1291. Payments Due: Invoices are payable upon their delivery to you (or upon our notice to you that they are available to you for downloading). After 30 days, outstanding amounts will be subject to a service charge of 1-1/2% per month or, if less, the maximum rate allowed by applicable law. Unless otherwise specifically set forth in the Order Confirmation or in a separate written agreement signed by CCC, invoices are due and payable on "net 30" terms. While User may exercise the rights licensed immediately upon issuance of the Order Confirmation, the license is automatically revoked and is null and void, as if it had never been issued, if complete payment for the license is not received on a timely basis either from User directly or through a payment agent, such as a credit card company.

TH-1971_126122025

3.3 Unless otherwise provided in the Order Confirmation, any grant of rights to User (i) is "one-time" (including the editions and product family specified in the license), (ii) is non-exclusive and non-transferable and (iii) is subject to any and all limitations and restrictions (such as, but not limited to, limitations on duration of use or circulation) included in the Order Confirmation or invoice and/or in these terms and conditions. Upon completion of the licensed use, User shall either secure a new permission for further use of the Work(s) or immediately cease any new use of the Work(s) and shall render inaccessible (such as by deleting or by removing or severing links or other locators) any further copies of the Work (except for copies printed on paper in accordance with this license and still in User's stock at the end of such period).

3.4 In the event that the material for which a republication license is sought includes third party materials (such as photographs, illustrations, graphs, inserts and similar materials) which are identified in such material as having been used by permission, User is responsible for identifying, and seeking separate licenses (under this Service or otherwise) for, any of such third party materials; without a separate license, such third party materials may not be used.

3.5 Use of proper copyright notice for a Work is required as a condition of any license granted under the Service. Unless otherwise provided in the Order Confirmation, a proper copyright notice will read substantially as follows: "Republished with permission of [Rightsholder's name], from [Work's title, author, volume, edition number and year of copyright]; permission conveyed through Copyright Clearance Center, Inc. " Such notice must be provided in a reasonably legible font size and must be placed either immediately adjacent to the Work as used (for example, as part of a by-line or footnote but not as a separate electronic link) or in the place where substantially all other credits or notices for the new work containing the republished Work are located. Failure to include the required notice results in loss to the Rightsholder and CCC, and the User shall be liable to pay liquidated damages for each such failure equal to twice the use fee specified in the Order Confirmation, in addition to the use fee itself and any other fees and charges specified.

3.6 User may only make alterations to the Work if and as expressly set forth in the Order Confirmation. No Work may be used in any way that is defamatory, violates the rights of third parties (including such third parties' rights of copyright, privacy, publicity, or other tangible or intangible property), or is otherwise illegal, sexually explicit or obscene. In addition, User may not conjoin a Work with any other material that may result in damage to the reputation of the Rightsholder. User agrees to inform CCC if it becomes aware of any infringement of any rights in a Work and to cooperate with any reasonable request of CCC or the Rightsholder in connection therewith.

4. Indemnity. User hereby indemnifies and agrees to defend the Rightsholder and CCC, and their respective employees and directors, against all claims, liability, damages, costs and expenses, including legal fees and expenses, arising out of any use of a Work beyond the scope of the rights granted herein, or any use of a Work which has been altered in any unauthorized way by User, including claims of defamation or infringement of rights of copyright, publicity, privacy or other tangible or intangible property.

5. Limitation of Liability. UNDER NO CIRCUMSTANCES WILL CCC OR THE RIGHTSHOLDER BE LIABLE FOR ANY DIRECT, INDIRECT, CONSEQUENTIAL OR INCIDENTAL DAMAGES (INCLUDING WITHOUT LIMITATION DAMAGES FOR LOSS OF BUSINESS PROFITS OR INFORMATION, OR FOR BUSINESS INTERRUPTION) ARISING OUT OF THE USE OR INABILITY TO USE A WORK, EVEN IF ONE OF THEM HAS BEEN ADVISED OF THE POSSIBILITY OF SUCH DAMAGES. In any event, the total liability of the Rightsholder and CCC (including their respective employees and directors) shall not exceed the total amount actually paid by User for this license. User assumes full liability for the actions and omissions of its principals, employees, agents, affiliates, successors and assigns.

6. Limited Warranties. THE WORK(S) AND RIGHT(S) ARE PROVIDED "AS IS". CCC HAS THE RIGHT TO GRANT TO USER THE RIGHTS GRANTED IN THE ORDER CONFIRMATION DOCUMENT. CCC AND THE RIGHTSHOLDER DISCLAIM ALL OTHER WARRANTIES RELATING TO THE WORK(S) AND RIGHT(S), EITHER EXPRESS OR IMPLIED, INCLUDING WITHOUT LIMITATION IMPLIED WARRANTIES OF MERCHANTABILITY OR FITNESS FOR A PARTICULAR

PURPOSE. ADDITIONAL RIGHTS MAY BE REQUIRED TO USE ILLUSTRATIONS, GRAPHS, PHOTOGRAPHS, ABSTRACTS, INSERTS OR OTHER PORTIONS OF THE WORK (AS OPPOSED TO THE ENTIRE WORK) IN A MANNER CONTEMPLATED BY USER; USER UNDERSTANDS AND AGREES THAT NEITHER CCC NOR THE RIGHTSHOLDER MAY HAVE SUCH ADDITIONAL RIGHTS TO GRANT.

7. Effect of Breach. Any failure by User to pay any amount when due, or any use by User of a Work beyond the scope of the license set forth in the Order Confirmation and/or these terms and conditions, shall be a material breach of the license created by the Order Confirmation and these terms and conditions. Any breach not cured within 30 days of written notice thereof shall result in immediate termination of such license without further notice. Any unauthorized (but licensable) use of a Work that is terminated immediately upon notice thereof may be liquidated by payment of the Rightsholder's ordinary license price therefor; any unauthorized (and unlicensable) use that is not terminated immediately for any reason (including, for example, because materials containing the Work cannot reasonably be recalled) will be subject to all remedies available at law or in equity, but in no event to a payment of less than three times the Rightsholder's ordinary license price for the most closely analogous licensable use plus Rightsholder's and/or CCC's costs and expenses incurred in collecting such payment.

8. **Miscellaneous.**

8.1 User acknowledges that CCC may, from time to time, make changes or additions to the Service or to these terms and conditions, and CCC reserves the right to send notice to the User by electronic mail or otherwise for the purposes of notifying User of such changes or additions; provided that any such changes or additions shall not apply to permissions already secured and paid for.

8.2 Use of User-related information collected through the Service is governed by CCC's privacy policy, available online here: http://www.copyright.com/content/cc3/en/tools/footer/privacypolicy.html.

8.3 The licensing transaction described in the Order Confirmation is personal to User. Therefore, User may not assign or transfer to any other person (whether a natural person or an organization of any kind) the license created by the Order Confirmation and these terms and conditions or any rights granted hereunder; provided, however, that User may assign such license in its entirety on written notice to CCC in the event of a transfer of all or substantially all of User's rights in the new material which includes the Work(s) licensed under this Service.

8.4 No amendment or waiver of any terms is binding unless set forth in writing and signed by the parties. The Rightsholder and CCC hereby object to any terms contained in any writing prepared by the User or its principals, employees, agents or affiliates and purporting to govern or otherwise relate to the licensing transaction described in the Order Confirmation, which terms are in any way inconsistent with any terms set forth in the Order Confirmation and/or in these terms and conditions or CCC's standard operating procedures, whether such writing is prepared prior to, simultaneously with or subsequent to the Order Confirmation, and whether such writing appears on a copy of the Order Confirmation or in a separate instrument.

8.5 The licensing transaction described in the Order Confirmation document shall be governed by and construed under the law of the State of New York, USA, without regard to the principles thereof of conflicts of law. Any case, controversy, suit, action, or proceeding arising out of, in connection with, or related to such licensing transaction shall be brought, at CCC's sole discretion, in any federal or state court located in the County of New York, State of New York, USA, or in any federal or state court whose geographical jurisdiction covers the location of the Rightsholder set forth in the Order Confirmation. The parties expressly submit to the personal jurisdiction and venue of each such federal or state court.If you have any comments or questions about the Service or Copyright Clearance Center, please contact us at 978-750-8400 or send an e-mail to info@copyright.com.

v 1.1

Questions? customercare@copyright.com or +1-855-239-3415 (toll free in the US) or +1-978-646-2777.

TH-1971_126122025

TH-1971_126122025

SPRINGER NATURE LICENSE
TERMS AND CONDITIONS

Aug 11, 2018

This Agreement between Mr. SHILAJ ROY ("You") and Springer Nature ("Springer Nature") consists of your license details and the terms and conditions provided by Springer Nature and Copyright Clearance Center.

License Number	4405990758959
License date	Aug 11, 2018
Licensed Content Publisher	Springer Nature
Licensed Content Publication	Nature Materials
Licensed Content Title	The surface science of nanocrystals
Licensed Content Author	Michael A. Boles, Daishun Ling, Taeghwan Hyeon, Dmitri V. Talapin
Licensed Content Date	Jan 22, 2016
Licensed Content Volume	15
Licensed Content Issue	2
Type of Use	Thesis/Dissertation
Requestor type	academic/university or research institute
Format	print and electronic
Portion	figures/tables/illustrations
Number of figures/tables/illustrations	2
High-res required	no
Will you be translating?	no
Circulation/distribution	<501
Author of this Springer Nature content	no
Title	Complexation on the Surface of Zinc Chalcogenide Quantum Dots:Binding, Kinetics and Application
Instructor name	Prof. Arun Chattopadhyay
Institution name	Indian Institute of Technology Guwahati
Expected presentation date	Aug 2018
Portions	Figure 3 and Figure 4
Requestor Location	Mr. SHILAJ ROY Department of Chemistry INDIAN INSTITUTE OF TECHNOLOGY GUWAHATI INDIA GUWAHATI, ASSAM 781039 India Attn: Mr. SHILAJ ROY
Billing Type	Invoice
Billing Address	Mr. SHILAJ ROY Department of Chemistry INDIAN INSTITUTE OF TECHNOLOGY GUWAHATI INDIA GUWAHATI, India 781039 Attn: Mr. SHILAJ ROY
Total	0.00 USD

TH-1971_126122025

Terms and Conditions

Springer Nature Terms and Conditions for RightsLink Permissions

Springer Customer Service Centre GmbH (the Licensor) hereby grants you a non-exclusive, world-wide licence to reproduce the material and for the purpose and requirements specified in the attached copy of your order form, and for no other use, subject to the conditions below:

1. The Licensor warrants that it has, to the best of its knowledge, the rights to license reuse of this material. However, you should ensure that the material you are requesting is original to the Licensor and does not carry the copyright of another entity (as credited in the published version).

   If the credit line on any part of the material you have requested indicates that it was reprinted or adapted with permission from another source, then you should also seek permission from that source to reuse the material.

2. Where **print only** permission has been granted for a fee, separate permission must be obtained for any additional electronic re-use.

3. Permission granted **free of charge** for material in print is also usually granted for any electronic version of that work, provided that the material is incidental to your work as a whole and that the electronic version is essentially equivalent to, or substitutes for, the print version.

4. A licence for 'post on a website' is valid for 12 months from the licence date. This licence does not cover use of full text articles on websites.

5. Where **'reuse in a dissertation/thesis'** has been selected the following terms apply: Print rights for up to 100 copies, electronic rights for use only on a personal website or institutional repository as defined by the Sherpa guideline (www.sherpa.ac.uk/romeo/).

6. Permission granted for books and journals is granted for the lifetime of the first edition and does not apply to second and subsequent editions (except where the first edition permission was granted free of charge or for signatories to the STM Permissions Guidelines http://www.stm-assoc.org/copyright-legal-affairs/permissions/permissions-guidelines/), and does not apply for editions in other languages unless additional translation rights have been granted separately in the licence.

7. Rights for additional components such as custom editions and derivatives require additional permission and may be subject to an additional fee. Please apply to Journalpermissions@springernature.com/bookpermissions@springernature.com for these rights.

8. The Licensor's permission must be acknowledged next to the licensed material in print. In electronic form, this acknowledgement must be visible at the same time as the figures/tables/illustrations or abstract, and must be hyperlinked to the journal/book's homepage. Our required acknowledgement format is in the Appendix below.

9. Use of the material for incidental promotional use, minor editing privileges (this does not include cropping, adapting, omitting material or any other changes that affect the meaning, intention or moral rights of the author) and copies for the disabled are permitted under this licence.

10. Minor adaptations of single figures (changes of format, colour and style) do not require the Licensor's approval. However, the adaptation should be credited as shown in Appendix below.

Appendix — Acknowledgements:

For Journal Content:

Reprinted by permission from [**the Licensor**]: [**Journal Publisher** (e.g. Nature/Springer/Palgrave)] [**JOURNAL NAME**] [**REFERENCE CITATION** (Article name, Author(s) Name), [**COPYRIGHT**] (year of publication)

TH-1971_126122025

For **Advance Online Publication papers:**
Reprinted by permission from [**the Licensor**]: [**Journal Publisher** (e.g. Nature/Springer/Palgrave)] [**JOURNAL NAME**] [**REFERENCE CITATION** (Article name, Author(s) Name), [**COPYRIGHT**] (year of publication), advance online publication, day month year (doi: 10.1038/sj.[JOURNAL ACRONYM].)

For Adaptations/Translations:
Adapted/Translated by permission from [**the Licensor**]: [**Journal Publisher** (e.g. Nature/Springer/Palgrave)] [**JOURNAL NAME**] [**REFERENCE CITATION** (Article name, Author(s) Name), [**COPYRIGHT**] (year of publication)

Note: For any republication from the British Journal of Cancer, the following credit line style applies:

Reprinted/adapted/translated by permission from [**the Licensor**]: on behalf of Cancer Research UK: : [**Journal Publisher** (e.g. Nature/Springer/Palgrave)] [**JOURNAL NAME**] [**REFERENCE CITATION** (Article name, Author(s) Name), [**COPYRIGHT]** (year of publication)

For **Advance Online Publication** papers:
Reprinted by permission from The [**the Licensor**]: on behalf of Cancer Research UK: [**Journal Publisher** (e.g. Nature/Springer/Palgrave)] [**JOURNAL NAME**] [**REFERENCE CITATION** (Article name, Author(s) Name), [**COPYRIGHT**] (year of publication), advance online publication, day month year (doi: 10.1038/sj.[JOURNAL ACRONYM])

For Book content:
Reprinted/adapted by permission from [**the Licensor**]: [**Book Publisher** (e.g. Palgrave Macmillan, Springer etc) [**Book Title**] by [**Book author**(s)] [**COPYRIGHT**] (year of publication)

Other Conditions:

Version 1.0

Questions? customercare@copyright.com or +1-855-239-3415 (toll free in the US) or +1-978-646-2777.

TH-1971_126122025

Title: Surface Ion Engineering of Mn2 -Doped ZnS Quantum Dots Using Ion-Exchange Resins

Author: Raihana Begum, Satyapriya Bhandari, Arun Chattopadhyay

Publication: Langmuir

Publisher: American Chemical Society

Date: Jun 1, 2012

PERMISSION/LICENSE IS GRANTED FOR YOUR ORDER AT NO CHARGE

This type of permission/license, instead of the standard Terms & Conditions, is sent to you because no fee is being charged for your order. Please note the following:

- Permission is granted for your request in both print and electronic formats, and translations.
- If figures and/or tables were requested, they may be adapted or used in part.
- Please print this page for your records and send a copy of it to your publisher/graduate school.
- Appropriate credit for the requested material should be given as follows: "Reprinted (adapted) with permission from (COMPLETE REFERENCE CITATION). Copyright (YEAR) American Chemical Society." Insert appropriate information in place of the capitalized words.
- One-time permission is granted only for the use specified in your request. No additional uses are granted (such as derivative works or other editions). For any other uses, please submit a new request.

If credit is given to another source for the material you requested, permission must be obtained from that source.

Title: In Situ Reversible Tuning of Photoluminescence of Mn2 -Doped ZnS Quantum Dots by Redox Chemistry

Author: Raihana Begum, Arun Chattopadhyay

Publication: Langmuir

Publisher: American Chemical Society

Date: May 1, 2011

PERMISSION/LICENSE IS GRANTED FOR YOUR ORDER AT NO CHARGE

This type of permission/license, instead of the standard Terms & Conditions, is sent to you because no fee is being charged for your order. Please note the following:

- Permission is granted for your request in both print and electronic formats, and translations.
- If figures and/or tables were requested, they may be adapted or used in part.
- Please print this page for your records and send a copy of it to your publisher/graduate school.
- Appropriate credit for the requested material should be given as follows: "Reprinted (adapted) with permission from (COMPLETE REFERENCE CITATION). Copyright (YEAR) American Chemical Society." Insert appropriate information in place of the capitalized words.
- One-time permission is granted only for the use specified in your request. No additional uses are granted (such as derivative works or other editions). For any other uses, please submit a new request.

If credit is given to another source for the material you requested, permission must be obtained from that source.

Title: Ligand Exchange and the Stoichiometry of Metal Chalcogenide Nanocrystals: Spectroscopic Observation of Facile Metal-Carboxylate Displacement and Binding

Author: Nicholas C. Anderson, Mark P. Hendricks, Joshua J. Choi, et al

Publication: Journal of the American Chemical Society

Publisher: American Chemical Society

Date: Dec 1, 2013

PERMISSION/LICENSE IS GRANTED FOR YOUR ORDER AT NO CHARGE

This type of permission/license, instead of the standard Terms & Conditions, is sent to you because no fee is being charged for your order. Please note the following:

- Permission is granted for your request in both print and electronic formats, and translations.
- If figures and/or tables were requested, they may be adapted or used in part.
- Please print this page for your records and send a copy of it to your publisher/graduate school.
- Appropriate credit for the requested material should be given as follows: "Reprinted (adapted) with permission from (COMPLETE REFERENCE CITATION). Copyright (YEAR) American Chemical Society." Insert appropriate information in place of the capitalized words.
- One-time permission is granted only for the use specified in your request. No additional uses are granted (such as derivative works or other editions). For any other uses, please submit a new request.

If credit is given to another source for the material you requested, permission must be obtained from that source.

Title: Double Channel Emission from a Redox Active Single Component Quantum Dot Complex

Author: Satyapriya Bhandari, Shilaj Roy, Sabyasachi Pramanik, et al

Publication: Langmuir

Publisher: American Chemical Society

Date: Jan 1, 2015

PERMISSION/LICENSE IS GRANTED FOR YOUR ORDER AT NO CHARGE

This type of permission/license, instead of the standard Terms & Conditions, is sent to you because no fee is being charged for your order. Please note the following:

- Permission is granted for your request in both print and electronic formats, and translations.
- If figures and/or tables were requested, they may be adapted or used in part.
- Please print this page for your records and send a copy of it to your publisher/graduate school.
- Appropriate credit for the requested material should be given as follows: "Reprinted (adapted) with permission from (COMPLETE REFERENCE CITATION). Copyright (YEAR) American Chemical Society." Insert appropriate information in place of the capitalized words.
- One-time permission is granted only for the use specified in your request. No additional uses are granted (such as derivative works or other editions). For any other uses, please submit a new request.

If credit is given to another source for the material you requested, permission must be obtained from that source.

Title: Synchronous Tricolor Emission-Based White Light from Quantum Dot Complex

Author: Sabyasachi Pramanik, Satyapriya Bhandari, Shilaj Roy, et al

Publication: Journal of Physical Chemistry Letters

Publisher: American Chemical Society

Date: Apr 1, 2015

PERMISSION/LICENSE IS GRANTED FOR YOUR ORDER AT NO CHARGE

This type of permission/license, instead of the standard Terms & Conditions, is sent to you because no fee is being charged for your order. Please note the following:

- Permission is granted for your request in both print and electronic formats, and translations.
- If figures and/or tables were requested, they may be adapted or used in part.
- Please print this page for your records and send a copy of it to your publisher/graduate school.
- Appropriate credit for the requested material should be given as follows: "Reprinted (adapted) with permission from (COMPLETE REFERENCE CITATION). Copyright (YEAR) American Chemical Society." Insert appropriate information in place of the capitalized words.
- One-time permission is granted only for the use specified in your request. No additional uses are granted (such as derivative works or other editions). For any other uses, please submit a new request.

If credit is given to another source for the material you requested, permission must be obtained from that source.

Royal Society of Chemistry LICENSE TERMS AND CONDITIONS

Aug 12, 2018

This is a License Agreement between Mr. SHILAJ ROY ("You") and Royal Society of Chemistry ("Royal Society of Chemistry") provided by Copyright Clearance Center ("CCC"). The license consists of your order details, the terms and conditions provided by Royal Society of Chemistry, and the payment terms and conditions.

All payments must be made in full to CCC. For payment instructions, please see information listed at the bottom of this form.

License Number	4406330651876
License date	Aug 12, 2018
Licensed content publisher	Royal Society of Chemistry
Licensed content title	Journal of materials chemistry. C, Materials for optical and electronic devices
Licensed content date	Jan 1, 2013
Type of Use	Thesis/Dissertation
Requestor type	Academic institution
Format	Print, Electronic
Portion	chart/graph/table/figure
Number of charts/graphs /tables/figures	1
The requesting person/organization is:	Person
Title or numeric reference of the portion(s)	TOC graphics
Title of the article or chapter the portion is from	NA
Editor of portion(s)	NA
Author of portion(s)	NA
Volume of serial or monograph.	NA
Issue, if republishing an article from a serial	NA
Page range of the portion	NA
Publication date of portion	NA
Rights for	Main product
Duration of use	Life of current edition
Creation of copies for the disabled	yes
With minor editing privileges	no
For distribution to	Worldwide
In the following language(s)	Original language of publication
With incidental promotional use	no

TH-1971_126122025

The lifetime unit quantity of new product	Up to 499
Title	Complexation on the Surface of Zinc Chalcogenide Quantum Dots:Binding, Kinetics and Application
Instructor name	Prof. Arun Chattopadhyay
Institution name	Indian Institute of Technology Guwahati
Expected presentation date	Aug 2018
Billing Type	Invoice
Billing Address	Mr. SHILAJ ROY Department of Chemistry INDIAN INSTITUTE OF TECHNOLOGY GUWAHATI INDIA GUWAHATI, India 781039 Attn: Mr. SHILAJ ROY
Total (may include CCC user fee)	0.00 USD

Terms and Conditions

TERMS AND CONDITIONS

The following terms are individual to this publisher:

None

Other Terms and Conditions:

STANDARD TERMS AND CONDITIONS

1. Description of Service; Defined Terms. This Republication License enables the User to obtain licenses for republication of one or more copyrighted works as described in detail on the relevant Order Confirmation (the "Work(s)"). Copyright Clearance Center, Inc. ("CCC") grants licenses through the Service on behalf of the rightsholder identified on the Order Confirmation (the "Rightsholder"). "Republication", as used herein, generally means the inclusion of a Work, in whole or in part, in a new work or works, also as described on the Order Confirmation. "User", as used herein, means the person or entity making such republication.

2. The terms set forth in the relevant Order Confirmation, and any terms set by the Rightsholder with respect to a particular Work, govern the terms of use of Works in connection with the Service. By using the Service, the person transacting for a republication license on behalf of the User represents and warrants that he/she/it (a) has been duly authorized by the User to accept, and hereby does accept, all such terms and conditions on behalf of User, and (b) shall inform User of all such terms and conditions. In the event such person is a "freelancer" or other third party independent of User and CCC, such party shall be deemed jointly a "User" for purposes of these terms and conditions. In any event, User shall be deemed to have accepted and agreed to all such terms and conditions if User republishes the Work in any fashion.

3. Scope of License; Limitations and Obligations.

3.1 All Works and all rights therein, including copyright rights, remain the sole and exclusive property of the Rightsholder. The license created by the exchange of an Order Confirmation (and/or any invoice) and payment by User of the full amount set forth on that document includes only those rights expressly set forth in the Order Confirmation and in these terms and conditions, and conveys no other rights in the Work(s) to User. All rights not expressly granted are hereby reserved.

3.2 General Payment Terms: You may pay by credit card or through an account with us payable at the end of the month. If you and we agree that you may establish a standing account with CCC, then the following terms apply: Remit Payment to: Copyright Clearance

Center, 29118 Network Place, Chicago, IL 60673-1291. Payments Due: Invoices are payable upon their delivery to you (or upon our notice to you that they are available to you for downloading). After 30 days, outstanding amounts will be subject to a service charge of 1-1/2% per month or, if less, the maximum rate allowed by applicable law. Unless otherwise specifically set forth in the Order Confirmation or in a separate written agreement signed by CCC, invoices are due and payable on "net 30" terms. While User may exercise the rights licensed immediately upon issuance of the Order Confirmation, the license is automatically revoked and is null and void, as if it had never been issued, if complete payment for the license is not received on a timely basis either from User directly or through a payment agent, such as a credit card company.

3.3 Unless otherwise provided in the Order Confirmation, any grant of rights to User (i) is "one-time" (including the editions and product family specified in the license), (ii) is non-exclusive and non-transferable and (iii) is subject to any and all limitations and restrictions (such as, but not limited to, limitations on duration of use or circulation) included in the Order Confirmation or invoice and/or in these terms and conditions. Upon completion of the licensed use, User shall either secure a new permission for further use of the Work(s) or immediately cease any new use of the Work(s) and shall render inaccessible (such as by deleting or by removing or severing links or other locators) any further copies of the Work (except for copies printed on paper in accordance with this license and still in User's stock at the end of such period).

3.4 In the event that the material for which a republication license is sought includes third party materials (such as photographs, illustrations, graphs, inserts and similar materials) which are identified in such material as having been used by permission, User is responsible for identifying, and seeking separate licenses (under this Service or otherwise) for, any of such third party materials; without a separate license, such third party materials may not be used.

3.5 Use of proper copyright notice for a Work is required as a condition of any license granted under the Service. Unless otherwise provided in the Order Confirmation, a proper copyright notice will read substantially as follows: "Republished with permission of [Rightsholder's name], from [Work's title, author, volume, edition number and year of copyright]; permission conveyed through Copyright Clearance Center, Inc. " Such notice must be provided in a reasonably legible font size and must be placed either immediately adjacent to the Work as used (for example, as part of a by-line or footnote but not as a separate electronic link) or in the place where substantially all other credits or notices for the new work containing the republished Work are located. Failure to include the required notice results in loss to the Rightsholder and CCC, and the User shall be liable to pay liquidated damages for each such failure equal to twice the use fee specified in the Order Confirmation, in addition to the use fee itself and any other fees and charges specified.

3.6 User may only make alterations to the Work if and as expressly set forth in the Order Confirmation. No Work may be used in any way that is defamatory, violates the rights of third parties (including such third parties' rights of copyright, privacy, publicity, or other tangible or intangible property), or is otherwise illegal, sexually explicit or obscene. In addition, User may not conjoin a Work with any other material that may result in damage to the reputation of the Rightsholder. User agrees to inform CCC if it becomes aware of any infringement of any rights in a Work and to cooperate with any reasonable request of CCC or the Rightsholder in connection therewith.

4. Indemnity. User hereby indemnifies and agrees to defend the Rightsholder and CCC, and their respective employees and directors, against all claims, liability, damages, costs and expenses, including legal fees and expenses, arising out of any use of a Work beyond the scope of the rights granted herein, or any use of a Work which has been altered in any unauthorized way by User, including claims of defamation or infringement of rights of

copyright, publicity, privacy or other tangible or intangible property.
5. Limitation of Liability. UNDER NO CIRCUMSTANCES WILL CCC OR THE RIGHTSHOLDER BE LIABLE FOR ANY DIRECT, INDIRECT, CONSEQUENTIAL OR INCIDENTAL DAMAGES (INCLUDING WITHOUT LIMITATION DAMAGES FOR LOSS OF BUSINESS PROFITS OR INFORMATION, OR FOR BUSINESS INTERRUPTION) ARISING OUT OF THE USE OR INABILITY TO USE A WORK, EVEN IF ONE OF THEM HAS BEEN ADVISED OF THE POSSIBILITY OF SUCH DAMAGES. In any event, the total liability of the Rightsholder and CCC (including their respective employees and directors) shall not exceed the total amount actually paid by User for this license. User assumes full liability for the actions and omissions of its principals, employees, agents, affiliates, successors and assigns.
6. Limited Warranties. THE WORK(S) AND RIGHT(S) ARE PROVIDED “AS IS”. CCC HAS THE RIGHT TO GRANT TO USER THE RIGHTS GRANTED IN THE ORDER CONFIRMATION DOCUMENT. CCC AND THE RIGHTSHOLDER DISCLAIM ALL OTHER WARRANTIES RELATING TO THE WORK(S) AND RIGHT(S), EITHER EXPRESS OR IMPLIED, INCLUDING WITHOUT LIMITATION IMPLIED WARRANTIES OF MERCHANTABILITY OR FITNESS FOR A PARTICULAR PURPOSE. ADDITIONAL RIGHTS MAY BE REQUIRED TO USE ILLUSTRATIONS, GRAPHS, PHOTOGRAPHS, ABSTRACTS, INSERTS OR OTHER PORTIONS OF THE WORK (AS OPPOSED TO THE ENTIRE WORK) IN A MANNER CONTEMPLATED BY USER; USER UNDERSTANDS AND AGREES THAT NEITHER CCC NOR THE RIGHTSHOLDER MAY HAVE SUCH ADDITIONAL RIGHTS TO GRANT.
7. Effect of Breach. Any failure by User to pay any amount when due, or any use by User of a Work beyond the scope of the license set forth in the Order Confirmation and/or these terms and conditions, shall be a material breach of the license created by the Order Confirmation and these terms and conditions. Any breach not cured within 30 days of written notice thereof shall result in immediate termination of such license without further notice. Any unauthorized (but licensable) use of a Work that is terminated immediately upon notice thereof may be liquidated by payment of the Rightsholder's ordinary license price therefor; any unauthorized (and unlicensable) use that is not terminated immediately for any reason (including, for example, because materials containing the Work cannot reasonably be recalled) will be subject to all remedies available at law or in equity, but in no event to a payment of less than three times the Rightsholder's ordinary license price for the most closely analogous licensable use plus Rightsholder's and/or CCC's costs and expenses incurred in collecting such payment.
8. **Miscellaneous.**
8.1 User acknowledges that CCC may, from time to time, make changes or additions to the Service or to these terms and conditions, and CCC reserves the right to send notice to the User by electronic mail or otherwise for the purposes of notifying User of such changes or additions; provided that any such changes or additions shall not apply to permissions already secured and paid for.
8.2 Use of User-related information collected through the Service is governed by CCC’s privacy policy, available online here: http://www.copyright.com/content/cc3/en/tools/footer/privacypolicy.html.
8.3 The licensing transaction described in the Order Confirmation is personal to User. Therefore, User may not assign or transfer to any other person (whether a natural person or an organization of any kind) the license created by the Order Confirmation and these terms and conditions or any rights granted hereunder; provided, however, that User may assign such license in its entirety on written notice to CCC in the event of a transfer of all or substantially all of User’s rights in the new material which includes the Work(s) licensed under this Service.

8.4 No amendment or waiver of any terms is binding unless set forth in writing and signed by the parties. The Rightsholder and CCC hereby object to any terms contained in any writing prepared by the User or its principals, employees, agents or affiliates and purporting to govern or otherwise relate to the licensing transaction described in the Order Confirmation, which terms are in any way inconsistent with any terms set forth in the Order Confirmation and/or in these terms and conditions or CCC's standard operating procedures, whether such writing is prepared prior to, simultaneously with or subsequent to the Order Confirmation, and whether such writing appears on a copy of the Order Confirmation or in a separate instrument.
8.5 The licensing transaction described in the Order Confirmation document shall be governed by and construed under the law of the State of New York, USA, without regard to the principles thereof of conflicts of law. Any case, controversy, suit, action, or proceeding arising out of, in connection with, or related to such licensing transaction shall be brought, at CCC's sole discretion, in any federal or state court located in the County of New York, State of New York, USA, or in any federal or state court whose geographical jurisdiction covers the location of the Rightsholder set forth in the Order Confirmation. The parties expressly submit to the personal jurisdiction and venue of each such federal or state court.If you have any comments or questions about the Service or Copyright Clearance Center, please contact us at 978-750-8400 or send an e-mail to info@copyright.com.
v 1.1

Questions? customercare@copyright.com or +1-855-239-3415 (toll free in the US) or +1-978-646-2777.

TH-1971_126122025

Title: Quantum Dot Surface Mediated Unprecedented Reaction of Zn2 and Copper Quinolate Complex

Author: Shilaj Roy, Satyapriya Bhandari, Arun Chattopadhyay

Publication: The Journal of Physical Chemistry C

Publisher: American Chemical Society

Date: Sep 1, 2015

PERMISSION/LICENSE IS GRANTED FOR YOUR ORDER AT NO CHARGE

This type of permission/license, instead of the standard Terms & Conditions, is sent to you because no fee is being charged for your order. Please note the following:

- Permission is granted for your request in both print and electronic formats, and translations.
- If figures and/or tables were requested, they may be adapted or used in part.
- Please print this page for your records and send a copy of it to your publisher/graduate school.
- Appropriate credit for the requested material should be given as follows: "Reprinted (adapted) with permission from (COMPLETE REFERENCE CITATION). Copyright (YEAR) American Chemical Society." Insert appropriate information in place of the capitalized words.
- One-time permission is granted only for the use specified in your request. No additional uses are granted (such as derivative works or other editions). For any other uses, please submit a new request.

Title: Complex Transfer Reaction from ZnO to ZnS Quantum Dots Driven by Surface Anions

Author: Shilaj Roy, Mihir Manna, Arun Chattopadhyay

Publication: The Journal of Physical Chemistry C

Publisher: American Chemical Society

Date: May 1, 2018

PERMISSION/LICENSE IS GRANTED FOR YOUR ORDER AT NO CHARGE

This type of permission/license, instead of the standard Terms & Conditions, is sent to you because no fee is being charged for your order. Please note the following:

- Permission is granted for your request in both print and electronic formats, and translations.
- If figures and/or tables were requested, they may be adapted or used in part.
- Please print this page for your records and send a copy of it to your publisher/graduate school.
- Appropriate credit for the requested material should be given as follows: "Reprinted (adapted) with permission from (COMPLETE REFERENCE CITATION). Copyright (YEAR) American Chemical Society." Insert appropriate information in place of the capitalized words.
- One-time permission is granted only for the use specified in your request. No additional uses are granted (such as derivative works or other editions). For any other uses, please submit a new request.

Title: Surface Complexed ZnO Quantum Dot for White Light Emission with Controllable Chromaticity and Color Temperature

Author: Shilaj Roy, Sabyasachi Pramanik, Satyapriya Bhandari, et al

Publication: Langmuir

Publisher: American Chemical Society

Date: Dec 1, 2017

PERMISSION/LICENSE IS GRANTED FOR YOUR ORDER AT NO CHARGE

This type of permission/license, instead of the standard Terms & Conditions, is sent to you because no fee is being charged for your order. Please note the following:

- Permission is granted for your request in both print and electronic formats, and translations.
- If figures and/or tables were requested, they may be adapted or used in part.
- Please print this page for your records and send a copy of it to your publisher/graduate school.
- Appropriate credit for the requested material should be given as follows: "Reprinted (adapted) with permission from (COMPLETE REFERENCE CITATION). Copyright (YEAR) American Chemical Society." Insert appropriate information in place of the capitalized words.
- One-time permission is granted only for the use specified in your request. No additional uses are granted (such as derivative works or other editions). For any other uses, please submit a new request.

BACK | CLOSE WINDOW